

Aims and Scope: Cell Journal (Yakhteh) is a peer review quarterly English publication of Royan Institute of Iran. The aim of the journal is to disseminate information through publishing the most recent scientific research studies on exclusively Cellular, Molecular and other related topics. Cell J, has been certified by Ministry of Culture and Islamic Guidance since 1999 and also accredited as a scientific and research journal by HBI (Health and Biomedical Information) Journal Accreditation Commission since 2000. **This journal holds the membership of the Committee on Publication Ethics (COPE).**

1. Types of articles

The articles in the field of Fertility and Sterility can be considered for publications in Cell J. These articles are as below:

A. Original articles are scientific reports of the original research studies. The article consists of English Abstract (structured), Introduction, Materials and Methods, Results, Discussion, Conclusion, Acknowledgements, Author's Contributions, and References (**Up to 40**).

B. Review articles are the articles written by well experienced authors and those who have excellence in the related fields. The corresponding author of the review article must be one of the authors of at least three published articles appearing in the references. The review article consists of English Abstract (unstructured), Introduction, Conclusion, Author's Contributions, and References (**Up to 70**).

C. Systematic Reviews

Systematic reviews are a type of literature review that collect and critically analyzes multiple research studies or papers. The Systematic reviews consist of English Abstract (unstructured), Introduction, Materials and Methods, Results, Discussion, Conclusion, Acknowledgements, Author's Contributions, and References (**Up to 70**).

D. Short communications are the articles containing new findings. Submissions should be brief reports of ongoing researches. The short communication consists of English Abstract (unstructured), the body of the manuscript (should not hold heading or subheading), Acknowledgements, Author's Contributions, and References (**Up to 30**).

E. Case reports are short discussions of a case or case series with unique features not previously described which make an important teaching point or scientific observation. They may describe novel techniques or use equipment, or new information on diseases of importance. It consists of English Abstracts (Unstructured), Introduction, Case Report, Discussion, Acknowledgements, Author's Contributions, and References (**Up to 30**).

F. Editorial should be written by either the editor in chief or the editorial board.

G. Imaging in biology should focus on a single case with an interesting illustration such as a photograph, histological specimen or investigation. Color images are welcomed. The text should be brief and informative.

H. Letter to the editors are welcome in response to previously published Cell J articles, and may also include interesting cases that do not meet the requirement of being truly exceptional, as well as other brief technical or clinical notes of general interest.

I. Debate.

2. Submission Process

It is recommended to see the guidelines for reporting different kinds of manuscripts here. This guide explains how to prepare the manuscript for submission. Before submitting, we suggest authors familiarize themselves with Cell J format and content by reading the journal via website (www.celljournal.org). The corresponding author ensures that all authors are included in the author list and agree with its order, and they must be aware of the manuscript submission.

A. Author contributions statements

It is essential for authors to include a statement of responsibility in the manuscript that specifies the contribution of every one of them. This participation must include conception and design of the manuscript, data acquisition or data analysis and interpretation, drafting of the manuscript and/or revising it for critically important intellectual content, revision and final approval of the manuscript and statistical analysis, obtaining funding, administrative, technical, or material support, or supervision. Authors who do not meet the above criteria should be acknowledged in the **Acknowledgements Section**.

B. Cover letter

Each article should be accompanied by a cover letter, signed by all authors specifying the following statement: "The manuscript has been seen and approved by all authors and is not under active consideration for publication. It has neither been accepted for publication nor published in another journal fully or partially (except in abstract form). I hereby assign the copyright of the enclosed manuscript to Cell J. Corresponding author must confirm the proof of the manuscript before online publishing. Also, is it needed to suggest three peer reviewers in the field of their manuscript.

C. Manuscript preparation

Authors whose first language is not English encouraged to consult a native English speaker in order to confirm his manuscripts to US or British (not a mixture) English usage and grammar. The manuscript should be prepared in accordance with the "International Committee of Medical Journal Editors (ICMJE)". Please send your manuscript in two formats (word and Pdf). The abstract and text pages should have consecutive line numbers in the left margin beginning with title page and continuing through the last page of the written text. Each abbreviation must be defined in the abstract and text when they are mentioned for the first time. Avoid using abbreviation in title. Please use the

international and standard abbreviations and symbols.

It should be added that an essential step toward the integration and linking of scientific information reported in published literature is using standardized nomenclature in all fields of science and medicine. Species names must be italicized (e.g., *Homo sapiens*) and also the full genus and species written out in full, both in the title of the manuscript and at the first mention of an organism in a paper.

It is necessary to mention that genes, mutations, genotypes, and alleles must be indicated in italics. Please use the recommended name by consulting the appropriate genetic nomenclature database, e.g., HUGO for human genes. In another words; if it is a human gene, you must write all the letters in capital and italic (e.g., *OCT4*, *c-MYC*). If not, only write the first letter in capital and italic (e.g., *Oct4*, *c-Myc*). **In addition, protein designations are the same as the gene symbol but are not italicized.**

Of note, Cell J will only consider publishing genetic association study papers that are novel and statistically robust. Authors are advised to adhere to the recommendations outlined in the STREGA statement (<http://www.strega-statement.org>). The following criteria must be met for all submissions:

1. Hardy-Weinberg Equilibrium (HWE) calculations must be carried out and reported along with the P-values if applicable [see Namipashaki et al. 2015 (Cell J, Vol 17, N 2, Pages: 187-192) for a discussion].
2. Linkage disequilibrium (LD) structure between SNPs (if multiple SNPs are reported) must be presented.
3. Appropriate multiple testing correction (if multiple independent SNPs are reported) must be included.

Submissions that fail to meet the above criteria will be rejected before being sent out for review.

Each of the following manuscript components should begin in the following sequence:

Authors' names and order of them must be carefully considered (full name(s), highest awarded academic degree(s), email(s), and institutional affiliation(s) of all the authors in English. Also, you must send mobile number and full postal address of the corresponding author).

Changes to Authorship such as addition, deletion or rearrangement of author names must be made only before the manuscript has been accepted in the case of approving by the journal editor. In this case, the corresponding author must explain the reason of changing and confirm them (which has been signed by all authors of the manuscript). If the manuscript has already been published in an online issue, an erratum is needed.

Title is providing the full title of the research (do not use abbreviations in title).

Running title is providing a maximum of 7 words (no more than 50 characters).

Abstract must include Background, Materials and Methods, Results, and Conclusion (no more than **300** words).

Keywords, three to five, must be supplied by the authors at the foot of the abstract chosen from the Medical Subject Heading (MeSH). Therefore; they must be specific and relevant to the paper.

The following components should be identified after the abstract:

Introduction: The Introduction should provide a brief background to the subject of the paper, explain the importance of the study, and state a precise study question or purpose.

Materials and Methods: It includes the exact methods or observations of experiments. If an apparatus is used, its manufacturer's name and address should be stipulated in parenthesis. If the method is established, give reference but if the method is new, give enough information so that another author can perform it. If a drug is used, its generic name, dose, and route of administration must be given. Standard units of measurements and chemical symbols of elements do not need to be defined.

Statistical analysis: Type of study and statistical methods should be mentioned and specified by any general computer program used.

Ethical considerations: Please state that informed consent was obtained from all human adult participants and from the parents or legal guardians of minors and include the name of the appropriate institutional review board that approved the project. It is necessary to indicate in the text that the maintenance and care of experimental animals complies with National Institutes of Health guidelines for the humane use of laboratory animals, or those of your Institute or agency.

Clinical trial registration: All of the Clinical Trials performing in Iran must be registered in Iranian Registry of Clinical Trials (www.ircct.ir). The clinical trials performed abroad, could be considered for publication if they register in a registration site approved by WHO or www.clinicaltrials.gov. If you are reporting phase II or phase III randomized controlled trials, you must refer to the CONSORT Statement for recommendations to facilitate the complete and transparent reporting of trial findings. Reports that do not conform to the CONSORT guidelines may need to be revised before peer reviewing.

Results: They must be presented in the form of text, tables, and figures. Take care that the text does not repeat data that are presented in tables and/or figures. Only emphasize and summarize the essential features of the main results. Tables and figures must be numbered consecutively as appeared in the text and should be organized in separate pages at the end of article while their location should be mentioned in the main text.

Tables and figures: Tables should have a short descriptive heading above them and also any footnotes. Figure's legend should contain a brief title for the whole figure and continue with a short explanation of each part and also the symbols used (no more than 100 words). All figures must be prepared based on cell journal's guideline in color (no more than **6** Figures and Tables) and also in GIF or JPEG format with 300 dpi resolutions.

Supplementary materials would be published on the online version of the journal. This material is important to the understanding

and interpretation of the report and should not repeat material within the print article. The amount of supplementary material should be limited. Supplementary material should be original and not previously published and will undergo editorial and peer review with the main manuscript. Also, they must be cited in the manuscript text in parentheses, in a similar way as when citing a figure or a table. Provide a legend for each supplementary material submitted.

Discussion: It should emphasize the present findings and the variations or similarities with other researches done by other researchers. The detailed results should not be repeated in the discussion again. It must emphasize the new and important aspects of the study.

Conclusion: It emphasizes the new and important aspects of the study. All conclusions are justified by the results of the study.

Acknowledgements: This part includes a statement thanking those who contributed substantially with work relevant to the study but does not have authorship criteria. It includes those who provided technical help, writing assistance and name of departments that provided only general support. You must mention financial support in the study. Otherwise; write this sentence "There is no financial support in this study".

Conflict of Interest: Any conflict of interest (financial or otherwise) and sources of financial support must be listed in the Acknowledgements. It includes providers of supplies and services from a commercial organization. Any commercial affiliation must be disclosed, regardless of providing the funding or not.

References: The references must be written based on the Vancouver style. Thus the references are cited numerically in the text and listed in the bibliography by the order of their appearance. The titles of journals must be abbreviated according to the style used in the list of Journals Indexed in PubMed. Write surname and initials of all authors when there are six or less. In the case of seven or more authors, the names of first six authors followed by "et al." must be listed. The reference of information must be based on the following order:

Article:

Surname(s) and first letter of name & middle name(s) of author(s). Manuscript title. Journal title (abbr).publication date (year); Volume (Issue): Page number.

Example: Manicardi GC, Bianchi PG, Pantano S, Azzoni P, Bizzaro D, Bianchi U, et al. Presence of endogenous nicks in DNA of ejaculated human spermatozoa and its relationship to chromomycin A3 accessibility. *Biol Reprod.* 1995; 52(4): 864-867.

Book:

Surname(s) and first letter of name & middle name(s) of author(s). Book title. Edition. Publication place: publisher name; publication date (year); Page number.

Example: Edelman CL, Mandle CL. Health promotion throughout the life span. 2nd ed. ST Louis: Mosby; 1998; 145-163.

Chapter of book:

Surname(s) and first letter of name & middle name(s) of author(s). Chapter title. In: Surname(s) and first letter of name & middle name(s) of editor(s), editors. Book title. Edition. Publication place: publisher name; publication date (year); Page number.

Example: Phillips SJ, Whisnant JP. Hypertension and stroke. In: Laragh JH, Brenner BM, editors. Hypertension: pathophysiology, diagnosis, and management. 2nd ed. New York: Raven Press; 1995; 465-478.

Abstract book:

Example: Nabavi SM. Stem cell therapy for multiple sclerosis. *Cell J.* 2013; 5 Suppl 1: Os-13.

Thesis:

Name of author. Thesis title. Degree. City name. University. Publication date (year).

Example: Eftekhari Yazdi P. Comparison of fragment removal and co-culture with Vero cell monolayer's on development of human fragmented embryos. Presented for the Ph.D., Tehran. Tarbiyat Modarres University. 2004.

Internet References

Article:

Surname(s) and first letter of name & middle name(s) of author(s). Manuscript title. Journal title (abbr). Publication date (year); Volume (Issue): Page number. Available from: URL link. (Observation date).

Example: Jahanshahi A, Mirnajafi-Zadeh J, Javan M, Mohammad-Zadeh M, Rohani M. Effect of low-frequency stimulation on adenosine A1 and A2A receptors gene expression in dentate gyrus of perforant path kindled rats. *Cell J.* 2008; 10 (2): 87-92. Available from: <http://www.celljournal.org>. (20 Oct 2008).

Book:

Example: Anderson SC, Poulsen KB. Anderson's electronic atlas of hematology.[CD-ROM]. Philadelphia: Lippincott Williams & Wilkins; 2002.

Law:

Example: Embryo donation law. Iran Judicature, Official Gazette of the Islamic Republic of Iran. Available from: <http://www.dastour.ir/Brows/?lid=245069>. (20 Jul 2013).

D. Proofs are sent by email as PDF files and should be checked and returned within 72 hours of receipt. It is the authors' responsibility to

check that all the text and data as contained in the page proofs are correct and suitable for publication. **We are requested to pay particular attention to author's names and affiliations as it is essential that these details be accurate when the article is published.**

E. Pay for publication: Authors do not have to pay any Manuscript Processing Charge or Open Access Publication Fee. **Before publishing author's article, it would be the author's responsibility to pay for the expenses, if the editor feels the level of English used in the manuscript requires editing.**

F. Ethics of scientific publication: Manuscripts that have been published elsewhere with the same intellectual material will refer to duplicate publication. If authors have used their own previously published work or work that is currently under review, as the basis for a submitted manuscript, they are required to cite the previous work and indicate how their submitted manuscript offers novel contributions beyond those of the previous work. Research and publication misconduct is considered a serious breach of ethics. The Journal systematically employs iThenticate, a plagiarism detection and prevention software designed to ensure the originality of written work before publication.

Plagiarism of text from a previously published manuscript by the same or another author is a serious publication offence. Some parts of text may be used, only where the source of the quoted material is clearly acknowledged.

3. General information

A. You can send your article via online submission system which is available at our website: <http://www.celljournal.org>. If the article is not prepared according to the format of **Cell J**, it will be returned to authors.

B. The order of article appearance in the Journal is not demonstrating the scientific characters of the authors.

C. **Cell J** has authority to accept or reject the articles.

D. The received articles will be evaluated by one epidemiologist. Then associate editor will determine its reviewers. If three reviewers pass their judgments on the article, it will be presented to the editorial board of **Cell J**. If the editorial board has a positive judgment about the article, reviewers' comments will be presented to the corresponding author (the identification of the reviewers will not be revealed). The executive member of journal will contact the corresponding author directly within 7-8 weeks by email. If authors do not receive any reply from journal office after the specified time, they can contact journal office. Executive manager will respond promptly to authors' message.

The Final Checklist

The authors must ensure that before submitting the manuscript for publication, they have to consider the following parts:

1. Title page should contain title, name of the author/coauthors, their academic qualifications, designation & institutions they are affiliated with, mailing address for future correspondence, email address, phone, and fax number.
2. Text of manuscript and References prepared as stated in the "guide for authors" section.
3. Tables should be in a separate page. Figures must be sent in color and also in GIF or JPEG format with 300 dpi resolutions.
4. Covering Letter.

The Editor-in-Chief: Ahmad Hosseini, Ph.D.

Cell Journal (Yakhteh),

P.O. Box: 16635-148, Iran

Tel/Fax: + 98-21-22510895

Emails: Celljournal@royaninstitute.org

info@celljournal.org



IN THE NAME OF GOD

Gone But not Forgotten

In the memory of the late Director of Royan Institute,
Founder of Stem Cells Research in Iran and Chairman of
Cell Journal ^(Yakhteh). May he rest in peace.

Dr. Saeed Kazemi Ashtiani

OWNED:

Royan Institute, Iranian Academic Center for Education Culture and Research (ACECR)

CHAIRMAN:

Hamid Gourabi, Ph.D., (Professor, Royan Institute, Tehran, Iran)

EDITOR IN CHIEF:

Ahmad Hosseini, Ph.D., (Professor, Shahid Beheshti Medical University, Tehran, Iran)

EDITOR ASSOCIATE:

Saeid Abroun, Ph.D., (Associate Professor, Tarbiat Modares University, Tehran, Iran)

EDITORIAL BOARD:

Saeid Abroun, Ph.D., (Associate Professor, Tarbiat Modares University, Tehran, Iran)
Kamran Alimoghadam, M.D., (Associate Professor, Tehran Medical University, Tehran, Iran)
Alireza Asgari, Ph.D., (Professor, Baghyatallah University, Tehran, Iran)
Mohammad Kazem Aghaee Mazaheri, D.D.S., (Assistant Professor, ACECR, Tehran, Iran)
Gila Behzadi, Ph.D., (Professor, Shahid Beheshti Medical University, Tehran, Iran)
Hossein Baharvand, Ph.D., (Professor, Royan Institute, Tehran, Iran)
Mary Familiari, Ph.D., (Senior Lecturer, University of Melbourne, Melbourne, Australia)
Hamid Gourabi, Ph.D., (Professor, Royan Institute, Tehran, Iran)
Jurgen Hescheler, M.D., (Professor, Institute of Neurophysiology of University Zu Koln, Germany)
Ghasem Hosseini Salekdeh, Ph.D., (Assistant Professor, Agricultural Biotechnology Research Institute, Karaj, Iran)
Esmail Jabbari, Ph.D., (Associate Professor, University of South Carolina, Columbia, USA)
Suresh Jesuthasan, Ph.D., (Associate Professor, National University of Singapore, Singapore)
Bahram Kazemi, Ph.D., (Professor, Shahid Beheshti Medical University, Tehran, Iran)
Saadi Khochbin, Ph.D., (Professor, Inserm/Grenoble University, France)
Ali Khademhosseini, Ph.D., (Associate Professor, Harvard Medical School, USA)
Kun Ping Lu, M.D., Ph.D., (Professor, Harvard Medical School, Boston, USA)
Navid Manuchehrabadi, Ph.D., (Angio Dynamics, Marlborough, USA)
Hosseinali Mehrani, Ph.D., (Professor, Baghyatallah University, Tehran, Iran)
Marcos Meseguer, Ph.D., (Clinical Embryology Laboratory IVI Valencia, Valencia, Spain)
Seyed Javad Mowla, Ph.D., (Professor, Tarbiat Modares University, Tehran, Iran)
Mohammad Hossein Nasr Esfahani, Ph.D., (Professor, Royan Institute, Tehran, Iran)
Toru Nakano, M.D., Ph.D., (Professor, Osaka University, Osaka, Japan)
Donald Newgreen, Ph.D., (Professor, Murdoch Children Research Institute, Melbourne, Australia)
Mojtaba Rezaezadeh Valojerdi, Ph.D., (Professor, Tarbiat Modares University, Tehran, Iran)
Mohammad Hossein Sanati, Ph.D., (Associate Professor, National Institute for Genetic Engineering and Biotechnology, Tehran, Iran)
Eimei Sato, Ph.D., (Professor, Tohoku University, Sendai, Japan)
Andreas Serra, M.D., (Professor, University of Zurich, Zurich, Switzerland)
Abdolhossein Shahverdi, Ph.D., (Professor, Royan Institute, Tehran, Iran)
Michele Catherine Studer, Ph.D., (Institute of Biology Valrose, IEV University of Nice Sophia-Antipolis, France)
Daniela Toniolo, Ph.D., (Head, Unit of Common Disorders, San Raffaele Research Institute, Milano, Italy)
Christian van den Bos, Ph.D., (Managing Director MARES Ltd, Greven, Germany)
Gianpaolo Zerbini, M.D., Ph.D., (San Raffaele Scientific Institute, Italy)
Shubing Zhang, Ph.D., (Associate Professor, Central South University, China)
Daniele Zink, Ph.D., (Institute of Bioengineering and Nanotechnology, Agency for Science Technology & Science, Singapore)

EXECUTIVE MANAGER:

Farideh Malekzadeh, M.Sc., (Royan Institute, Tehran, Iran)

EXECUTIVE BOARD:

Parvaneh Afsharian, Ph.D., (Royan Institute, Tehran, Iran)
Reza Azimi, B.Sc., (Royan Institute, Tehran, Iran)
Reza Omani-Samani, M.D., (Royan Institute, Tehran, Iran)
Elham Amirchaghmaghi, M.D., Ph.D., (Royan Institute, Tehran, Iran)
Leila Daliri, M.Sc., (Royan Institute, Tehran, Iran)
Mahdi Lotfipanah, M.Sc., (Royan Institute, Tehran, Iran)

ENGLISH EDITOR:

Saman Eghtesad, Ph.D., (Royan Institute, Tehran, Iran)
Vahid Ezzatizadeh, Ph.D., (Royan Institute, Tehran, Iran)
Jane Elizabeth Ferrie, Ph.D., (University College of London, London, UK)
Mojtaba Nemati, M.Sc., (Royan Institute, Tehran, Iran)
Ramin Rezaee, Pharm.D., Ph.D., (Mashhad University of Medical Sciences, Mashhad, Iran)
Kim Vagharfard, M.Sc., (Royan Institute, Tehran, Iran)
Hamid Zahednasab, M.Sc., (Royan Institute, Tehran, Iran)

GRAPHICS:

Laleh Mirza Ali Shirvani, B.Sc., (Royan Institute, Tehran, Iran)

PUBLISHED & SPONSORED BY:

Publication of Royan Institute (ACECR)

Indexed in:

1. Thomson Reuters (ISI); *Impact Factor*: 2.363
2. PubMed
3. PubMed Central (PMC)
4. National Library Medicine (NLM)
5. Biosis Preview
6. Index Medicus for the Eastern Mediterranean Region (IMEMR)
7. Index Copernicus International
8. Cambridge Scientific Abstract (CSA)
9. EMBASE
10. Scopus
11. Cinahl Database
12. Google Scholar
13. Chemical Abstract Service (CAS)
14. Proquest
15. Directory of Open Access Journals (DOAJ)
16. Open Academic Journals Index (OAJI)
17. Directory of Research Journals Indexing (DRJI)
18. Scientific Information Database (SID)
19. Iranmedex
20. Regional Information Center for Sciences and Technology (RICeST)
21. Islamic World Science Citation Center (ISC)
22. Magiran
23. Science Library Index

ACECR

Copyright and license information:

The *Cell Journal* ^(Yakhteh) is an open access journal which means the articles are freely available online for any individual author to download and use the providing address. The journal is licensed under a Creative Commons Attribution-Non Commercial 3.0 Unported License which allows the author(s) to hold the copyright without restrictions that is permitting unrestricted use, distribution, and reproduction in any medium provided the original work is properly cited.

Editorial Office Address (Dr. Ahmad Hosseini):

Royan Institute, P.O.Box: 16635-148,
Tehran, Iran
Tel & Fax: (+9821)22510895
Website: www.celljournal.org
Emails: info@celljournal.org
celljournal@royaninstitute.org

Printing Company:

Naghsh e Johar Co.
NO. 103, Fajr alley, Tehranpars Street, Tehran, Iran



CONTENTS

Review Article

- **A Review on The Protective Effects of Metformin in Sepsis-Induced Organ Failure**
Fatima Ismail Hassan, Tina Didari, Fazlullah Khan, Kamal Niaz, Mojtaba Mojtahedzadeh, Mohammad Abdollahi 363

Original Articles

- **The Synergistic Effect of Glucagon-Like Peptide-1 and Chamomile Oil on Differentiation of Mesenchymal Stem Cells into Insulin-Producing Cells**
Saeid Saghahazrati, Seyed Abdulmajid Ayatollahi, Farzad Kobarfard, Bagher Minaii Zang 371
- **Incorporation of Silver Sulfadiazine into An Electrospun Composite of Polycaprolactone as An Antibacterial Scaffold for Wound Healing in Rats**
Fereshteh Nejaddehbash, Mahmoud Hashemitabar, Vahid Bayati, Eskandar Moghimipour, Jabrael Movaffagh, Mahmoud Orazizadeh, Mohammadreza Abbaspour 379
- **Histological Evidence for Therapeutic Induction of Angiogenesis Using Mast Cells and Platelet-Rich Plasma within A Bioengineered Scaffold following Rat Hindlimb Ischemia**
Ali Karimi, Rasoul Shahrooz, Rahim Hobbenaghi, Rahim Mohammadi, Nowruz Delirez, Saeede Amani, Johan Garssen, Esmacil Mortaz, Ian M Adcock 391
- **Spermatogenesis Recovery Potentials after Transplantation of Adipose Tissue-Derived Mesenchymal Stem Cells Cultured with Growth Factors in Experimental Azoospermic Mouse Models**
Masoumeh Eliyasi Dashtaki, Masoud Hemadi, Ghasem Saki, Javad Mohammadiasl, Ali Khodadadi 401
- **Three-Dimensional Culture of Mouse Spermatogonial Stem Cells Using A Decellularised Testicular Scaffold**
Nasrin Majidi Gharenaz, Mansoureh Movahedin, Zohreh Mazaheri 410
- **The Use of β -Elemene to Enhance Radio Sensitization of A375 Human Melanoma Cells**
Zahra Balavandi, Ali Neshasteh-Riz, Fereshteh Koosha, Samira Eynali, Mahmood Hoormand, Mino Shahidi 419
- **Characterization and In Silico Analysis of The Structural Features of G-CSF Derived from Lysates of *Escherichia coli***
Sharareh Peymanfar, Rasoul Roghanian, Kamran Ghaedi, Sayed-Hamid Zarkesh-Esfahani, Reza Yari 426
- **Biosimilar Gene Therapy: Investigational Assessment of Secukinumab Gene Therapy**
Ali Fallah, Hajar Estiri, Elizabeth Parrish, Mansoureh Soleimani, Sirous Zeinali, Azita Zadeh-Vakili 433
- **Repression of TGF- β Signaling in Breast Cancer Cells by miR-302/367 Cluster**
Mona Ahmadalizadeh Khanehsar, Moslem Hoseinbeyki, Masoumeh Fakhr Taha, Arash Javeri 444
- **CD44 Gene rs8193 C Allele Is Significantly Enriched in Gastric Cancer Patients**
Roya Mokhtarian, Hossein Tabatabaeian, Pardis Saadatmand, Mansoureh Azadeh, Negar Balmeh, Bagher Yakhchali, Kamran Ghaedi 451
- **Regulatory Network Analysis to Reveal Important miRNAs and Genes in Non-Small Cell Lung Cancer**
Xingni Zhou, Zhenghua Zhang, Xiaohua Liang 459
- **Down-Regulation of *miR-200c* and Up-Regulation of miR-30c Target both Stemness and Metastasis Genes in Breast Cancer**
Mahsa Rahimi, Ali Sharifi-Zarchi, Nosratollah Zarghami, Lobat Geranpayeh, Marzieh Ebrahimi, Effat Alizadeh 467
- **Chitosan Hydrogel Supports Integrity of Ovarian Follicles during *In Vitro* Culture: A Preliminary of A Novel Biomaterial for Three Dimensional Culture of Ovarian Follicles**
Fatemeh Hassani, Bitah Ebrahimi, Ashraf Moini, Ali Ghiaseddin, Mahshid Bazrafkan, Gholamreza Hassanzadeh, Mojtaba Rezazadeh Valojerdi 479
- **Front page of Cell Journal_(Yakhteh): Figure 6B, Page: 387**

A Review on The Protective Effects of Metformin in Sepsis-Induced Organ Failure

Fatima Ismail Hassan, M.Sc.¹, Tina Didari, M.Sc.¹, Fazlullah Khan, M.Sc.¹, Kamal Niaz, Ph.D.¹,
Mojtaba Mojtahedzadeh, Pharm.D.^{1, 2, 3}, Mohammad Abdollahi, Ph.D.^{1, 2*}

1. The Institute of Pharmaceutical Sciences (TIPS), Tehran University of Medical Sciences, Tehran, Iran
2. Department of Toxicology and Pharmacology, Tehran University of Medical Sciences, Tehran, Iran
3. Department of Clinical Pharmacy, Tehran University of Medical Sciences, Tehran, Iran

*Corresponding Address: The Institute of Pharmaceutical Sciences (TIPS), Tehran University of Medical Sciences, Tehran, Iran
Email: mohammad@tums.ac.ir

Received: 11/August/2018, Accepted: 17/November/2018

Abstract

Despite advances in sepsis management, it remains a major intensive-care-unit (ICU) concern. From new prospective, positive effects of metformin, such as anti-oxidant and anti-inflammatory properties are considered potentially beneficial properties for management of septic patients. This article reviewed the potential ameliorative effects of metformin in sepsis-induced organ failure. Information were retrieved from PubMed, Scopus, Embase, and Google Scholar. Multi-organ damage, oxidative stress, inflammatory cytokine stimulation, and altered circulation are hallmarks of sepsis. Metformin exerts its effect via adenosine monophosphate-activated protein kinase (AMPK) activation. It improves sepsis-induced organ failure by inhibiting the production of reactive oxygen species (ROS) and pro-inflammatory cytokines, preventing the activation of transcription factors related to inflammation, decreasing neutrophil accumulation/infiltration, and also maintaining mitochondrial membrane potential. Studies reported the safety of metformin therapeutic doses, with no evidence of lactic acidosis, in septic patients.

Keywords: Adenosine Monophosphate-Activated Protein Kinase, Metformin, Multi-Organ Failure, Oxidative Stress, Sepsis

Cell Journal(yakhteh), Vol 21, No 4, January-March (Winter) 2020, Pages: 363-370

Citation: Ismail Hassan F, Didari T, Khan F, Niaz K, Mojtahedzadeh M, Abdollahi M. A review on the protective effects of metformin in sepsis-induced organ failure. Cell J. 2020; 21(4): 363-370. doi: 10.22074/cellj.2020.6286.

Introduction

Recently, at the 45th Congress of Society of Critical Care Medicine in Florida, sepsis was defined as a life-threatening condition associated with organ damage as a result of dysregulated host immune response (1). Septic shock has been described as persistent elevation in lactate levels above 2 mmol/L despite adequate fluid resuscitation and elevation in mean arterial pressure to over 65 mmHg that requires administration of a vasopressor (2). Recent evidence suggests that people at risk of developing sepsis, are usually critically ill, elderly, and immunocompromised patients (3). There are other acute and chronic conditions that can cause systemic inflammatory response and events similar to those observed in sepsis, including burst of inflammatory mediators, hemorrhagic shock, pancreatitis, trauma, and ischemic conditions (4). To date, management of sepsis has been challenged due to its complex nature. Experimental studies have proven the possible alleviative effect of anti-inflammatory drugs in sepsis. The protective effects of metformin mediated by anti-oxidative and anti-inflammatory mechanisms, were demonstrated in recent studies (5-7). Such evidence made metformin a potential candidate for sepsis management. Lactic acidosis has emerged as the most concerning issue in metformin users, since it affects lactate clearance and metabolism (8). However, some studies abrogated of the association between therapeutic doses of metformin and lactic acidosis occurrence. Studies on

metformin reported an improvement in sepsis-induced inflammatory and oxidative stress conditions, as well as improved mortality at different tested doses and in various models (9, 10). This article aimed at reviewing the ameliorative effects of metformin in sepsis-related organ failure and discussing the underlying molecular mechanisms.

Overview of sepsis

Sepsis is a lethal situation with a high mortality rate in intensive-care-unit (ICU) hospitalized persons (11). It is characterized by severe blood or tissue infection with a burst of inflammatory markers and subsequent mitochondrial dysfunction due to the presence of molecules released by microbes or stressed cells. Molecules released from these microbes stimulate inflammatory responses, which in turn lead to tissue damage and production of some mediators that can exacerbate inflammation and tissue damage, and eventually cause organ failure (12). These include inflammatory mediators such as high mobility box protein (HMGB1) which can serve as a classic damage-associated molecular pattern (DAMP) molecule in the late phase of sepsis. Sepsis is associated with risk factors such as age, delayed treatment, persistent infection, immune suppression, and previous illness (13). Polymorphism of genes encoding inflammatory mediators, heat shock proteins, and toll-like receptors (TLRs), can influence the incidence and severity of sepsis (14).

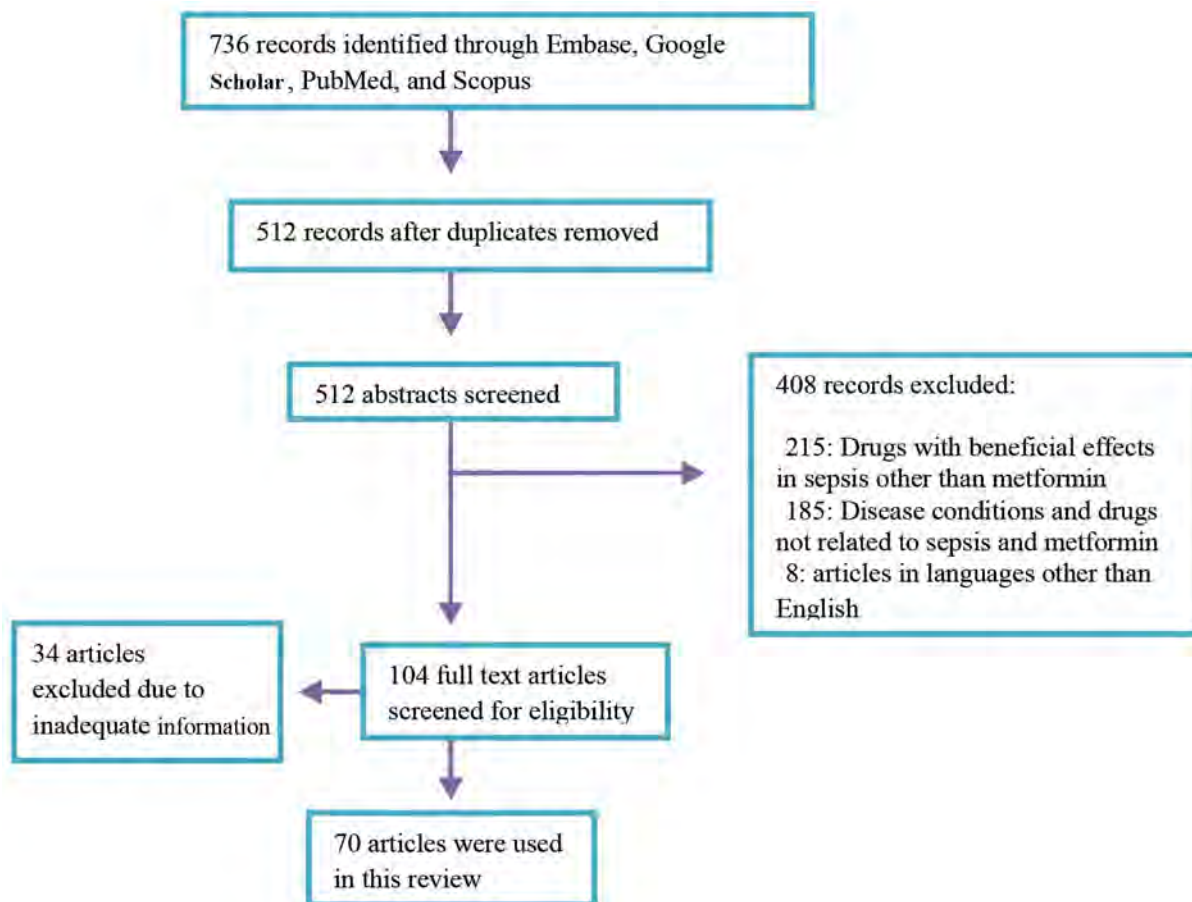


Fig.1: Search strategy indicating inclusion and exclusion criteria.

Biochemical events in sepsis

Sepsis involves the release of molecules exclusively synthesized by microbes [lipopolysaccharides (LPS), peptidoglycan, and bacterial lipoproteins] recognized by pattern recognition receptors (CD14, TLRs) which send warning signals to the host, and induce stimulation of cytokines, chemokines, and complement system, and subsequent activation of the immune system cells neutrophils, monocytes, and macrophages (15-17). It involves both cellular and molecular events which occur as a result of stimulation of inflammatory mediators, oxidative stress markers, apoptosis, as well as interference with some neurotransmitters and signaling pathways (Fig.1). These events lead to tissue injury and subsequent organ damage/failure. Sepsis is associated with increased production of inflammatory cytokines in response to the entrance of microorganisms into the blood (18). Sepsis is comprised of two inflammatory stages namely, an acute phase and subsequently, a late-phase characterized by a systemic inflammatory response syndrome (SIRS) and a complimentary anti-inflammatory response syndrome (CARS), respectively (19). The typical characteristic of these stages are exaggerated productions of pro- and anti-inflammatory cytokines or chemokines which lead to a cytokine storm. These

cytokines exhibit both beneficial and deleterious effects as although they are produced to eliminate infection, their overproduction/overactivity can lead to immunosuppression, tissue damage, and organ failure (19, 20). Proinflammatory cytokines stimulate systemic responses while anti-inflammatory cytokines inhibit such responses and initiate wound healing (19). These early response regulators (i.e. proinflammatory cytokines) are implicated in SIRS, while the anti-inflammatory mediators secreted during CARS play immunoregulatory roles in sepsis (20, 21). These hyper-inflammatory responses affect the balance between endogenous oxidants and antioxidants and cause immunosuppression which leads to tissue injury, cell death, and organ failure. Excessive activation of NF- κ B stimulated the production of reactive oxygen species (ROS) and affected endogenous antioxidant activity, which in turn caused lung damage and distal organs apoptosis in septic mice (22). Redox imbalance due to production of ROS can affect respiratory chain activities and mitochondrial structure (23). These events increase oxidative stress, tissue injury, and organ failure by affecting blood flow of various organs. Increased production of ROS leads to vasoconstriction and subsequent decreased blood flow of vital organs (24). Another important parameter in

sepsis is accumulation of lactate which is associated with inactivation of pyruvate dehydrogenase (PDH) enzyme. Tumor necrosis factor (TNF) may be involved in preventing PDH activity in the skeletal muscles of rats with chronic abdominal sepsis (25). Blood or serum lactate concentration during sepsis is regarded as the most important indicator of morbidity and mortality during sepsis. Hyperlactatemia was shown to be associated with sepsis severity. In this regard, increment of lactate clearance was found to be associated with improved clinical outcomes and decreased mortality probably by resolving hypoxia. Several clinical trials reported the improved clinical outcomes in patients with sepsis and septic shock, following adequate lactate clearance. A 10% increase in lactate clearance was associated with one-score decrease in acute physiology and chronic health evaluation II (APACHE II), and an approximately 11% decrease in mortality among the septic patients (26). Decreased APACHE II score, days spent in the ICU, and 28-day mortality in groups with 10-30% lactate clearances were also observed in patients with severe sepsis and septic shock (27). Recent findings

using *Escherichia coli*-infected cells (*in vitro*), and LPS and cecal ligation and puncture (CLP)-induced septic mice (*in vivo*) revealed the role of adenosine monophosphate kinase (AMPK) pathway in sepsis severity as suppression of this pathway led to an increase in pyruvate kinase isozyme M2 (PKM2)-dependent aerobic glycolysis. This increases HMGB1 release, lactate accumulation, and mortality (28). Activation of NF- κ B pathway that involves nitric oxide (NO) production was shown to be associated with activation of pro-apoptotic proteins signaling such as the Fas and FasL which led to apoptosis in A549 human lung epithelial cells and mice treated with LPS (29). Common molecular events that occur during sepsis are inflammation, oxidative stress, and apoptosis which lead to the observed deleterious effects. Hence, agents that have the ability to block these effects, may be beneficial in sepsis management. Studies reported that the antioxidant, anti-inflammatory, and anti-apoptotic effects of metformin are mediated by blockade or enhancement of the involved molecular pathways; thus, it may affect sepsis via same mechanisms (Fig.2).

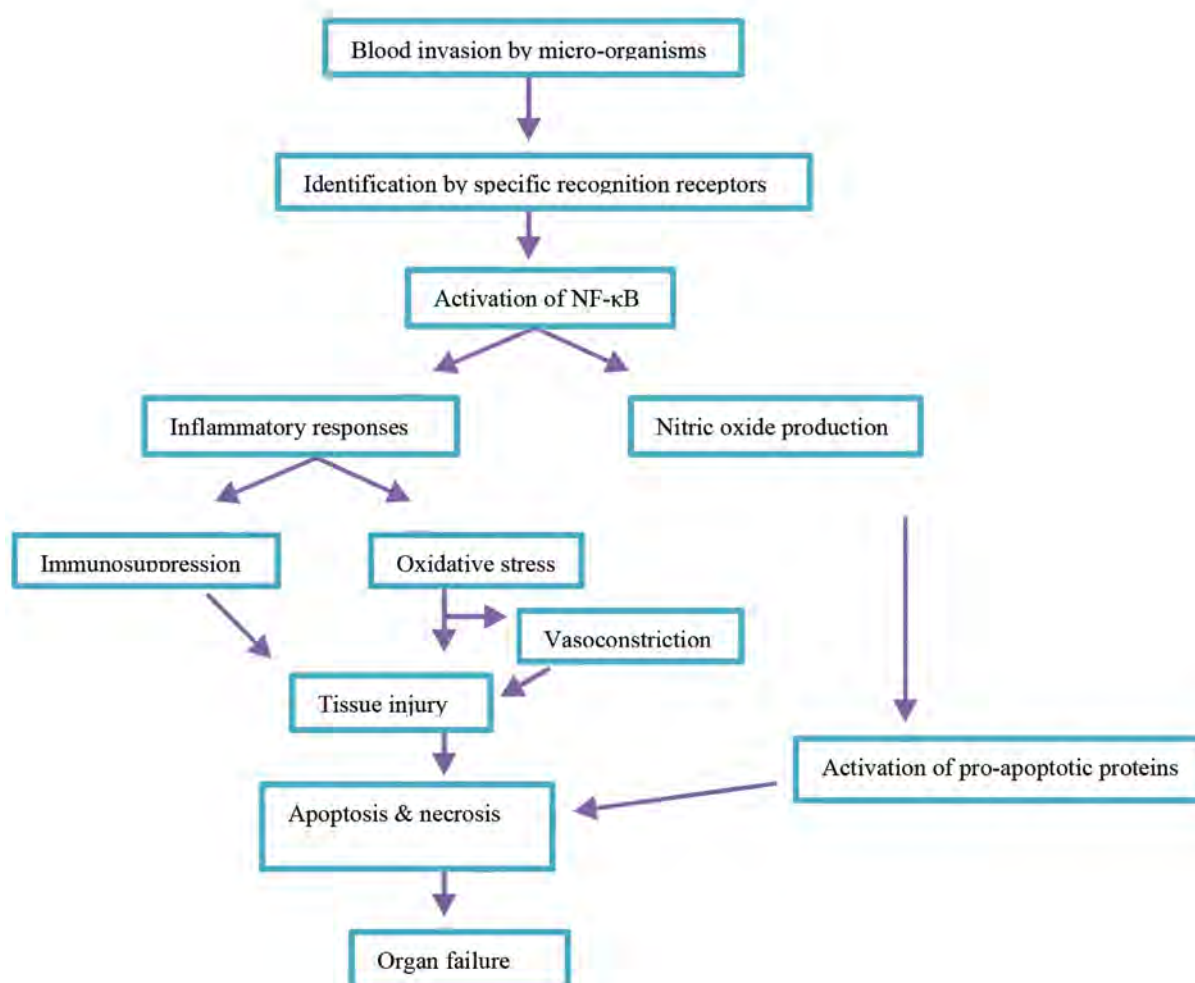


Fig.2: A summary of biochemical events occurring during sepsis.

Metformin

Metformin has several functions in addition to its anti-hyperglycemic effects. Inhibition of respiratory chain complex in the mitochondria is a primary action of metformin (30). It exerts its effect by inhibiting complex I of the electron transport chain (ETC) which increases AMP/ATP ratio and subsequently induces AMPK activation (31). This effect was observed in perfused liver, skeletal muscles, endothelial cells, pancreatic beta cells, and neurons (32-34). AMPK plays significant roles in cellular responses to danger signals (35).

The protective effect of metformin is majorly mediated through activation of AMPK and inhibition of NF- κ B pathway (36). It decreases mitochondrial respiration which renders cells less energetic, increases aerobic glycolysis, and reduces glucose metabolism through the citric cycle. Metformin reduces tumor cell growth by preventing lipid membrane biosynthesis in the mitochondria (37). It was shown that inhibition of complex I of ETC in cancer cells prevented oxidative phosphorylation, which in turn, decreased cell multiplication both *in vitro* and *in vivo*. Metformin lessened the activation of apoptotic cascade by inhibiting the permeability transition pore (PTP) opening (38). It also attenuated kidney injury induced by gentamicin in rats (7).

Co-administration of metformin with garlic also prevented gentamicin-induced kidney injury and suppressed diabetes-induced podocyte loss in diabetic neuropathy (39, 40). Metformin was reported to exert potent antioxidant activity, especially in oxidative stress-induced damage in diabetic patients (5). It reduces cardiovascular-associated mortality and morbidity in both diabetic and non-diabetic patients (6). Metformin was shown to decrease blood pressure, left ventricular mass, and cholesterol, triglycerides, and fibrinogen levels in obese non-diabetic hypertensive women (41). It also decreased blood pressure and hyperandrogenemia in women with polycystic ovarian syndrome (42). Metformin also reduced myocardial infarct size by preventing membrane PTP (mPTP) opening via the phosphatidylinositol-3-kinase (PI3K) pathway (43). Metformin prevented brain mitochondrial dysfunction by decreasing oxidative stress levels and reducing insulin resistance (44). A combination of metformin and insulin given to critically ill patients reduced the incidence of insulin resistance, adverse effects associated with high-dose insulin therapy, as well as inflammatory cytokines production (45-47).

Other animal studies reported metformin's ability to promote neurogenesis, enhance spatial memory, protect against cerebral ischemia, and stimulate angiogenesis (48, 49). Sepsis includes similar biochemical events; hence, metformin may protect against sepsis-induced organ injury via above-noted mechanisms. Some studies reported beneficial effects of metformin on sepsis. Despite these promising effects, metformin is still contraindicated in organ failure due to risk of lactic acidosis. However, some studies reported the safety of metformin at therapeutic doses with little or no incidence of lactic acidosis but improvement of morbidity and mortality.

The safety of metformin in sepsis

Metformin was shown to cause lactate accumulation by inhibiting or reducing lactate metabolism and clearance in the liver through induction of hypoxia or excessive inhibition of mitochondrial respiration (50). Metformin was also found to be associated with non-hypoxic lactic acidosis with an increased mortality rate of about 50%. This is the main reason for metformin contraindication in critically ill patients, especially in sepsis. However, this effect of metformin on mitochondrial respiration that causes lactate accumulation was reported at therapeutic doses. Some studies reported metformin-associated lactic acidosis (MALA) only in case of overdose which is rare, while some studies found no MALA even at very high doses of the drug. MALA in sepsis may not be significant as the benefit outweighs the risk and the usual doses are within the therapeutic limit. The following studies reported little or no aggravating effects for metformin in terms of sepsis-related mortality. Metformin did not affect survival rate in sepsis at high doses (500 mg/kg) in mice, which was similar to smaller doses (50 mg/kg) used in clinical practice (9). In another study, patients with suspected sepsis were recruited from the emergency department (ED); higher lactate levels and incidence of hyperlactatemia were more common in metformin users compared to non-users though it did not indicate poor prognosis (51). A clinical trial reported lower incidence of hospital mortality in metformin users compared to non-users, while lactate, bicarbonate, and blood pH levels were similar between the two groups (10). This inferred that metformin did not increase the lactate level, but improved mortality. Another study similarly reported that metformin had no significant impact on lactate levels, clearance, and normalization, over a 24-hour period in patients with severe sepsis and septic shock (52). These studies suggest that though high lactate concentration indicates poor prognosis in sepsis, metformin use may not increase lactate levels, which is proportional to disease severity or increase in mortality rate. Further studies on the effect of metformin on lactate are needed to clarify MALA incidence at therapeutic doses.

The effects of metformin on sepsis-induced organ failure

The biochemical events that occur in sepsis usually result in organ failure and death. Studies reported metformin induces beneficial effects against sepsis by interfering with inflammatory markers and other molecular processes, which are mainly mediated via AMPK activation. Metformin was reported to increase bacterial killing by enhancing neutrophil chemotaxis via AMPK activation. It promoted the chemotactic and bacterial killing ability of neutrophils in an LPS-induced model (53). This suggests that AMPK activation by metformin may prevent the influence of molecules released by microbes and their subsequent deleterious events. Some reported protective effects of metformin on sepsis-induced organ failure are presented in Table 1.

Table 1: Protective effects of metformin on sepsis

Organ	Model	Mechanism	References
Brain	CLP	Inhibition of oxidative stress and apoptosis, and increased BBB integrity.	(54)
Heart	LPS	Suppression of TLRs, and inhibition of MPO activity and inflammatory responses.	(55-58)
Lungs	LPS, CLP	Inhibition of inflammatory cytokines, activation of ATF-3, and enhance neutrophil chemotaxis, inhibition of neutrophil and macrophage infiltration, and suppression of TLR signaling.	(59-63)
Liver	LPS	Inhibition of pro-inflammatory cytokine production, decreased the expression of PAI-1 mRNA and PAI-1 protein, decreased MPO activity and tissue asymmetric dimethylarginine levels, and restored glutathione.	(64, 65)

CLP; Cecal ligation and puncture, LPS; Lipopolysaccharides, BBB; Blood brain barrier, TLR; Toll-like receptor, MPO; Myeloperoxidase, ATF; Activating transcription factor, and PAI-1; Plasminogen activator inhibitor type-1.

The brain

Metformin in different brain injury models could improve brain function and prevent injury. The effects of metformin on sepsis-induced brain injury were also reported; metformin could enhance blood brain barrier (BBB) integrity and attenuate brain injury (54). Metformin improved brain function by preventing brain injury through increased expression of specialized tight junction proteins (claudins), decreased oxidative stress markers, and attenuated apoptosis. Tight junction proteins regulate the passage of molecules across the BBB; thus, any alteration in their concentration will affect the permeability leading to increased brain injury (54, 66). More studies on involved mechanisms and pathways are needed.

The heart

In the heart, the consequence of sepsis is microcirculatory failure, right and left ventricular dysfunction, myocardial infarction, and many other forms of heart failure. Metformin exerts its cardioprotective effects via suppression of TLRs. It preserved left ventricular function by reducing myeloperoxidase (MPO) activity and TNF alpha (TNF- α) level, both in the serum and heart tissue. This effect was observed to be mediated via AMPK activation (55). Metformin also inhibited local immune response in the isolated rat heart through AMPK and TLRs pathways (56). Also, metformin could protect against myocardial dysfunction by increasing the expression of genes related to cardiac metabolism, enhancement of fatty acid oxidation and ATP synthesis, while decreasing glucose transport and inflammatory responses (57). Metformin protected against endotoxin-induced acute myocarditis by inhibiting pro-inflammatory cytokines, suppressing the expression of MPO, and decreasing creatine kinase myocardial band and brain natriuretic peptide (58).

The lungs

Metformin can reduce inflammation-induced endotoxemia via inhibition of TNF- α , interleukin

1 beta (IL-1 β), and HMGB1 release as well as suppression of MPO activity (59). Metformin was shown to decrease LPS-induced edema and lung permeability through AMPK activation (35). Its anti-inflammatory effects were reported to be mediated through activating transcription factor (ATF-3) (60). The anti-inflammatory effects of metformin via inhibition of TNF- α activity was studied in an *in vitro* equine whole blood assay (61). Through induction of AMPK pathway, metformin protected against sepsis and improved survival in diabetic mice by reducing lung permeability and decreasing the expression of pro-inflammatory cytokines (67). AMPK activation by metformin was shown to restore and increase the levels of ETC complexes, diminish accumulation of the immunosuppressive transcriptional factor alpha (HIF-1 α), reduce cells' tolerance to endotoxin challenge, and prevent the abnormal neutrophil movement caused by LPS (68). In the same study, metformin also improved innate immune ability to eliminate *Pseudomonas aeruginosa* and restore lung balance by inhibiting pro-inflammatory cytokines in bronchioalveolar lavage (BAL). In another study, metformin decreased cytokine production, BAL protein expression, and decreased lung edema in LPS-treated rats; also, neutrophil and macrophage infiltration and MPO activity were prevented, while AMPK- α 1 expression was promoted by metformin (62). Metformin decreased acute lung injury by suppressing TLR-4 signaling in LPS-treated rats (63). This effect was mediated via activation of AMPK which reduced LPS-induced expression of TLR4, levels of myeloid differentiation primary response protein 88 (MyD88), NF- κ B, and TNF α . It also up-regulated the p-AMPK α /AMPK α ratio by 22% and reduced the congestion and inflammatory cells infiltration into the alveolar walls. It also decreased MPO activity by 37%. Recently, the anti-inflammatory and anti-oxidative effects of metformin on sepsis-induced lung injury were reported (69).

The liver

Liver injury due to sepsis was shown to be induced via oxidative damage, inflammatory response, and neutrophil infiltration. Metformin decreased the expression of inflammatory biomarkers and thrombosis by reducing the expression of hepatic plasminogen activator inhibitor type-1 (PAI-1) mRNA and plasma PAI-1 protein, which was related to the inhibition of hepatic urokinase plasminogen activator activity and an increase in fibrin deposition in a rat model of endotoxic shock (64). Metformin prevented LPS-induced liver injury by reducing MPO activity and asymmetric dimethylarginine tissue level, as well as restoring the activity of antioxidants such as glutathione (65).

The kidney

Activation of the innate immune system can cause renal failure by stimulating the secretion of pro-inflammatory mediators which trigger the release of toxic oxygen radicals, protease, and cytokines, that in turn lead to increased vascular permeability, capillary leakage, and impaired oxygen extraction, with subsequent hypoperfusion and hypoxia (70).

The beneficial effects of metformin on sepsis-induced kidney injury were not reported. However, the importance of oxidative stress and inflammation in the pathophysiology of kidney injury/failure indicates the potential role of metformin in management of such conditions. The beneficial effects reported in other models may support this claim. Studies on the effect of metformin on sepsis-induced kidney injury are required.

Conclusion

Sepsis leads to multi-organ damage via inflammation and oxidative stress induced by production of pro-inflammatory cytokines and ROS. This happens through NF- κ B and other signaling pathways. Metformin, through AMPK activation, suppresses NF- κ B signaling which leads to inhibition of the production of pro-inflammatory cytokines especially IL-1 β , IL-6, and TNF- α , in different organs. Hence, metformin was shown to improve organ injury and mortality in sepsis via its action on these mediators. The major limitation of metformin therapy may be the induction of lactic acidosis (MALA) which may not be a matter of concern as its occurrence was only reported at high doses of metformin in the presence of other risk factors. Further experimental studies are required to ascertain the impact of metformin on sepsis-induced organ failure and its safety.

Acknowledgements

This is an in-house study that received no financial support. Authors wish to thank Tehran University of Medical Sciences and Iran National Science Foundation (INSF). Authors declare no conflict of interest.

Authors' Contribution

M.A., M.M.; Contributed to conception and design of

the study. F.I.H., T.D., F.K., K.N.; Contributed to drafting the manuscript which was revised by M.A. and M.M. All authors have read and approved the final manuscript.

References

1. Singer M, Deutschman CS, Seymour CW, Shankar-Hari M, Annane D, Bauer M, et al. The third international consensus definitions for sepsis and septic shock (Sepsis-3). *JAMA*. 2016; 315(8): 801-810.
2. Shankar-Hari M, Phillips GS, Levy ML, Seymour CW, Liu VX, Deutschman CS, et al. Developing a new definition and assessing new clinical criteria for septic shock: for the Third International Consensus Definitions for Sepsis and Septic Shock (Sepsis-3). *JAMA*. 2016; 315(8): 775-787.
3. Angus DC, Linde-Zwirble WT, Lidicker J, Clermont G, Carcillo J, Pinsky MR. Epidemiology of severe sepsis in the United States: analysis of incidence, outcome, and associated costs of care. *Crit Care Med*. 2001; 29(7): 1303-1310.
4. Bone RC, Balk RA, Cerra FB, Dellinger RP, Fein AM, Knaus WA, et al. Definitions for sepsis and organ failure and guidelines for the use of innovative therapies in sepsis. The ACCP/SCCM Consensus Conference Committee. American College of Chest Physicians/Society of Critical Care Medicine. *Chest*. 1992; 101(6): 1644-1655.
5. Esteghamati A, Eskandari D, Mirmiranpour H, Noshad S, Mousavizadeh M, Hedayati M, et al. Effects of metformin on markers of oxidative stress and antioxidant reserve in patients with newly diagnosed type 2 diabetes: a randomized clinical trial. *Clin Nutr*. 2013; 32(2): 179-185.
6. Batchuluun B, Sonoda N, Takayanagi R, Inoguchi T. The cardiovascular effects of metformin: conventional and new insights. *J Endocrinol Diabetes Obes*. 2014; 2(2): 1035.
7. Amini FG, Rafieian-Kopaei M, Nematbakhsh M, Baradaran A, Nasri H. Ameliorative effects of metformin on renal histologic and biochemical alterations of gentamicin-induced renal toxicity in Wistar rats. *J Res Med Sci*. 2012; 17(7): 621-625.
8. Wang DS, Kusuhara H, Kato Y, Jonker JW, Schinkel AH, Sugiyama Y. Involvement of organic cation transporter 1 in the lactic acidosis caused by metformin. *Mol Pharmacol*. 2003; 63(4): 844-848.
9. Gras V, Bouffandeau B, Montravers PH, Lalau JD. Effect of metformin on survival rate in experimental sepsis. *Diabetes Metab*. 2006; 32(2): 147-150.
10. Doenya-Barak K, Beberashvili I, Marcus R, Efrati S. Lactic acidosis and severe septic shock in metformin users: a cohort study. *Crit Care*. 2016; 20: 10.
11. Dellinger RP, Carlet JM, Masur H, Gerlach H, Calandra T, Cohen J, et al. Surviving Sepsis Campaign guidelines for management of severe sepsis and septic shock. *Crit Care Med*. 2004; 32(3): 858-873.
12. Castellheim A, Brekke OL, Espevik T, Harboe M, Mollnes TE. Innate immune responses to danger signals in systemic inflammatory response syndrome and sepsis. *Scand J Immunol*. 2009; 69(6): 479-491.
13. Bilevicius E, Dragosavac D, Dragosavac S, Araújo S, Falcão AL, Terzi RG. Multiple organ failure in septic patients. *Braz J Infect Dis*. 2001; 5(3): 103-110.
14. Holmes CL, Russell JA, Walley KR. Genetic polymorphisms in sepsis and septic shock: role in prognosis and potential for therapy. *Chest*. 2003; 124(3): 1103-1115.
15. Mannick JA, Rodrick ML, Lederer JA. The immunologic response to injury. *J Am Coll Surg*. 2001; 193(3): 237-244.
16. Wang JH, Doyle M, Manning BJ, Blankson S, Wu QD, Power C, et al. Cutting edge: bacterial lipoprotein induces endotoxin-independent tolerance to septic shock. *J Immunol*. 2003; 170(1): 14-18.
17. Power CP, Wang JH, Manning B, Kell MR, Aherne NJ, Wu QD, et al. Bacterial lipoprotein delays apoptosis in human neutrophils through inhibition of caspase-3 activity: regulatory roles for CD14 and TLR-2. *J Immunol*. 2004; 173(8): 5229-5237.
18. van der Poll T, Opal SM. Host-pathogen interactions in sepsis. *Lancet Infect Dis*. 2008; 8(1): 32-43.
19. Bone RC. Immunologic dissonance: a continuing evolution in our understanding of the systemic inflammatory response syndrome (SIRS) and the multiple organ dysfunction syndrome (MODS). *Ann Intern Med*. 1996; 125(8): 680-687.
20. Ward NS, Casserly B, Ayala A. The compensatory anti-inflammatory response syndrome (CARS) in critically ill patients. *Clin Chest Med*. 2008; 29(4): 617-625.
21. Opal SM, DePalo VA. Anti-inflammatory cytokines. *Chest*. 2000; 117(4): 1162-1172.

22. Santos RS, Silva PL, de Oliveira GP, Santos CL, Cruz FF, de Assis EF, et al. Oleanolic acid improves pulmonary morphofunctional parameters in experimental sepsis by modulating oxidative and apoptotic processes. *Respir Physiol Neurobiol.* 2013; 189(3): 484-490.
23. Torraco A, Carrozzo R, Piemonte F, Pastore A, Tozzi G, Verrigni D, et al. Effects of levosimendan on mitochondrial function in patients with septic shock: a randomized trial. *Biochimie.* 2014; 102: 166-173.
24. Krysztolik RJ, Bentley FR, Spain DA, Wilson MA, Garrison RN. Free radical scavenging by lazaroids improves renal blood flow during sepsis. *Surgery.* 1996; 120(4): 657-662.
25. Vary TC, Hazen SA, Maish G, Cooney RN. TNF binding protein prevents hyperlactatemia and inactivation of PDH complex in skeletal muscle during sepsis. *J Surg Res.* 1998; 80(1): 44-51.
26. Nguyen HB, Rivers EP, Knoblich BP, Jacobsen G, Muzzin A, Ressler JA, et al. Early lactate clearance is associated with improved outcome in severe sepsis and septic shock. *Crit Care Med.* 2004; 32(8): 1637-1642.
27. Tian HH, Han SS, Lv CJ, Wang T, Li Z, Hao D, et al. The effect of early goal lactate clearance rate on the outcome of septic shock patients with severe pneumonia. *Zhongguo Wei Zhong Bing Ji Jiu Yi Xue.* 2012; 24(1): 42-45.
28. Huang J, Liu K, Zhu S, Xie M, Kang R, Cao L, et al. AMPK regulates immunometabolism in sepsis. *Brain Behav Immun.* 2018; 72: 89-100.
29. Lin WC, Chen CW, Huang YW, Chao L, Chao J, Lin YS, et al. Kallistatin protects against sepsis-related acute lung injury via inhibiting inflammation and apoptosis. *Sci Rep.* 2015; 5: 12463.
30. Viollet B, Guigas B, Sanz Garcia N, Leclerc J, Foretz M, Andreelli F. Cellular and molecular mechanisms of metformin: an overview. *Clin Sci (Lond).* 2012; 122(6): 253-270.
31. Detaille D, Guigas B, Chauvin C, Batandier C, Fontaine E, Wiernsperger N, et al. Metformin prevents high-glucose-induced endothelial cell death through a mitochondrial permeability transition-dependent process. *Diabetes.* 2005; 54(7): 2179-2187.
32. Hinke SA, Martens GA, Cai Y, Finsi J, Heimberg H, Pipeleers D et al. Methyl succinate antagonises biguanide-induced AMPK-activation and death of pancreatic beta-cells through restoration of mitochondrial electron transfer. *Br J Pharmacol.* 2007; 150(8): 1031-1043.
33. El-Mir MY, Detaille D, Gloria R, Delgado-Esteban M, Guigas B, Attia S, et al. Neuroprotective role of antidiabetic drug metformin against apoptotic cell death in primary cortical neurons. *J Mol Neurosci.* 2008; 34(1): 77-87.
34. Griss T, Vincent EE, Egnatchik R, Chen J, Ma EH, Faubert B, et al. Metformin antagonizes cancer cell proliferation by suppressing mitochondrial-dependent biosynthesis. *PLoS Biol.* 2015; 13(12): e1002309.
35. Jian MY, Alexeyev MF, Wolkowicz PE, Zmijewski JW, Creighton JR. Metformin-stimulated AMPK- α 1 promotes microvascular repair in acute lung injury. *Am J Physiol Lung Cell Mol Physiol.* 2013; 305(11): L844-L855.
36. Cameron A, Forteath C, Beall C, Rena G. Anti-inflammatory effects of metformin and their relationship to the therapeutic action of the drug. *Endocrine Abstracts.* 2015; 38: P-229.
37. Wheaton WW, Weinberg SE, Hamanaka RB, Soberanes S, Sullivan LB, Anso E, et al. Metformin inhibits mitochondrial complex I of cancer cells to reduce tumorigenesis. *Elife.* 2014; 3: e02242.
38. Haugrud AB, Zhuang Y, Coppock JD, Miskimins WK. Dichloroacetate enhances apoptotic cell death via oxidative damage and attenuates lactate production in metformin-treated breast cancer cells. *Breast Cancer Res Treat.* 2014; 147(3): 539-550.
39. Kim J, Shon E, Kim CS, Kim JS. Renal podocyte injury in a rat model of type 2 diabetes is prevented by metformin. *Exp Diabetes Res.* 2012; 2012: 210821.
40. Taheri N, Azarmi Y, Neshat M, Garjani A, Doustar Y. Study the effects of metformin on renal function and structure after unilateral ischemia-reperfusion in rat. *Res Pharm Sci.* 2012; 7(5): S77.
41. Giugliano D, De Rosa N, Di Maro G, Marfella R, Acampora R, Buoninconti R, et al. Metformin improves glucose, lipid metabolism, and reduces blood pressure in hypertensive, obese women. *Diabetes Care.* 1993; 16(10): 1387-1390.
42. Velazquez EM, Mendoza S, Hamer T, Sosa F, Glueck CJ. Metformin therapy in polycystic ovary syndrome reduces hyperinsulinemia, insulin resistance, hyperandrogenemia, and systolic blood pressure, while facilitating normal menses and pregnancy. *Metabolism.* 1994; 43(5): 647-654.
43. Bhamra GS, Hausenloy DJ, Davidson SM, Carr RD, Paiva M, Wynne AM, et al. Metformin protects the ischemic heart by the Akt-mediated inhibition of mitochondrial permeability transition pore opening. *Basic Res Cardiol.* 2008; 103(3): 274-284.
44. Pintana H, Apaijai N, Pratchayasakul W, Chattipakorn N, Chattipakorn SC. Effects of metformin on learning and memory behaviors and brain mitochondrial functions in high fat diet induced insulin resistant rats. *Life Sci.* 2012; 91(11-12): 409-414.
45. Ansari G, Mojtahedzadeh M, Kajbaf F, Najafi A, Khajavi MR, Khalili H, et al. How does blood glucose control with metformin influence intensive insulin protocols? Evidence for involvement of oxidative stress and inflammatory cytokines. *Adv Ther.* 2008; 25(7): 681-702.
46. Mojtahedzadeh M, Rouini MR, Kajbaf F, Najafi A, Ansari G, Gholipour A, et al. Is there a role for metformin in the ICU? *Arch Med Sci.* 2008; 4(2): 174-181.
47. Mojtahedzadeh M, Rouini MR, Kajbaf F, Najafi A, Ansari G, Gholipour A, et al. Advantage of adjunct metformin and insulin therapy in the management of glycemia in critically ill patients. Evidence for nonoccurrence of lactic acidosis and needling to parenteral metformin. *Arch Med Sci.* 2008; 4(2): 174-181.
48. Jiang T, Yu JT, Zhu XC, Wang HF, Tan MS, Cao L, et al. Acute metformin preconditioning confers neuroprotection against focal cerebral ischaemia by pre-activation of AMPK-dependent autophagy. *Br J Pharmacol.* 2014; 171(13): 3146-3157.
49. Venna VR, Li J, Hammond MD, Mancini NS, McCullough LD. Chronic metformin treatment improves post-stroke angiogenesis and recovery after experimental stroke. *Eur J Neurosci.* 2014; 39(12): 2129-2138.
50. Wang DS, Kusuhara H, Kato Y, Jonker JW, Schinkel AH, Sugiyama Y. Involvement of organic cation transporter 1 in the lactic acidosis caused by metformin. *Mol Pharmacol.* 2003; 63(4): 844-848.
51. Green JP, Berger T, Garg N, Suarez A, Hagar Y, Radeos MS, et al. Impact of metformin use on the prognostic value of lactate in sepsis. *Am J Emerg Med.* 2012; 30(9): 1667-1673.
52. Park J, Hwang SY, Jo JJ, Jeon K, Suh GY, Lee TR, et al. Impact of metformin use on lactate kinetics in patients with severe sepsis and septic shock. *Shock.* 2017; 47(5): 582-587.
53. Park DW, Jiang S, Tadie JM, Stigler WS, Gao Y, Deshane J, et al. Activation of AMPK enhances neutrophil chemotaxis and bacterial killing. *Mol Med.* 2013; 19(1): 387-398.
54. Tang G, Yang H, Chen J, Shi M, Ge L, Ge X, et al. Metformin ameliorates sepsis-induced brain injury by inhibiting apoptosis, oxidative stress and neuroinflammation via the PI3K/Akt signaling pathway. *Oncotarget.* 2017; 8(58): 97977-97989.
55. Vaez H, Rameshrad M, Najafi M, Barar J, Barzegari A, Garjani A. Cardioprotective effect of metformin in lipopolysaccharide-induced sepsis via suppression of toll-like receptor 4 (TLR4) in heart. *Eur J Pharmacol.* 2016; 772: 115-123.
56. Vaez H, Najafi M, Rameshrad M, Toutouchi NS, Garjani M, Barar J, et al. AMPK activation by metformin inhibits local innate immune responses in the isolated rat heart by suppression of TLR 4-related pathway. *Int Immunopharmacol.* 2016; 40: 501-507.
57. Tzanavari T, Varela A, Theocharis S, Ninou E, Kapelouzou A, Cokinos DV, et al. Metformin protects against infection-induced myocardial dysfunction. *Metabolism.* 2016; 65(10): 1447-1458.
58. Liu G, Wu K, Zhang L, Dai J, Huang W, Lin L, et al. Metformin attenuated endotoxin-induced acute myocarditis via activating AMPK. *Int Immunopharmacol.* 2017; 47: 166-172.
59. Tsoyi K, Jang HJ, Nizamutdinova IT, Kim YM, Lee YS, Kim HJ, et al. Metformin inhibits HMGB1 release in LPS-treated RAW 264.7 cells and increases survival rate of endotoxaemic mice. *Br J Pharmacol.* 2011; 162(7): 1498-1508.
60. Kim J, Kwak HJ, Cha JY, Jeong YS, Rhee SD, Kim KR et al. Metformin suppresses lipopolysaccharide (LPS)-induced inflammatory response in murine macrophages via activating transcription factor-3 (ATF-3) induction. *J Biol Chem.* 2014; 289(33): 23246-23255.
61. Bauquier JR, Tudor E, Bailey SR. Anti-inflammatory effects of four potential anti-endotoxaemic drugs assessed in vitro using equine whole blood assays. *J Vet Pharmacol Ther.* 2015; 38(3): 290-296.
62. Zhang X, Shang F, Hui L, Zang K, Sun G. The alleviative effects of metformin for lipopolysaccharide-induced acute lung injury rat model and its underlying mechanism. *Saudi Pharm J.* 2017; 25(4): 666-670.
63. Vaez H, Najafi M, Toutouchi NS, Barar J, Barzegari A, Garjani A. Metformin alleviates lipopolysaccharide-induced acute lung injury through suppressing toll-like receptor 4 signaling. *Iran J Allergy Asthma Immunol.* 2016; 15(6): 498-507.
64. Bergheim I, Luyendyk JP, Steele C, Russell GK, Guo L, Roth RA, et al. Metformin prevents endotoxin-induced liver injury after partial hepatectomy. *J Pharmacol Exp Ther.* 2006; 316(3): 1053-1061.

65. Bal F, Bekpinar S, Unlucerci Y, Kusku-Kiraz Z, Önder S, Uysal M, et al. Antidiabetic drug metformin is effective on the metabolism of asymmetric dimethylarginine in experimental liver injury. *Diabetes Res Clin Pract.* 2014; 106(2): 295-302.
 66. Chiba H, Osanai M, Murata M, Kojima T, Sawada N. Transmembrane proteins of tight junctions. *Biochim Biophys Acta.* 2008; 1778(3): 588-600.
 67. Yang Y, Dong R, Hu D, Chen Z, Fu M, Wang DW, et al. Liver kinase B1/AMP-activated protein kinase pathway activation attenuated the progression of endotoxemia in the diabetic mice. *Cell Physiol Biochem.* 2017; 42(2): 761-779.
 68. Liu Z, Bone N, Jiang S, Park DW, Tadie JM, Deshane J, et al. AMP-activated protein kinase and Glycogen Synthase Kinase 3 β modulate the severity of sepsis-induced lung injury. *Mol Med.* 2015; 21(1): 937-950.
 69. Ghavimi H, Sheidaei S, Vaez H, Zolali E, Asgharian P, Hamishehkar H. Metformin-attenuated sepsis-induced oxidative damages: a novel role for metformin. *Iran J Basic Med Sci.* 2018; 21(5): 469-475.
 70. De Vriese AS. Prevention and treatment of acute renal failure in sepsis. *J Am Soc Nephrol.* 2003; 14(3): 792-805.
-

The Synergistic Effect of Glucagon-Like Peptide-1 and Chamomile Oil on Differentiation of Mesenchymal Stem Cells into Insulin-Producing Cells

Saeid Saghahazrati, Ph.D.¹, Seyed Abdulmajid Ayatollahi, Ph.D.^{1,2,3*}, Farzad Kobarfard, Ph.D.⁴,
Bagher Minaei Zang, Ph.D.^{5*}

1. Phytochemistry Research Center, Shahid Beheshti University of Medical Sciences, Tehran, Iran

2. Department of Chemistry, Richardson College for The Environmental Science Complex, The University of Winnipeg, Winnipeg, Canada

3. Department of Pharmacognosy, School of Pharmacy, Shahid Beheshti University of Medical Sciences, Tehran, Iran

4. Department of Medicinal Chemistry, Shahid Beheshti School of Pharmacy, Tehran, Iran

5. Department of Histology, Faculty of Medicine, Tehran University of Medical Sciences, Tehran, Iran

*Corresponding Addresses: P.O.Box: 141556163, Phytochemistry Research Center, Shahid Beheshti University of Medical Sciences, Tehran, Iran
P.O.Box: 1417613151, Department of Histology, Faculty of Medicine, Tehran University of Medical Sciences, Tehran, Iran
Emails: majid_ayatollahi@yahoo.com, minaezb@tums.ac.ir

Received: 27/August/2018, Accepted: 17/November/2018

Abstract

Objective: Glucagon-like peptide-1 (GLP-1) has attracted tremendous attention for treatment of diabetes. Likewise, it seems that active ingredients of chamomile oil might have anti-diabetic effects. This work was conducted to investigate the effects of the combination of GLP-1 and chamomile oil on differentiation of mesenchymal stem cells (MSCs) into functional insulin-producing cells (IPCs).

Materials and Methods: In this experimental study, adipose MSCs derived from the adult male New Zealand white rabbits were assigned into four groups: control (without any treatment); GLP-1 (in which cells were treated with 10 nM GLP-1 every other day for 5 days); chamomile oil (in which cells were treated with 100 µg/ml *Matricaria chamomilla* L. flower oil every other day for 5 days); and GLP-1+ chamomile oil (in which cells were treated with 10 nM GLP-1 and 100 µg/ml *M. chamomilla* flower oil every other day for 5 days). Characterization of isolated MSCs was performed using flow cytometry, Alizarin red S staining and Oil red O staining. The expressions of genes specific for IPCs were measured using reverse transcriptase-polymerase chain reaction (RT-PCR) assay. Measurement of insulin and the cleaved connecting peptide (C-peptide) in response to different concentrations of glucose, were performed using ELISA kits.

Results: Our results demonstrated that isolated cells highly expressed MSC markers and were able to differentiate into osteocytes and adipocytes. Additionally, using GLP-1 in combination with chamomile oil exhibited higher levels of IPCs gene markers including NK homeobox gene 2.2 (*NKX-2.2*), paired box gene 4 (*PAX4*), insulin (*INS*) and pancreatic duodenal homeobox-1 (*PDX1*) as well as insulin and C-peptide secretion in response to different glucose concentrations compared to GLP-1 or chamomile oil alone ($P < 0.05$).

Conclusion: Collectively, these findings establish a substantial foundation for using peptides in combination with natural products to obtain higher efficiency in regenerative medicine and peptide therapy.

Keywords: Chamomile Oil, Differentiation, Glucagon-Like Peptide-1, Insulin-Producing Cells, Mesenchymal Stem Cell

Cell Journal (Yakhteh), Vol 21, No 4, January-March (Winter) 2020, Pages: 371-378

Citation: Saghahazrati S, Ayatollahi SAM, Kobarfard F, Minaei Zang D. The synergistic effect of glucagon-like peptide-1 and chamomile oil on differentiation of mesenchymal stem cells into insulin-producing cells. Cell J. 2020; 21(4): 371-378. doi: 10.22074/cellj.2020.6325.

Introduction

Type 1 diabetes mellitus (T1DM) is an autoimmune disease that is responsible for about 5-10% of all cases of diabetes around the world (1). During T1DM, initiation of chronic inflammatory responses gives rise to apoptotic and necrotic death of pancreatic β -cells, and absolute insulin deficiency which, in turn, results in serious short-term and long-term side effects (2). It is urgent to discover new therapeutic options for treatment of T1DM and other degenerative diseases considering their high rate of morbidity and mortality (3-6). In recent years, stem cell-based therapy has been regarded as a promising strategy to treat immune-mediated diseases such as T1DM (7). Unique properties of mesenchymal stem cells

(MSCs) including modulation of immune response, differentiation plasticity, easy attainability, and ability for inhibition of key factors involved in initiation of autoimmune disorders, make them excellent candidates to treat T1DM (8, 9). Although MSCs have demonstrated safety and efficacy in treatment of immune-mediated diseases such as T1DM, several drawbacks such as differentiation into undesired cells and migration to other body organs might limit their clinical applications (10).

Glucagon-like peptide-1 (GLP-1) is an incretin hormone and food intake acts as a potent stimulator of its secretion by intestinal cells. GLP-1 plays an important role in a large number of physiological processes such as modulation of gastric emptying, blood glucose

level, insulin secretion, glucose metabolism and appetite (11). Some previous studies have shown that GLP-1 might promote the growth and differentiation of β -cells. For example, Abraham et al. (12) reported that GLP-1 contributed to the differentiation of nestin-positive islet-derived progenitor cells, present in the ducts and islet of the pancreas, into insulin-producing cells (IPCs). They concluded that GLP-1 exerted this function through alterations of gene expression profile. In fact, GLP-1 increased the expression of *PDX-1* and insulin promoter factor (*IPF-1*) gene. Moreover, previous reports have shown that natural products may exert therapeutic effects by targeting different cellular signaling pathways (13-15). Likewise, it is well-documented that natural products can enhance proliferation and differentiation of stem cells into desired cells (16). Chamomile (*Matricaria chamomilla* L.) is one of the well-documented medicinal herbs that belong to the Asteraceae (Compositae) family. Antioxidant and therapeutic properties of chamomile are due to the presence of terpenoids and flavonoids in its flowers (17). Some previous studies have shown that active ingredients of chamomile such as coumarins, quercetin, apigenin, and luteolin can reduce diabetes risk factors (18, 19). According to the aforementioned researches, we examined possible synergistic effects of GLP-1 and *M. chamomilla* L. oil on differentiation of MSCs into IPCs and their potential mechanisms.

Methods and Materials

Reagents

GLP-1, Collagenase type I, and *Matricaria chamomilla* L. flower oil were purchased from Sigma (Sigma-Aldrich Chemical, USA). Dulbecco's modification of Eagle medium (DMEM/F12) and fetal bovine serum (FBS) were obtained from Gibco Company (USA). Rabbit Insulin ELISA Kit was purchased from Crystal Chem. Company (Crystal Chem. Inc., Downers Grove, IL). cDNA Synthesis Kit was supplied by EURx Company (Gdańsk, Poland). SYBR® Premix Ex Taq™ II (TliRNaseH Plus, RR820Q) was purchased from Takara company (Japan). Rabbit C-peptide ELISA Kit was purchased from Mybiosource Company.

Animals

In this experimental study, male New Zealand white rabbits with a mean weight of 2.5 kg, were obtained from Razi Institute, Iran. All procedures and experimental tests were approved by the Animal Ethics Committee of Shahid Beheshti University of Medical Sciences (reference No. 1392. 49270). Rabbits were maintained in a temperature-controlled chamber set at $25 \pm 1^\circ\text{C}$, with 12/12-hour light/dark cycles. They were fed with standard pellet chow and water ad libitum. After surgery and isolation of cells, the animals were permitted to recover spontaneous breathing and placed

in their cage with free access to food and water.

Isolation of adipose-derived mesenchymal stem cells

Rabbits were anesthetized intraperitoneally (IP) using ketamine (40 mg/kg) and xylazine (5 mg/kg). A midline incision was made in abdominal region. Approximately, 100 ml of adipose tissue was dissected from the perivisceral area. The adipose tissue was divided into small pieces in cold phosphate-buffered saline (PBS, Biochrom, Germany, pH=7.4). Then, small pieces of adipose tissue were homogenized and centrifuged at 175 g for 5 minutes. After removing supernatant, pellet was digested using 0.1% collagenase type I at 37°C under continuous shaking for 60 minutes. Then, the cell suspension was centrifuged at 175 g for 5 minutes. The supernatant was removed, and pellets were resuspended in an appropriate volume of the DMEM (Gibco, USA) supplemented with 10% FBS, and 1% penicillin-streptomycin and incubated at 37°C in a humid incubator with 5% CO_2 to acquire enough cell density.

Identification of mesenchymal stem cells

To determine cell surface antigen profile of MSCs, fluorescence-activated cell sorting (FACS) was performed. In brief, after trypsinizing and washing with cold PBS containing 1% fetal calf serum (FCS), cells were incubated for 30 minutes with 10 $\mu\text{g}/\text{ml}$ antibodies in PBS per 1×10^6 cells at 25°C in the dark. Antibodies applied in this work included CD45-FITC, CD34-FITC, CD105-PE and CD73-PE (Dako, Denmark). To determine nonspecific fluorescence, cells were incubated with the isotype-matched antibody. A flow cytometer (Partec Pas III, Germany) was used to quantify the results.

Evaluation of osteogenic and adipogenic differentiation

To evaluate adipogenic differentiation, Oil red O staining was performed. MSCs were incubated in a medium including 100 $\mu\text{g}/\text{ml}$ 3-isobutyl-1-methylxanthine, 10 $\mu\text{g}/\text{ml}$ insulin, 10^{-6} M dexamethasone, 50 μM indomethacin in alpha-MEM medium supplemented with 10% FBS, for 3 weeks. To determine osteogenic differentiation, cells were incubated with a medium including 10 mM glycerophosphate disodium, 10^{-7} M dexamethasone, 50 $\mu\text{g}/\text{ml}$ ascorbic acid in alpha-MEM medium supplemented with 10% FBS, for 4 weeks. Alizarin red S staining was used to observe calcium deposits.

Study design

MSCs were cultured at a density of 1.5×10^6 cells/mL in alpha-MEM medium supplemented with 10% FBS containing 20 ng/ml of basic fibroblast growth factor (bFGF) and epidermal growth factor (EGF).

Cells were randomly divided into the following four groups of 12 flasks in each. For control groups, cells did not receive any treatment (control). GLP-1 group only received 10 nM GLP-1 every other day for 5 days. Chamomile oil group only was treated with 100 µg/ml *Matricaria chamomilla* flower oil every other day for 5 days. GLP-1+chamomile oil group was treated with 10 nM GLP-1+100 µg/ml *M. chamomilla* L. flower oil every other day for 5 days.

Reverse transcription polymerase chain reaction

Qiagen RNeasy kit (Qiagen Company, Valencia, CA, USA) was used to extract total RNA from 1×10^6 differentiated cells following the manufacturer's instructions. RNA concentration was determined using NanoDrop Microvolume Spectrophotometer and stored at -80°C . Then, total RNA was converted into cDNA following the manufacturer's protocol using a Dart cDNA kit. Quantitative polymerase chain reaction (PCR) was carried out using SYBR® Premix Ex Taq™ II on a Rotor-Gene Q 5plex System (30-40 cycles). *β-actin* was used as the internal control. The expression levels of each target gene was normalized against the internal control expression using $2^{-\Delta\Delta C_t}$ method. Reverse transcription-PCR (RT-PCR) primer pairs are shown in Table 1.

Assessment of insulin/C-peptide release

To evaluate C-peptide release, we used Rabbit C-Peptide ELISA Kit. Measurement of insulin levels in culture media was performed using rabbit insulin ELISA kit. First, cells were pre-incubated with Krebs-Ringer buffer at 37°C for 2 hours. Then, cells were incubated with Krebs-Ringer buffer containing different doses of glucose (0, 15, and 30 mM) at 37°C

for 1 hour. Finally, culture media was collected and assessments were performed.

Statistical analysis

All the data were presented as mean \pm SD. GraphPad Prism software version 5.0 (CA, USA) was employed to analyze data. Values were subjected to a one-way analysis of variance (ANOVA) followed by Tukey multiple comparison tests. $P < 0.05$ was accepted to be statistically significant.

Results

Characterization of mesenchymal stem cells

Three days after initial plating, we found that MSCs possess fibroblast-like morphology. Fourteen days after the initial plating, a confluent monolayer of MSCs was formed. Flowcytometric analysis demonstrated that CD105 (MSC marker) was expressed in 95.76% of cultured MSCs. Additionally, CD73 (MSC marker) was expressed in 96.86% of MSCs.

The hematopoietic progenitor marker CD34 (expressed in 0.04% of MSCs) and the pan-leukocyte marker CD45 (expressed in 0.02% of MSCs) did not indicate significant expression levels (Fig.1).

Osteogenic and adipogenic differentiation

Oil red O staining demonstrated that isolated MSCs have the ability to differentiate into adipocytes (Fig.2A). Alizarin red S staining showed the ability of the isolated MSCs for mineralization and formation of calcium deposits. These findings confirmed that isolated MSCs are able differentiate into osteocytes (Fig.2B).

Table 1: Primer sequences for reverse transcription polymerase chain reaction (RT-PCR) analysis

Gene	Primer sequence (5'-3')	Accession number	Sequence detected (bp)
<i>NKX-2.2</i>	F: GGGGTTTTTCAGTCAAGGACA	XM_002710941.3	246
	R: AGTCCGTGCAGGGAGTATTG		
<i>PAX4</i>	F: GGGCTCTTTGTGAATGGCCG	XM_008258399.1	108
	R: TACCTTAAGGCTCCGGGAGAT		
<i>INS</i>	F: TCCTGCCCCTGCTGGC	NM_001082335.1	312
	R: AGTTGCAGTAGTTCTCCAG		
<i>PDX1</i>	F: AAAGCTCACGCGTGGAAAGG	XM_008275214.2	175
	R: TCAACATGACAGCCAGCTCCA		
<i>β-actin</i>	F: AAGATGACCCAGATCATGT	NM_001101683.1	188
	R: AGGTCCAGACGCAGGATG		

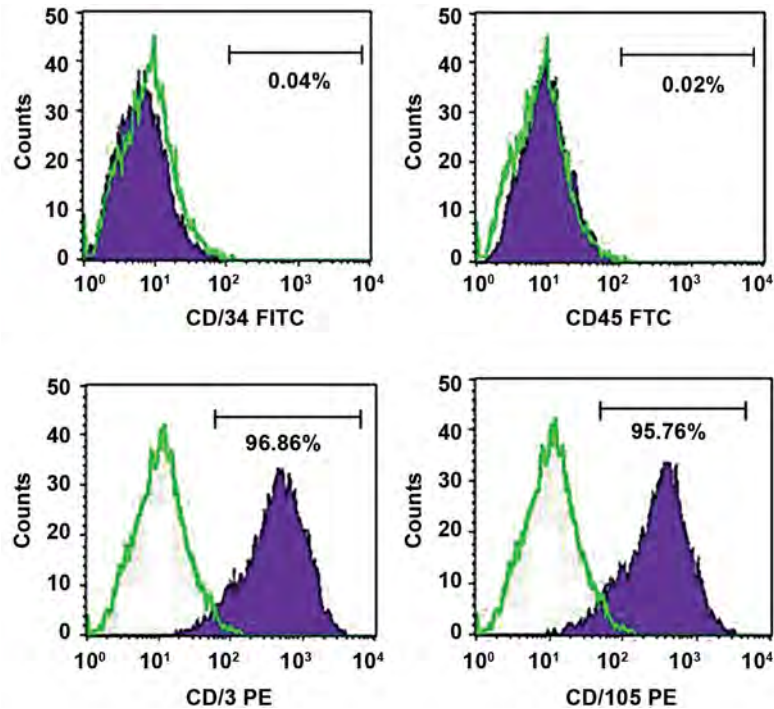


Fig.1: Immunophenotypic characterization of adipose-derived cells. The expressions of mesenchymal stem cell (MSC) markers such as CD73-PE and CD 105 PE, were higher than those of the hematopoietic progenitor marker CD34 and the pan-leukocyte marker CD45.

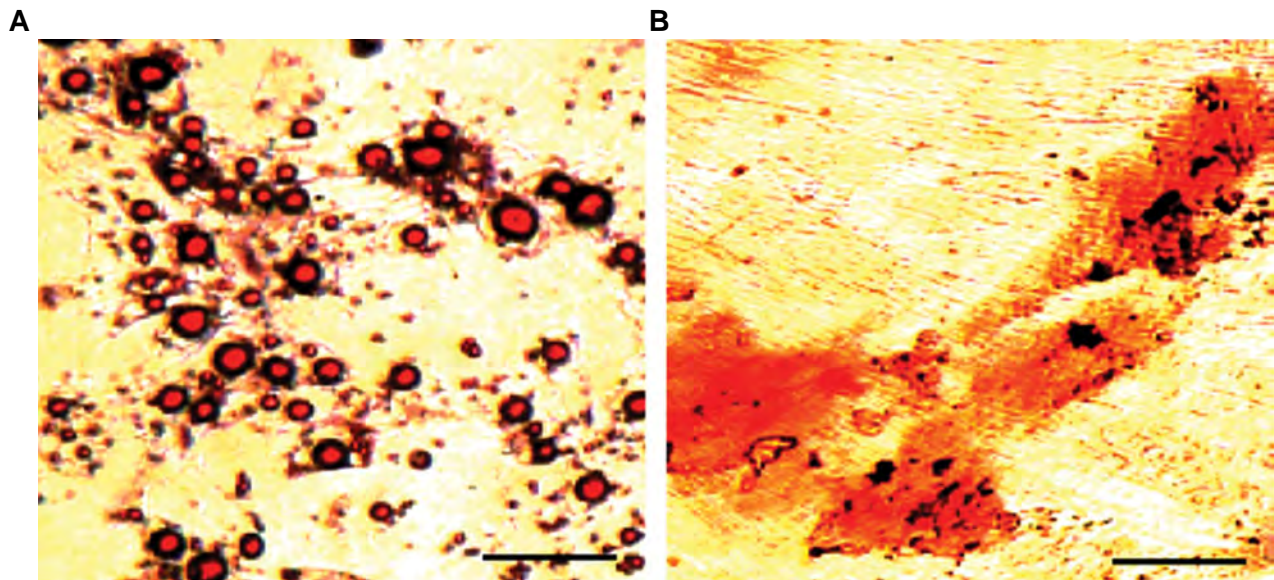


Fig.2: Evaluation of differentiation ability of mesenchymal stem cells (MSCs). **A.** Oil red O staining confirmed post-differentiation lipid accumulation in cultured cells and **B.** Alizarin red S staining showed mineralization and formation of calcium deposits in MSCs (scale bar: 100 μ m).

The effects of GLP-1 and chamomile oil on morphology of cultured MSCs

The cells treated with GLP-1 and chamomile oil exhibited changes in their morphology. These cells were more flattened compared with control after 5 days, suggesting their differentiation into IPCs (Fig.3A).

The effects of GLP-1 and chamomile oil on differentiation of MSCs into IPCs

To confirm differentiation of cells treated with GLP-

1 and chamomile oil into IPCs, we measured mRNA levels of *NKX-2.2*, *PAX4*, *INS* and *PDX1* using RT-PCR assay. Our results demonstrated that although cells treated with GLP-1 and cells treated with chamomile oil significant expressed *NKX-2.2*, *PAX4*, *INS* and *PDX1*, the expression of these IPCs markers was higher in cells treated with GLP-1+chamomile oil group (Fig.3B-E).

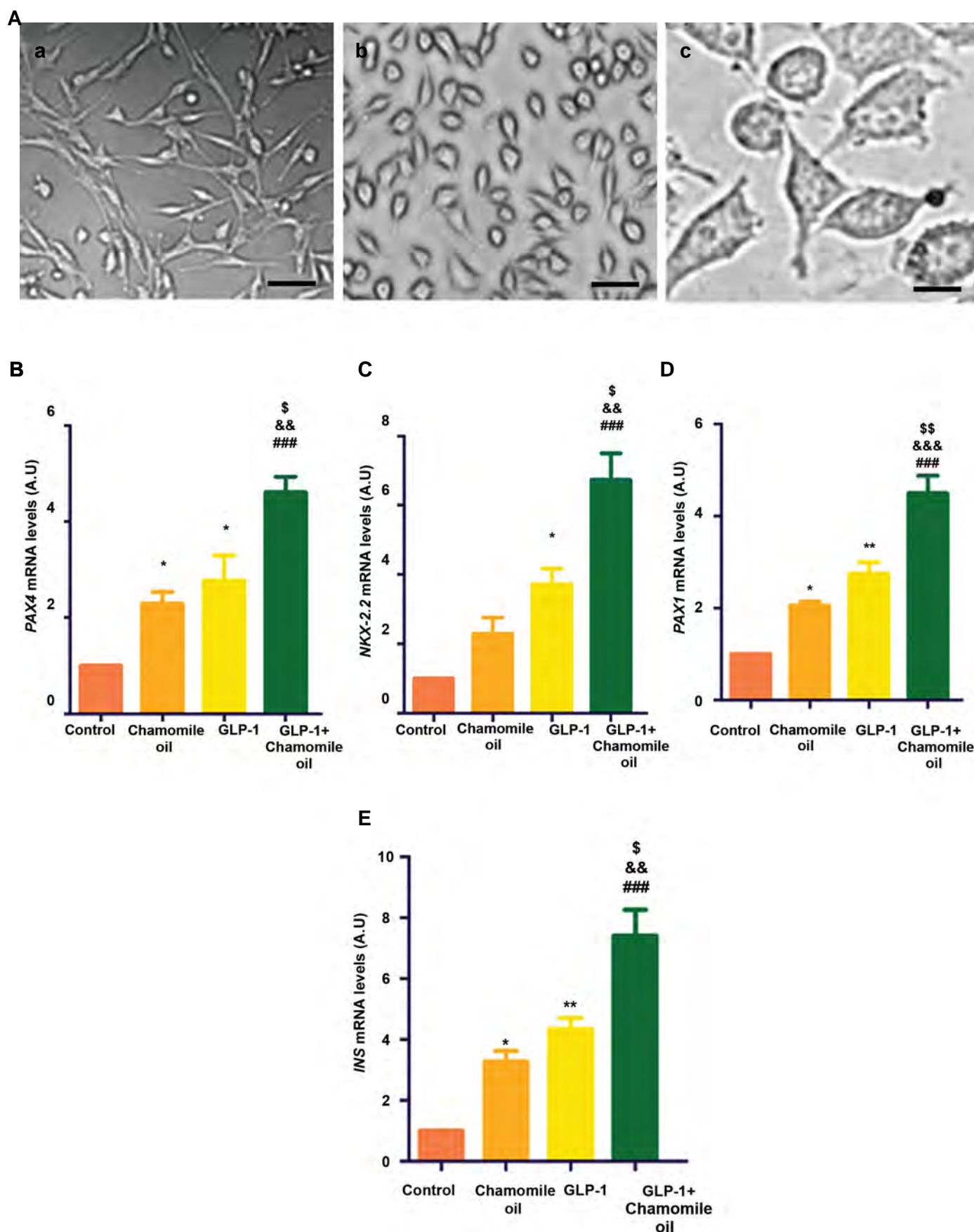


Fig.3: The effects of GLP-1+chamomile oil on cell morphology and gene markers of IPCs. **A.** The effects of GLP-1+chamomile oil on morphology of cells after 5 days. a. Control (scale bar: 100 μ m), b and c. Presentation of cells treated with GLP-1+chamomile oil for 5 days at low and high magnifications (scale bars: 100 μ m and 20 μ m, respectively). The effects of GLP-1+chamomile oil on the expression of gene markers of insulin-secreting cells including: **B.** *PAX4*, **C.** *NKX-2.2*, **D.** *PDX1*, and **E.** *INS*. GLP-1; Glucagon-like peptide-1, IPCs; Insulin-producing cells, *; $P < 0.05$, **; $P < 0.01$ versus control, ###; $P < 0.001$ versus the control, &&; $P < 0.01$, &&&; $P < 0.001$ versus chamomile oil, \$; $P < 0.05$, and \$\$; $P < 0.01$ versus GLP-1.

The effects of GLP-1 and chamomile oil on the cleaved C-peptide levels in culture media

To evaluate the function of treated cells, we measured C-peptide secretion by cells in response to different concentrations of glucose. As shown in Figure 4A, no significant differences were found among different groups in the absence of glucose (0 mM). Significant differences were observed in response to 15 and 30 mM concentrations of glucose. GLP-1+ chamomile oil group exhibited higher C-peptide secretion than cells treated either with chamomile oil alone or GLP-1 alone.

The effects of GLP-1 and chamomile oil on insulin levels in culture media

There were no significant differences among different groups in the absence of glucose (0 mM). Compared with other groups, GLP-1+chamomile oil showed the highest insulin secretion in response to 15 and 30 mM concentrations of glucose (Fig.4B).

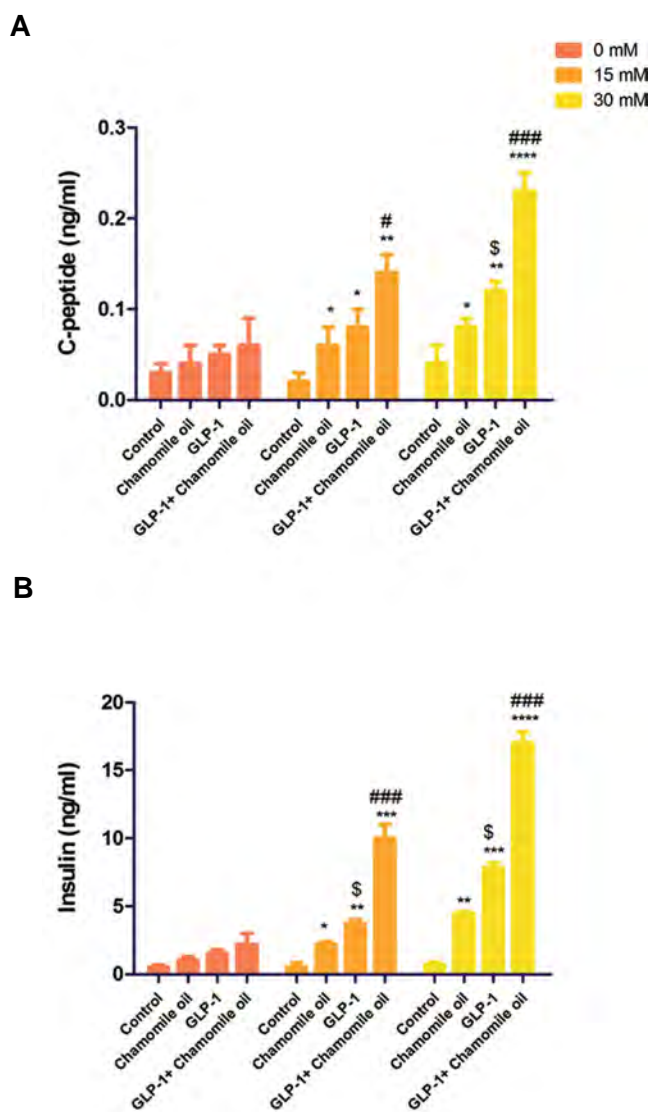


Fig.4: The effects of GLP-1 and chamomile oil on C-peptide and insulin levels in culture media. **A.** C-peptide level and **B.** Insulin level in culture media. GLP-1; Glucagon-like peptide-1, *, P<0.05, **, P<0.01, ***, P<0.001, ****, P<0.0001 versus control, \$, P<0.05 versus chamomile oil, #, P<0.05, and ###, P<0.001 versus chamomile oil or GLP-1 alone.

Discussion

In this work, we demonstrated that using peptide therapy and natural products together can produce synergistic effects on differentiation of MSCs into IPCs. In recent years, GLP-1, a peptide produced by dipeptidyl peptidase-4 (DPP4) cleavage of the gut incretin hormone, has attracted tremendous attention from scientific community for T1DM therapy because it can act as a growth factor to increase mass expansion of β -cells and subsequently, insulin secretion. In fact, it is well known that this peptide promotes survival and proliferation of β -cells (20). However, some recent studies have shown that GLP-1 facilitated the formation of new mature β -cells (neogenesis) in the adult pancreases (21). Moreover, many previous reports have demonstrated that chamomile oil possesses many active ingredients that act as anti-diabetic, antioxidant, anti-inflammatory and antibacterial agents (22-24). For example, luteolin, a bioactive compound present in chamomile oil, increases insulin secretion and activates adipokines/cytokines in adipocytes through induction of the peroxisome proliferator-activated receptor- γ (PPAR γ) pathway (25, 26).

In this study, we investigated the synergistic effect of GLP-1 and chamomile oil on differentiation of MSCs into insulin-secreting cells. The isolated MSCs exhibited an increased expression of MSCs markers, whereas they did not demonstrate a significant expression of the hematopoietic progenitor and pan-leukocyte markers. These findings confirmed a highly purified MSC population. In agreement with the results of the present study, Razavi Tousi et al. (27) reported that the isolated MSCs strongly expressed MSCs marker CD105, but not CD 45 and CD34. On the other hand, isolated cells were able to differentiate into osteocytes and adipocytes. In agreement with this study, a previous report showed that the isolated MSCs can be differentiated into osteocytes and adipocytes (28). Furthermore, a previous study indicated that addition of GLP-1 to the culture media of mouse embryonic stem cells, contributed to differentiation into IPCs (29).

To examine the synergistic effects of GLP-1 and chamomile oil, we measured mRNA levels of *PAX4* and *NKX-2.2*. The activity of homeodomain protein *NKX-2.2* and the NK-family members is necessary for differentiation and the maturation of β -cells. It seems that *NKX-2.2* contributes to differentiation of β -cells through interaction with *PAX4*. Loss of *PAX4* results in downregulation of *INS*, *PDX1* and *HB9* in β -cell precursors (30). Our findings showed that using peptide and chamomile oil significantly increased mRNA levels of *PAX4* and *NKX-2.2* compared to control, GLP-1 group only and chamomile oil only treated groups. Recent studies have shown that expression of *PDX1* is necessary for maintaining β -cell identity and function via suppression of α -cell program (31). To examine whether GLP-1 and chamomile oil can contribute to formation of β -cells and maintain their function, we also measured

mRNA levels of *PDX1* and *INS*. Our findings showed that although both peptide and chamomile oil administered alone, increased the mRNA levels of *PDX1* and *INS* in cultured cells, the effects of their co-administration was higher than single treatments. Consistent with the present study, increased mRNA levels of *NKX-2.2*, *PAX4*, *PDX1*, *INS* were found after differentiation of human embryonic stem cells (hESCs) into IPCs during a seven-stage protocol (32). The cleaved C-peptide is a byproduct and a hallmark of average daily insulin production. To form mature insulin hormone, a single-chain proinsulin peptide is translated and then converted into C-peptide and disulfide-linked insulin (33). It has been reported that C-peptide secretion of IPCs derived from hESCs in response to 15 mM glucose was about 0.15 ng/ml after 33 days (34). Compared with this report, the present study showed that C-peptide secretion of MSCs treated with chamomile oil+GLP-1 in response to 15 mM glucose was about 0.15 ng/ml after 5 days. Likewise, differentiated cells exhibited higher insulin secretion in response to higher concentrations of glucose. Other studies also indicated that IPCs derived from embryonic stem cells displayed higher insulin secretion in response to higher concentrations of glucose (35). Additionally, the highest insulin levels in culture media were found in chamomile oil+GLP-1 group. The cells treated with peptide and chamomile oil exhibited more flattened morphology. Consistent with our study, Abraham et al. (12) reported that differentiation of human pancreatic islet-derived progenitor cells into IPCs in the presence of GLP-1 resulted in more flattened morphology. Also, this research group reported that insulin concentration in media was about 2.4 ng/ml after treatment of nestin-positive islet-derived progenitor cells (NIPs) with 10 nM GLP-1 for 7 days. Consistently, the present study demonstrated that insulin concentration in media of cells treated with 10 nM GLP-1 alone in the absence of glucose, was about 2.5 ng/ml, whereas it was increased to 4-7 ng/ml in response to 15 and 30 mM glucose.

Conclusion

Collectively, our finding demonstrated that chamomile oil in combination with GLP-1 more efficiently enhances the differentiation of adipose-derived MSCs into IPCs. These findings establish a substantial foundation for using peptides in combination with natural products to obtain higher efficiencies in regenerative medicine.

Acknowledgements

This study was financially supported by a research grant from Phytochemistry Research Center of Shahid Beheshti University of Medical Sciences. The authors declare no conflict of interest.

Authors' Contributions

S.A.A., B.M.Z.; Contributed to conception and design, and were responsible for overall supervision. S.S., F.K.; Contributed to all experimental work, data and statistical

analysis, and interpretation of data. S.A.A.; Drafted the manuscript, which was revised by S.S. All authors read and approved the final manuscript.

References

- Daneman D. Type 1 diabetes. *The Lancet*. 2006; 367(9513): 847-858.
- Shehata AM, Quintanilla-Fend L, Bettio S, Singh CB, Ammon HP. Prevention of multiple low-dose streptozotocin (MLD-STZ) diabetes in mice by an extract from gum resin of *Boswellia serrata* (BE). *Phytomedicine*. 2011; 18(12): 1037-1044.
- Rodriguez-Calvo T, Atkinson M, von Herrath M. β -Cell mass versus function in type 1 diabetes mellitus: truth or dare? *Nat Rev Endocrinol*. 2017; 13(9): 1.
- Amani H, Habibey R, Hajmiresmail SJ, Latifi S, Pazoki-Toroudi H, Akhavan O. Antioxidant nanomaterials in advanced diagnoses and treatments of ischemia reperfusion injuries. *J Mater Chem B*. 2017; 5(48): 9452-9476.
- Pazoki-Toroudi H, Nilforoushzadeh MA, Ajami M, Jaffary F, Aboutaleb N, Nassiri-Kashani M, et al. Combination of azelaic acid 5% and clindamycin 2% for the treatment of acne vulgaris. *Cutan Ocul Toxicol*. 2011; 30(4): 286-291.
- Firooz A, Bouzari N, Mojtahed F, Pazoki-Toroudi H, Nassiri-Kashani M, Davoudi M, et al. Topical immunotherapy with diphenecyprone in the treatment of extensive and/or long-lasting alopecia areata. *J Eur Acad Dermatol Venerol*. 2005; 19(3): 393-394.
- Abdi R, Fiorina P, Adra CN, Atkinson M, Sayegh MH. Immunomodulation by mesenchymal stem cells: a potential therapeutic strategy for type 1 diabetes. *Diabetes*. 2008; 57(7): 1759-1767.
- Vija L, Farge D, Gautier JF, Vexiau P, Dumitrache C, Bourgarit A, et al. Mesenchymal stem cells: Stem cell therapy perspectives for type 1 diabetes. *Diabetes Metab*. 2009; 35(2): 85-93.
- Amani H, Mostafavi E, Arzaghi H, Davaran S, Akbarzadeh A, Akhavan O, et al. Three-dimensional graphene foams: synthesis, properties, biocompatibility, biodegradability, and applications in tissue engineering. *ACS Biomater Sci Eng*. 2019; 5(1): 193-214.
- Jiang Q, Yu T, Huang K, Zhang H, Zheng Z, Hu S. Systemic redistribution of the intramyocardially injected mesenchymal stem cells by repeated remote ischaemic post-conditioning. *J Cell Mol Med*. 2018; 22(1): 417-428.
- Lee YS, Jun HS. Anti-diabetic actions of glucagon-like peptide-1 on pancreatic beta-cells. *Metabolism*. 2014; 63(1): 9-19.
- Abraham EJ, Leech CA, Lin JC, Zulewski H, Habener JF. Insulinotropic hormone glucagon-like peptide-1 differentiation of human pancreatic islet-derived progenitor cells into insulin-producing cells. *Endocrinology*. 2002; 143(8): 3152-3161.
- Pazoki-Toroudi H, Amani H, Ajami M, Nabavi SF, Braidy N, Kasi PD, et al. Targeting mTOR signaling by polyphenols: a new therapeutic target for ageing. *Ageing Res Rev*. 2016; 31: 55-66.
- Ajami M, Pazoki-Toroudi H, Amani H, Nabavi SF, Braidy N, Vacca RA, et al. Therapeutic role of sirtuins in neurodegenerative disease and their modulation by polyphenols. *Neurosci Biobehav Rev*. 2017; 73: 39-47.
- Ajami M, Davoodi SH, Habibey R, Namazi N, Soleimani M, Pazoki-Toroudi H, et al. Effect of DHA+ EPA on oxidative stress and apoptosis induced by ischemia-reperfusion in rat kidneys. *Fundam Clin Pharmacol*. 2013; 27(6): 593-602.
- Shin DW, Kim SN, Lee SM, Lee W, Song MJ, Park SM, et al. (-)-Catechin promotes adipocyte differentiation in human bone marrow mesenchymal stem cells through PPAR gamma transactivation. *Biochem Pharmacol*. 2009; 77(1): 125-133.
- Srivastava JK, Shankar E, Gupta S. Chamomile: a herbal medicine of the past with a bright future. *Mol Med Rep*. 2010; 3(6): 895-901.
- Zemestani M, Rafrat M, Asghari-Jafarabadi M. Chamomile tea improves glycemic indices and antioxidants status in patients with type 2 diabetes mellitus. *Nutrition*. 2016; 32(1): 66-72.
- Kato A, Minoshima Y, Yamamoto J, Adachi I, Watson AA, Nash RJ. Protective effects of dietary chamomile tea on diabetic complications. *J Agric Food Chem*. 2008; 56(17): 8206-8211.
- Drucker DJ. Glucagon-like peptide-1 and the islet beta-cell: augmentation of cell proliferation and inhibition of apoptosis. *Endocrinology*. 2003; 144(12): 5145-5148.
- Dadheech N, Buteau J. Glucagon-like peptide-1 treatment stimulates Neurogenin3 expression and pancreatic beta-cell neogenesis in adult mice. *FASEB J*. 2017; 31(1 Supplement): 883.14.
- Rafrat M, Zemestani M, Asghari-Jafarabadi M. Effectiveness of chamomile tea on glycemic control and serum lipid profile in pa-

- tients with type 2 diabetes. *J Endocrinol Invest.* 2015; 38(2): 163-170.
23. Khan SS, Najam R, Anser H, Riaz B, Alam N. Chamomile tea: herbal hypoglycemic alternative for conventional medicine. *Pak J Pharm Sci.* 2014; 27(5 Spec no): 1509-1514.
 24. Stanojevic LP, Marjanovic-Balaban ZR, Kalaba VD, Stanojevic JS, Cvetkovic DJ. Chemical composition, antioxidant and antimicrobial activity of chamomile flowers essential oil (*Matricaria chamomilla* L.). *Journal of Essential Oil Bearing Plants.* 2016; 19(8): 2017-2028.
 25. Ding L, Jin D, Chen X. Luteolin enhances insulin sensitivity via activation of PPAR γ transcriptional activity in adipocytes. *J Nutr Biochem.* 2010; 21(10): 941-947.
 26. Amani H, Ajami M, Nasser Maleki S, Pazoki-Toroudi H, Daglia M, Tsetegho Sokeng AJ, et al. Targeting signal transducers and activators of transcription (STAT) in human cancer by dietary polyphenolic antioxidants. *Biochimie.* 2017; 142: 63-79.
 27. Razavi Tousi SM, Faghihi M, Nobakht M, Molazem M, Kalantari E, Darbandi Azar A, et al. Improvement of heart failure by human amniotic mesenchymal stromal cell transplantation in rats. *J Tehran Heart Cent.* 2016; 11(3): 123-138.
 28. Li L, Zhang Y, Li Y, Yu B, Xu Y, Zhao S, et al. Mesenchymal stem cell transplantation attenuates cardiac fibrosis associated with isoproterenol-induced global heart failure. *Transpl Int.* 2008; 21(12): 1181-1189.
 29. Bai L, Meredith G, Tuch BE. Glucagon-like peptide-1 enhances production of insulin in insulin-producing cells derived from mouse embryonic stem cells. *J Endocrinol.* 2005; 186(2): 343-352.
 30. Wang J, Elghazi L, Parker SE, Kizilocak H, Asano M, Sussel L, et al. The concerted activities of Pax4 and Nkx2. 2 are essential to initiate pancreatic β -cell differentiation. *Dev Biol.* 2004; 266(1): 178-189.
 31. Gao T, McKenna B, Li C, Reichert M, Nguyen J, Singh T, et al. Pdx1 maintains β cell identity and function by repressing an α cell program. *Cell Metab.* 2014; 19(2): 259-271.
 32. Rezaia A, Bruin JE, Arora P, Rubin A, Batushansky I, Asadi A, et al. Reversal of diabetes with insulin-producing cells derived in vitro from human pluripotent stem cells. *Nat Biotechnol.* 2014; 32(11): 1121-1133.
 33. Zhu X, Orci L, Carroll R, Norrbom C, Ravazzola M, Steiner DF. Severe block in processing of proinsulin to insulin accompanied by elevation of des-64, 65 proinsulin intermediates in islets of mice lacking prohormone convertase 1/3. *Proc Natl Acad Sci USA.* 2002; 99(16): 10299-10304.
 34. Bruin JE, Erener S, Vela J, Hu X, Johnson JD, Kurata HT, et al. Characterization of polyhormonal insulin-producing cells derived in vitro from human embryonic stem cells. *Stem Cell Res.* 2014; 12(1): 194-208.
 35. Lumelsky N, Blondel O, Laeng P, Velasco I, Ravin R, McKay R. Differentiation of embryonic stem cells to insulin-secreting structures similar to pancreatic islets. *Science.* 2001; 292(5520): 1389-1394.
-

Incorporation of Silver Sulfadiazine into An Electrospun Composite of Polycaprolactone as An Antibacterial Scaffold for Wound Healing in Rats

Fereshteh Nejaddehbashi, M.Sc.¹, Mahmoud Hashemitabar, Ph.D.^{1,2}, Vahid Bayati, Ph.D.^{1,2}, Eskandar Moghimipour, Ph.D.^{1,3}, Jabraeel Movaffagh, Ph.D.⁴, Mahmoud Orazizadeh, Ph.D.^{1,2*}, Mohammadreza Abbaspour, Ph.D.^{4*}

1. Cellular and Molecular Research Center, Ahvaz Jundishapur University of Medical Sciences, Ahvaz, Iran

2. Department of Anatomical Sciences, School of Medicine, Ahvaz Jundishapur University of Medical Sciences, Ahvaz, Iran

3. Nanotechnology Research Center, Faculty of Pharmacy, Ahvaz Jundishapur University of Medical Sciences, Ahvaz, Iran

4. Targeted Drug Delivery Research Center, Pharmaceutical Technology Institute, Mashhad University of Medical Sciences, Mashhad, Iran

*Corresponding Addresses: P.O.Box: 45, Cellular and Molecular Research Center, Ahvaz Jundishapur University of Medical Sciences, Ahvaz, Iran
P.O.Box: 91775-1365, Targeted Drug Delivery Research Center, Pharmaceutical Technology Institute, Mashhad University of Medical Sciences, Mashhad, Iran

Emails: orazizadehm@gmail.com, abbaspourmr@mums.ac.ir

Received: 2/September/2018, Accepted: 2/December/2018

Abstract

Objective: Fabrication of an antibiotic-loaded scaffold with controlled release properties for wound dressing is one of tissue engineering challenges. The aim of this study was to evaluate the wound-healing effectiveness of 500- μ m thick polycaprolactone (PCL) nanofibrous mat containing silver sulfadiazine (SSD) as an antibacterial agent.

Materials and Methods: In this experimental study, an electrospun membrane of PCL nanofibrous mat containing 0.3% weight SSD with 500 μ m thickness, was prepared. Morphological and thermomechanical characteristics of nanofibers were evaluated. Drug content and drug release properties as well as the surface hydrophobicity of the nanofibrous membrane were determined. Antimicrobial properties and cellular viability of the scaffold were also examined. A full thickness wound of 400 mm² was created in rats, to evaluate the wound-healing effects of PCL/SSD blend in comparison with PCL and vaseline gas used as the control group.

Results: SSD at a concentration of 0.3% improved physicochemical properties of PCL. This concentration of SSD did not inhibit the attachment of human dermal fibroblasts (HDFs) to nanofibers *in vitro*, but showed antibacterial activity against Gram-positive *Staphylococcus aureus* (ST) and Gram-negative *Pseudomonas aeruginosa* (PS). Overall, results showed that SSD improves characteristics of PCL nanofibrous film and improves wound-healing process in one-week earlier compared to control.

Conclusion: Cytotoxicity of SSD in fabricated nanofibrous mat is a critical challenge in designing an effective wound dressing that neutralizes cellular toxicity and improves antimicrobial activity. The PCL/SSD nanofibrous membrane with 500- μ m thickness and 0.3% (w/v) SSD showed applicable characteristics as a wound dressing and it accelerated wound healing process *in vivo*.

Keywords: Nanofibers, Polycaprolactone, Silver Sulfadiazine, Tissue Engineering, Wound Healing

Cell Journal (Yakhteh), Vol 21, No 4, January-March (Winter) 2020, Pages: 379-390

Citation: Nejaddehbashi F, Hashemitabar M, Bayati V, Moghimipour E, Movaffagh J, Orazizadeh M, Abbaspour MR. Incorporation of silver sulfadiazine into an electrospun composite of polycaprolactone as an antibacterial scaffold for wound healing in rats. Cell J. 2020; 21(4): 379-390. doi: 10.22074/cellj.2020.6341.

Introduction

The skin structure and function is often damaged by several factors such as chronic wounds, diabetic foot ulcers, surgical incisions, ruptures and burns. This unique tissue following exposure to these external threats, shows different reactions depending on the severity of the injury and the size of injured area (1). When over 1 cm of the skin is lost, skin grafting is necessary for avoiding bacterial infections, water and blood losses and extensive scar formation.

As commonly used clinical approaches, autologous, allogenic and xenogeneic skin grafts have limitations such as availability of donor sites, risk of immune rejection and transmission of disease, respectively. Therefore, researchers are looking for ways to overcome these limitations. Various skin substitutes are used in the clinic, but none of them can restore the structure and function of the skin alone (2).

Several studies have focused on tissue engineering methods using different types of biomaterials and electrospinning techniques (3, 4).

The important aim in this field is finding an ideal candidate for wound dressing. An acceptable biomaterial should present a panel of biomimetic characteristics such as extra cellular matrix (ECM) manifestations, biocompatibility, sustained release of drugs and reagents, very low cytotoxicity, wettability, biomechanical integrity, optimal biodegradability and anti-bacterial potency (5, 6). Polycaprolactone (PCL) is used in a broad spectrum of tissue engineering applications (7) and showed unique properties making it a good candidate for skin tissue engineering or wound dressing. The main advantage of PCL is its proper mechanical and handling characteristics, while the main drawback of PCL is its hydrophobicity that impedes the process of wound healing (8). To overcome this problem, and prepare a hydrophilic environment

with antibacterial properties, silver sulfadiazine (SSD) as a hydrophilic antibacterial agent was added to PCL and a nanofibrous mat composed of PCL/SSD was fabricated (9).

SSD as a wide spectrum antibacterial and antifungal agent was used in formulation of burn ointments for several decades. It was shown that in addition to the anti-infective effects of SSD against a wide range of Gram-positive and negative bacteria, it promotes epithelialization and decreases inflammation and contraction of wound area (10, 11). However, the impact of incorporating SSD into nanofibrous mat, and its wound-healing properties have not been clarified yet.

The aim of this study, at the first step, was to prepare and evaluate the efficiency of a cell-seeded nanofibrous mat of PCL comprising 0.3% w/v SSD. Then, a 400-mm² wound was created in rats and fully covered by 500- μ m thick PCL/SSD mats and the effectiveness of mats was evaluated.

Materials and Methods

Study design

In this experimental study, SSD was incorporated into the PCL solution at the concentration of 0.3% and nanofibrous membrane of 500- μ m thickness was produced using electrospinning technique. Then, main characteristics of the scaffold for transplantation in rats skin were evaluated. The rats were divided into the following 3 groups: rats treated with vaseline gas used as control group, rats treated with PCL/SSD, and rats treated PCL without SSD.

Materials

Poly (ϵ - caprolactone Mw of 80KDa) (PCL), 3-(4,5-dimethylthiazol-2-yl)-2,5-diphenyltetrazolium bromide (MTT) (M2128), dialysis bag (12 KDa), triphenyltetrazolium chloride (T8877), Muller Hinton agar, and Muller Hinton broth (70192) were purchased from Sigma-Aldrich (USA). Acetic acid (purity 99.8%) was acquired from Merck (Germany). Fetal bovine serum (FBS), phosphate buffered saline (PBS), DMEM'F12, Trypsin, and penicillin/streptomycin (pen/strep) were purchased from Gibco (USA), and SSD was acquired from Sinadaru (Iran).

Methods

Preparation and characterization of polymeric solutions and nanofibers

The PCL pellets were dissolved in 90% acetic acid to produce 15% w/v polymer solutions; then, 3 mg/ml SSD was dissolved in the solution. The solutions were mixed using a magnetic stirrer overnight.

In order to evaluate the influence of SSD on the rheological characteristics of PCL, the relative viscosity of the composite was assessed using Rheometer R/S plus Brookfield (Waukesha County, USA) at 20°C.

The electrospinning of the composite was performed at 17 kV, flow rate 0.5 ml/hour, nozzle to collector distance 17 cm and drum rotation speed 125 rpm.

Characterization of electrospun nanofibers was done under a field-emission microscope (Mira3Tescan, Czech), and prior to the examination, the samples were sputter coated with a thin layer of gold. Moreover, the SSD-loaded nanofibers were also characterized by energy-dispersive X-ray spectroscopy (EDX) (VEGA TESCAN, XMU, USA) to prove the presence of SSD in the nanofibers.

Physicochemical characterization

Differential scanning calorimetry

Differential scanning calorimetry (DSC) was carried out using STAR^e system (Mettler Toledo, Swiss). Then, 2 mg of the samples was heated in sealed aluminum pans under nitrogen flow (50 ml/minute) at a scanning rate of 10°C/minute from 25 to 300°C.

Thermogravimetric analysis

To evaluate the thermal behavior of the samples, thermogravimetric analysis (TGA) was analyzed from room temperature to 600°C at heating rate 10°C/minute (STA503, Germany) under N₂ flow. All the experiments were carried out in triplicate and the mean was reported.

Mechanical test

Tensile test was performed to evaluate mechanical characteristics of the mats. The scaffolds were cut in rectangular shapes (2×5 cm). Then, the film thickness was measured by thickness gauge and the tensile test was performed using a universal tensile machine (INSTRON 5967 USA) fitted with a 60 N load cell at 2 mm/minute speed until the samples were ruptured.

Fourier transform infrared spectroscopy

FTIR was performed to confirm presence or distribution of material in nanofibrous mat. The procedure was performed for PCL and SSD powders by mixing 50 mg samples with KBr and compressing to form pellets. The pellets were inserted into the FTIR spectrometer (Vertex 70 Bruker, Germany) connected to a PC and 30 scans with a resolution of 20 cm⁻¹ were performed. For nanofibers, a sheet of nanofibers was detected and the data was analyzed using FTIR software.

Contact angle analysis

Water contact angles of PCL/SSD and PCL nanofibrous membranes were measured by a water contact angle analyzer (FTA-125, First Ten Angstroms, USA). Samples (2×2 cm) were cut and placed on the testing plate; distilled water drops (3 μ l) were used in all analyses.

Drug release studies

To determine the drug release rate, PCL/SSD nanofibrous

mat (average weight 30 mg) was placed in the dialysis bag (cutoff 12,000 Da) with 5 ml PBS, immersed in 25 ml PBS (PH=7.4) in a 50-ml centrifuge tube and incubated at 37°C in a continuous horizontal shaker. At predetermined time-points, 2 ml of dissolution medium was retrieved and replenished with 2 ml of fresh PBS. Drug release profile was determined using UV absorption spectrophotometer (Shimadzu model uv-1700, USA) at 241 nm.

Determination of PCL/SSD nanofibers degradation rate

PCL/SSD matrices degradation rate evaluation was carried out in PBS (pH=7.2, at 37°C) in a shaking incubator for 7 days. Dry weight of matrices was measured on incubation days 1 and 17. Degradation was determined according to the following equation where w_0 is initial weight, w is weight of matrix after degradation and w_1 is degradation rate percentage.

$$w_1(\%) = \left[\frac{w_0 - w}{w_0} \right] \times 100$$

Antibacterial test

The minimum inhibitory concentration (MIC) of SSD on *Staphylococcus aureus* (ST) (ATCC29213) and *Pseudomonas aeruginosa* (PS) (ATCC27853) was briefly determined by using an antibiotic tube dilution method in supplemented Muller-Hinton Broth (12). The antibacterial properties of the PCL/SSD nanofibrous mat against ST (ATCC29213) and PS (ATCC27853) were briefly evaluated by zone inhibition test (13).

Isolation of human dermal fibroblasts

Human skin specimens were obtained by plastic surgery (2×2 cm) from healthy individuals in compliance with a protocol approved by Ethics Committee of Ahvaz Jundishapur University of Medical Sciences (1394/657). The skin samples were kept in culture medium on the ice during transportation. The culture medium was composed of DMEM containing 0.5 µg/ml amphotericin B, 100 IU/ml gentamycin, 100 IU/ml penicillin and 100 µg/ml streptomycin. The procedure of cell isolation was commenced as soon as possible in cell culture room of Cellular and Molecular Research Center (CMRC, Ahvaz Jundishapur University of Medical Sciences, Iran). The samples were sterilized in 70% ethanol for 10 seconds and rinsed 3 times with sterile PBS. The whole hypodermal adipose tissue and blood vessels were removed and discarded and cells were isolated according to a previously explained method (14).

Cytotoxicity and cell adhesion studies

For cytotoxicity studies, nanofibrous mats were punched and put onto 96-well culture plates. Human dermal fibroblasts (HDFs) were seeded at 5×10^3 cells per well on

both PCL/SSD, and PCL nanofibrous mat. MTT assays were performed on days 1, 3, 6, and 9 using a microplate reader (Bio-Rad 680, USA) at 570 nm.

The cell adhesion studies on the PCL/SSD nanofibers were carried out using HDFs after 24 hours. Electrospun nanofibrous mats were sterilized by 1-hour UV radiation done prior to cell studies. Cells were added to each nanofibrous mat at a seeding density of 10^4 cells/cm mat. After 24 hours, the fibers were washed thrice with PBS, then fixed using 2.5% glutaraldehyde for 1 hour at 4°C, dehydrated by graded ethanol and allowed to air-dry overnight. The dried samples were imaged using field emission-scanning electron microscope (FE-SEM).

In vivo evaluation

Creation of full thickness wound

Fifty-four male Sprague-Dawley rats (250 g) were housed under standard conditions at controlled temperature ($21 \pm 2^\circ\text{C}$) with 12/12 hour light/dark cycles. All protocols were done according to the Ethics Committee of Ahvaz Jundishapur University of Medical Sciences (1394/657). Animals were anesthetized by 40 mg/kg ketamine and 5 mg/kg xylazine; then, dorsal surface was shaved by an electric hair clipper and sterilized using 10% povidone-iodine. A full thickness square wound (400 mm²) was cut with a scissor from the back along the dorsal side of the skin of each rat. The scaffolds were affixed using 5-0 nylon sutures. One wound was created on each rat and 18 rats were used in each group but some of them were lost during anesthesia. The following three groups were used in this study: control group treated with vaseline gas (n=12), PCL/SSD-treated group (n=12) and PCL nanofibrous mats-treated group (n=12). Considering the mean thickness of nanofibrous mat, approximately 500-µm thick scaffolds were applied. On days 14, 21, and 28, animals were euthanized, and the process of wound closure was observed by using a digital camera, and then the surrounding skin and muscle including wound area were removed, fixed in formalin and embedded in paraffin.

Histological analysis

The reconstituted wound region of all groups was removed to the level of hypoderm layer. The specimens were fixed in 10% formaldehyde. Samples were cut into 2-µm thick sections by a rotating microtome for histological studies and for evaluation of wound area and repairing process. Hematoxylin and eosin (H&E) and Masson's trichrome staining were performed.

Statistical analysis

The statistical analysis was performed using the SPSS for windows, version 16 (SPSS Inc., IL, USA). The difference in means of the continuous data was evaluated using one-way analysis of variance (ANOVA) followed by Tukey post hoc analysis. All experimental data were presented as mean \pm SEM. Each experiment was repeated at least 3 times. A $P < 0.05$ was considered statistically significant.

Results

Solutions and nanofibers characterization

The viscosity (η) of PCL solutions in the presence and absence of SSD, at different shear rates (SR), are shown in Figure 1A. Compared to 15% wt PCL alone, the viscosity of composite of 15% PCL and 0.3% weight/volume SSD was slightly increased. The viscosity of both solutions decreased due to increase in SR, which indicated a non-Newtonian type of fluid. For both PCL and PCL/SSD, SR were in the range of 40-120 second^{-1} , while the viscosity was in a range of 180-184 pa.s for PCL and 181-186 pa.s for PCL/SSD. Thus SSD increased viscosity of the composite, but did not affect the integrity of nanofibers.

FE-SEM images of electrospun PCL and PCL/SSD mats showed uniform and beadless nanofibers (Fig. 1B, C). Mean diameter for PCL and PCL/SSD was 116.82 and 218.62 nm, respectively. Therefore, SSD incorporated uniformly in solution and nanofibrous mat.

EDX evaluations are shown in Figure 1D and E and the peak of Ag shown in the Figure 1E confirmed the presence of SSD in PCL nanofibrous mat. Elementary analysis of nanofibers was carried out by using SEM-EDX (Fig. 1D). Carbon and oxygen as the main elements presented in the PCL nanofibers, and also that of silver as a marker of SSD agent, were detected (Fig. 1E).

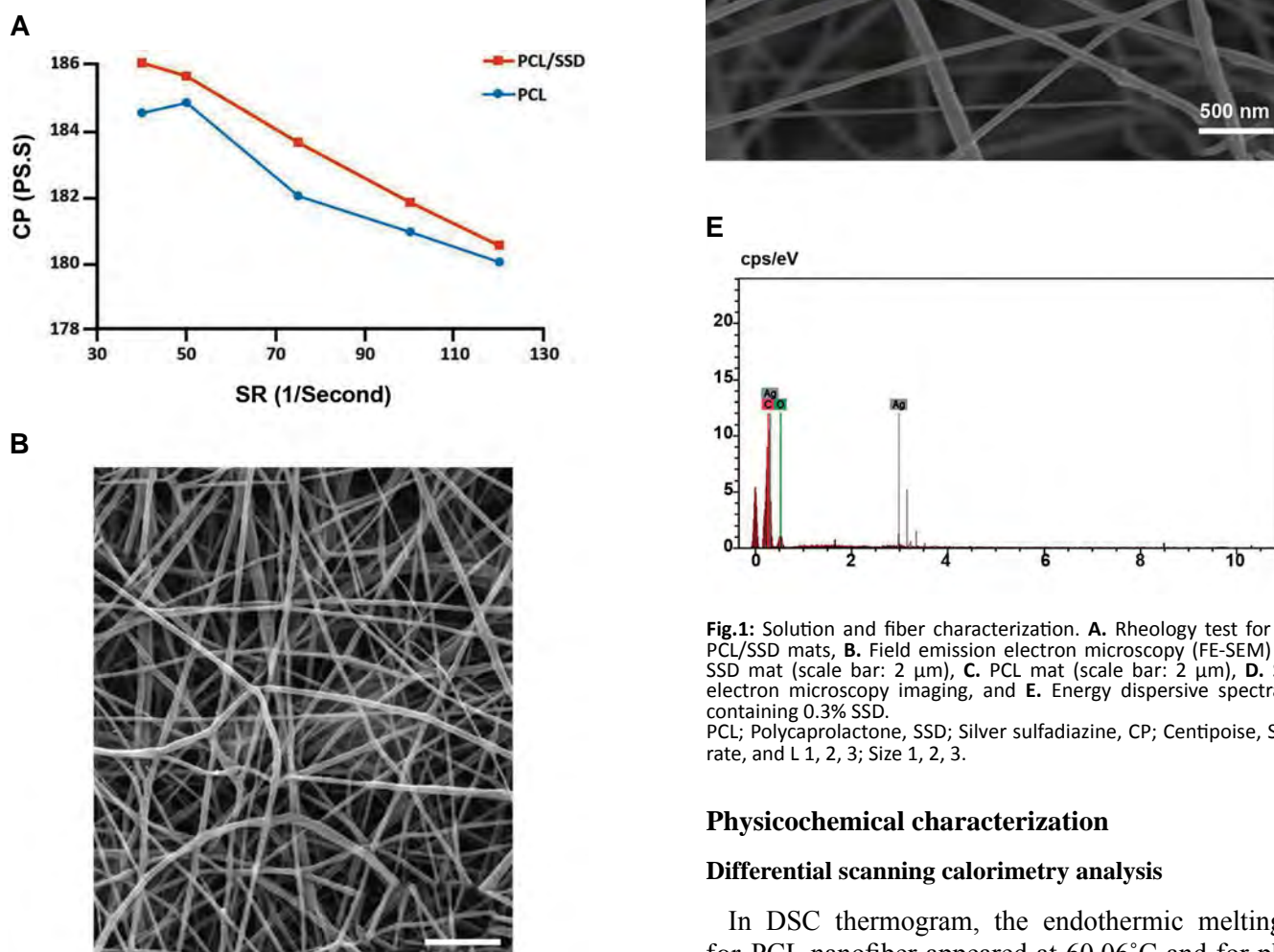


Fig.1: Solution and fiber characterization. **A.** Rheology test for PCL and PCL/SSD mats, **B.** Field emission electron microscopy (FE-SEM) for PCL/SSD mat (scale bar: 2 μm), **C.** PCL mat (scale bar: 2 μm), **D.** Scanning electron microscopy imaging, and **E.** Energy dispersive spectra of PCL containing 0.3% SSD.

PCL; Polycaprolactone, SSD; Silver sulfadiazine, CP; Centipoise, SR; Shear rate, and L 1, 2, 3; Size 1, 2, 3.

Physicochemical characterization

Differential scanning calorimetry analysis

In DSC thermogram, the endothermic melting peak for PCL nanofiber appeared at 60.06 $^{\circ}\text{C}$ and for physical

mixture of PCL and SSD was 60°C, while for PCL/SSD nanofibrous mat was 56.6°C. This shift in melting point from 60 to 56.6°C could be attributed to the interaction between drug and polymer during electrospinning process and changes in their physical structure Figure 2A.

Thermogravimetric analysis

TGA curves of PCL, SSD and PCL/SSD nanofiber are presented in Figure 2B. The initial decomposition temperature for PCL was around 300°C, for SSD was 288.7°C, and for PCL/SSD was around 300°C.

Tensile test

The Young's modulus of PCL and PCL/SSD nanofibrous membranes were 1.3 and 0.65 MPa, respectively (Fig.2C). These results were in the range of elastic modulus in normal human skin (i.e. 0.2-20 MPa) indicating acceptable mechanical strength and elasticity for both nanofibrous mats (15).

Fourier Transform Infrared spectroscopy analysis

FTIR spectrum for SSD, PCL and PCL/SSD nanofibrous mats are shown in Figure 3A. FTIR spectrum of the PCL exhibited characteristic peaks at 2945.91 cm⁻¹ (-CH₂, asymmetric and stretching), 2870.75 cm⁻¹ (-CH₂, symmetric stretching) and 1729.26 cm⁻¹ (-C=O, stretching). The chemical structure of the PCL/SSD nanofibrous mats was evaluated by FTIR to examine chemical interactions between the PCL and SSD, as shown in Figure 3A. Moreover, PCL/SSD nanofibrous mats showed additional bands at approximately 1045.95, and 727.84 cm⁻¹, which are representative of various vibration modes of N-C, N-O bonds. The broad peak observed at 3500 cm⁻¹ might be due to the hydrogen bond interaction between PCL and SSD.

Contact angle test

Contact angle of nanofibers was 97 ± 2° and 56 ± 2° for PCL and PCL/SSD nanofibers, respectively Figure 3B, C. These measurements showed that incorporation of SSD into PCL nanofibers leads to higher hydrophilic surface of the nanofibrous membrane.

Drug release and antibacterial effects

The cumulative release profile of SSD from the nanofibrous mat is shown in Figure 4A. The profile exhibits an almost fast release of the drug (up to 60%) in 4 days followed by a sustained release of 80% drug during 20 days. It was shown that PCL could modulate the release profile of anti-infection reagent (12). Antibacterial properties of scaffold were assessed against *Staphylococcus aureus* (ST, ATCC 29213) and *Pseudomonas aeruginosa* (PS, ATCC 27853) using inhibition zone measurements. Clear inhibition areas around the samples containing SSD affirm their antibacterial properties (Fig.4B, C). Considering the MIC for *Pseudomonas aeruginosa* (15 µg/ml) and *Staphylococcus aureus* (30 µg/ml), it can be concluded that the concentration of drug released over a period of

20 days, was above the MIC of the microorganisms. Moreover, the release of 50% drug within the first 3 days has merits for fast effectiveness of the nanofibrous mats.

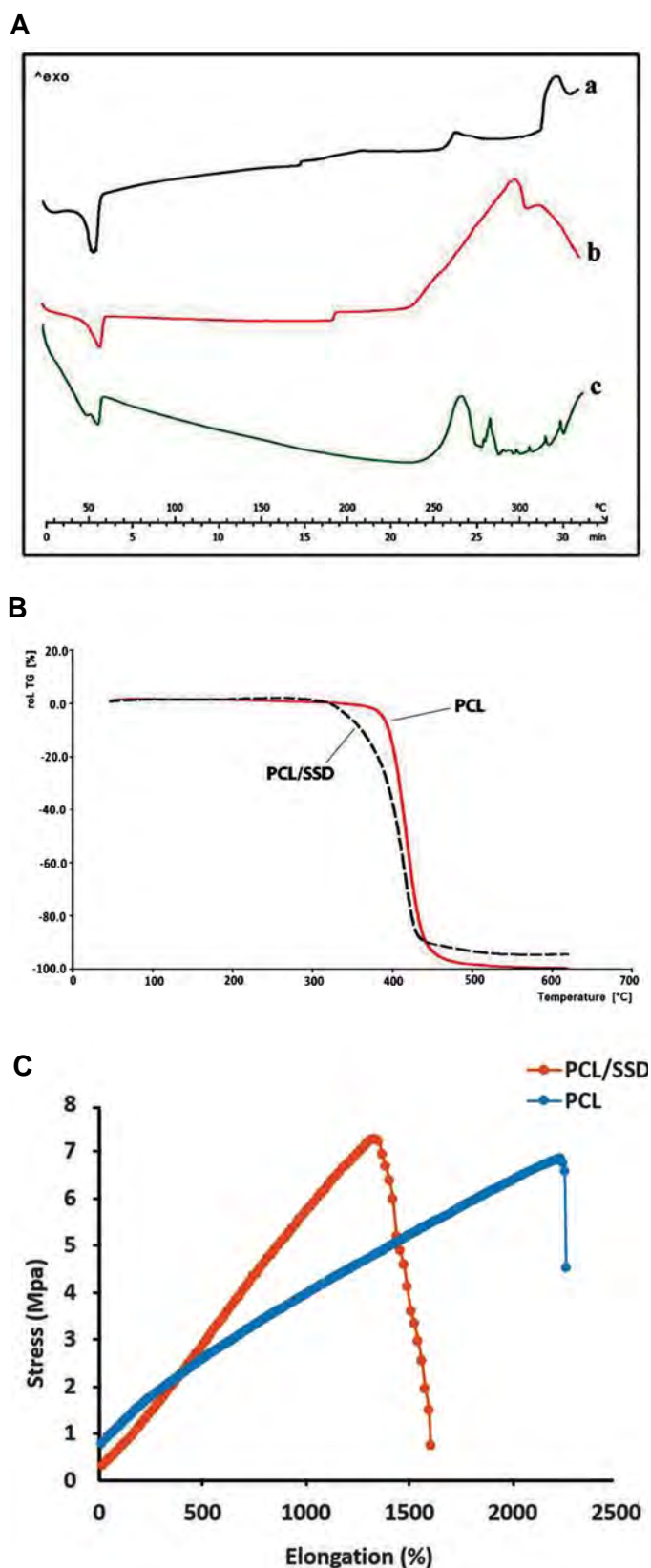


Fig.2: Physicochemical characterization. **A.** DSC thermogram for (a) PCL/SSD nanofibrous mat, for (b) PCL nanofibrous mat, and (c) physical mixing of PCL and SSD, **B.** TGA results for PCL and PCL/SSD nanofibrous mat, and **C.** Mechanical behavior of the mats with and without SSD. DSC; Differential scanning calorimetry, PCL; Polycaprolactone, SSD; Silver sulfadiazine, and TGA; Thermogravimetric analysis.

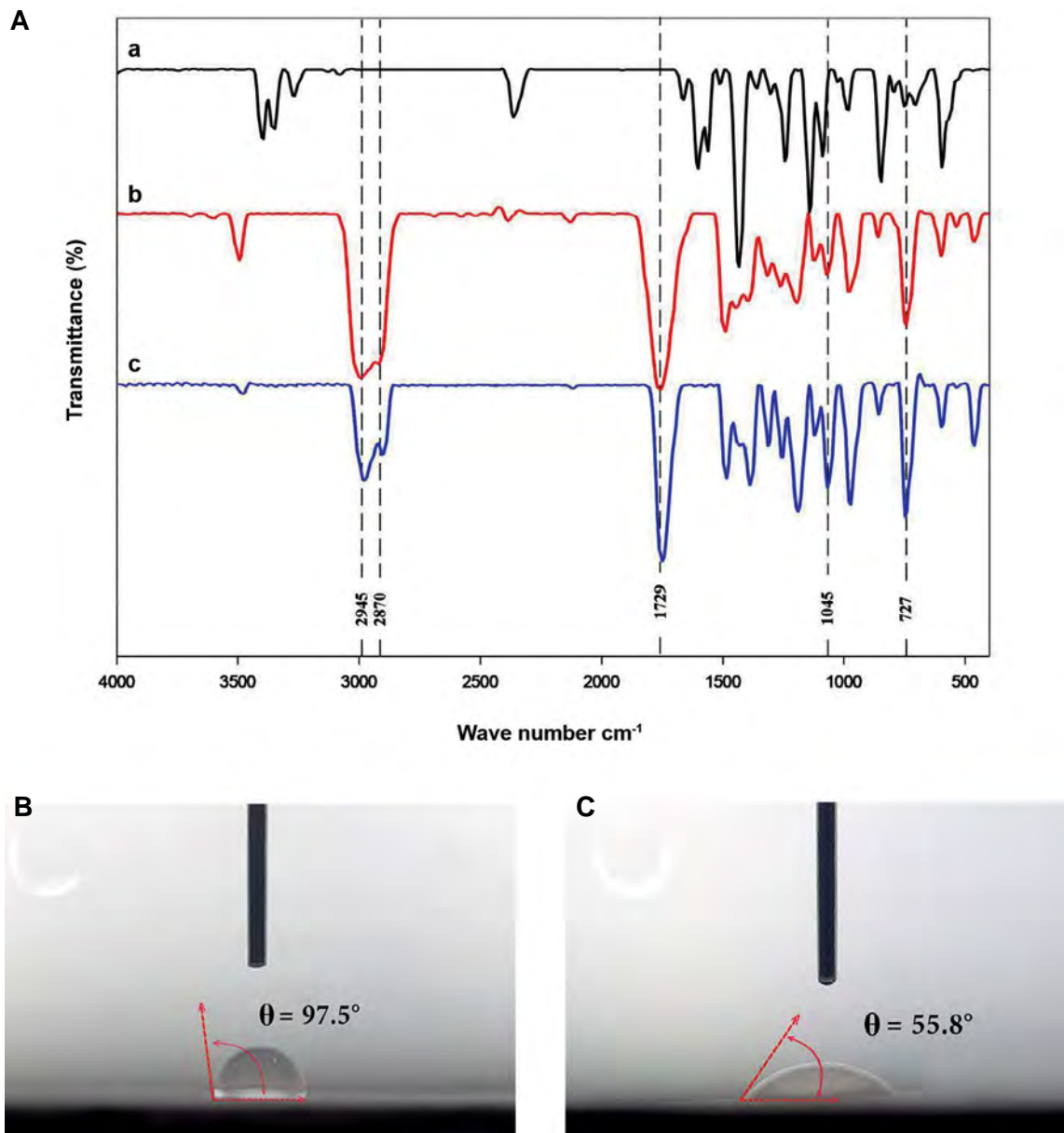


Fig.3: FTIR and contact angle for nanofibrous mat. **A.** FTIR for (a) SSD, (b) PCL, and (c) PCL/SSD nanofibrous mat are shown, **B.** Contact angle for PCL, and **C.** PCL/SSD are shown. FTIR; Fourier Transform Infrared spectroscopy analysis, SSD; Silver sulfadiazine, and PCL; Polycaprolac.

Biodegradability

Among many classes of biodegradable and biocompatible polymers, PCL is a suitable polymer for producing nanofibers by electrospinning. Slow degradation and release rate of this polymer is an advantage for its application in drug delivery systems, and PCL shows little degradation in an aqueous environment (16).

Biodegradability for PCL/SSD nanofibrous mats is an important parameter that shows controlled release of SSD during incubation days. In this way, we digested 3 mg of the scaffold using a 90% acetic acid as solvent at once, measured the absorbance of the solution, and plotted the standard curve for different concentrations of the drug. Absorption of 0.19 is equivalent to 3 μg of the drug that is present in 3 mg of scaffold. After incubation of 30 mg scaffold for 7 days,

approximately 30 μg of drug were released. Therefore, the degradation rate was 0.1%.

Cytotoxicity and cell attachment studies

MTT assay was done on days 1, 3, 6, and 9 to study the toxic effects of SSD incorporated into nanofibers and evaluate the biocompatibility of mats (Fig.4D). In order to evaluate cell adhesion and spreading on PCL/SSD nanofibrous mat, HDFs cells were seeded in PCL/SSD mat for a period of 24 hours. FE-SEM images (Fig.4E, F) showed cell adhesion on this nanofibrous mat. Cell proliferation and cell adhesion were obviously observed when cultured on both nanofibers. Due to hydrophilicity of PCL/SSD nanofibrous mat, cells attachment and proliferation rates were clearly higher than PCL nanofibrous mat (Fig.4E, F).

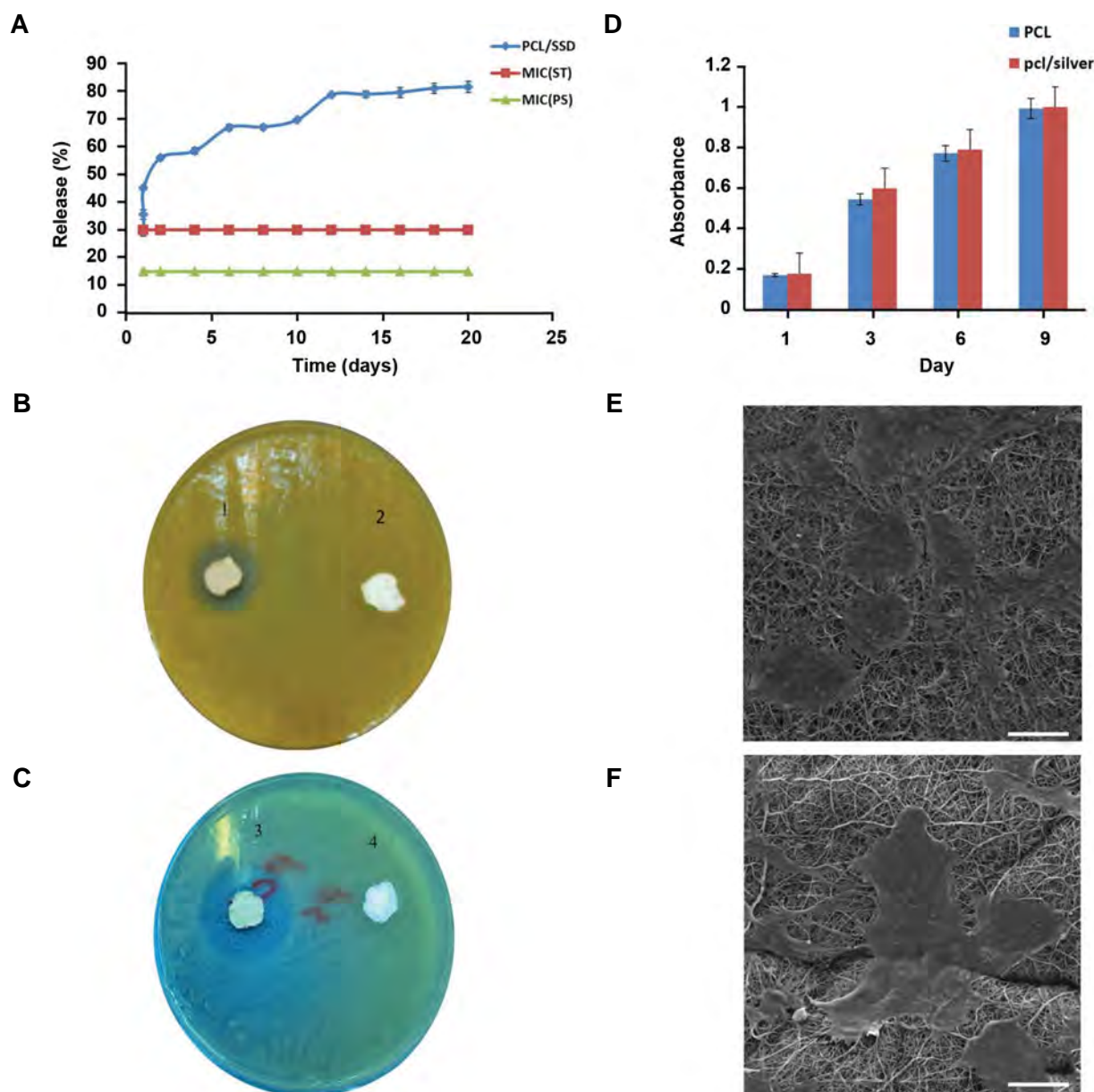


Fig.4: Drug release profile. **A.** *In vitro* SSD release from PCL/SSD nanofibrous mat, **B.** Antibacterial test for PCL/SSD, 1 and 3 are PCL mat containing SSD, and 2 and 4 are PCL mat. B. is *Staphylococcus aureus* and C. is *Pseudomonas aeruginosa*. MTT assay for PCL and PCL/SSD nanofibrous mat, **D.** Differences between two nanofibrous mat were not significant, **E.** Attachment of cells on PCL nanofibrous mat (scale bar: 50 μ m), and **F.** PCL/SSD nanofibrous mat are shown (scale bar: 50 μ m).

SSD; Silver sulfadiazine, PCL; Polycaprolactone, and MTT; 3-(4,5-dimethylthiazol-2-yl)-2,5-diphenyltetrazolium bromide.

Macroscopic evaluation

The appearance of each wound was observed on days 14, 21, and 28 of treatment. As shown in PCL/SSD group, wound healing process was remarkable compared to PCL and control after 14, 21 and 28 days. The extent of wound healing was evaluated by comparing wound size at each time-point with the primary wound size on day 0 (Fig.5) (1, 5, 9). Electrospun PCL/SSD mat and PCL alone were placed and adhered on the wound site of the test groups. From day 14 to 28, the PCL/SSD nanofibrous mat showed faster contraction compared to both open wound samples as control and PCL samples. On day 21 of treatment (Fig.5) (3, 7, 11) scab fell off the skin wound in all samples, but PCL/SSD sample showed a faster healing

with more regenerated skin and more hair growth. On day 28 of treatment (Fig.5) (4, 8, 12), all wounds appeared to be closed, and scab was observed upon open wound in control and PCL group.

The wound size in different groups was measured; in PCL/SSD group, more than 80% wound closure was found by day 14, while in PCL group, about 40% wound closure was observed. In PCL/SSD group, wound closure finalized (~90%) until day 21, while in PCL group and control group it reached 60 and 40%, respectively on day 21. Thus, PCL/SSD as wound dressing accelerated the healing process and shortened the final healing time to 14 days compared to 21 and 28 days for PCL group and open wound, respectively.

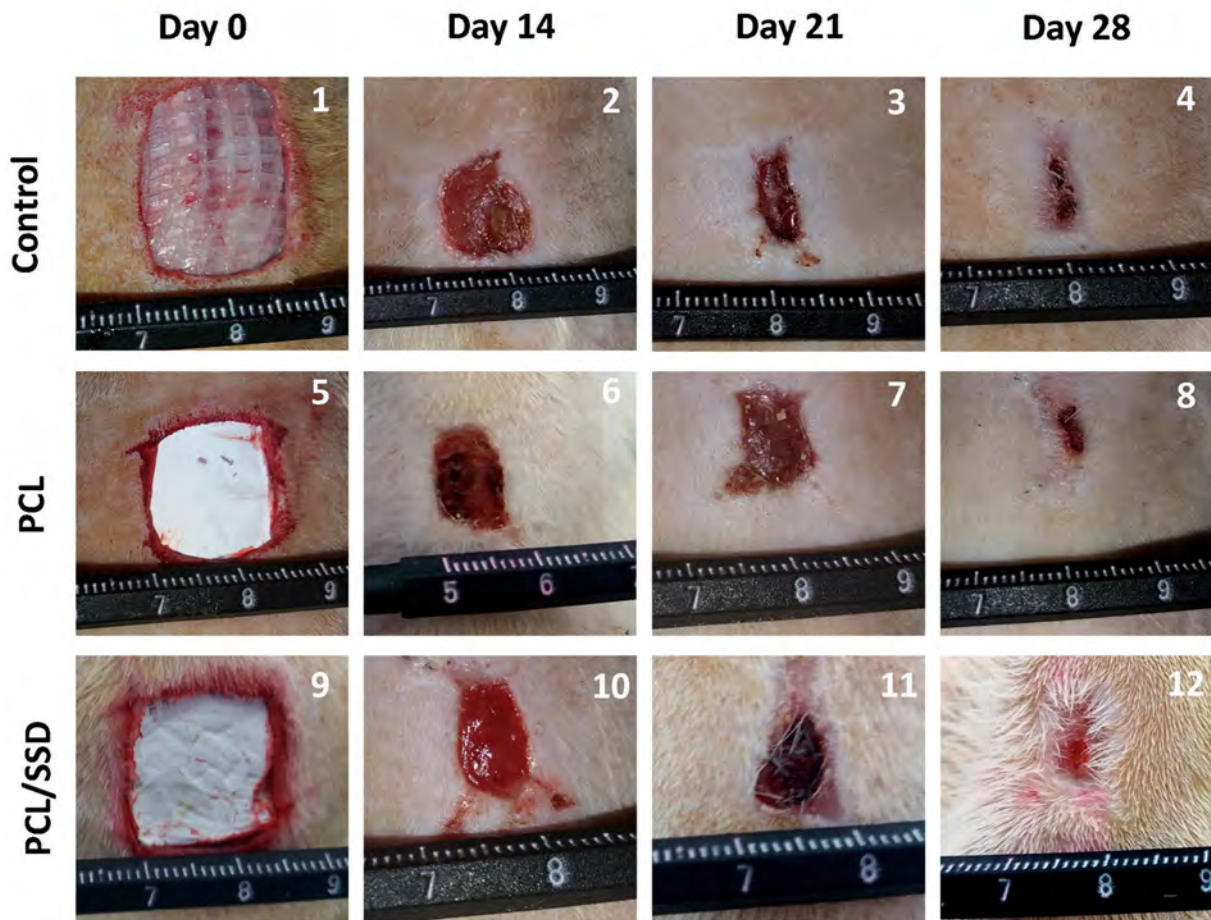


Fig.5: Macroscopic observation. The process of wound closure during the healing time was evaluated for assessment of PCL and PCL/SSD nanofibrous mat. PCL; Polycaprolactone and SSD; Silver sulfadiazine.

Microscopic and histological evaluation

To evaluate the *in vivo* efficacy of nanofibrous mat, H&E staining was done on sectioned tissue samples obtained from the wound site. The results for H&E staining on days 14, 21, and 28 post-wounding were summarized in Figure 6A. Histological studies showed accelerated healing time for PCL/SSD used as a wound dressing.

On day 14, in control group, thick granulation tissue with inflammatory cells including lymphocytes and neutrophils, obviously occupied wound site. However, in PCL group, the thickness and density of granulation tissues was clearly decreased and distribution of inflammatory cells was moderate. The granulation tissue and related inflammatory cells in PCL/SSD group were decreasing, but, fibroblast-like cells were increased and the repair process was promoting.

On day 21, both test groups showed noticeable improvements in regeneration of epidermis and dermis. Proliferation of fibroblasts and reformation of collagen fibers were observed. All these changes were observed in PCL group but in at a moderate level compared to test groups, in control group, in epidermis

and dermis, the tissue characteristics were similar to a skin in primary stages of regeneration and no blood vessels and collagen formation were clearly found. On day 21, epithelialization showed perfect thickness and morphology in PCL/SSD group compared to PCL and control group (Fig.6A). Typical vascular morphology, normal and desirable format of collagen fibers and bundles, were clearly observed. Thus, on day 21, in PCL/SSD group, the healing process was fully completed. But, in PCL group, the epithelialization, vascularization and collagen forming showed undesirable results. Therefore, by using the PCL/SSD as a wound dressing, healing time was accelerated, and the process moved to an acceptable and optimal route, to produce a normal skin with high quality and proper appearance. In other words, the process of healing was completed during 14 days and after that, the appearance and morphology was similar to a final perfect manifestation of the normal skin.

Overall, in histological analysis, inflammatory cells, fibroblasts and fibroid debris were seen in control group until day 21, but these features were seen in PCL/SSD and PCL nanofibrous mat group until day 14.

On day 28, all these groups showed final steps of regeneration and skin formation. These alterations in PCL/SSD showed very clear and developed stages of skin reformation toward a normal skin. Epithelialization and also skin appendages like hair follicles and sebaceous glands in PCL/SSD were obviously visible. Although in the two other groups, these presentations were observed, but, these changes were similar to PCL/SSD group on day 14. In other words, the process of regeneration was clearly shortened for about one week. The shape of wounds covered with PCL/SSD and PCL was rounded whereas the open wound was elongated, due to contraction of the rat skin. The results showed significantly reduced scar at both macroscopic and histological levels in the PCL/SSD mat compared with PCL mat and open wound, on day 28.

Masson's trichrome staining (Fig.6B) was used for evaluation of collagen formation and remodeling presented very sharp difference among PCL/SSD and other groups. In control group, collagen formation was in early steps and maturation of fibers and bundle formation was not occurred properly. In PCL group, when compared with control, the development of collagen bundles was promoted but compared to PCL/SSD group, the process of collagen formation was in earlier stages. Compared to the other groups, the PCL/SSD group showed the final and developed collagen bundles with desirable morphology which was similar to normal skin. This morphology and arrangement of collagen bundles in PCL/SSD clearly showed the production of a high-quality skin that could function as a perfect skin.

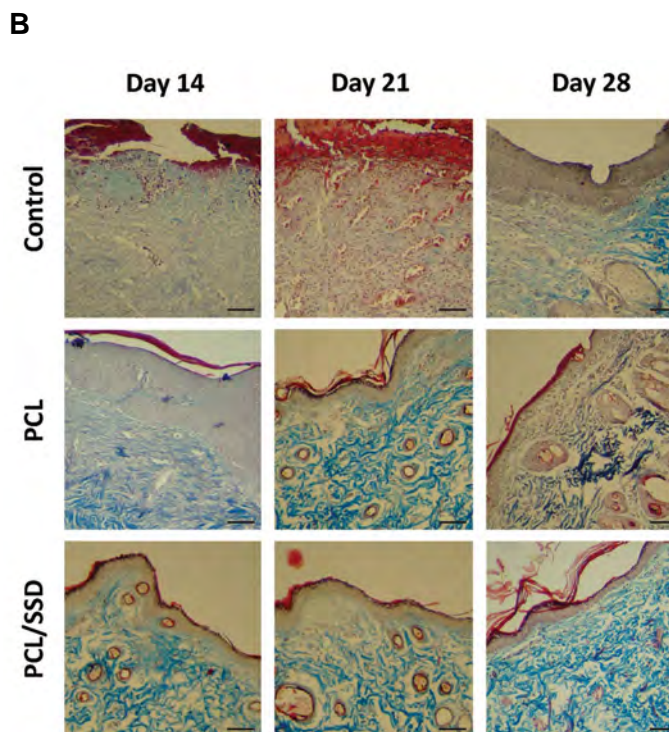
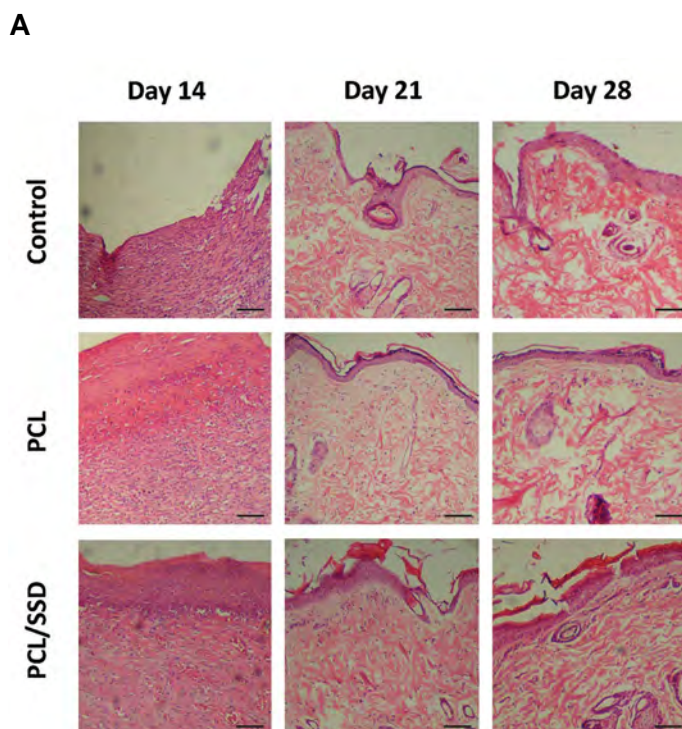


Fig.6: Microscopic observation: histological evaluations of wounds treated with PCL, PCL/SSD and control, on days 14, 21, and 28 of the healing process are shown. **A.** H&E staining and **B.** Masson's trichrome staining (scale bar: 50 μ m).

PCL; Polycaprolactone and SSD; Silver sulfadiazine.

On day 21, when different groups were compared, the skin overview of PCL group was similar to that of PCL/SSD group on day 14.

In other words, the PCL group with about one-week delay showed presentations similar to those of the PCL/SSD group. Development of dermis and collagen bundles in PCL/SSD group were also observed. On day 28, different groups showed progressive phase of repairing, but in PCL/SSD group, final skin remodeling in dermis layer was visible and PCL group still needed more time to produce the final form of a normal skin.

Discussion

As a wound dressing, a proper biomaterial with optimized characteristics should be able to decrease inflammation, infection, and scar formation and promote normal skin remodeling. Moreover, it should possess a proper surface for cell attachment and proliferation. Loading of drug into nanofibrous mat is a way to deliver drug into target region in a sustained manner. Nanofibrous mats with similar characteristics to those of ECM, are desirable candidates to be used as an optimum wound dressing and possess an acceptable potential for loading antibiotics to decrease the risk of infection (17, 18).

This study presents three main findings as follows: i. Design and fabrication of nanofibrous mat containing effective concentrations of SSD against *Staphylococcus aureus* and *Pseudomonas aeruginosa* that were approved *in vitro*, ii. Construction of a nanofibrous mat with 500-

μm thickness, similar to wound thickness, as a wound dressing, and iii. Creation of an expanded wound area (400 mm^2) compared to similar studies.

In this study, functionality of optimized nanocomposite PCL containing 0.3% SSD was evaluated in treatments of full area and thickness (400 mm^2 and $500\ \mu\text{m}$, respectively) wound healing in wistar rats and healing process were compared to that of rats treated with PCL nanofibers and vaseline gas used as control group.

Results of the present study showed that the PCL solution containing 0.3% SSD, has suitable viscosity and it was successfully synthesized by electrospinning in the range of nanoscale fibers. This concentration of SSD showed effective antibacterial properties *in vitro* and a controlled release profile for SSD during 20 days. Physicochemical and mechanical analysis such as TGA, DSC, and contact angle showed suitable characteristics of this scaffold in regeneration of skin tissue.

For several decades, SSD has been used as an antibiotic for wound healing. However, there are few studies that focused on nanofibers containing SSD. Using electrospun mats containing SSD is a promising method to fabricate antimicrobial wound dressings. For this reason, it is necessary to evaluate the physical and antimicrobial features as well as the biocompatibility of nanofibers loaded with SSD, to optimize the concentration of SSD.

The proper physical and mechanical integrity of the nanofibrous mat and similar viscoelasticity and flexibility to skin tissue, are the main characteristics of a desirable mat designed for wound dressing applications (1, 19). Therefore, in the first step to obtain an economic, nontoxic, and also an optimum backbone of scaffold, the unique solvent system (90% acetic acid) was selected as solvent (20, 21) for dissolving PCL. In addition, a very low but effective and nontoxic concentration of SSD (0.3%) was incorporated into the polymeric solution (22, 23). Fabricated PCL/SSD nanofibers showed acceptable characteristics with respect to biocompatibility, drug loading potential, anti-infection properties, and improved wettability to promote cell attachment, which play crucial roles in wound healing.

Some studies showed that modification of solutions viscosity affects the nanofiber characteristics. Some other works used different active ingredients such as plant extract, silver nanoparticles and Ag ions to increase the hydrophilicity and antimicrobial activity of the scaffold (24, 25). According to our results, the diameter of nanofibers in mats and also the elasticity of their composite showed an optimum range in nanoscale dimensions. In our study, by addition of SSD, viscosity of PCL/SSD composite was increased, and uniform and beadless nanofibers with a continuous, uniform and randomly-oriented morphology was formed.

Contact angle and tensile test showed that incorporation of SSD results in weaker mechanical properties and more hydrophilic surfaces of PCL nanofibers. It was shown

that a hydrophilic surface leads to higher affinity for cell interactions (22). MTT and FE-SEM analysis of scaffold with HDFs and their ability for cellular attachment, also showed that cellular proliferation pattern with applied concentration of SSD (0.3% wt) did not significantly alter PCL nanofibers integrity and cell tolerability.

SSD release profile showed that the amount of SSD released from the nanofibers was above the MIC for *Pseudomonas aeruginosa* and *Staphylococcus aureus* even at the very starting time-points.

In a previous study, Mohseni et al. (19) studied the effect of three different concentrations of SSD on the characteristics of PVA/PCL nanofibers *in vitro*; but, the study did not evaluate the *in vivo* effect of SSD-loaded nanofibers on wound healing. In another *in vitro* study, Mim et al. showed that Ag/PCL/Ge nanofibrous can protect wounds from bacterial infection and promote tissue regeneration, but they did not perform *in vivo* studies for evaluation of the effect of this scaffold on wound healing process (26).

In this study, PCL nanofibrous mat containing SSD was fabricated and applied *in vitro* and *in vivo*. PCL is a nontoxic polymer that is commonly used in tissue engineering because of its great biocompatibility and biodegradability characteristics, as well as its ability to provide a sustained release of anti-infection agents.

Some previous studies used higher concentrations of SSD such as 1, 2, and 3% (22), it was shown that using a silk biomaterial treated by dipping in a mixture solution of EGF and SSD for 48 hours at 4°C , can improve the wound healing (26).

Semnani et al. (27) impregnated SSD into PVP/gelatin scaffold by electrospinning; this membrane showed antibacterial activities against Gram-negative and -positive bacteria *in vitro*. However, the *in vivo* study was not performed for this scaffold. In this study, different ratios of loaded drug (0.1, 0.2, and 0.3 %) were tested and it was shown that samples with 0.3% drug had higher drug release rate and in turn, a greater antibacterial activity.

In the final step of our study, we applied the nanofibrous mats as a wound dressing on animal wounds and followed the healing process for 14, 21, and 28 days. Histological staining of repaired tissue in PCL/SSD group after 28 days did not show scarring in wound area in comparison to control. Jin et al. (28) created a wound size of around 8 mm^2 on mice and after 20 days, the wound was not closed completely. But, in our study, a wound size of about 400 mm^2 was created on the back of rats, and after 28 days, the wound was completely closed in PCL/SSD groups. Jeong et al. (22) designed a silk fibroin nanofibers containing 0.5, 0.1, and 1 % wt SSD that 1% wt SSD inhibited the attachment of epidermal cells to SF nanofibers *in vitro* and were cytotoxic to attachment of normal human epidermal keratinocyte (NHEK) and normal human epidermal fibroblast (NHEF). A 6-mm diameter biopsy punch was created on the dorsum of the rats and after 15 days, the healing process was comparable to control group.

In the study of jasmine stojkovska in 2018, silver nanoparticles accelerated the healing process of a thermal burn model with 10 mm in diameter between 19-21 days, but in our study, full thickness wound with 20 mm in diameter repaired after 21 days in PCL/SSD nanofibrous mat with 500- μm thickness. In this group, dermis and epidermis and collagen bundles with normal features similar to normal tissue were seen (29).

Comparing the regeneration stages and reformation of wounded skin, obviously presented this idea that by using PCL/SSD electrospun mat, wound healing accelerated for about one week. In other words, PCL/SSD as a wound dressing could finalize the regeneration and reformation by the end of week two. When this macroscopic presentation was examined by histological assessment, epidermis and hypodermis showed a reformed and remodeled skin. A favorite reepithelialization, rearrangement the collagen fibers and bundles similar to normal skin by specific staining, and also formation and dispersing of blood vessels in dermis were the main alterations that were clearly observed.

The main strength and novel points in this study are application of a mat with 500 μm - thickness *in vivo* on a larger wound area (about 400 mm^2). A thickness of 500 μm nanofibrous mat is similar to epidermis plus dermis thickness in normal skin. Since the smaller wounds are healed in shorter time points, we applied a larger wound area in our study, to examine the effectiveness of PCL/SSD mat.

It seems that application of PCL with 0.3% SSD and 500 μm -thickness could accelerate wound healing in about one-week shorter period. Specific staining for collagen showed thick collagen bundles in dermal layer in PCL/SSD group compared to PCL and control group. Additionally, the rate of epithelialization and formation of skin appendages such as new hair follicles and sebaceous glands were higher in PCL/SSD group compared with PCL and control. Moreover, these findings are supported by the previous studies (29-31).

Conclusion

This study demonstrated that PCL/SSD blended mat could be considered a wound dressing for fast and effective repairing and remodeling of skin tissue. Further studies are needed to assess the effect of PCL/SSD nanofibrous mat containing higher concentrations of SSD during a short period of wound healing to accelerate the healing process.

Acknowledgements

This work was financial supported by a grant (CMRC-9427) from the vice-chancellor for research affairs of Ahvaz Jundishapur University of Medical Sciences. This study is part of a Ph.D. thesis done by Fereshteh Nejaddehbashi at Cellular and Molecular Research Center. The authors have no commercial, proprietary, or financial interest in the products or companies described

in this manuscript. The authors declare that there is no conflict of interest.

Authors' Contributions

F.N., M.O., M.A., V.B. M.H.; Participated in study design, data collection and evaluation. F.N., M.A. J.M., E.M.; Participated in designing scaffold. F.N.; Transplanted the scaffold into rats. F.N., M.O.; Evaluated *in vivo* evaluation. F.N., M.O., M.A.; Prepared the draft of the manuscript, participated in the finalization of the manuscript. All authors read and approved the final manuscript.

References

1. Boakye MAD, Rijal NP, Adhikari U, Bhattarai N. Fabrication and characterization of electrospun PCL-MgO-keratin-based composite nanofibers for biomedical applications. *Materials (Basel)*. 2015; 8(7): 4080-4095.
2. Klama-Baryla A, Kitala D, Łabuś W, Kraut M, Glik J, Nowak M, et al. Autologous and allogeneic skin cell grafts in the treatment of severely burned patients: retrospective clinical study. *Transplant Proc*. 2018; 50(7): 2179-2187.
3. Mahoney C, McCullough MB, Sankar J, Bhattarai N. Nanofibrous structure of chitosan for biomedical applications. *J Nanomedic Biotherapeu Discover*. 2012; 2(1): 102.
4. Leung V, Ko F. Biomedical applications of nanofibers. *Polym Adv Technol*. 2011; 22(3): 350-365.
5. Edwards A, Jarvis D, Hopkins T, Pixley S, Bhattarai N. Poly (ϵ -caprolactone)/keratin-based composite nanofibers for biomedical applications. *J Biomed Mater Res B Appl Biomater*. 2015; 103(1): 21-30.
6. Chung TW, Yang MC, Tseng CC, Sheu SH, Wang SS, Huang YY, et al. Promoting regeneration of peripheral nerves in-vivo using new PCL-NGF/Tirofiban nerve conduits. *Biomaterials*. 2011; 32(3): 734-743.
7. Cipitria A, Skelton A, Dargaville TR, Dalton PD, Huttmacher DW. Design, fabrication and characterization of PCL electrospun scaffolds-a review. *J Mater Chem*. 2011; 21(26): 9419-9453.
8. Gholipour-Kanani A, Bahrami SH, Joghataie MT, Samadikuchak-saraei A, Ahmadi-Taftie H, Rabhani S, et al. Tissue engineered poly (caprolactone)-chitosan-poly (vinyl alcohol) nanofibrous scaffolds for burn and cutting wound healing. *IET Nanobiotechnol*. 2014; 8(2): 123-131.
9. Shafiee A, Soleimani M, Chamheidari GA, Seyedjafari E, Dodel M, Atashi A, et al. Electrospun nanofiber-based regeneration of cartilage enhanced by mesenchymal stem cells. *J Biomed Mater Res A*. 2011; 99(3): 467-478.
10. Ip M, Lui SL, Poon VK, Lung I, Burd A. Antimicrobial activities of silver dressings: an in vitro comparison. *J Med Microbiol*. 2006; 55(Pt 11): 59-63.
11. Srivastava P, Durgaprasad S. Burn wound healing property of *Cocos nucifera*: an appraisal. *Indian J Pharmacol*. 2008; 40(4): 144-146.
12. Chen DW, Hsu YH, Liao JY, Liu SJ, Chen JK, Ueng SW. Sustainable release of vancomycin, gentamicin and lidocaine from novel electrospun sandwich-structured PLGA/collagen nanofibrous membranes. *Int J Pharm*. 2012; 430(1-2): 335-341.
13. Lim MM, Sultana N. In vitro cytotoxicity and antibacterial activity of silver-coated electrospun polycaprolactone/gelatine nanofibrous scaffolds. *3 Biotech*. 2016; 6(2): 211.
14. Orazizadeh M, Hashemitabar M, Bahramzadeh S, Dehbashi FN, Saremy S. Comparison of the enzymatic and explant methods for the culture of keratinocytes isolated from human foreskin. *Biomed Rep*. 2015; 3(3): 304-308.
15. Jin G, Prabhakaran MP, Ramakrishna S. Stem cell differentiation to epidermal lineages on electrospun nanofibrous substrates for skin tissue engineering. *Acta Biomater*. 2011; 7(8): 3113-3122.
16. Gümüşderelioğlu M, Dalkıranoğlu S, Aydın RS, Çakmak S. A novel dermal substitute based on biofunctionalized electrospun PCL nanofibrous matrix. *J Biomed Mater Res A*. 2011; 98(3): 461-472.
17. Song W, Yu X, Markel DC, Shi T, Ren W. Coaxial PCL/PVA electrospun nanofibers: osseointegration enhancer and controlled drug release device. *Biofabrication*. 2013; 5(3):035006.

18. Qi R, Guo R, Zheng F, Liu H, Yu J, Shi X. Controlled release and antibacterial activity of antibiotic-loaded electrospun halloysite/poly (lactic-co-glycolic acid) composite nanofibers. *Colloids Surf B Biointerface*. 2013; 110: 148-155.
19. Mohseni M, Shamloo A, Aghababaei Z, Vossoughi M, Moravvej H. Antimicrobial wound dressing containing silver sulfadiazine with high biocompatibility: in vitro study. *Artif Organs*. 2016; 40(8): 765-773.
20. Pok SW, Wallace KN, Madhally SV. In vitro characterization of polycaprolactone matrices generated in aqueous media. *Acta Biomater*. 2010; 6(3): 1061-1068.
21. Ghasemi-Mobarakeh L, Prabhakaran MP, Morshed M, Nasr-Esfahani MH, Ramakrishna S. Electrospun poly (ϵ -caprolactone)/gelatin nanofibrous scaffolds for nerve tissue engineering. *Biomaterials*. 2008; 29(34): 4532-4539.
22. Jeong L, Kim MH, Jung JY, Min BM, Park WH. Effect of silk fibroin nanofibers containing silver sulfadiazine on wound healing. *Int J Nanomedicine*. 2014; 9: 5277-5287.
23. Lakshman LR, Shalumon KT, Nair SV, Jayakumar R, Nair SV. Preparation of silver nanoparticles incorporated electrospun polyurethane nano-fibrous mat for wound dressing. *Journal of Macromolecular Science, Part A: Pure and Applied Chemistry*. 2010; 47(10): 1012-1018.
24. Li JH, Shao XS, Zhou Q, Li MZ, Zhang QQ. The double effects of silver nanoparticles on the PVDF membrane: surface hydrophilicity and antifouling performance. *Applied Surface Science*. 2013; 265: 663-670.
25. de Mel A, Chaloupka K, Malam Y, Darbyshire A, Cousins B, Seifalian AM. A silver nanocomposite biomaterial for blood-contacting implants. *J Biomed Mater Res A*. 2012; 100(9): 2348-2357.
26. Gil ES, Panilaitis B, Bellas E, Kaplan DL. Functionalized silk biomaterials for wound healing. *Adv Healthc Mater*. 2013; 2(1): 206-217.
27. Semnani D, Poursharifi N, Banitaba N, Fakhrali A. Electrospun polyvinylidene pyrolidone/gelatin membrane impregnated with silver sulfadiazine as wound dressing for burn treatment. *Bull Mater Sci*. 2018; 41(3): 72 -79.
28. Jin G, Li Y, Prabhakaran MP, Tian W, Ramakrishna S. In vitro and in vivo evaluation of the wound healing capability of electrospun gelatin/PLLCL nanofibers. *Journal of Bioactive and Compatible Polymers*. 2014; 29(6): 628-645.
29. Stojkowska J, Djurdjevic Z, Jancic I, Bufan B, Milenkovic M, Jankovic R, Miskovic-Stankovic V, Obradovic B. Comparative in vivo evaluation of novel formulations based on alginate and silver nanoparticles for wound treatments. *J Biomater Appl*. 2018; 32(9): 1197-1211.
30. Mirnezami M, Rahimi H, Fakhar HE, Rezaei K. The role of topical estrogen, phenytoin, and silver sulfadiazine in time to wound healing in rats. *Ostomy Wound Manage*. 2018; 64(8): 30-34.
31. Bayati V, Abbaspour MR, Neisi N, Hashemitabar M. Skin-derived precursors possess the ability of differentiation into the epidermal progeny and accelerate burn wound healing. *Cell Biol Int*. 2017; 41(2): 187-196.

Histological Evidence for Therapeutic Induction of Angiogenesis Using Mast Cells and Platelet-Rich Plasma within A Bioengineered Scaffold following Rat Hindlimb Ischemia

Ali Karimi, Ph.D.¹, Rasoul Shahrooz, D.V.Sc.^{1*}, Rahim Hobbenagh, D.V.Sc.², Rahim Mohammadi, D.V.Sc.³, Nowruz Delirezh, Ph.D.², Saeede Amani, Ph.D.¹, Johan Garssen, Ph.D.^{4,5}, Esmaeil Mortaz, Ph.D.^{4,6,7*}, Ian M Adcock, Ph.D.^{8,9}

1. Department of Basic Science, Faculty of Veterinary Medicine, Urmia University, Urmia, Iran

2. Department of Pathobiology, Faculty of Veterinary Medicine, Urmia University, Urmia, Iran

3. Department of Surgery and Diagnostic Imaging, Faculty of Veterinary Medicine, Urmia University, Urmia, Iran

4. Division of Pharmacology, Utrecht Institute for Pharmaceutical Sciences, Faculty of Science, Utrecht University, Utrecht, Netherlands

5. Nutricia Research Centre for Specialized Nutrition, Utrecht, Netherlands

6. Department of Immunology, School of Medicine, Shahid Beheshti University of Medical Sciences, Tehran, Iran

7. Clinical Tuberculosis and Epidemiology Research Center, National Research Institute for Tuberculosis and Lung Disease (NRITLD), Shahid Beheshti University of Medical Sciences, Tehran, Iran

8. Cell and Molecular Biology Group, Airways Disease Section, Faculty of Medicine, National Heart and Lung Institute, Imperial College London, London, United Kingdom

9. Priority Research Centre for Asthma and Respiratory Disease, Hunter Medical Research Institute, University of Newcastle, Newcastle, NSW, Australia

*Corresponding Addresses: P.O.Box: 57153-1177, Department of Basic Science, Faculty of Veterinary Medicine, Urmia University, Urmia, Iran
P.O.Box: 19575154, Clinical Tuberculosis and Epidemiology Research Center, National Research Institute for Tuberculosis and Lung Disease (NRITLD), Shahid Beheshti University of Medical Sciences, Tehran, Iran
Emails: r.shahrooze@urmia.ac.ir, emortaz@gmail.com

Received: 12/August/2018, Accepted: 26/November/2018

Abstract

Objective: Peripheral arterial disease results from obstructed blood flow in arteries and increases the risk of amputation in acute cases. Therapeutic angiogenesis using bioengineered tissues composed of a chitosan scaffold that was enriched with mast cells (MCs) and/or platelet-rich plasma (PRP) was used to assess the formation of vascular networks and subsequently improved the functional recovery following hindlimb ischemia. This study aimed to find an optimal approach for restoring local vascularization.

Materials and Methods: In this experimental study, thirty rats were randomly divided into six experimental groups: a. Ischemic control group with right femoral artery transection, b. Ischemia with phosphate-buffered saline (PBS) control group, c. Ischemia with chitosan scaffold, d. Ischemia with chitosan and MCs, e. Ischemia with chitosan and PRP, and f. Ischemia with chitosan, PRP, and MCs. The left hind limbs served as non-ischemic controls. The analysis of capillary density, arterial diameter, histomorphometric analysis and immunohistochemistry at the transected locations and in gastrocnemius muscles was performed.

Results: The group treated with chitosan/MC significantly increased capillary density and the mean number of large blood vessels at the site of femoral artery transection compared with other experimental groups ($P < 0.05$). The treatment with chitosan/MC also significantly increased the muscle fiber diameter and the capillary-to-muscle fiber ratio in gastrocnemius muscles compared with all other ischemic groups ($P < 0.05$).

Conclusion: These findings suggested that chitosan and MCs together could offer a new approach for the therapeutic induction of angiogenesis in cases of peripheral arterial diseases.

Keywords: Chitosan, Histology, Ischemia, Mast Cells, Platelet-Rich Plasma

Cell Journal (Yakhteh), Vol 21, No 4, January-March (Winter) 2020, Pages: 391-400

Citation: Karimi A, Shahrooz R, Hobbenaghi R, Mohammadi R, Delirezh N, Amani S, Garssen J, Mortaz E, M Adcock I. Histological evidence for therapeutic induction of angiogenesis using mast cells and platelet-rich plasma within a bioengineered scaffold following rat hindlimb ischemia. Cell J. 2020; 21(4): 391-400. doi: 10.22074/cellj.2020.6287.

Introduction

The prevalence of peripheral artery disease (PAD), which affects approximately 200 million people globally, is increasing (1). These patients are at increased risk of acute limb ischemia (ALI), a painful event that can lead to limb loss due to inadequate angiogenesis and collateral artery ramification which may stimulate additional functional disorders (2).

A few attempts have been made to reduce limb morbidity in prospective randomized trials in PAD (3). However, current pharmacological treatment is ineffective, and not all patients are eligible for surgical procedure (4). Therefore, developing a new treatment

strategy that will reduce both the symptoms of the disease but also the underlying pathological processes is critical. Therapeutic angiogenesis provides a potential approach to improve and increase the function of ischemic tissue via stimulating blood vessel growth, enabling tissue perfusion and therefore supporting tissue regeneration and healing (5).

Pro-angiogenic approaches have been used in numerous studies investigating growth factor and cell-based therapies (2). Clinical trials have been performed to examine the effects of modulating growth factors including fibroblast growth factor (FGF), hepatocyte growth factor (HGF), and vascular endothelial growth factor (VEGF). However,

the results yielded little clinical significance apart from evidence of increased vascularity (5) Cell transplantation is a novel strategy for the treatment of critical limb ischemia (CLI) and specific bone marrow cells can be targeted to the sites of ischemia, and they contribute to blood vessel regeneration (6).

Mast cells (MC) are circulating bone marrow-derived cells found in all connective tissues and mucosal environments particularly in perivascular regions (7). MCs release various angiogenic factors including interleukin-8 (IL-8), FGF, VEGF, and transforming growth factors- α and β (TGF- α and TGF- β) (8). Many documents indicate an association between angiogenesis and the presence of MCs in body tissues. The presence of MCs near the site of capillary sprouting is one of the evidence for the association between angiogenesis and MCs (9).

Activated MCs synthesize large amounts of inducible nitric oxide (NO) which regulates processes such as inflammation and angiogenesis (10). NO upregulates the VEGF expression and enhances viability, proliferation, migration, association with intercellular matrix and the differentiation of endothelial cells and their formation into capillaries (11). MCs are implicated in most stages of wound healing including the initiation and modulation via acute inflammation at the growth and proliferation stages, as well as in the final remodeling of the newly formed connective tissue matrix (12). Furthermore, MCs increase the proliferation and migration of mesenchymal cells in the murine heart following infarction (13). In addition, the ability of platelet-rich plasma (PRP) to stimulate tissue regeneration is thought to be due to the effects of growth factors on progenitor cell proliferation, migration, and tube formation resulting in local angiogenesis (14).

Tissue engineering combines the use of cells, biochemical factors and various materials such as extracellular matrix to construct a scaffold that enables the formation of new viable tissue (15). Chitosan, derived from chitin, has been used as a tissue engineering scaffold as it has unique biopolymer, biocompatibility, and biodegradability properties (16). We hypothesized that the combination of MCs and PRP within a chitosan scaffold would synergize the repair processes in an ischemic model. In the current study, we examined the effects of mouse xenograft MCs and allograft platelets, in comparison with tissue modeling and bioengineering, on the promotion of angiogenesis in a rat hindlimb model of local ischemia. Murine MCs were used to more closely mimic the human clinical situation where sufficient MCs are unlikely to be obtained from the patients.

Materials and Methods

Study design and animals

In this experimental study, 30 healthy white male Wistar rats, weighing approximately 200-250 g, were obtained from the animal house of the Faculty of Veterinary Medicine, Urmia University, and randomly divided into six experimental groups: a. Ischemic control group (ischemia): the femoral

artery of right hind limb was transected, the proximal branches, superficial caudal epigastric, and lateral muscular arteries and veins were also resected, b. Phosphate-buffered saline (PBS group): the transected area around the femoral artery in the ischemic animals was immersed with PBS, c. Chitosan control group (chitosan): the transected area around the femoral artery in the ischemic animals was exposed to 50 μ L chitosan gel (see below), d. MC-transplanted group (MC): the transected area around the femoral artery in the ischemic animals was immersed with 50 μ L chitosan gel and 10^6 MCs, e. PRP-transplanted group (PRP): the transected location was immersed with chitosan and 13×10^6 platelets, and f. PRP- and MC-transplanted group (mix): the transected location was immersed with chitosan, 13×10^6 platelets, and 10^6 MCs. The left hindlimbs served as non-ischemic controls (17). Animals were kept in separate chambers with stable condition including $23 \pm 3^\circ\text{C}$ temperature, adequate air, humidity, and a natural light cycle for a fortnight before and throughout the experimental protocol. Standard rodent laboratory water and food were freely accessible. Samples were obtained on day 21 post-surgery. All procedures were administrated according to Ethics Committee guidelines of the Urmia University, Urmia, Iran (AECVU-175-2018).

Surgical procedure

Surgical procedures were carried out under the rules and regulations of the International Association of Pain Research (18). The animals were anesthetized by intraperitoneal injection of ketamine-xylazine (5% ketamine-90 mg/kg and 2% xylazine-5 mg/kg). The animals were positioned dorsally, and the feet pulled back. The femoral artery was located, and a 5 mm length was transected before the resected stumps were ligated to initiate hindlimb ischemia.

Histological analysis

The animals were anesthetized and euthanized on day 21, using an overdose of ketamine-xylazine, and tissue specimens were taken and fixed in 10% formaldehyde buffer solution. After tissue processing, 6 μ m paraffin sections were prepared using a rotary microtome (Microm GmbH, Germany). The sections were stained with hematoxylin and eosin (H&E) for histology, Masson's trichrome for collagen distribution, Periodic Acid-Schiff (PAS) to assess muscle glycogen, and CD31 antibody for the analysis of capillary density and vessel diameter at both the transected location and in gastrocnemius muscles.

Tissue samples were photographed with a digital camera (Dino-Eye-AM-7023) and analyzed using the Dino Capture 2.0 software (Dino-Lite Europe, The Netherlands) for morphometric analysis.

Hematoxylin and eosin staining

In brief, slides were deparaffinized with xylene and sections rehydrated using an ethanol gradient. Sections were stained in Harris' hematoxylin for 8 minutes, washed under running tap water for 5 minutes before 3 fast dips in 1% acid alcohol

to enhance differentiation. Sections were rewashed under running tap water for 1 minute and the blue stain revealed by placing in saturated lithium carbonate solution for 1 minute. The sections were washed in running water, counterstained with eosin for 5 minutes prior to examination under light microscopy. The number of capillaries and fibers were counted at 5 random 0.025 mm² areas at $\times 1000$ magnification, and their ratios were calculated. For the histomorphometric evaluation of fibers, cross-sectional muscles were photographed with a digital camera (Dino-Eye-AM-7023) and analyzed using the Dino Capture 2.0 software at 848-fold magnification.

Platelet preparation

Platelets were isolated from rat peripheral blood flow using differential centrifugation, as previously described (19).

Mouse bone marrow-derived mast cells

Murine MCs were obtained from hematopoietic progenitor cells generated from the bone marrow of male mice modified from a method described previously (20). In brief, the marrow from femurs and tibia were removed from 6-9 week old donor animals by flushing the bone shafts repeatedly with flushing medium using a syringe and a 27-gauge needle. The suspension of bone marrow cells was centrifuged at 1500 rpm for 10 min, and 0.5×10^6 cells/ml were cultured for 21 days. The culture medium was composed of RPMI 1640 medium (Gibco, UK) supplemented with 15% heat-inactivated fetal bovine serum, penicillin (100 IU/mL) and streptomycin (100 μ g/mL). Two mM L-glutamine, 0.1 mM nonessential amino acids, 5×10^{-5} M 2-mercaptoethanol, and 1 mM sodium pyruvate were also added to enrich the medium. Conditioned medium from pokeweed mitogen-stimulated spleen cells (PWM-SCM) was added to the enriched media to 20% (v/v), and the cells were incubated at 37-38°C for a further 5-7 days. At this point, non-adherent cells were transferred to new flasks, containing a fresh medium. After 3-4 weeks, MC purity was assessed by toluidine blue staining and flow cytometry.

Pokeweed mitogen-stimulated spleen cell conditioned medium (PWM-SCM)

Mice splenocytes (2×10^6 cells/ml) were cultured in a 75-cm² flask in RPMI 1640 medium with 15% FBS containing 1 mM sodium pyruvate, 0.5 M 2-mercaptoethanol, 4 mM L-glutamine 100 U penicillin/0.1 mg/ml streptomycin and nonessential amino acids (0.1 mM) containing lectin (8 μ g/ml) from *Phytolacca americana* (Pokeweed mitogen; Sigma, St. Louis MO). The culture medium was collected after 5-6 days of the culture when the color of the medium was completely yellow. The supernatant (PWM-SCM) was obtained by centrifugation at 3000 rpm for 15 minutes; then, gently filtration through a 0.2 μ m filter.

Toluidine blue staining

The purity of the MC population was determined by staining with toluidine blue (pH=2.7). Briefly, the harvested cells were centrifuged and stained for 2 minutes after fixation using Carnoy fluid. Cellular granularity was

assessed by light microscopy (21).

Characterization of mast cells

The expression of the high-affinity IgE receptor (Fc ϵ RI) and c-Kit on harvested MCs was assessed using flow cytometry. Briefly, the cells were washed with cold PBS before blocking of cell-surface Fc receptors with 2.4G2 (PharMingen, San Diego, CA, USA). Cells were incubated with fluorescein isothiocyanate (FITC)-conjugated anti-mouse Fc ϵ RI antibody (PharMingen, USA), Phycoerythrin (PE)-conjugated anti-mouse c-kit (PharMingen, USA) or matched isotype controls for 1 hour at 4°C. Cells were washed with PBS before being analyzed by flow cytometry (FACSCalibur BD, USA). Dead cells were separated during the data analysis.

Preparation of chitosan solution

Chitosan solution was prepared, as previously described. In brief, 2% (w/v) chitosan was prepared by dissolving crab shell chitosan (~400kDa, 85% deacetylated) (Fluka, Sigma-Aldrich St. Louis, MO, USA) in an aqueous solution (1% v/v) of glacial acetic acid (Merck, Darmstadt, Germany) by stirring on a hot plate at 50°C for 3 hours. The product was vacuum filtered through Whatman paper No.3 to remove any undissolved particles. Glycerol (Sigma Chemical Co., St. Louis, MO, USA) was added to 30% (w/w) of the total solid weight in solution to prepare a non-brittle product. The product [chitosan (2% w/v)] was lyophilized in acetic acid and cross-linked with 5% (w/v) tri-polyphosphate to produce a sponge-like matrix (22). The jelly-like chitosan scaffolds were prepared and 50 μ L implanted at the site of femoral artery transection.

Immunohistochemical analysis

Tissue sections were heated at 60°C, dewaxed with xylene, and rehydrated using an ethanol gradient. Endogenous peroxidase was blocked in 0.03% hydrogen peroxide for 5 minutes. Then, sections were gently washed in buffer before incubation for 15 minutes with anti-CD31 antibody (1:500 rabbit anti-mouse, Spain) to detect endothelial cells or with anti-CD34 antibody (1:5000 ab81289) as a marker of endothelial progenitor cells and blood vessel endothelial cells according to the manufacturer's instructions (Biocare, USA). Sections were gently rinsed in washing buffer, placed in a wet chamber with streptavidin-HRP (streptavidin conjugated to horseradish peroxidase in PBS-containing, the antimicrobial agent). Sections were gently washed by the use of washing buffer and placed in a buffer dish. Diaminobenzidine-substrate-chromogen (DAKO, Denmark) was added to tissue slides and incubated for 5 minutes. Sections were then washed and counterstained using hematoxylin for 5 seconds before being immersed 10 times in weak ammonia solution (0.037 M/L). Sections were washed with distilled water, immunohistochemically stained and visualized as a brown stain under light microscopy.

DNA-laddering

DNA laddering was performed using a commercial apoptotic DNA laddering kit (Roche Diagnostics GmbH, Mannheim, Germany). DNA was separated through a 0.8% agarose gel for 60 minutes at 60 V. IPST1-digested DNA was loaded as a control for the DNA content. Gels were stained with ethidium bromide and visualized with the Gel Doc 2000 system (Bio-Rad, California). Necrosis leads to rapid non-specific cleavage of DNA which is visualized as a smear whilst apoptosis results in 100-3000 bp DNA ladders.

Collagen fiber density

Using Masson's trichrome stain, collagen fibers were visualized by light microscopy (Zeiss, Cyber-Shot, Japan) using the MEZZURE software (Image pro-vision insight software) with a $\times 2.4$ optical zoom. Staining intensity and distribution were evaluated by pixel counting.

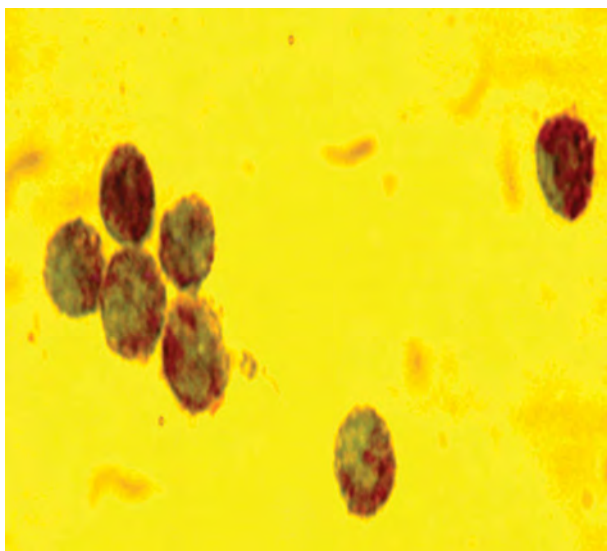
Statistics

We used the SPSS 20 software (SPSS Inc., Chicago, USA) to analyze the data. All data are expressed as the mean and standard error of the mean (mean \pm SEM). One-way ANOVA was used to compare the differences between the groups followed by Bonferroni post hoc test. The $P < 0.05$ was considered statistically significant.

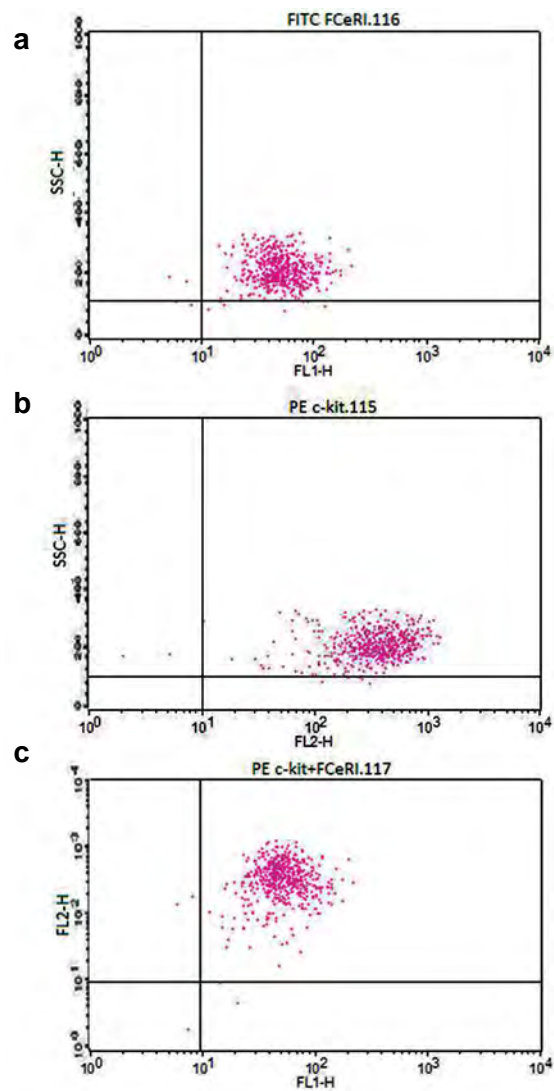
Results

After 3 weeks of cell culture, more than 92% of bone marrow cells differentiated into MCs as determined by Toluidine Blue staining (Fig.1A) and flow cytometry (Fig.1B). Scanning electron microscopy demonstrated the porosity of the chitosan scaffold (Fig.1C) On the 21st day, after the operation, macroscopically visible connective tissue was present in the graft region of the cell transplantation groups (Fig.2A). In the ischemia groups, due to femoral artery transections, the evidence of necrosis was observed in the foot pads and fingers (Fig.2B).

A



B



C

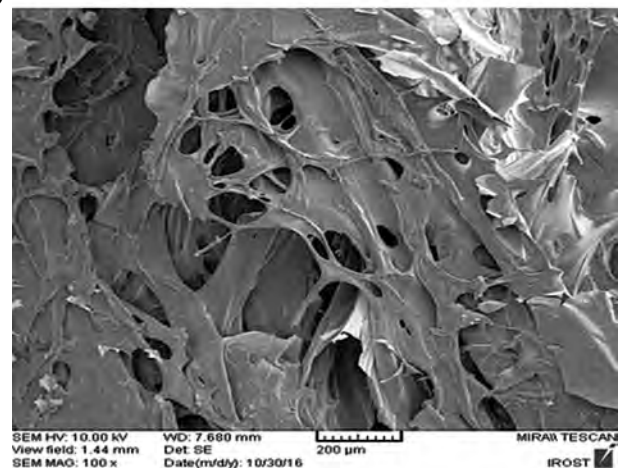


Fig.1: Presentation of the cell characterizations and scaffold microstructure. **A.** Murine bone marrow mast cells (BMMC) were cultured in pokeweed mitogen-stimulated spleen cell conditioned medium (PWM-SCM), 20% (v/v) for 3 weeks and cells were stained with toluidine blue (representative image at $\times 1000$ magnification), **B.** Representative flow cytometry analysis of BMMC. (a) Cells positive for FcεRI, (b) Cells positive for CD117 (c-kit), and (c) Double positive cells (92%), and **C.** Representative micrograph of scanning electron microscope to evaluate ultra-structure of porosity of the chitosan scaffold. Images are representative of at least $n=3$ independent experiments.

Capillary density findings in the femoral artery resected area

A combination of H&E, Masson's trichrome staining, and CD31 antibody verified the presence of endothelial cells within capillaries. Capillaries were counted at the site of femoral artery resection using an optical microscope (magnification $\times 400$) and a graded lens (1.16 mm square mesh size) (Fig.2C). Ischemia resulted in a significant decrease in capillary density that was significantly ($P < 0.05$) reversed in both the chitosan and the chitosan/MC groups (Fig.2D). The other treatments did not significantly enhance the capillary density compared with PBS treatment. Interestingly, the presence of PRP significantly reduced the ability of MCs to enhance capillary density (Fig.2D, comparison of MIX versus MC groups).

Histomorphometric analysis of vessels in the femoral artery resected area

The histomorphometric analysis of tissue vessels was stratified into 3 groups according to the cross-sectional

thickness (20-50, 50-100, and $>100 \mu\text{m}$) at the site of femoral artery transection (Fig.3A). Ischemia resulted in a significant increase in the number of small vessels ($P < 0.05$) and a considerable reduction in the number of large vessels ($P < 0.05$, Fig.3B). There was no significant change in the number of intermediate-sized vessels (50-100 μm).

Chitosan alone had no effect on the ischemia-induced reduction in large vessels, increased the number of small vessels ($P < 0.05$) and decreased the numbers of intermediate vessels ($P < 0.05$) compared with ischemia, PBS and control animals. The number of large vessels in the chitosan/MC-treated ischemia group was significantly higher than the other groups ($P < 0.05$) although did not reach the control levels (Fig.3B).

Collagen fiber density in femoral artery resected area

Ischemia induced a significant increase in the distribution of collagen fibers at the site of femoral artery resection ($P < 0.05$). No intervention affected this distribution (Fig.3C).

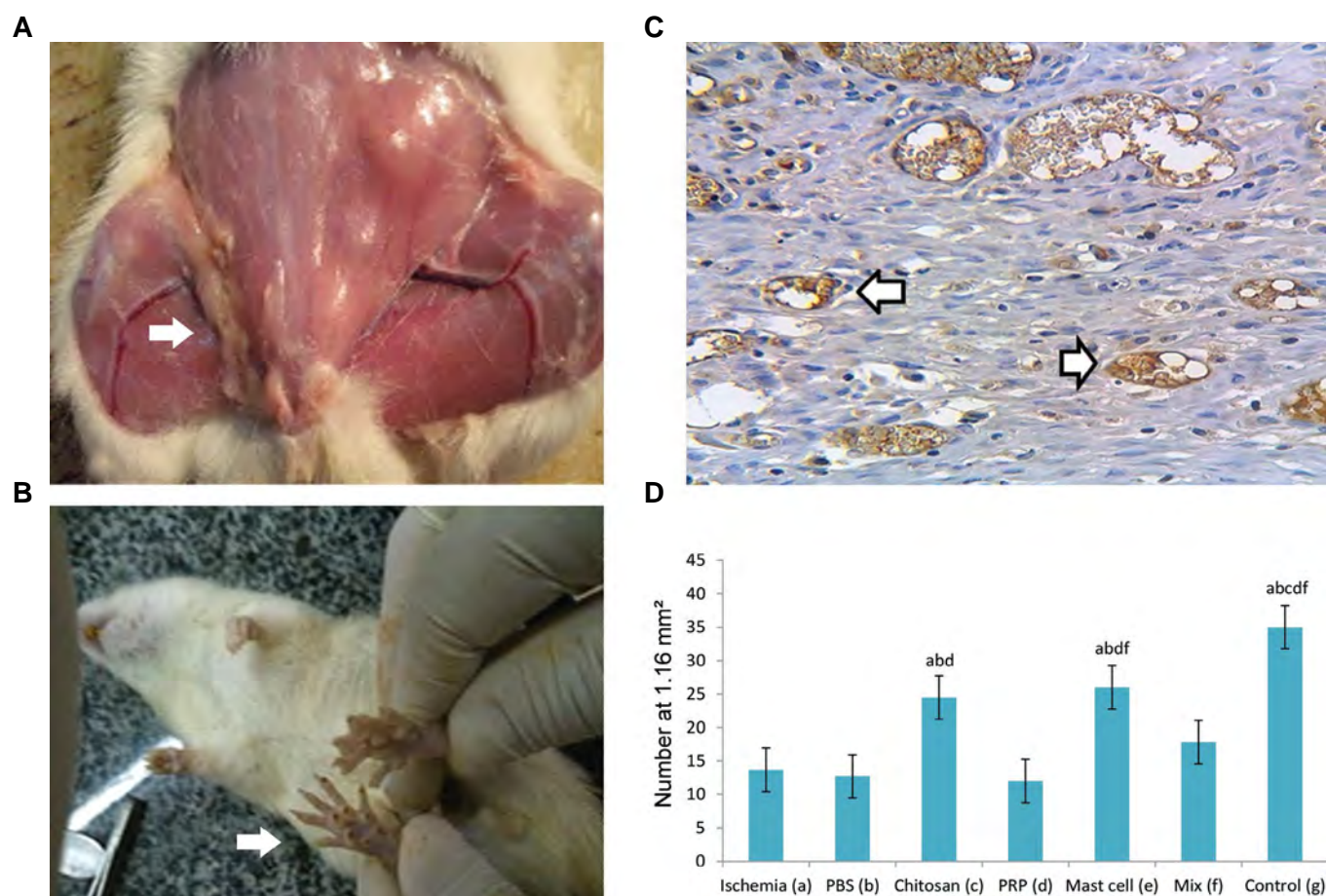
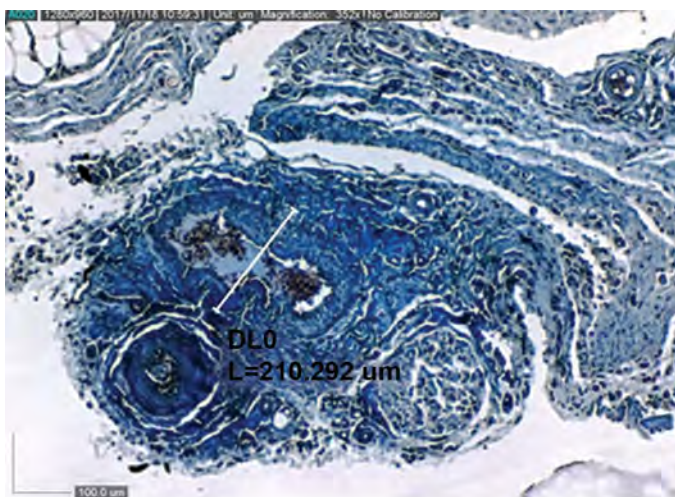
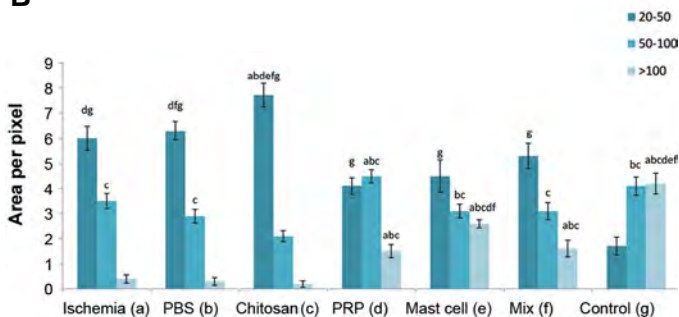


Fig.2: Illustrations for gross morphology of femoral artery and presentation of Immunohistochemical staining for endothelial cells and capillary density. **A.** Gross morphology of right femoral artery transection. The arrow shows the transected and transplanted area, **B.** The visual presentation of ischemia-induced necrosis of the foot pad, **C.** Immunohistochemical staining for CD31-positive endothelial cells (brownish yellow staining, arrowed) within the transplantation area ($\times 600$ magnification). Images are representative of at least $n=5$ independent analyses, and **D.** Bar graph shows the effect of ischemia on capillary density. All values are expressed as the mean \pm SEM, a-f represent statistically significant differences ($P < 0.05$) among indicated groups. Pictures are representative of the results from 5 animals with the left hind paw acting as a control. In this study, we used 5 animals in each group. PRP; Platelet-rich plasma, Mix; Chitosan, PRP, and mast cell group, and PBS; Phosphate-buffered saline.

A



B



C

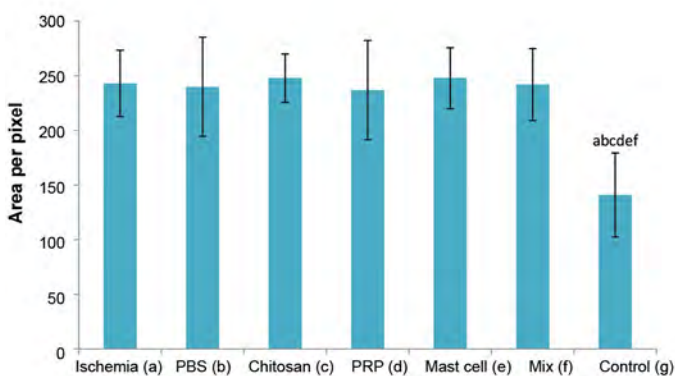


Fig.3: Micrograph and histograms presented collagen distribution and vessel morphometry in the cell transplanted area. **A.** Representative micrograph ($\times 352$ magnification) showing individual morphometric analysis of blood vessels (collagen deposition is shown as blue color) stained with Masson's trichrome staining method and evaluated with the Dino Capture 2.0 software, **B.** The bar graph shows vessel morphometry in experimental groups in femoral artery transected area according to cross-sectional thickness (20-50, 50-100, and $>100 \mu\text{m}$), and **C.** Histogram showed a semi-quantitative comparison of connective tissue density (intensity and distribution) Ischemia-induced distribution of collagen fibers at the site of femoral artery resection was unaffected by any intervention. All values are expressed as the mean \pm SEM, a-g represent statistically significant differences ($P < 0.05$) among indicated groups. In this study, we used 5 animals in each group. PRP; Platelet-rich plasma, Mix; Chitosan, PRP, and mast cell group, and PBS; Phosphate-buffered saline.

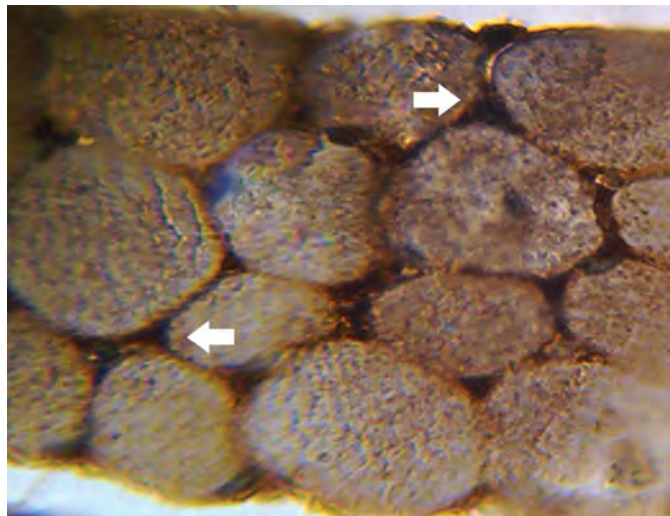
Capillaries to muscle fiber ratio

A combination of H&E staining, Masson's trichrome stain and vessel endothelial cell staining (CD34+ cells) was used to count capillaries (Fig.4A). Ischemia significantly reduced the ratio of capillaries to muscle fibers at the site of femoral artery transection. This reduced ratio was significantly increased and restored to the control levels in the chitosan alone and the chitosan/MC-treated groups ($P < 0.05$). Neither the chitosan/PRP nor chitosan/MIX groups showed significant differences when compared with the ischemia or PBS groups (Fig.4B).

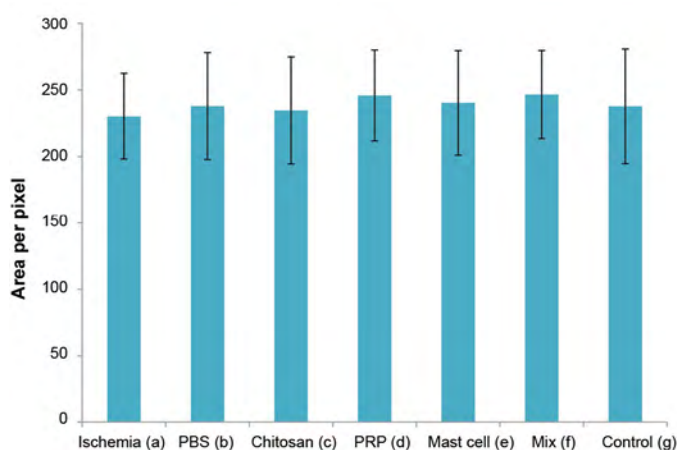
Endomysium and perimysium (connective tissue) density in different groups

Masson's trichrome staining was carried out to determine the connective tissue density in the endomysium and perimysium area of gastrocnemius muscles. It demonstrated a high variability within the groups with no significant effect of ischemia or the various interventions on stained sections (Fig.4C).

A



B



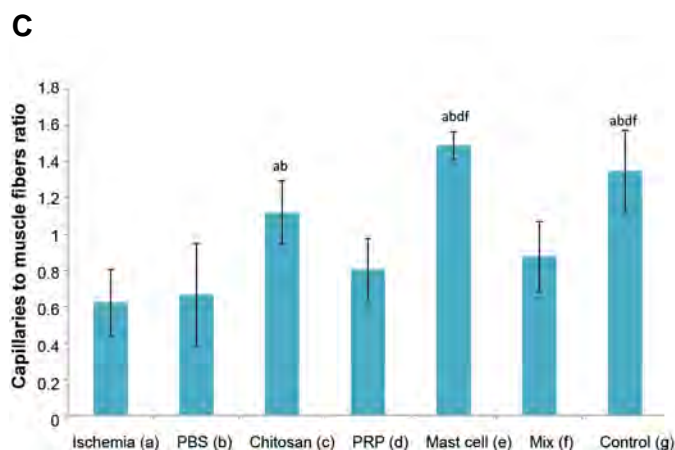


Fig.4: Micrograph and histogram presented the blood vessels data's and connective tissue density in the gastrocnemius muscles. **A.** Immunohistochemical staining for CD34-positive endothelial cells (dark brown, arrowed) between the gastrocnemius muscle fibers ($\times 1500$ magnification), **B.** The graph indicates semi quantitative intensity of endomysium and perimysium (connective tissue) density in different groups, and **C.** The effect of ischemia and interventions on the capillary to gastrocnemius muscle fiber ratio. All values are expressed as the mean \pm SEM, a-f represent statistically significant differences ($P < 0.05$) among indicated groups. In this study, we used 5 animals in each group. PRP; Platelet-rich plasma, Mix; Chitosan, PRP, and mast cell group, and PBS; Phosphate-buffered saline.

Comparison of gastrocnemius muscle fiber diameter

Gastrocnemius muscle fiber diameter, as determined using

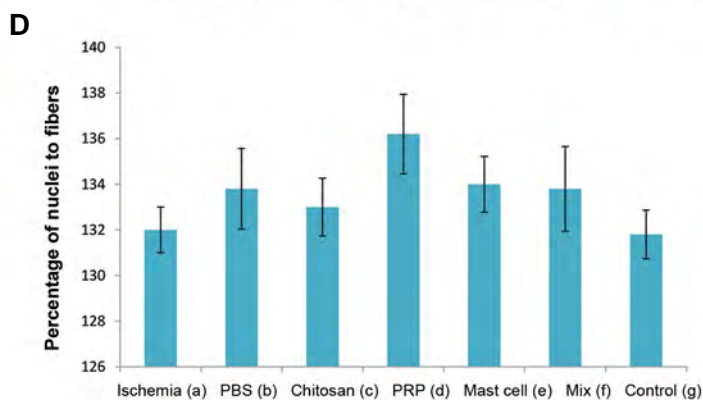
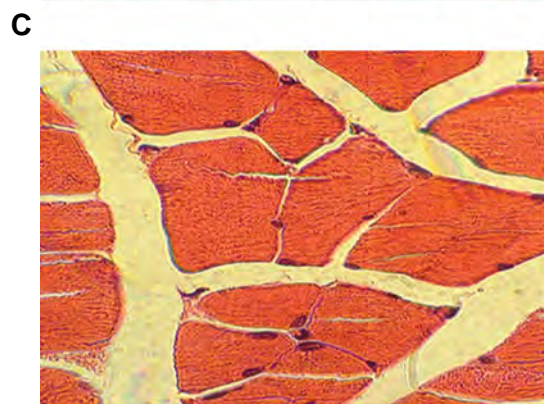
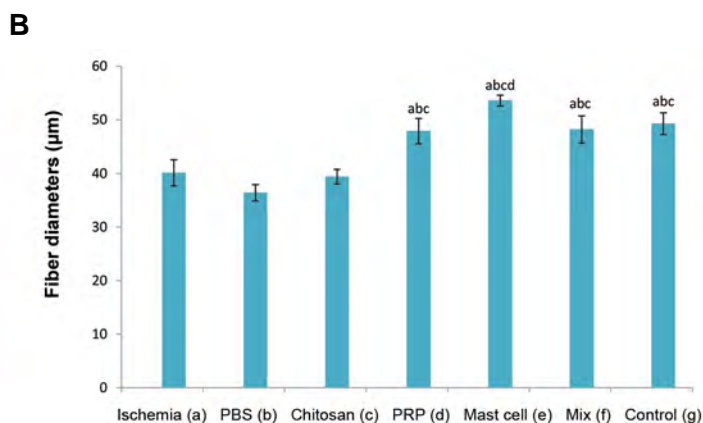
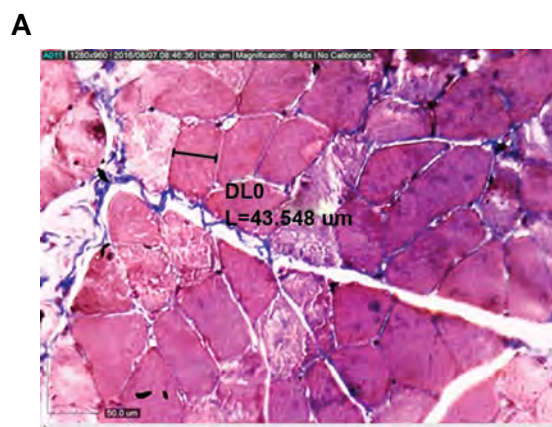


Fig.5: Illustrations for histomorphometric analysis of gastrocnemius muscles. **A.** Representative morphometric analysis of gastrocnemius muscle fibers ($\times 848$ magnification) stained with Masson's trichrome stain and determined using the Dino Capture 2.0 software, **B.** Histogram showed the effect of ischemia and various interventions on fiber diameter, **C.** Representative H&E stained a transverse section of muscle demonstrating the calculation of the ratio of the nuclei to the number of muscle fibers ($\times 1000$ magnification), and **D.** Histogram showed the percentage of nuclei to muscle fibers. All values are expressed as the mean \pm SEM, a-d represent statistically significant differences ($P < 0.05$) among indicated groups. In this study, we used 5 animals in each group. PRP; Platelet-rich plasma, Mix; Chitosan, PRP, and mast cell group, PBS; Phosphate-buffered saline, and H&E; Hematoxylin and eosin.

the Dino Capture 2.0 software (Fig.5A), was significantly ($P < 0.05$) reduced in the ischemia group. Chitosan alone had no effect on the muscle fiber diameter, but this parameter was significantly ($P < 0.05$) restored to the levels of the control group in the chitosan/PRP, chitosan/MC and chitosan/MIX groups (Fig.5B).

Estimation of the percentage of nuclei to muscle fibers

The percentage of nuclei within muscle fibers was highly variable, and no significant effect of ischemia or any intervention was observed (Fig.5C).

Estimations the amount of muscle glycogen in different groups

PAS staining indicated no difference in tissue glycogen of muscle fibers due to ischemia or following any intervention (Fig.6A).

Investigation of necrosis in various muscle groups

The evaluation of DNA smearing, as a marker of necrosis, and DNA laddering, indicative of apoptosis, demonstrated the presence of ischemia-induced necrosis (smearing) rather than apoptosis (laddering) (Fig.6B). The degree of DNA smearing was not significantly affected by any of the interventions studied.

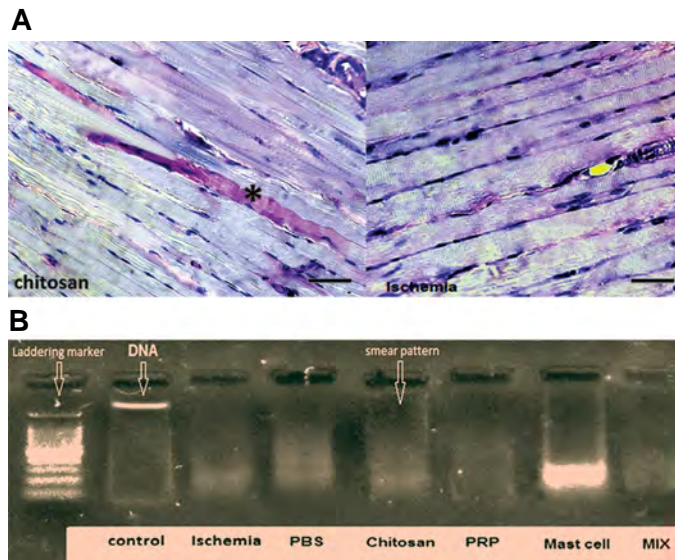


Fig.6: Illustration of PAS staining method and DNA fragmentation analysis of gastrocnemius muscles. **A.** Representative micrograph showing pink-red periodic acid-Schiff (PAS) staining to assess muscle glycogen. PAS staining was intense in some muscle fibers (*) but overall was nearly the same for all groups and **B.** DNA was isolated from rat muscle and prepared for the DNA fragmentation analysis. Ischemia induced DNA smearing considered a marker of necrosis, which was not affected by any of the interventions studied. The left column is a DNA marker indicating DNA "laddering," associated with apoptosis. All sham and treated groups demonstrate a "smear" pattern, indicating the typical sign of necrosis (100-3000 bp). In this study, we used 5 animals in each group.

Discussion

Our results indicate that ischemia causes a marked reduction in capillary density and the number of large vessels, but increased the number of small vessels and the distribution of collagen fibers. These changes were associated with reduced gastrocnemius muscle fiber diameter and the capillary: gastrocnemius muscle fiber ratio. Bioengineering using a chitosan scaffold alone restored ischemia-induced capillary density and the capillary: muscle fiber ratio and further enhanced ischemia-induced small vessel formation. The combination of a chitosan scaffold and activated MCs reversed the ischemia-induced reduction in capillary density and increased the mean number of small blood vessels. This combination also enhanced the ischemia-induced reduction in large blood vessels at the site of femoral artery transection and significantly increased the muscle fiber diameter and the capillary-to-gastrocnemius muscle fiber ratio.

The pathophysiology of major artery blockade indicates that ischemia occurs when the blood flow from arteries within regions adjacent to the affected tissue is reduced, and the resulting peripheral artery expansion is insufficient to allow normal blood flow to be restored to the tissue (23). To overcome this ischemia, the microvasculature and vessels of the affected area create anastomosis leading to the formation of large blood vessels. This results in increased blood flow to the tissues overcoming the requirement for small vessels and allowing the effect of ischemia to be decreased (9). The reversal of the

reduction in the capillary density in response to ischemia by all the interventions studied may result from the activation of signals released from the existing vascular tissue inducing new vessel formation (24) or factors released from platelets and MCs.

The release of MC-derived factors including VEGF, bFGF, TGF- β , TNF- α , and IL-8 have been implicated in this increased angiogenesis (8). Previous studies have reported various roles of bFGF in the initiation of vascularization, with the modulation of endothelial cell migration, proliferation, and differentiation (25). bFGF can also stimulate the growth of large vessels in smooth muscle tissue (26). Moreover, VEGF can increase vascular permeability and vascularization (27). A limitation of the current study is the failure of analyzing the local growth factor levels. Furthermore, as this is a xerograph model, there is a potential occurrence of immunosuppression. Although unlikely to occur in the time-frame of the current experiment, future studies should look for markers of immunosuppression.

Several studies have focused on the impact of PRP on the vascularization including the role of PRP in the healing of stomach and diabetic wounds (28). In addition, the proliferation, differentiation, and migration of human microvascular endothelial cells are enhanced by PRP in *in vitro* and an *in vivo* model of neonatal mouse retinal angiogenesis (29).

We hypothesized that MCs and platelets would have a synergistic effect on neovascularization due to the ability of platelet-derived growth factor (PDGF) to enhance MC differentiation through activation of stem cell factor (SCF) receptors and MC-derived platelet-activating factor (PAF) which are able to assemble and degranulate platelets (30). However, no additive or synergistic effects on the induction of vascularization was observed in the present study. Indeed, for most of the reported outcomes, a combination of PRP and MCs had a lesser effect than MCs when used alone, indicating a degree of functional antagonism. Also, MCs and platelets induce stimulating effects on collagen synthesis and contribute to tissue fibrosis (31, 32). In our current study, ischemia induced the formation of collagen fiber which was unaffected by the presence of MCs or platelets either alone or in combination.

We investigated the effects of ischemia and potential neovascularization interventions on the gastrocnemius muscle due to a link between general blood circulation and hindlimb musculoskeletal systems. Ischemia reduced the diameter of gastrocnemius muscle fiber and capillary-to-muscle ratio without affecting the density of connective tissue in gastrocnemius endomysium and perimysium areas or the number of muscle nuclei. MCs, PRP, and mixed treatment completely reversed the decreased diameter of muscle fiber induced by ischemia with no difference between each treatment. These results were similar to those seen with micro-fractured fat tissue (Lipogems) containing human adipose-derived stem

cells (hASCs) which produced greater tissue repair and reduced localized inflammation in a rat model of chronic hindlimb ischemia downstream of enhanced endothelial cell proliferation (33). Furthermore, recent studies have demonstrated that ischemia-induced gastrocnemius muscle atrophy was significantly reversed by VEGF, nerve growth factor (NGF) (34), and human smooth muscle cell transplantation (17).

Our data support the hypothesis that the formation of a local microvasculature is essential for communication between the general blood circulatory system and the lower limb circulatory system. An increase in the number of capillaries in the chitosan alone group could enhance this interaction due to the porous nature of the structural scaffold allowing angiogenesis to occur (35). Furthermore, tissue engineering experiments have indicated that human microvascular endothelial cells can drive vascularization within the host liver after implantation following. Some recent surveys have shown that after transplantation, anastomosis of 25-250 μm diameter (36).

Despite the transection of the femoral artery and the induction of ischemia, our data show that gastrocnemius can maintain muscle glycogen even though the reduced blood flow would be unable to deliver the entire metabolic requirements to the affected muscles. This would indicate that a degree of metabolic reprogramming occurs in this muscle under ischemic conditions. This confirms a previous study which revealed that parallel with the increased absorption of glucose by insulin-dependent receptors (GLUT4) in hypoxic muscles, the amount of muscle glycogen was relatively constant (37). The switch from adipose to connective tissue following the ischemia may affect the overall tissue metabolic status due to the change in metabolic demands. A limitation of our study was the failure of measuring the expression of either GLUT4 or glucose uptake in specific tissue/cells types.

The current results also indicate that the density of connective tissue (endomysium and perimysium) is not a sign of structural changes during ALI. Previous studies indicated that although the inter-myofibrillar network in the endomysium of ischemic muscle tissue was coarser than the normal, the amount of connective tissue was not significantly increased (38). The change in fiber coarseness may result from altered muscle necrosis rather than apoptosis as demonstrated by the presence of DNA smearing rather than DNA laddering. This agrees with a previous study examining ischemia and reperfusion in rat leg muscles (39). This may reflect the apoptotic resistance observed in fully matured muscle (40).

Conclusion

These findings suggest that bioengineered tissues incorporating MCs within a chitosan scaffold could offer a new approach for therapeutic angiogenesis to improve arterial diseases. However, further research in this area is required to determine the optimal combination of scaffold and cells.

Acknowledgements

We wish to thank Mr. A. Aliari, Mr. H. Esmaili, from Immunology Laboratory and A. Piernejad from the central laboratory of the Faculty of Veterinary Medicine, Urmia University, Urmia, Iran, for their kind technical support. Ian M. Adcock is supported by Wellcome Trust grant 093080/Z/10/Z. The authors declare that there is no potential conflict of interest regarding the study.

Authors' Contributions

A.K.; Performed experiments, analyzed the data and co-authored the manuscript. R.S.; Designed and supervised the histological and histomorphometric experiments and co-wrote the manuscript. R.H.; Supervised the histopathological experiments. R.M.; Supervised the surgical experiments. N.D.; Advised in the cell culture process. S.A.; Participated in the cell culture process. J.G.; Participated in data analysis and approved the final draft. E.M.; Supervised in the generation of bone marrow-derived mast cells. I.M.A.; Participated in the data analysis and interpretation. All authors read and approved the final manuscript.

References

1. Creager MA. The crisis of vascular disease and the journey to vascular health: Presidential Address at the American Heart Association 2015 Scientific Sessions. *Circulation*. 2016; 133(24): 2593-2598.
2. Hamburg NM, Creager MA. Pathophysiology of intermittent claudication in peripheral artery disease. *Circ J*. 2017; 81(3): 281-289.
3. Bonaca MP, Gutierrez JA, Creager MA, Scirica BM, Olin J, Murphy SA, et al. Acute limb ischemia and outcomes with vorapaxar in patients with peripheral artery disease: results from the trial to assess the effects of vorapaxar in preventing heart attack and stroke in patients with atherosclerosis-thrombolysis in myocardial infarction 50 (TRA2 degrees P-TIMI 50). *Circulation*. 2016; 133(10): 997-1005.
4. European Stroke Organisation, Tendera M, Aboyans V, Bartelink ML, Baumgartner I, Clement D, et al. ESC Guidelines on the diagnosis and treatment of peripheral artery diseases: Document covering atherosclerotic disease of extracranial carotid and vertebral, mesenteric, renal, upper and lower extremity arteries: the task force on the diagnosis and treatment of peripheral artery diseases of the European Society of Cardiology (ESC). *Eur Heart J*. 2011; 32(22): 2851-2906.
5. Ylä-Herttua S, Bridges C, Katz MG, Korpisalo P. Angiogenic gene therapy in cardiovascular diseases: dream or vision? *Eur Heart J*. 2017; 38(18): 1365-1371.
6. Aicher A, Rentsch M, Sasaki K, Ellwart JW, Fandrich F, Siebert R, et al. Nonbone marrow-derived circulating progenitor cells contribute to postnatal neovascularization following tissue ischemia. *Circ Res*. 2007; 100(4): 581-589.
7. Bataineh A, Al-Dwairi ZN. A survey of localized lesions of oral tissues: a clinicopathological study. *J Contemp Dent Pract*. 2005; 6(3): 30-39.
8. Kashyap B, Reddy PS, Nalini P. Reactive lesions of oral cavity: a survey of 100 cases in Eluru, West Godavari district. *Contemp Clin Dent*. 2012; 3(3): 294-297.
9. Jain RK. Molecular regulation of vessel maturation. *Nat Med*. 2003; 9(6): 685-693.
10. An S, Zong G, Wang Z, Shi J, Du H, Hu J. Expression of inducible nitric oxide synthase in mast cells contributes to the regulation of inflammatory cytokines in irritable bowel syndrome with diarrhea. *J Neurogastroenterol Motil*. 2016; 28(7): 1083-1093.
11. Cooke JP. NO and angiogenesis. *Atheroscler Suppl*. 2003; 4(4): 53-60.
12. Noli C, Miolo A. The mast cell in wound healing. *Vet Dermatol*. 2001; 12(6): 303-313.
13. Nazari M, Ni NC, Lüdke A, Li SH, Guo J, Weisel RD, et al. Mast cells promote proliferation and migration and inhibit differentia-

- tion of mesenchymal stem cells through PDGF. *J Mol Cell Cardiol.* 2016; 94: 32-42.
14. Kakudo N, Morimoto N, Kushida S, Ogawa T, Kusumoto K. Platelet-rich plasma releasate promotes angiogenesis in vitro and in vivo. *Med Mol Morphol.* 2014; 47(2): 83-89.
 15. Quade M, Knaack S, Akkineni AR, Gabrielyan A, Lode A, Rosen-Wolff A, et al. Central growth factor loaded depots in bone tissue engineering scaffolds for enhanced cell attraction. *Tissue Eng Part A.* 2017; 23(15-16): 762-772.
 16. Suh JK, Matthew HW. Application of chitosan-based polysaccharide biomaterials in cartilage tissue engineering: a review. *Biomaterials.* 2000; 21(24): 2589-2598.
 17. Hobo K, Shimizu T, Sekine H, Shin'oka T, Okano T, Kurosawa H. Therapeutic angiogenesis using tissue engineered human smooth muscle cell sheets. *Arterioscler Thromb Vasc Biol.* 2008; 28(4): 637-643.
 18. Zimmermann M. Ethical guidelines for investigations of experimental pain in conscious animals. *Pain.* 1983; 16(2): 109-110.
 19. Reis Messoria M, Hitomi Nagata MJ, Chaves Furlaneto FA, Menegati Dornelles RC, Mogami Bomfim SR, Miranda Deliberador T, et al. A standardized research protocol for platelet-rich plasma (PRP) preparation in rats. *RSBO.* 2011; 8(3): 299-304.
 20. Mortaz E, Redegeld FA, Nijkamp FP, Engels F. Dual effects of acetylsalicylic acid on mast cell degranulation, expression of cyclooxygenase-2 and release of pro-inflammatory cytokines. *Biochem Pharmacol.* 2005; 69(7): 1049-1057.
 21. Shao Z, Nazari M, Guo L, Li SH, Sun J, Liu SM, et al. The cardiac repair benefits of inflammation do not persist: evidence from mast cell implantation. *J Cell Mol Med.* 2015; 19(12): 2751-2762.
 22. Ojagh SM, Rezaei M, Razavi SH, Hosseini SMH. Development and evaluation of a novel biodegradable film made from chitosan and cinnamon essential oil with low affinity toward water. *Food Chem.* 2010; 122(1): 161-166.
 23. Losordo DW, Vale PR, Symes JF, Dunnington CH, Esakof DD, Maysky M, et al. Gene therapy for myocardial angiogenesis: initial clinical results with direct myocardial injection of phVEGF165 as sole therapy for myocardial ischemia. *Circulation.* 1998; 98(25): 2800-2804.
 24. Logsdon EA, Finley SD, Popel AS, Mac Gabhann F. A systems biology view of blood vessel growth and remodelling. *J Cell Mol Med.* 2014; 18(8): 1491-1508.
 25. Cross MJ, Claesson-Welsh L. FGF and VEGF function in angiogenesis: signalling pathways, biological responses and therapeutic inhibition. *Trends Pharmacol Sci.* 2001; 22(4): 201-207.
 26. Khurana R, Simons M. Insights from angiogenesis trials using fibroblast growth factor for advanced arteriosclerotic disease. *Trends Cardiovasc Med.* 2003; 13(3): 116-122.
 27. Henning RJ. Therapeutic angiogenesis: angiogenic growth factors for ischemic heart disease. *Future Cardiol.* 2016; 12(5): 585-599.
 28. Ma L, Elliott SN, Cirino G, Buret A, Ignarro LJ, Wallace JL. Platelets modulate gastric ulcer healing: role of endostatin and vascular endothelial growth factor release. *Proc Natl Acad Sci USA.* 2001; 98(11): 6470-6475.
 29. Mammoto T, Jiang A, Jiang E, Mammoto A. Platelet rich plasma extract promotes angiogenesis through the angiopoietin1-Tie2 pathway. *Microvasc Res.* 2013; 89: 15-24.
 30. Hiragun T, Morita E, Tanaka T, Kameyoshi Y, Yamamoto S. A fibrogenic cytokine, platelet-derived growth factor (PDGF), enhances mast cell growth indirectly via a SCF- and fibroblast-dependent pathway. *J Invest Dermatol.* 1998; 111(2): 213-217.
 31. Francis H. Mast cells promote biliary proliferation and hepatic fibrosis in normal and HDC-/- mice by interacting with cholangiocytes and hepatic stellate cells via TGF- β 1 signaling. *FASEB J.* 2016; 30(1 Supplement): 1251.4.
 32. Lee JI, Wright JH, Johnson MM, Bauer RL, Sorg K, Yuen S, et al. Role of Smad3 in platelet-derived growth factor-C-induced liver fibrosis. *Am J Physiol Cell Physiol.* 2016; 310(6): C436-C445.
 33. Bianchi F, Olivi E, Baldassarre M, Giannone FA, Laggetta M, Valente S, et al. Lipogems, a new modality of fat tissue handling to enhance tissue repair in chronic hind limb ischemia. *CellR4.* 2014; 2(6): e1289.
 34. Diao YP, Cui FK, Yan S, Chen ZG, Lian LS, Guo LL, et al. Nerve growth factor promotes angiogenesis and skeletal muscle fiber remodeling in a murine model of hindlimb ischemia. *Chin Med J (Engl).* 2016; 129(3): 313-319.
 35. Shigemasa Y, Minami S. Applications of chitin and chitosan for biomaterials. *Biotechnol Genet Eng Rev.* 1996; 13: 383-420.
 36. Chaturvedi RR, Stevens KR, Solorzano RD, Schwartz RE, Eyckmans J, Baranski JD, et al. Patterning vascular networks in vivo for tissue engineering applications. *Tissue Eng Part C Methods.* 2015; 21(5): 509-517.
 37. Gamboa JL, Garcia-Cazarin ML, Andrade FH. Chronic hypoxia increases insulin-stimulated glucose uptake in mouse soleus muscle. *Am J Physiol Regul Integr Comp Physiol.* 2011; 300(1): R85-R91.
 38. Karpati G, Carpenter S, Melmed C, Eisen AA. Experimental ischemic myopathy. *J Neurol Sci.* 1974; 23(1): 129-161.
 39. Cowled PA, Leonardos L, Millard SH, Fitridge RA. Apoptotic cell death makes a minor contribution to reperfusion injury in skeletal muscle in the rat. *Eur J Vasc Endovasc Surg.* 2001; 21(1): 28-34.
 40. Walsh K, Perlman H. Cell cycle exit upon myogenic differentiation. *Curr Opin Genet Dev.* 1997; 7(5): 597-602.

Spermatogenesis Recovery Potentials after Transplantation of Adipose Tissue-Derived Mesenchymal Stem Cells Cultured with Growth Factors in Experimental Azoospermic Mouse Models

Masoumeh Eliyasi Dashtaki, Ph.D.¹, Masoud Hemadi, Ph.D.¹, Ghasem Saki, Ph.D.^{2*}, Javad Mohammadiasl, Ph.D.³,
Ali Khodadadi, Ph.D.⁴

1. Cellular and Molecular Research Center, School of Medicine, Ahvaz Jundishapur University of Medical Sciences, Ahvaz, Iran

2. Physiology Research Center, School of Medicine, Ahvaz Jundishapur University of Medical Sciences, Ahvaz, Iran

3. Department of Medical Genetics, School of Medicine, Ahvaz University of Medical Sciences, Ahvaz, Iran

4. Cancer, Environmental and Petroleum Pollutants Research Center, Ahvaz Jundishapur University of Medical Sciences, Ahvaz, Iran

*Corresponding Address: P.O.Box: 61355189, Physiology Research Center, School of Medicine, Ahvaz Jundishapur University of Medical Sciences, Ahvaz, Iran

Email: ghasemsaki@yahoo.com

Received: 31/May/2018, Accepted: 17/November/2018

Abstract

Objective: Approximately 1% of the male population suffers from obstructive or non-obstructive azoospermia. Previous *in vitro* studies have successfully differentiated mesenchymal stem cells (MSCs) into germ cells. Because of immunomodulating features, safety, and simple isolation, adipose tissue-derived MSCs (AT-MSCs) are good candidates for such studies. However, low availability is the main limitation in using these cells. Different growth factors have been investigated to overcome this issue. In the present study, we aimed to comparatively assess the performance of AT-MSCs cultured under the presence or absence of three different growth factors, epidermal growth factor (EGF), leukemia inhibitory factor (LIF) and glial cell line-derived neurotrophic factor (GDNF), following transplantation in testicular torsion-detorsion mice.

Materials and Methods: This was an experimental study in which AT-MSCs were first isolated from male Naval Medical Research Institute (NMRI) mice. Then, the mice underwent testicular torsion-detorsion surgery and received bromodeoxyuridine (BrdU)-labeled AT-MSCs into the lumen of seminiferous tubules. The transplanted cells had been cultured in different conditioned media, containing the three growth factors and without them. The expression of germ cell-specific markers was evaluated with real-time polymerase chain reaction (PCR) and western-blot. Moreover, immunohistochemical staining was used to trace the labeled cells.

Results: The number of transplanted AT-MSCs resided in the basement membrane of seminiferous tubules significantly increased after 8 weeks. The expression levels of *Gcnf* and *Mvh* genes in the transplanted testicles by AT-MSCs cultured in the growth factors-supplemented medium was greater than those in the control group ($P < 0.001$ and $P < 0.05$, respectively). The expression levels of the *c-Kit* and *Scp3* genes did not significantly differ from the control group.

Conclusion: Our findings showed that the use of EGF, LIF and GDNF to culture AT-MSCs can be very helpful in terms of MSC survival and localization.

Keywords: Azoospermia, Epidermal Growth Factor, Glial Cell Line-Derived Neurotrophic Factor, Leukemia Inhibitory Factor, Mesenchymal Stem Cells

Cell Journal (Yakhteh), Vol 21, No 4, January-March (Winter) 2020, Pages: 401-409

Citation: Eliyasi Dashtaki M, Hemadi M, Saki G, Mohammadiasl J, Khodadadi A. Spermatogenesis recovery potentials after transplantation of adipose tissue-derived mesenchymal stem cells cultured with growth factors in experimental azoospermic mouse models. Cell J. 2020; 21(4): 401-409. doi: 10.22074/cellj.2020.6055.

Introduction

Infertility is among the common health issues worldwide that affects 15% of couples. Among infertile men, approximately 1% of the cases suffers from obstructive or non-obstructive azoospermia, with the latter being difficult to treat (1). One of the causes involved in the non-obstructive azoospermia is testicular torsion (2). Recently, researchers have offered a new approach to the treatment of infertility that involves differentiating stem cells into male or female germ cells *in vitro* (3-6). Adipose tissue-derived mesenchymal stem cells (AT-MSCs) have high proliferation rate and self-renewal capacity, as well as the potential to differentiate into various lineages (7). Recent studies have shown that both embryonic and adult stem cells are able to differentiate into primordial

germ cells (PGCs) and adult gametes (4, 8, 9). In 2006, Nayernia et al. (4, 9) demonstrated the production of a generation of mice from germ cells derived from embryonic stem cells (ESCs) for the first time, and in the same year, they were able to differentiate murine bone marrow-derived MSCs (BM-MSCs) into germ cells. Zhang et al. (10) recently reported that BM-MSCs have the potential to trans-differentiate into sperm-like cells, and can revive fertility in busulfan-treated azoospermic rats. Similarly, Cakici et al. (11) have shown that AT-MSCs cause regeneration of fertility in azoospermic rats.

However, amongst the important issues for therapeutic applications of these produced cells are their low numbers and viability (12). To overcome these problems, growth factors and several supplements are

often added to the culture media of these cells (13-15). Epidermal growth factor (EGF) is a 53 amino acid protein (16) involved in proliferation of spermatogonia and regulation of spermatogenesis in mammalian testis (17). It is also involved in the proliferation of MSCs (14). Leukemia inhibitory factor (LIF) is involved in the self-renewal process of stem cells, maintenance of the non-differentiated forms of ESCs, MSCs, and proliferation of PGCs (18, 19). The glial cell line-derived neurotrophic factor (GDNF) is expressed by glial cells in the brain (20), testicular and ovarian tissues during the development, and it has been found to be responsible for spermatogonial stem cells (SSCs) self-renewal both *in vitro* and *in vivo* (21). The present study is aimed to compare the performances of AT-MSCs cultured with or without the addition of three different growth factors EGF, LIF, and GDNF to their culture medium, following their transplantation in testicular torsion-detorsion mice.

Materials and Methods

Animals

In this experimental study, 6-8 week-old male Naval Medical Research Institute (NMRI) mice were housed under standard conditions (18-20°C and 12:12 hours light: dark cycles) at the Research Center and Experimental Animal House of Jundishapur University of Medical Sciences (Ahvaz, Iran). All the experiments presented in this study were approved by The Local Animal Care Committees of Ahvaz Jundishapur University of Medical Sciences (AJUMS) (IR.AJUMS.REC.2015.739), which were in complete accordance with the guidelines for the care and use of laboratory animals set by the national academy of sciences (National Institutes of Health Publication No. 86-23).

Isolation and culture of adipose tissue derived mesenchymal stem cells

Adipose tissue was taken from epididymis of 5-10 male NMRI mice in a sterile environment. Then, the samples were washed three times with phosphate buffered saline (PBS, Gibco Life Technologies, Paisley, UK) containing 3% penicillin/streptomycin (Pen/Strept) and 0.3% amphotericin B, then cut into 1-2 mm³ pieces. Blood vessels were removed from the tissue as much as possible and the pieces of fat were incubated in collagenase type I enzyme (Sigma-Aldrich, St. Louis, MO, 1 mg/ml) for 25-30 minutes at 37°C. To stop the enzyme activity, Dulbecco's Modified Eagle's Medium (DMEM, Life Technologies, USA) containing 10% fetal bovine serum (FBS, Gibco, Life Technologies, USA) was added to the sample. The suspension sample was centrifuged at 1200 rpm for 7 minutes, at room temperature and the cell pellet was cultured in 25 cm² flasks containing DMEM medium supplemented with 15% FBS and 1% Pen/Strep, and incubated at 37°C in the presence of 5% CO₂. After three days, the cell medium was replaced with fresh

medium and non-cohesive cells were removed. Medium was changed once every two days until the cell density reached 80-90%. The cells were then passaged for more proliferation and purification. For this purpose, 1 ml 0.25% trypsin-ethylenediaminetetraacetic acid (EDTA) was added to each flask and incubated for 2-3 minutes. When the cells were floating in the flask, the trypsin was neutralized using 3-4 ml of the medium containing FBS. Then, the cell suspension was centrifuged for 7 minutes. at 1200 rpm and the cell pellet was cultured in new flasks at a density of 20000/cm² (22).

Adipose tissue-derived mesenchymal stem cells identification

MSCs are fibroblast analogue cells with adhesion property and differentiation capacity (23). However, before any transplantation it is necessary to confirm the exact type of the cells isolated from donor animals. For this purpose, we used the commonly applied flow cytometry technique to confirm specific cell surface markers on the cultured cells. The expression of CD90 and CD44 markers (specific to MSCs) and the lack of expression of the two CD31 and CD45 markers (specific to hematopoietic stem cells and endothelial cells) were investigated, in our previous study (22).

In vitro osteogenic and adipogenic differentiation potentials of adipose tissue-derived mesenchymal stem cells

In order to further characterize of our cultured cells, we assessed their ability to differentiate into osteoblasts and adipocytes. For osteogenic differentiation, AT-MSCs (passage 3) were cultured in a 6-well plate (5×10⁴ cells/well). After 24 hours, the proliferative medium was replaced with osteogenic differentiation medium [DMEM (low glucose), 10⁻⁷ M dexamethasone, 50 µg/ml ascorbic acid, and 10 mM B-glycerol phosphate (Sigma-Aldrich, St. Louis, Mo, USA)]. The cells were incubated at 37°C and in 5% CO₂ for 21 days. Osteogenic medium was exchanged every 3 days. At the end of the differentiation period, AT-MSCs were fixed with 3% paraformaldehyde and the presence of calcium deposits was examined using 0.5% alizarin red solution.

For adipogenic differentiation, 5×10⁴ cells/well (passage 3) were seeded in a 6-well plate. After 24 hours, the proliferative medium was replaced with adipogenic differentiation medium [DMEM (low glucose) supplemented with 10⁻⁷ M dexamethasone, 66 nM insulin, 0.2 mM indomethacin and 0.5 mM isobutylmethylxanthine (Sigma-Aldrich, St. Louis, Mo, USA)]. The cells were incubated at 37°C and 5% CO₂. After 14 days, the cells were fixed with 3% paraformaldehyde and the presence of lipid follicles was examined by Oil Red O staining (0.5% in methanol, Sigma-Aldrich, St. Louis, Mo, USA) (22, 24).

Bromodeoxyuridine labeling of adipose tissue-derived mesenchymal stem cells

For labeling the AT-MSCs prior to transplantation we used Bromodeoxyuridine (BrdU), which is a base analogue substituted for thymine during DNA synthesis in proliferating cells. Following the denaturation of double-stranded DNA, BrdU is detected by immunohistochemistry, thus a population of cells that has proliferated is identified (25). Using this method we were able to trace the transplanted cells in the murine testicles. To do so, passage 3 AT-MSCs were incubated in 10 mM BrdU (Sigma-Aldrich, St. Louis, Mo, USA) overnight and BrdU immunohistochemistry kit (Merck, Germany) was used to confirm labeling of the cells.

Induction of azoospermia by surgical testicular torsion-detorsion procedure

To create azoospermic mice, we used the testicular torsion-detorsion method. For this purpose, twenty 6-8 week-old male NMRI mice (25-30 g) were first anesthetized by intraperitoneal injection of ketamine and xylazine, then the scrotal midline was cut, tunica vaginalis was opened and the testicle was twisted 720 degrees around its axis in a counterclockwise direction and was fixed with a 4-0 silk suture. Two hours later (26), the testicle was untwisted and fixed to the scrotal wall, which was then surgically closed (27). The right testicle of each group was also considered as the positive control for that group.

Labeled adipose tissue-derived mesenchymal stem cells transplantation

Six weeks after testicular torsion-detorsion surgery, the mice were anesthetized with ketamine/xylazine, scrotal walls were opened and 10^5 AT-MSCs were injected into the lumen of seminiferous tubules of testicular torsion-detorsion mice by Hamilton syringes. Testicles were fixed in their places and scrotal walls were closed again. The mice were divided into three groups. Group 1 was injected with AT-MSCs cultured in EGF (10 ng/ml), LIF (5 ng/ml), and GDNF (5 ng/ml) (MSCs-GF group), group 2 was injected with AT-MSCs that were cultured in a medium without growth factors (MSCs-T group), and group 3 was the testicular torsion-detorsion mice that did not receive any cells (negative control). The right testicles of all mice were considered as the positive control group for each treatment. To verify that the injected AT-MSCs have entered the testicles, the cells were stained with trypan blue. 8 weeks after cell transplantation, 5 testicles in each group were removed for molecular analysis. For histological analyses, 3 testicles in each group were removed and fixed in formalin and hematoxylin-eosin staining and immunohistochemical analysis were performed on tissue sections.

Hematoxylin-eosin staining

For histological assessment, hematoxylin-eosin staining was done. The stages of staining were performed according to the standard protocols, as summarized in the study by Cardiff et al. (28). All reagents were from Sigma-Aldrich (St. Louis, Mo, USA).

Immunohistochemical assessments of testicles

In order to trace the AT-MSCs labeled with BrdU, immunohistochemical staining was performed. For this purpose, the tissues containing BrdU were fixed in 4% formalin, then dehydrated and embedded in paraffin. Five-micron thick slices were prepared from the paraffin blocks and placed on slides for immunostaining. The slides were kept at 37°C overnight. Prior to staining, the sections were deparaffinized, then staining was performed according to the BrdU immunohistochemistry kit (Merck, Germany) instructions.

RNA extraction, cDNA synthesis and real time polymerase chain reaction

The RNeasy Mini Kit (Qiagen, Germany) was used to extract the total tissue RNA as per the company instructions. The cDNA was synthesized with Quanti Nova Reverse Transcription Kit (Qiagen, Germany) according to the company instructions. Primers for the selected genes were designed specifically using Gene Bank sequences. Primer sequences of *c-Kit*, *Mvh*, *Scp3*, *Gcnf* and *Gapdh* are as follows respectively:

c-Kit

F: 5'-GAGAAGGAAGCGTGACTCGT-3'

R: 5'-TCTTGCGGATCTCCTCTTGT-3',

Mvh

F: 5'-CGAAACATAGGTGATGAAAGAAC-3'

R: 5'-CCACTGAAGTAGCAACAAGAAC-3',

Scp3

F: 5'-AAAGCATTCTGGGAAATCTG-3'

R: 5'-GTACTTCACCTCCAACATCTTC-3',

Gcnf

F: 5'-CAACTGAACAAGCGGTATT-3'

R: 5'-GATGTATCGGATCTCTGGC-3',

Gapdh

F: 5'-AAGGTCATCCCAGAGCTGAA-3'

R: 5'-CTGCTTCACCACCTTCTTGA-3'.

Quantitative real-time polymerase chain reaction (qRT-PCR) stages were performed in Applied Biosystems 7500 Sequence Biosystem. Briefly, 100 nM of the primers and 100 ng cDNA were added to Syber Green PCR master mix to reach the overall volume of 10 μ l, then the reaction was carried out in 45 cycles, at 95°C for 15 seconds and 58-60°C for 1 minutes. The gene expression levels in every sample were normalized with the *Gapdh* gene and data was

evaluated using $2^{-\Delta\Delta CT}$ approach (22).

Western blot analysis

To assess the expression of c-Kit and Gcnf proteins, western blot analysis was performed. In this method, tissue samples were lysed in radioimmunoprecipitation assay buffer (RIPA) solution [150 mM NaCl, 25 mM Tris-HCl (pH=7.6), 1% Triton X-100, and, 1 mM EDTA pH=7.4, 3% sodium dodecyl sulfate (SDS, Sigma-Aldrich, St. Louis, Mo, USA), 1% Sodium deoxy collate] supplemented with 0.1% phosphatase inhibitor (Sigma-Aldrich, USA). The concentrations of the proteins was specified using bicinchoninic acid assay (BCA assay). The equivalent quantity of the protein samples (60 μ g) was loaded on 12% polyacrylamide gel, and then transferred to polyvinylidene fluoride (PVDF) membrane (Amersham, UK). PVDF membrane was blocked at room temperature for one hour in Tris Buffer/Tween 20 (TBST) solution containing 3% skim milk. Then, the membrane was incubated with primary antibodies in the blocking buffer at 4°C overnight: Gcnf (1:1000, Abcam, USA), c-Kit (1:250, Abcam, USA), β -actin (1:250, Santa Cruz Biotechnology, Germany). After washing with TBST, the membrane was exposed to the secondary antibody in the blocking buffer [goat anti rabbit IgG-HRP (1:15000, Abcam, USA)] for one hour at room temperature. The membrane was then washed in TBST and enhanced chemiluminescence

(ECL) western blotting substrate (Abcam, USA) was used for detection of the protein bands according to the manufacturer's instructions. Beta-actin protein was used as a loading control. Image J software was used to measure and compare the density of the protein bands in the experimental and control groups.

Statistical analysis

For the analysis of the real time PCR tests, the relative expression levels of the genes were calculated by the $2^{-\Delta\Delta CT}$ formula and SPSS version 16 (SPSS Ink., USA) was used for statistical analysis. All quantitative variables were expressed as mean \pm SD. The variations were evaluated using one way analysis of variance (ANOVA), Kruskal-Wallis test, Dunnett test and LSD test. For all statistical analyses, the statistical significance was set as $P=0.05$.

Results

Isolated adipose tissue-derived mesenchymal stem cells characterization

AT-MSCs were isolated from the adipose tissue around epididymis of male NMRI mice as was explained before. On the first day, the isolated cells were round shaped, but three days later, the cells became spindle-shaped and fibroblast-like. Other types of cells including endothelial and blood cells were also seen in the flask, however, these cells were eliminated during passaging (Fig.1).

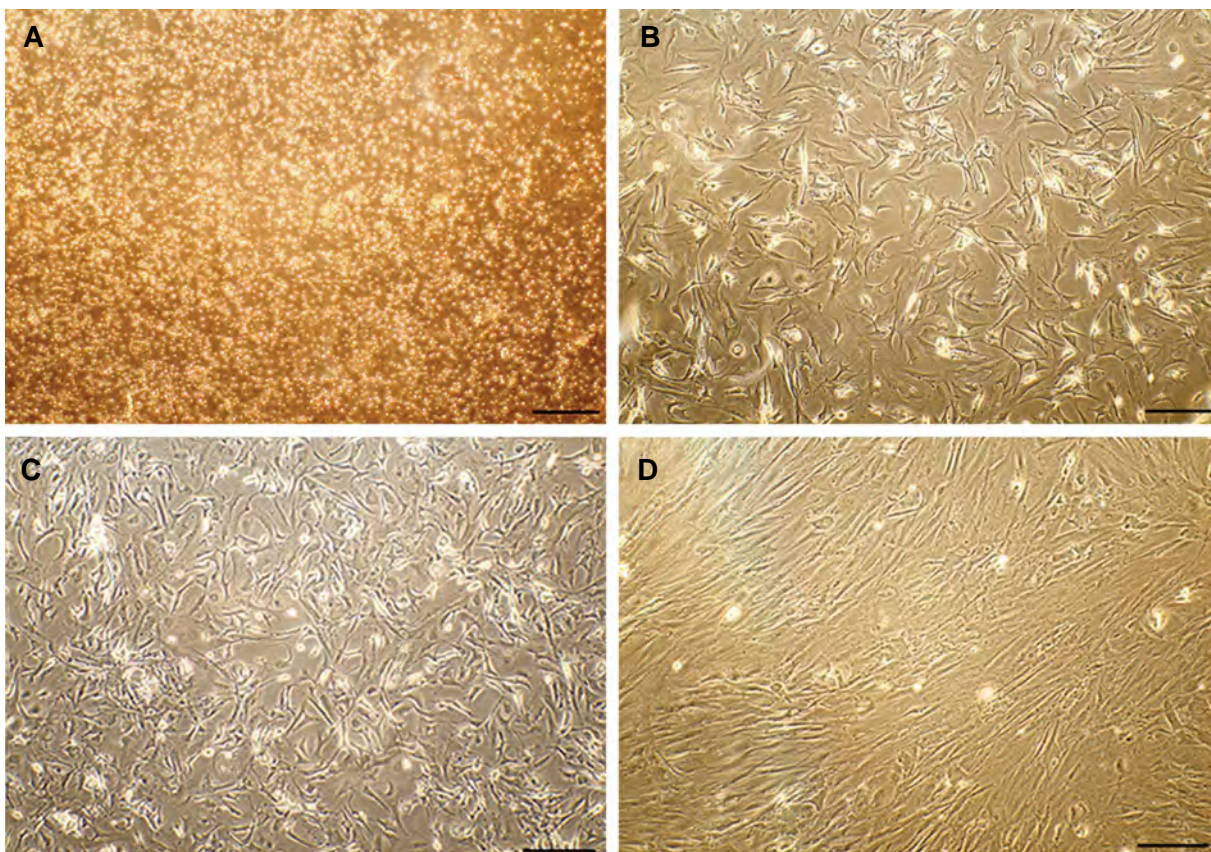


Fig.1: Morphology of the cultured adipose tissue derived mesenchymal stem cells. **A.** Day 0, **B.** Day 3, **C.** Day 5, and **D.** Passage 1 (scale bar: 100 μ m).

Nine days after the induction of adipogenic differentiation, lipid vacuoles within the cells were observed. After 14 days, the cells were stained with Oil Red O and the lipid particles turned red (Fig.2A). The first signs of change in the morphology of AT-MSCs and differentiation to osteocyte cells were seen 10 days after inducing osteogenic differentiation. After 21 days, the cells started forming calcium nodules. The cells formed mineral matrixes around themselves that were visible by Alizarin Red staining (Fig.2B). The results showed that these cells have the potentials to differentiate into both adipogenic and osteogenic lineages.

According to the results of our previous study, the isolated cells expressed high levels of CD90 and CD44 markers, and showed low expressions of CD31 and CD45. These values indicated a high level of purity of the isolated MSCs (22).

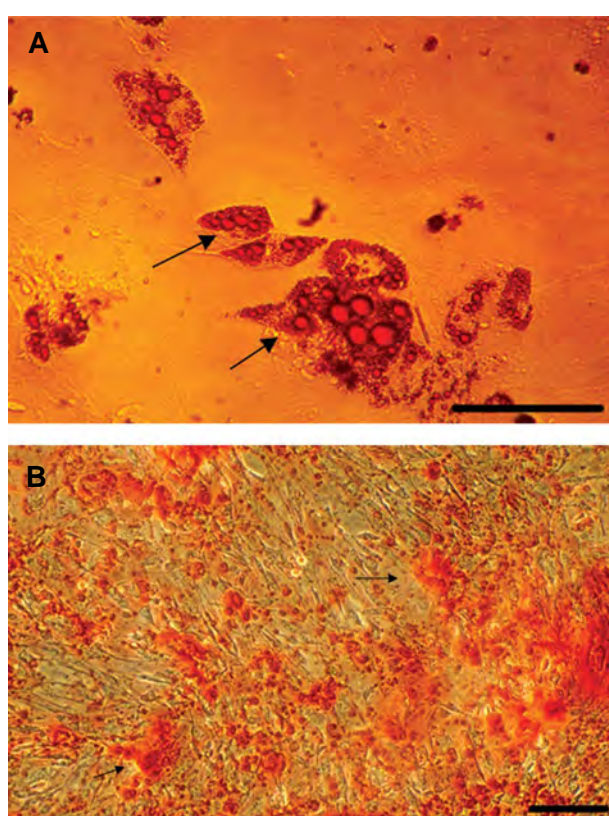


Fig.2: Adipose tissue derived mesenchymal stem cells exhibited stem cell characteristics. **A.** Adipocyte differentiation of the cells. Arrows show lipid vacuoles stained with oil red O and **B.** Differentiation of the cells into osteocytes. The arrows show the calcium nodules stained with alizarin red (scale bar: 100 μ m).

Histological analysis of recipient mice testis

Six weeks after torsion-detorsion surgery of mice, hematoxylin-eosin staining of testicle tissue sections was performed. In the seminiferous tubules of the testicular torsion-detorsion mice, most of the sperm cells were eliminated, spermatogenesis was arrested and the tubules were empty from spermatogenic cells, while Sertoli cells and seminiferous tubules structures were maintained (Fig.3). Eight weeks after cell transplantation, most of the labeled cells had survived and were resided in the basement membrane of the seminiferous tubules. Spermatogenesis process successfully occurred in seminiferous tubules and spermatogenic cells were observed in these tubules (Fig.4).

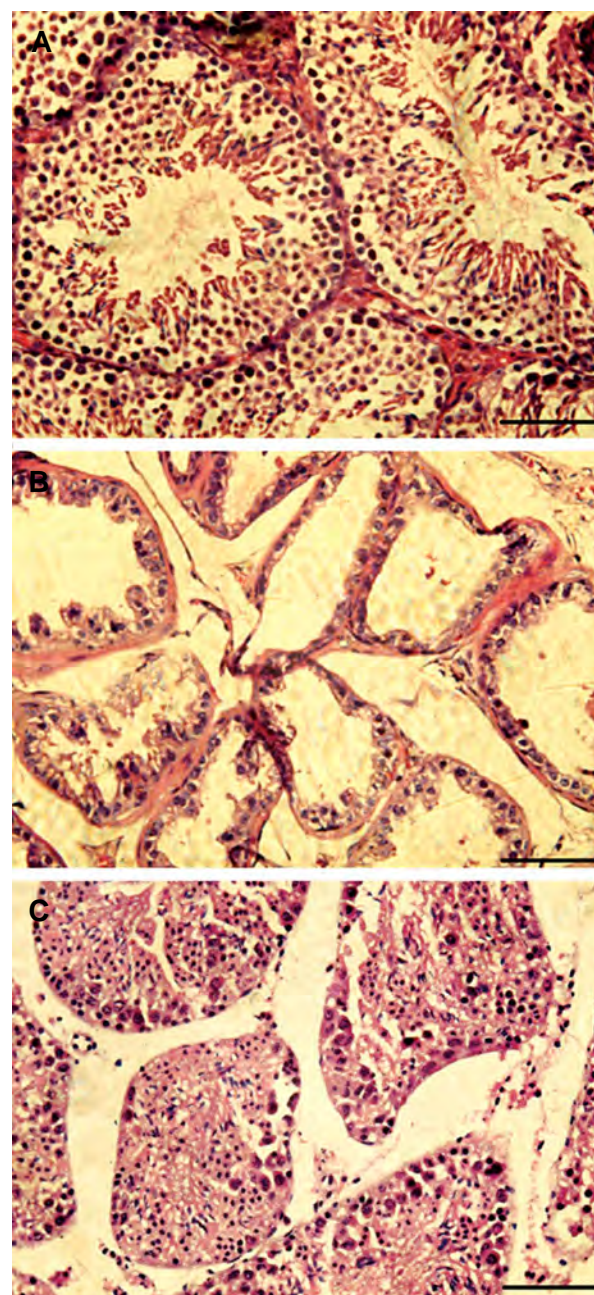


Fig.3: H&E staining of testis sections. **A.** Positive control (scale bar: 50 μ m), **B.** Torsion testis: six weeks after the torsion/detorsion, most of sperm cells were eliminated, and **C.** Cell transplanted testis after 8 weeks, spermatogenesis was observed in seminiferous tubules (scale bar: 100 μ m).

Expression of spermatogenic molecular markers in testicle of transplanted mice

The expression levels of *Gcnf* gene, a germ cell-specific marker, in both MSCs-GF ($P < 0.001$) and MSCs-T groups ($P < 0.01$) increased significantly compared to the control group. *Gcnf* gene expression in the MSCs-GF group was significantly higher than that in MSCs-T group ($P < 0.001$). The expression level of *Mvh* another germ cell-specific marker, in the MSCs-GF group was significantly higher compared to the control group ($P < 0.05$). The expression of this gene was not significantly different in the MSCs-T group. The expression levels of *Scp3* and *c-Kit* markers showed no significant difference in either experimental group compared to the control group (Fig.5).

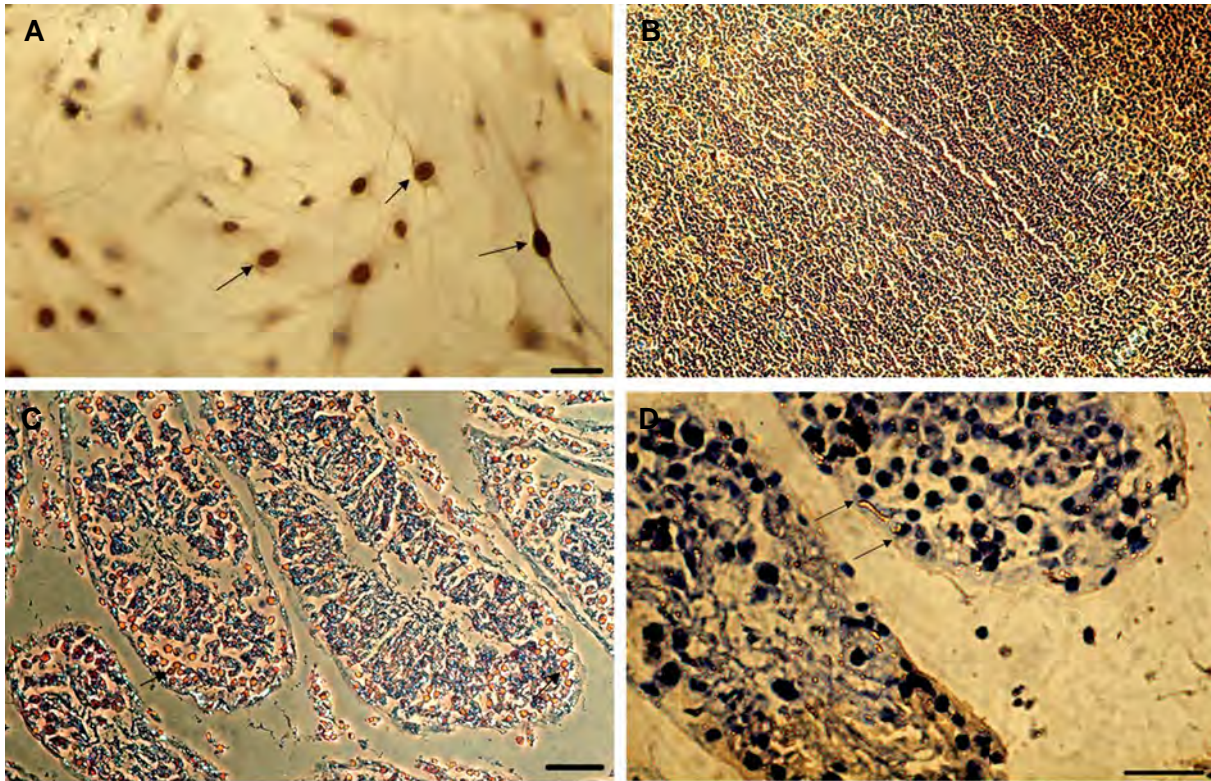


Fig.4: Bromodeoxyuridine (BrdU) staining of the cells and tissues. **A.** The labeled cells with BrdU before transplantation. Arrows show the labeled cells, **B.** Positive control, intestinal mouse cells, **C.** and **D.** BrdU labeled cells transplanted into mouse testis. Most of the cells were localized into the basement membrane of seminiferous tubules (the brown cells in C and the dark cells in D). BrdU-labeled cells are shown by arrows (scale bar: 50 μ m).

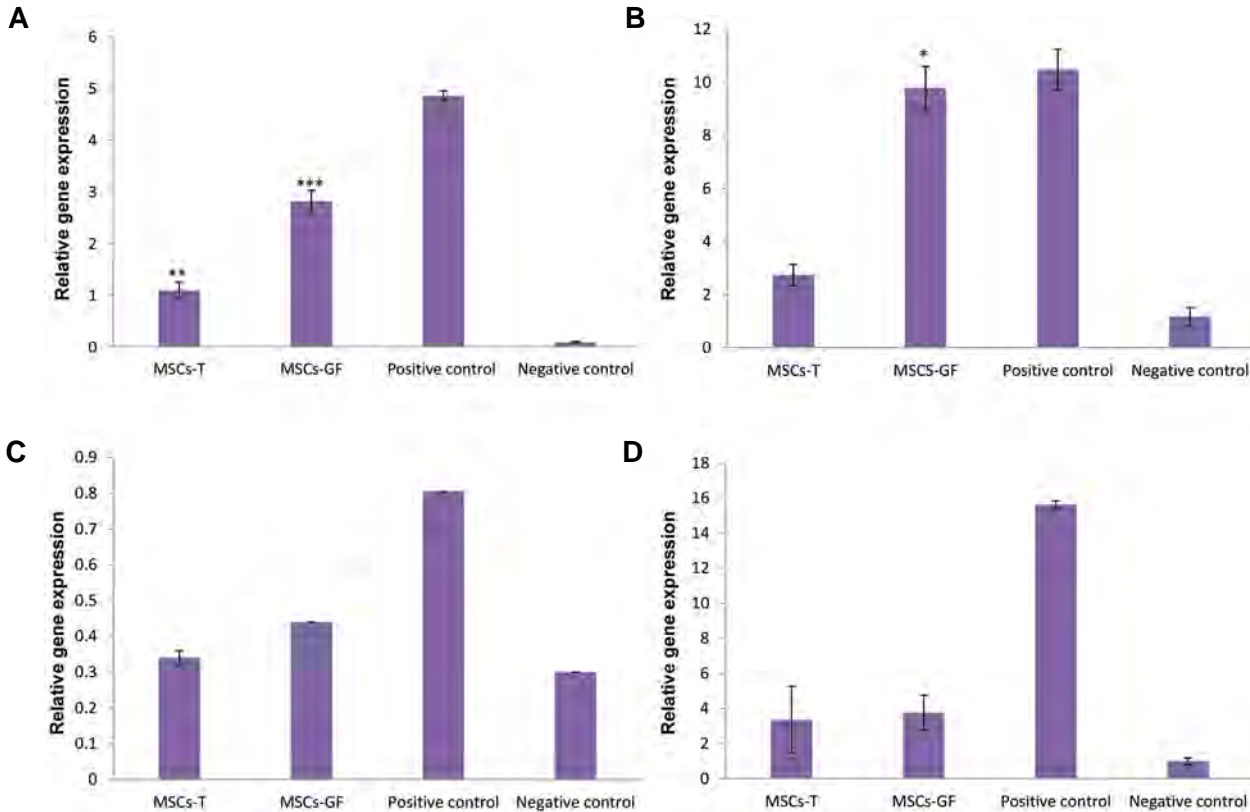


Fig.5: Expression of spermatogenic molecular markers in testicle of the transplanted mice. **A.** The *Gcnf* expression in MSCs-GF group ($P < 0.001$) and MSCs-T group ($P < 0.01$) increased compared to the control group, **B.** The expression of *Mvh*, in the MSCs-GF group showed a significantly higher level than the control group ($P < 0.05$), **C.** and **D.** Expression of *Scp3* and *c-Kit* markers showed no significant difference compared to the control group. *, $P < 0.05$, **, $P < 0.01$, ***, $P < 0.001$, MSCs; Mesenchymal stem cells, AT-MSCs; Adipose tissue-derived MSCs, MSCs-T; The group of mice injected with AT-MSCs, and MSCs-GF; The group of mice injected with AT-MSCs cultured with growth factors, torsion: negative control.

Protein analysis after adipose tissue-derived mesenchymal stem cell transplantation

c-Kit protein expression in both MSCs-GF and MSCs-T groups showed no difference compared to the control groups and confirmed the results of the real time PCR method. Expression of Gcnf protein in the MSCs-GF group was higher than the control group ($P < 0.05$), but the MSCs-T group showed no significant difference compared to the control group (Fig.6).

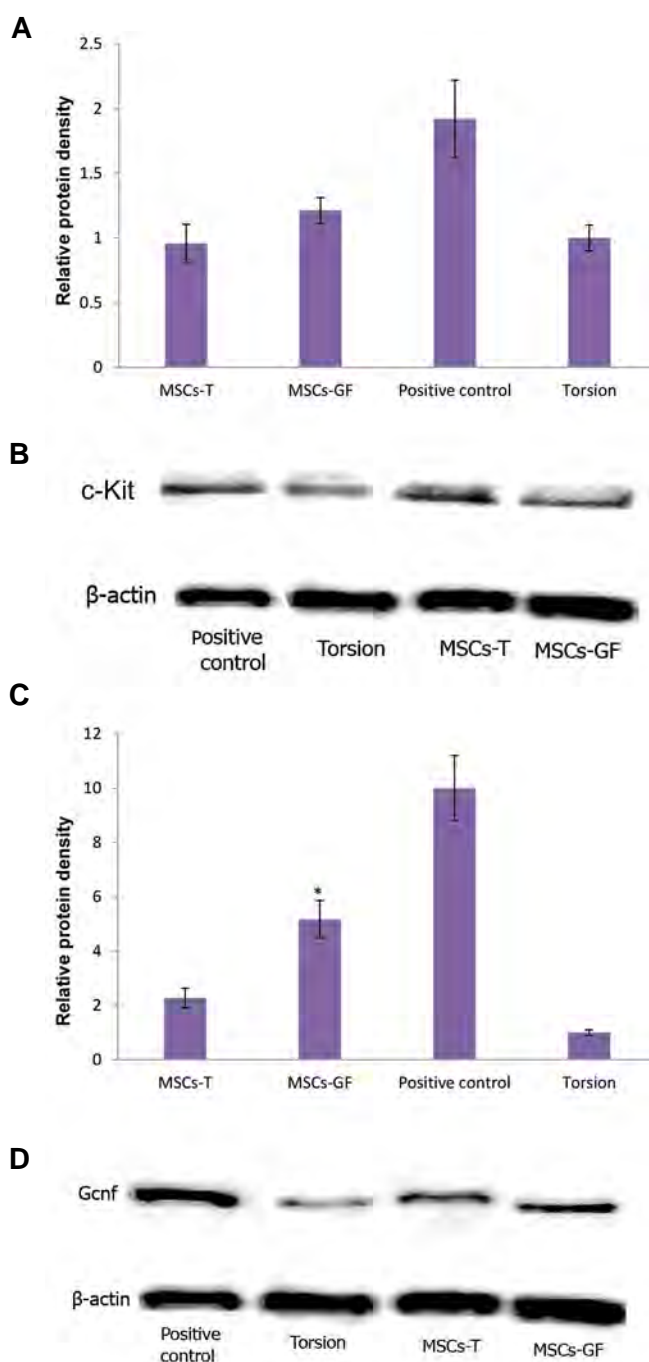


Fig.6: Western blot results. **A, B.** c-Kit protein expression results (not statistically significant), **C,** and **D.** Expression of Gcnf protein in the MSCs-GF group was higher but the MSCs-T group showed no significant difference compared to the control group. *; $P < 0.05$, MSCs; Mesenchymal stem cells, AT-MSCs; Adipose tissue-derived MSCs, MSCs-T; The group of mice that received AT-MSCs, and MSCs-GF; The group of mice that received AT-MSCs cultured with growth factors, torsion: negative control.

Discussion

Stem cell-based therapy has become one of the new potential treatment for the near future in regenerative medicine for the repair of damaged tissues and organs in many diseases such as infertility (29). AT-MSCs can be obtained easily and are highly capable of proliferation and differentiation into different lineages. These fibroblast-like cells have high immune-modulating properties. Therefore, they are considered appropriate options for autologous cell transplantation (30).

Most of the previous studies show that MSCs confer potential of spermatogenesis recovery in azoospermic animal models (5, 31-33). Nayernia et al. (9) was the first group who reported that murine (BM)-MSCs possess a high differentiating potential into male germ cells. Zhang et al. (10) demonstrated that BM-MSCs have the capability of differentiating into sperm-like cells and restoring fertility in busulfan treated azoospermic rats. Ghasemzadeh-Hasankolaei's group (34) as well as Anand et al. (35) have also reported similar results. Vahdati et al. (32) have shown that BM-MSCs revive spermatogenesis of infertile hamsters. Consistent with our results, Cakici et al. (11) also showed the restoration of the fertility of azoospermic rats after injection of AT-MSCs. Hsiao et al. (33) have reported that through inhibition of apoptosis and enhancement of testosterone secretion, MSCs prevent infertility in torsion rats. These findings indicate that MSCs successfully differentiate into germ cells in animal models and have the potentials to be used in the treatment of infertility in human patients as well.

In the present study, one group of mice was injected with AT-MSCs cultured in a medium supplemented with EGF, LIF, and GDNF growth factors. These factors increase proliferation and viability of the AT-MSCs *in vitro* (22). They are also secreted in the testicular niche that influences the proliferation process and maintenance of SSCs (17, 21). Spermatogenesis process occurs in seminiferous tubules. The core components of testicular niche include the basement membrane, Sertoli cells, peritubular myoid cells, and the extracellular signaling molecules. Sertoli cells are one of the most important of these components and provide the necessary growth factors for proliferation and maintenance of SSCs (36). We injected the cells into the seminiferous tubules of azoospermic mice. In fact, an appropriate microenvironment was provided for differentiation of MSCs. In previous studies, a busulfan-treated azoospermic mouse model was used as recipient (10, 11). One limitation of using this model is damaging seminiferous tubules structure and destroying the testicular niche, especially Sertoli cells through busulfan treatment.

Transplanted AT-MSCs migrate to the basement membrane of seminiferous tubules. They are affected by the seminiferous tubules niche and factors secreted by Sertoli cells, and begin to differentiate. In studies conducted by Zhang et al. (10) and Cakici et al. (11), a small number of the cells remained in the basement

membrane after injection. However, in our study, after 8 weeks, a large number of AT-MSCs were resided in the seminiferous tubules basement membrane, which can be due to the increase of viability of the cells induced by the growth factors as well as an appropriate mouse model, in which the structure of seminiferous tubules and testicular niche have been maintained.

After 8 weeks, *Gcnf* gene expression in the cell-transplanted groups (MSCs-GF and MSCs-T) was significantly higher compared to the control group. Interestingly, MSCs-GF group showed further increased expression of the germ cell-specific markers (*Mvh*, *Gcnf*). It could be due to the impact of the growth factors on viability of the cells. In addition, EGF, LIF, and GDNF are secreted from sertoli cells and testicular niches (17, 21). Therefore, they are probably effective in the process of differentiation of the injected cells into germ cells. Expression of *c-Kit* and *Scp3* genes in the AT-MSC recipient groups did not significantly differ from the control group. These genes are related to the final stages of sperm differentiation (37). However, this could be due to our short tracking time. Zhang et al. (10) showed increased expression of *Mvh* and *Gcnf* factors in the testicular tissues and reported that *c-Kit* expression was reduced after 8 weeks. The exact mechanism of function of the transplanted MSCs has not been specified. There are several possibilities in this regard: i. MSCs are differentiated into target tissue cells under the influence of their niche (38), ii. MSCs secrete factors, which stimulate inner stem cells or lead to revival of damaged tissue (7), and iii. In the case of infertility, MSCs can prevent infertility by inhibition of oxidative stress and apoptosis (33).

The observations in the present study may indicate that the injected AT-MSCs have entered spermatogenic pathway or have revived damaged testicular tissue and SSCs by secretion of trophic factors. To determine its exact mechanism, the cells should be tracked over a longer period of time in the future studies.

Conclusion

This study showed that the transplanted AT-MSCs were localized in the basement membrane of seminiferous tubules. The testicles of the mice injected with AT-MSCs expressed spermatogenesis-specific markers. The mice that received cells that were cultured in the presence of growth factors showed overexpression of germ cell-specific markers. According to these results, the use of EGF, LIF and, GDNF to culture AT-MSCs can be very helpful in terms of MSC survival and localization, but further preclinical studies in different animal models and with different time points are needed to develop an effective clinical application.

Acknowledgements

This study was funded by a grant from Physiology Research Center, Jundishapur University of Medical

Science, Ahvaz, Iran (grant number: CMRC-9432). The authors declare no conflict of interest.

Authors' Contributions

G.S., M.H., M.E.D.; Contributed to conception and design. M.E.D.; Contributed to all experimental work, data and statistical analysis, and interpretation of data. J.M.; Contributed to primer design and real time PCR. A.K.; Contributed to selection of antibodies for the western blot technique. G.S.; Supervised the experimental, data collection, and writing processes. M.H.; Drafted the manuscript, which was revised by G.S. All authors have read and approved the final version of the manuscript.

References

- Gudeloglu A, Parekattil SJ. Update in the evaluation of the azoospermic male. *Clinics (Sao Paulo)*. 2013; 68 Suppl 1: 27-34.
- Cocuzza M, Alvarenga C, Pagani R. The epidemiology and etiology of azoospermia. *Clinics (Sao Paulo)*. 2013; 68 Suppl 1: 15-26.
- Lacham-Kaplan O, Chy H, Trounson A. Testicular cell conditioned medium supports differentiation of embryonic stem cells into ovarian structures containing oocytes. *Stem Cells*. 2006; 24(2): 266-273.
- Nayernia K, Nolte J, Michelmann HW, Lee JH, Rathsack K, Drusenheimer N, et al. In vitro-differentiated embryonic stem cells give rise to male gametes that can generate offspring mice. *Dev Cell*. 2006; 11(1): 125-132.
- Abd Allah SH, Pasha HF, Abdelrahman AA, Mazen NF. Molecular effect of human umbilical cord blood CD34-positive and CD34-negative stem cells and their conjugate in azoospermic mice. *Mol Cell Biochem*. 2017; 428(1-2): 179-191.
- Ghasemzadeh-Hasankolaei M, Eslaminejad MB, Sedighi-Gilani M. Derivation of male germ cells from ram bone marrow mesenchymal stem cells by three different methods and evaluation of their fate after transplantation into the testis. *In Vitro Cell Dev Biol Anim*. 2016; 52(1): 49-61.
- Leatherman J. Stem cells supporting other stem cells. *Front Genet*. 2013; 4: 257.
- Hua J, Pan S, Yang C, Dong W, Dou Z, Sidhu KS. Derivation of male germ cell-like lineage from human fetal bone marrow stem cells. *Reprod Biomed Online*. 2009; 19(1): 99-105.
- Nayernia K, Lee JH, Drusenheimer N, Nolte J, Wulf G, Dressel R, et al. Derivation of male germ cells from bone marrow stem cells. *Lab Invest*. 2006; 86(7): 654-663.
- Zhang D, Liu X, Peng J, He D, Lin T, Zhu J, et al. Potential spermatogenesis recovery with bone marrow mesenchymal stem cells in an azoospermic rat model. *Int J Mol Sci*. 2014; 15(8): 13151-13165.
- Cakici C, Buyrukcu B, Duruksu G, Haliloglu AH, Aksoy A, Isik A, et al. Recovery of fertility in azoospermia rats after injection of adipose-tissue-derived mesenchymal stem cells: the sperm generation. *Biomed Res Int*. 2013; 2013: 529589.
- Ksiazek K. A comprehensive review on mesenchymal stem cell growth and senescence. *Rejuvenation Res*. 2009; 12(2): 105-116.
- Hu F, Wang X, Liang G, Lv L, Zhu Y, Sun B, et al. Effects of epidermal growth factor and basic fibroblast growth factor on the proliferation and osteogenic and neural differentiation of adipose-derived stem cells. *Cell Reprogram*. 2013; 15(3): 224-232.
- Tamama K, Fan VH, Griffith LG, Blair HC, Wells A. Epidermal growth factor as a candidate for ex vivo expansion of bone marrow-derived mesenchymal stem cells. *Stem Cells*. 2006; 24(3): 686-695.
- Shlush E, Maghen L, Swanson S, Kenigsberg S, Moskovtsev S, Barretto T, et al. In vitro generation of Sertoli-like and haploid spermatid-like cells from human umbilical cord perivascular cells. *Stem Cell Res Ther*. 2017; 8(1): 37.
- Abé K, Eto K, Abé S. Epidermal growth factor mediates spermatogonial proliferation in newt testis. *Reprod Biol Endocrinol*. 2008; 6: 7.
- Uguralp S, Bay Karabulut A, Mizrak B, Kaymaz F, Kiziltay A, Hasirci N. The effect of sustained and local administration of epidermal growth factor on improving bilateral testicular tissue after torsion.

- Urol Res. 2004; 32(5): 323-331.
18. Williams RL, Hilton DJ, Pease S, Willson TA, Stewart CL, Gearing DP, et al. Myeloid leukaemia inhibitory factor maintains the developmental potential of embryonic stem cells. *Nature*. 1988; 336(6200): 684-687.
 19. Jiang Y, Vaessen B, Lenvik T, Blackstad M, Reyes M, Verfaillie CM. Multipotent progenitor cells can be isolated from postnatal murine bone marrow, muscle, and brain. *Exp Hematol*. 2002; 30(8): 896-904.
 20. Golden JP, DeMaro JA, Osborne PA, Milbrandt J, Johnson EM Jr. Expression of neurturin, GDNF, and GDNF family-receptor mRNA in the developing and mature mouse. *Exp Neurol*. 1999; 158(2): 504-528.
 21. Hofmann MC, Braydich-Stolle L, Dym M. Isolation of male germline stem cells; influence of GDNF. *Dev Biol*. 2005; 279(1): 114-124.
 22. Eliyasi Dashtaki M, Kazemi Nezhad SR, Hemadi M, Saki G, Mohammadiasl J. Effects of Epidermal growth factor, glial cell line-derived neurotrophic and leukemia inhibitory factor on the proliferation and differentiation potential of adipose tissue-derived mesenchymal stem cells. *Iran Red Crescent Med J*. 2018; 20(1): e55943.
 23. Tholpady SS, Katz AJ, Ogle RC. Mesenchymal stem cells from rat visceral fat exhibit multipotential differentiation in vitro. *Anat Rec A Discov Mol Cell Evol Biol*. 2003; 272(1): 398-402.
 24. Hankamolsiri W, Manochantr S, Tantrawatpan C, Tantikanlayaporn D, Tapanadechopone P, Kheolamai P. The effects of high glucose on adipogenic and osteogenic differentiation of gestational tissue-derived MSCs. *Stem Cells Int*. 2016; 2016: 9674614.
 25. Nagyova M, Slovinska L, Blasko J, Grulova I, Kuricova M, Cigankova V, et al. A comparative study of PKH67, Dil, and BrdU labeling techniques for tracing rat mesenchymal stem cells. *In Vitro Cell Dev Biol Anim*. 2014; 50(7): 656-663.
 26. Azizollahi S, Aflatoonian R, Sedigi-Gilani MA, Jafarabadi MA, Behnam B, Azizollahi G, et al. Recruiting testicular torsion introduces an azoospermic mouse model for spermatogonial stem cell transplantation. *Urol J*. 2014; 11(3): 1648-1655.
 27. Cay A, Alver A, Küçük M, Işık O, Eminağaoğlu MS, Karahan SC, et al. The effects of N-acetylcysteine on antioxidant enzyme activities in experimental testicular torsion. *J Surg Res*. 2006; 131(2): 199-203.
 28. Cardiff RD, Miller CH, Munn RJ. Manual hematoxylin and eosin staining of mouse tissue sections. *Cold Spring Harb Protoc*. 2014; 2014(6): 655-658.
 29. Pfister O, Della Verde G, Liao R, Kuster GM. Regenerative therapy for cardiovascular disease. *Transl Res*. 2014; 163(4): 307-320.
 30. Ullah I, Subbarao R B, Rho G J. Human mesenchymal stem cells-current trends and future prospective. *Biosci Rep*. 2015; 35(2). pii: e00191.
 31. Karimaghani N, Tamadon A, Rahmanifar F, Mehrabani D, Raayat Jahromi A, Zare S, et al. Spermatogenesis after transplantation of adipose tissue-derived mesenchymal stem cells in busulfan-induced azoospermic hamster. *Iran J Basic Med Sci*. 2018; 21(7): 660-667.
 32. Vahdati A, Fathi A, Hajihoseini M, Aliborzi G, Hosseini E. The regenerative effect of bone marrow-derived stem cells in spermatogenesis of infertile hamster. *World J Plast Surg*. 2017; 6(1): 18-25.
 33. Hsiao CH, Ji AT, Chang CC, Cheng CJ, Lee LM, Ho JH. Local injection of mesenchymal stem cells protects testicular torsion-induced germ cell injury. *Stem Cell Res Ther*. 2015; 6: 113.
 34. Ghasemzadeh-Hasankolaei M, Batavani R, Eslaminejad MB, Sayahpour F. Transplantation of autologous bone marrow mesenchymal stem cells into the testes of infertile male rats and new germ cell formation. *Int J Stem Cells*. 2016; 9(2): 250-263.
 35. Anand S, Bhartiya D, Sriraman K, Mallick A. Underlying Mechanisms that restore spermatogenesis on transplanting healthy niche cells in busulphan treated mouse testis. *Stem Cell Rev*. 2016; 12(6): 682-697.
 36. Ebata KT, Yeh JR, Zhang X, Nagano MC. Soluble growth factors stimulate spermatogonial stem cell divisions that maintain a stem cell pool and produce progenitors in vitro. *Exp Cell Res*. 2011; 317(10): 1319-1329.
 37. Jan SZ, Hamer G, Repping S, de Rooij DG, van Pelt AM, Vormer TL. Molecular control of rodent spermatogenesis. *Biochim Biophys Acta*. 2012; 1822(12): 1838-1850.
 38. Gneccchi M, Melo LG. Bone marrow-derived mesenchymal stem cells: isolation, expansion, characterization, viral transduction, and production of conditioned medium. *Methods Mol Biol*. 2009; 482: 281-294.

Three-Dimensional Culture of Mouse Spermatogonial Stem Cells Using A Decellularised Testicular Scaffold

Nasrin Majidi Gharenaz, Ph.D.¹, Mansoureh Movahedin, Ph.D.^{1*}, Zohreh Mazaheri, Ph.D.²

1. Department of Anatomical Sciences, Faculty of Medical Sciences, Tarbiat Modares University, Tehran, Iran
2. Basic Medical Science Research Center, Histogenotech Company, Tehran, Iran

*Corresponding Address: P.O.Box: 14115-175, Department of Anatomical Sciences, Faculty of Medical Sciences, Tarbiat Modares University, Tehran, Iran
Email: movahed.m@modares.ac.ir

Received: 18/August/2018, Accepted: 17/November/2018

Abstract

Objective: Applications of biological scaffolds for regenerative medicine are increasing. Such scaffolds improve cell attachment, migration, proliferation and differentiation. In the current study decellularised mouse whole testis was used as a natural 3 dimensional (3D) scaffold for culturing spermatogonial stem cells.

Materials and Methods: In this experimental study, adult mouse whole testes were decellularised using sodium dodecyl sulfate (SDS) and Triton X-100. The efficiency of decellularisation was determined by histology and DNA quantification. Masson's trichrome staining, alcian blue staining, and immunohistochemistry (IHC) were done for validation of extracellular matrix (ECM) proteins. These scaffolds were recellularised through injection of mouse spermatogonial stem cells in to rete testis. Then, they were cultured for eight weeks. Recellularised scaffolds were assessed by histology, real-time polymerase chain reaction (PCR) and IHC.

Results: Haematoxylin-eosin (H&E) staining showed that the cells were successfully removed by SDS and Triton X-100. DNA content analysis indicated that 98% of the DNA was removed from the testis. This confirmed that our decellularisation protocol was efficient. Masson's trichrome and alcian blue staining respectively showed that glycosaminoglycans (GAGs) and collagen are preserved in the scaffolds. IHC analysis confirmed the preservation of fibronectin, collagen IV, and laminin. MTT assay indicated that the scaffolds were cell-compatible. Histological evaluation of recellularised scaffolds showed that injected cells were settled on the basement membrane of the seminiferous tubule. Analyses of gene expression using real-time PCR indicated that expression of the *Plzf* gene was unchanged over the time while expression of *Sycp3* gene was increased significantly ($P=0.003$) after eight weeks in culture, suggesting that the spermatogonial stem cells started meiosis. IHC confirmed that PLZF-positive cells (spermatogonial stem cells) and SYCP3-positive cells (spermatocytes) were present in seminiferous tubules.

Conclusion: Spermatogonial stem cells could proliferate and differentiated in to spermatocytes after being injected in the decellularised testicular scaffolds.

Keywords: Extracellular Matrix, Scaffold, Spermatogonial Cells, Testis

Cell Journal (Yakhteh), Vol 21, No 4, January-March (Winter) 2020, Pages: 410-418

Citation: Majidi Gharenaz N, Movahedin M, Mazaheri Z. Three-dimensional culture of mouse spermatogonial stem cells using a decellularised testicular scaffold. Cell J. 2020; 21(4): 410-418. doi: 10.22074/cellj.2020.6304.

Introduction

The process of spermatogenesis is regulated by the endocrine system and testicular paracrine factors (1). In this process, germ cells are in contact with basement membrane and somatic cells that were located in seminiferous tubules. Hormonal and paracrine factors along with Sertoli cells and basement membrane are the main component of specialized microenvironment called a niche that promotes self-renewal of germ cells (2, 3). Impairment of each of these hormones and factors could lead to infertility.

In order to study the biology of spermatogonial stem cells and for a better-understanding of factors that regulate male fertility, *in vitro* culture techniques are commonly used (4). The chosen *in vitro* culture system for establishment of spermatogenesis should provide the right situation for communication between somatic and germ cells and the extracellular matrix (ECM). This could provide an environment similar to somniferous tubules of the testis (5). So, in order to mimic the local microenvironment for homing and attachment of germ

and somatic cells, biological scaffolds and growth factors could be considered. These scaffolds have been successfully used for the regeneration of several organs including the lungs, pancreas, liver, and small veins (6, 7). Biological scaffolds are produced by decellularisation of actual tissues. In this process, the cells are removed from the tissues while the ECM components remain on what is referred to as a scaffold (8). These proteins provide structural and biochemical support for cell adhesion, proliferation, migration, and cell to cell interactions. Therefore, development of biological and biocompatible scaffolds could be beneficial for *in vitro* culture systems of germ cells. In recent years, applications of these scaffolds for *in vitro* spermatogenesis have been considered. Baert et al. (9) demonstrated natural testicular scaffold could support the self-assembly of human testicular cells to organoid structures. However, they reported that seeding testicular cells on decellularised scaffolds could not produce a testis with a typical cytoarchitecture.

In another paper, Sertoli cells (10) were seeded on a testicular scaffold. Their results showed that the testicular

scaffold could increase the proliferative activity of the Sertoli cells. They did not, however, investigate the spermatogonial stem cells differentiation in the presence of testicular scaffolds. In the present study mouse spermatogonial stem cells were injected in to whole testicular scaffolds via efferent ductuli, then cultured on agarose gels for evaluation of spermatogonial stem cells differentiation.

Materials and Methods

Testes donors

In this experimental study, fifteen male Naval Medical Research Institute (NMRI) mice (8 weeks old) were used for the production of whole testicular scaffolds. The mice were in an animal house under controlled conditions (12 hour light/dark cycles). All animal procedures were conducted using guidelines approved by the Ethical Committee of Medical Sciences Faculty at the Tarbiat Modares University (Permission No. IR.TMU.REC.1394.269).

Organ harvest and decellularisation protocol

Mice were euthanized using chloroform, then sacrificed by cervical dislocation. Subsequently, testes were removed from the mice. The capsules of the testes were perforated using an insulin syringe (29 gauge) and then washed with phosphate-buffered saline (PBS, Invitrogen, Switzerland) to remove residual blood. Decellularisation was done at 25°C using an orbital shaker (50 rpm). The washed testes were immersed in 0.5% (v/v) sodium dodecyl sulfate (SDS, Sigma, USA), then in 0.5% (v/v) Triton X-100 (Sigma, USA), both of which had been diluted in distilled water for 18 hours. Next, the scaffolds were washed extensively with PBS for 24 hours. Decellularised scaffolds were disinfected by 0.1% peracetic acid in 4% ethanol for 2 hours, and washed three times in sterile PBS for 4 hours each (11).

Scaffolds analyses

Fixation of the scaffolds was performed by incubation in 10% formalin solution in PBS at 25°C for 24–48 hours. The fixed scaffolds were then dehydrated by incubation in graded alcohol (each alcohol for 20 minutes). After embedding them in paraffin, they were cut into 5 µm-thick sections for histological evaluation. H&E (Sigma, USA) staining was performed on paraffin sections for evaluation of detergent efficacy to remove the cells and debris from the testes. Preservation of glycosaminoglycans (GAGs) and collagen in decellularised scaffolds were assessed by alcian blue (Sigma, USA) and Masson's trichrome staining (Sigma, USA), respectively. Alcian blue was diluted 1:100 in hydrochloric acid (0.1 M). On these samples nuclear fast red (Sigma, USA) was used for counter-staining (12, 13). Also, preservation of ECM proteins, including fibronectin, collagen IV, and laminin in decellularised scaffolds was evaluated by immunohistochemistry (IHC). Initially, the sections were transferred to a 60°C oven for de-waxing, then further cleared in xylene. Later,

they were rehydrated by alcohol gradient and washing in water. Then they were incubated in citrate (10 mM pH=6.0) for 20 min for antigen retrieval. Then the samples were permeabilized by triton X-100 for 40 minutes and incubated with anti-fibronectin (mouse monoclonal IgG, Elabscience Biotechnology Inc., USA), anti-collagen IV (mouse monoclonal IgG, Elabscience Biotechnology Inc., USA), and anti-laminin (rabbit polyclonal IgG, Abcam, USA). The secondary antibody was Alexa Fluor 488 (goat anti-mouse IgG, Invitrogen, USA) and Texas Red (Goat anti-rabbit IgG, Abcam, USA). Photomicrographs were taken with an Olympus microscope (Olympus, Center Valley, PA, USA).

Analysis of DNA content

DNA was isolated from 25 mg wet weight of intact and decellularised testes using a QIAamp DNA Mini Kit (Qiagen, Germany) (14). The concentration of DNA content was measured using a NanoDrop 2000 C UV-Vis spectrophotometer (Thermo Scientific, Venlo, Netherlands) at 260 nm. Each experiment was repeated five times.

DAPI staining

Intact and decellularised testes were evaluated using 0.5 mg/mL blue-fluorescent 4, 6-diamidino-2-phenylindole (DAPI, Sigma, USA) for visualizing dsDNA. The DAPI solutions were diluted in PBS to 30 nM and were pipetted directly on each tissue section. They were kept in a dark room for 30 minutes. After washing with PBS, the slides were examined using an inverted fluorescence microscope (15).

Cytotoxicity assay

Cytotoxicity of the scaffolds was evaluated by 3-[4, 5-dimethyl (thiazol-2-yl)-3,5-diphenyl] tetrazolium bromide (MTT, Sigma, USA) test, which assesses the viability of the cells. The scaffolds were cut into 2×2×2 mm³ fragments and placed in a 96-well plate. Mouse embryonic fibroblast (MEF) cells were isolated according to Jozefczuk's protocol (16). Then, 3×10⁴ cells per well were seeded on the testicular scaffolds and cultivated in DMEM containing 10% fetal bovine serum (FBS, Gibco, Germany) for 72 hours. MTT assay was performed after 24 and 72 hours using the following protocol. Initially, 200 µL of medium containing MTT (0.5 mg/mL) was added to each well. Then they were incubated at 37°C for 4 hours for formazan formation. After removing the medium, the obtained formazan was dissolved in dimethyl sulfoxide (DMSO, Sigma, USA). The optical density (OD) of the supernatants was measured using a microplate reader (Beckman, Fullerton, CA) at 570 nm. Five replicates were performed for each sample (17).

Recellularization of testicular scaffolds

Isolation and culture of spermatogonial stem cells

After euthanizing 5 male NMRI mouse pups (6 days

old), their testes were removed and placed immediately in a 3.5-cm dish containing PBS and were cooled on ice. Spermatogonial stem cells were isolated according to the protocol described by Mirzapour et al (18) and subjected to a two-step enzymatic digestion with 0.5 mg/ml trypsin, 0.5 mg/ml collagenase IV and 0.5 mg/ml hyaluronidase (all from Sigma, USA). For cell viability assay, a sample of the cells was mixed with trypan blue and transferred to a hemocytometer, where the live unstained cells were counted under a light microscope. Following the enzymatic digestion step, the cell suspension was cultivated in alpha minimum essential medium (α MEM, Bio-Ideal, Iran) supplemented with 10% FBS at 34°C in 5% CO₂ for two weeks.

Identification of spermatogonial stem cells

The identity of the isolated spermatogonial stem cells was verified by tracing the PLZF protein (19) in the obtained colonies from the cell suspension after two weeks in culture. Fixed cells were incubated overnight with a mouse monoclonal anti-PLZF antibody (mouse monoclonal IgG, sc-28319 Santa Cruz Biotechnology, USA, diluted 1:100) at 37°C. Following PBS washes they were incubated with an Alexa 488-conjugated secondary antibody (goat anti-mouse IgG, USA, diluted 1:200 in PBS) for 1 hour in the dark at 25°C. Nuclei were stained by propidium iodide (PI).

In vitro transplantation of spermatogonial stem cells in to whole testicular scaffolds

Initially, the cell suspension was stained with trypan blue, then 10 μ l of the stained cells were injected by a glass needle into the end of the efferent ductuli and the opening of the rete decellularised testes. Then recellularized testicular scaffolds were cut into 1×1×1 mm pieces under a stereomicroscope and cultured on agarose gel. An agarose support layer and a culture medium with specific compositions and growth factors were prepared according to the protocol by Yokonishi and colleagues (20). The culture medium supplemented with 10% knockout serum replacement (KSR, USA), 60 ng/ml progesterone (Invitrogen, UK), 30 ng/ml beta-estradiol (Pepro Tech, USA), 20 ng/ml epithelial growth factor (EGF, Pepro Tech, USA), 10 ng/ml basic fibroblast growth factor (bFGF, Pepro Tech, USA), and 10 ng/ml leukemia inhibitory factor (LIF, Royan, Iran). Pieces of the recellularized scaffolds were placed gently in the middle of the agarose layer to prevent them from floating. They were cultivated under static

conditions at 37°C with 5% CO₂ for up to 8 weeks. Cell-free testicular scaffolds were cultured under the same conditions as the control. The culture medium was replaced with fresh medium twice a week. The samples (20 pieces) were collected for histological and molecular evaluation at the end of the second and eighth weeks of culturing.

Histology and immunohistochemistry

Recellularized testicular scaffolds and intact testes as the positive control group were fixed in 10% formalin solution in PBS at 25°C for 24-48 hours. Then samples were dehydrated by graded alcohol. After embedding in paraffin, they were cut into 5 μ m-thick sections for histological evaluation. H&E staining was performed on samples cultured for two and eight weeks. For IHC, primary antibody PLZF (mouse monoclonal IgG, sc-28319 Santa Cruz Biotechnology, USA, diluted 1:100) and SYCP3 (mouse monoclonal IgG, Santa Cruz Biotechnology, USA, diluted 1:100) were used. The secondary antibody was Alexa Fluor 488 (goat anti-mouse IgG, Invitrogen, USA) and the nuclear stain DAPI (Life Technologies, USA) was used for counterstaining. Photomicrographs were taken with an Olympus Microscope (Olympus, Center Valley, PA).

Real-time polymerase chain reaction studies for analysis of gene expression

The expression of *Plzf* and *Sycp3* genes were assessed by real-time PCR. For extraction of total RNA from samples, RNX-Plus™ KIT (Cinna Gen, Iran) was used, then RNA was treated with DNase I (Fermentase, USA) to remove the genomic contamination. The RNA concentrations were measured by a biophotometer (Eppendorf, USA). cDNA was synthesized from 1000 ng RNA using a cDNA kit (Fermentase, Germany) (21). Primers for *Plzf* and *Sycp3* genes were designed using the NCBI website and were synthesized by Cinna Gen (Iran, Table 1). The PCR reactions were done using Master Mix and SYBR Green (Fluka, Switzerland) in a StepOne™ thermal cycler (Applied Biosystems, USA). Melting curve analyses were used for confirmation of the quality of the PCR reactions. A standard curve was used to determine the efficiency of each gene (logarithmic dilution of cDNA from the samples). In addition, this process was repeated in triplicates for all the target and reference (*β -actin*) genes. The target genes were normalized to the reference gene.

Table 1: Primer sequences for real time- polymerase chain reaction

Gene	Primer sequence (5'-3')	Accession number	Product length
<i>β-actin</i>	F:TTACTGAGCTGCGTTTTACAC R:ACAAAGCCATGCCAATGTTG	NM_007393.5	90
<i>Plzf</i>	F:GCTGCTGTCTCTGTGATGG R:GGGCTGATGGAACATAGGGG	NM_001033324.3	153
<i>Sycp3</i>	F:TCAGCAGAGAGCTTGGTCGG R:GATGTTTGCTCAGCGGCTCC	NM_011517.21	118

Statistical analysis

All data are presented as mean values \pm standard error. SPSS software (version 16.0, Chicago, USA) was used for data analysis. DNA content and MTT data analysis were conducted using an independent sample t test. Real-time PCR data analysis was performed by one-way analysis of variance (ANOVA) followed by Tukey's post hoc test. Three replicates were done per sample. $P \leq 0.05$ was considered statistically significant.

Results

Characterization of decellularised testicular scaffolds

Macroscopically decellularised testes, which retained the gross shape of the whole organ, were completely translucent (Fig.1A), while intact testes were opaque (Fig.1B). Histological evaluation by H&E staining showed that the cells were removed by SDS and Triton X-100 (Fig.1C). Intact testes were stained as control (Fig.1D). In order to evaluate the efficiency of the

decellularisation protocol more accurately, DNA content was measured as well. Analysis of DNA content indicated that approximately 98% of the DNA was successfully removed from the testes. This further confirmed that our decellularisation protocol was efficient (Fig.1E). Masson's trichrome staining showed blue stained collagen fibers in the decellularised testes, while no red stained areas, which would indicate cell residues, were observed (Fig.1F). Intact testes were stained as control (Fig.1G). The maintenance of GAGs in scaffolds was assessed by alcian blue staining, which demonstrated that GAGs were in fact preserved (Fig.1H). Intact testes were stained as control (Fig.1I). IHC staining verified the preservation of fibronectin (Fig.2A, B), collagen IV (Fig.2C, D), and laminin (Fig.2E, F) in the decellularised testes and intact testes respectively, with no detectable DAPI staining (Fig.2G) in the decellularised testes. Intact testes were stained as control (Fig.2H). These findings suggest that cellular elements were eliminated completely while ECM proteins including fibronectin, Collagen IV, and laminin have remained.

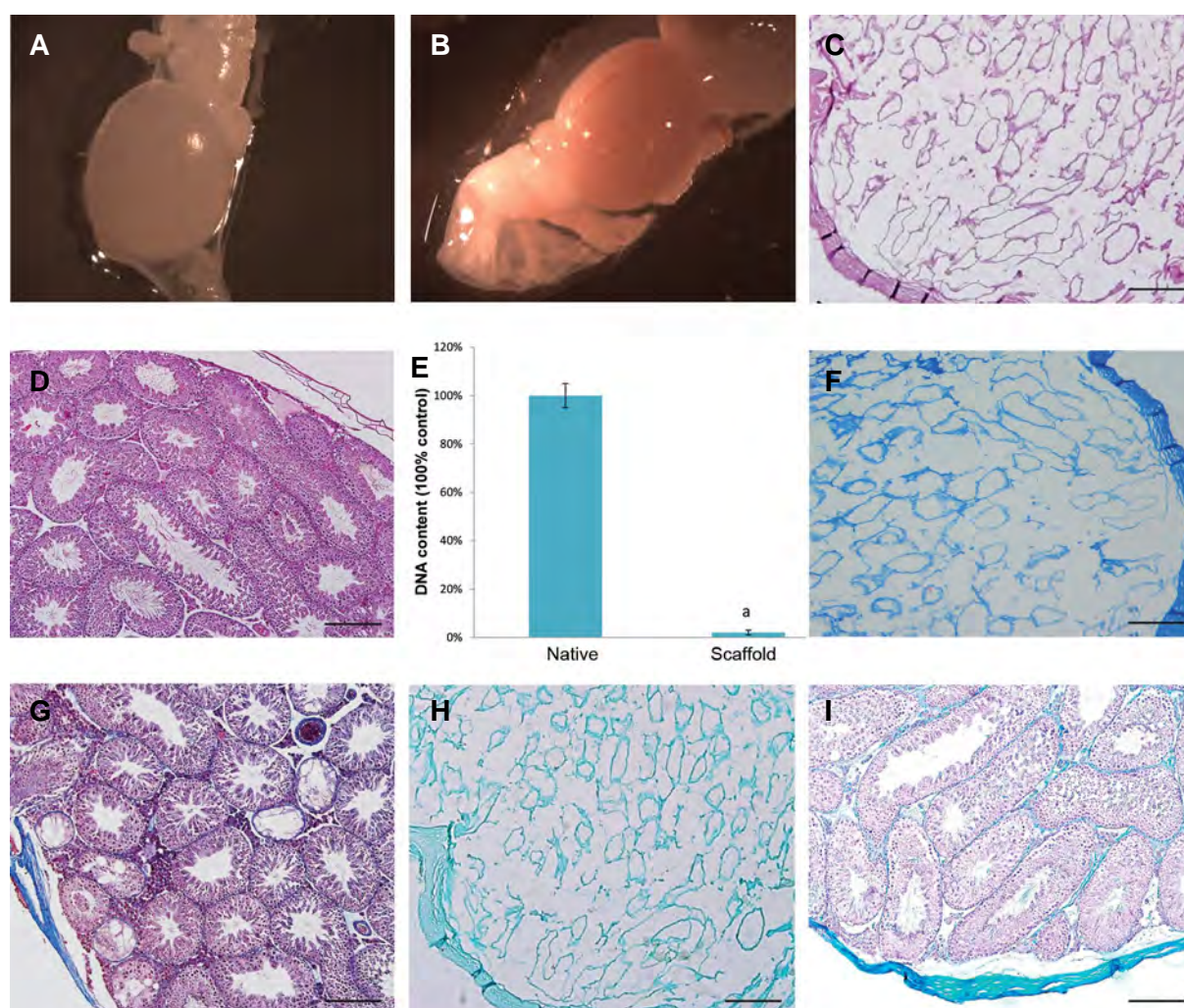


Fig.1: Characterization of decellularised testes. **A.** Macroscopic images showed that decellularised testes were completely translucent while, **B.** Intact testes were opaque, **C.** Histological comparison of decellularised, **D.** Intact testes by H&E staining exhibited the elimination of the cells, **E.** DNA quantification confirmed removal of 98% of the DNA from the tissue. a; Indicated significant difference with intact testis, **F.** Masson's trichrome staining showed collagen preservation in decellularised, **G.** Intact testes, **H.** Alcian blue staining confirmed glycosaminoglycans (GAGs) retention in decellularised, and **I.** Intact tests (scale bar: 100 μ m).

Recellularization of decellularised testicular scaffolds following *in vitro* transplantation

To evaluate the potentials of decellularised testicular tissue as a scaffold for tissue engineering, it was recellularized using *in vitro* transplantation (IVT) of murine spermatogonial stem cells. Initially, to determine the cytotoxicity of the scaffold, MTT testing was performed. The result of the MTT assay showed that decellularised testicular scaffolds had no detectable effects on the MEF proliferative activity after 24 and 72 hours of culture (Fig.2I). Spermatogonial colonies were obtained after two weeks culture of testicular cell suspension (Fig.3A). PLZF protein was expressed in these colonies (Fig.3B-D). After IVT of spermatogonial stem cells, which mixed with trypan blue was completed, the cell suspension was spread in the seminiferous tubules, and approximately 20 to 40% of the decellularised testis was filled (Fig.4A). Histological examination of recellularized scaffolds was conducted after two and eight weeks of culture. H&E staining showed that injected spermatogonial stem cells resided on the basement membrane of the seminiferous tubules and interstitium after two weeks of culture (Fig.4B). Organoid like structures was

seen after eight weeks of culture (Fig.4C).

In order to evaluate the expression of spermatogenesis-specific genes, real-time PCR was performed. Our results indicated that *Plzf* gene expression did not show any significant difference between samples cultured for two and eight weeks, while expression of *Sycp3* genes significantly increased ($P=0.003$). Also, expression of *Sycp3* gene in samples cultured for two and eight weeks was significantly lower compared to intact testes ($P=0.003$, Fig.4D). Bands of *Plzf* and *Sycp3*, and β -*actin* genes were detected on gel electrophoresis (Fig.4E). Detection of germ cell markers at the protein level was confirmed via immunostaining of recellularized scaffolds. IHC confirmed PLZF-positive cells (Fig.5A-C) were present in the recellularized scaffolds after eight weeks of culturing. The scaffolds without cell injection didn't expressed the PLZF protein (Fig.5D). SYCP3-positive cells (Fig.5E-G), were present in the recellularized scaffolds after eight weeks of culturing. The scaffolds without cell injection didn't expressed the SYCP3 protein (Fig.5H). Mouse adult testis was stained as a positive control for PLZF (Fig.5I, J) and SYCP3 (Fig.5K, L) markers.

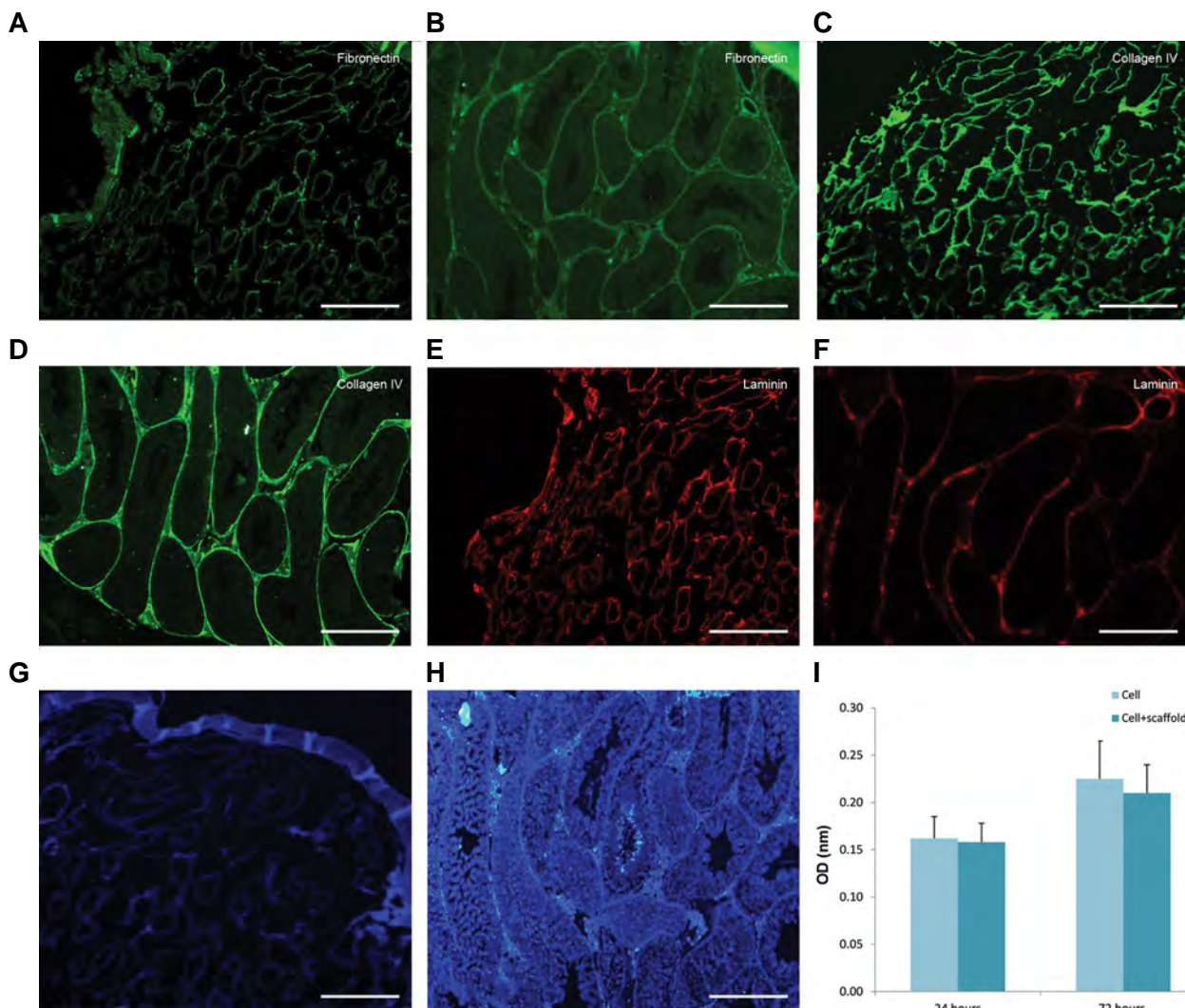


Fig.2: Protein and nucleic acid analyses of the decellularised scaffolds and intact testes. **A.** Representative images of fibronectin expression in decellularised scaffolds, **B.** Intact testis, **C.** Collagen IV expression in decellularised scaffolds, **D.** Intact testis, **E.** Laminin expression in decellularised scaffolds, **F.** Intact testis, **G.** DAPI staining of decellularised scaffolds, **H.** Intact testis, and **I.** Evaluation of scaffold cytocompatibility using MTT test did not show any significant difference in the optical density (OD) values, meaning that the cells proliferated at a rate similar to that of the controls (scale bar: 100 μ m).

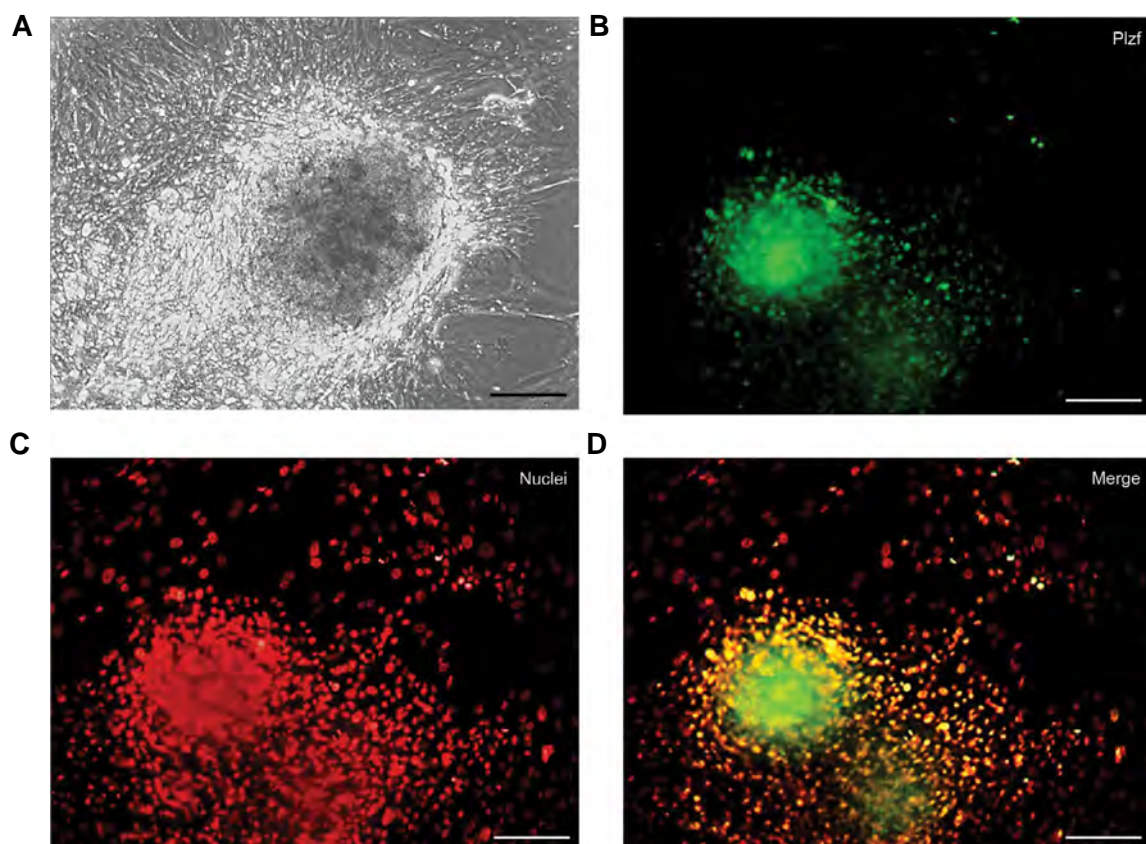


Fig.3: Characterization of spermatogonial stem cells harvested from neonatal mouse testes. **A.** Phase contrast images of spermatogonial stem cell colonies after two weeks of culture, and **B-D.** IHC staining of spermatogonial stem cell colonies with PLZF marker. Cell nuclei were stained by propidium iodide (PI) (scale bar: 30 μ m).

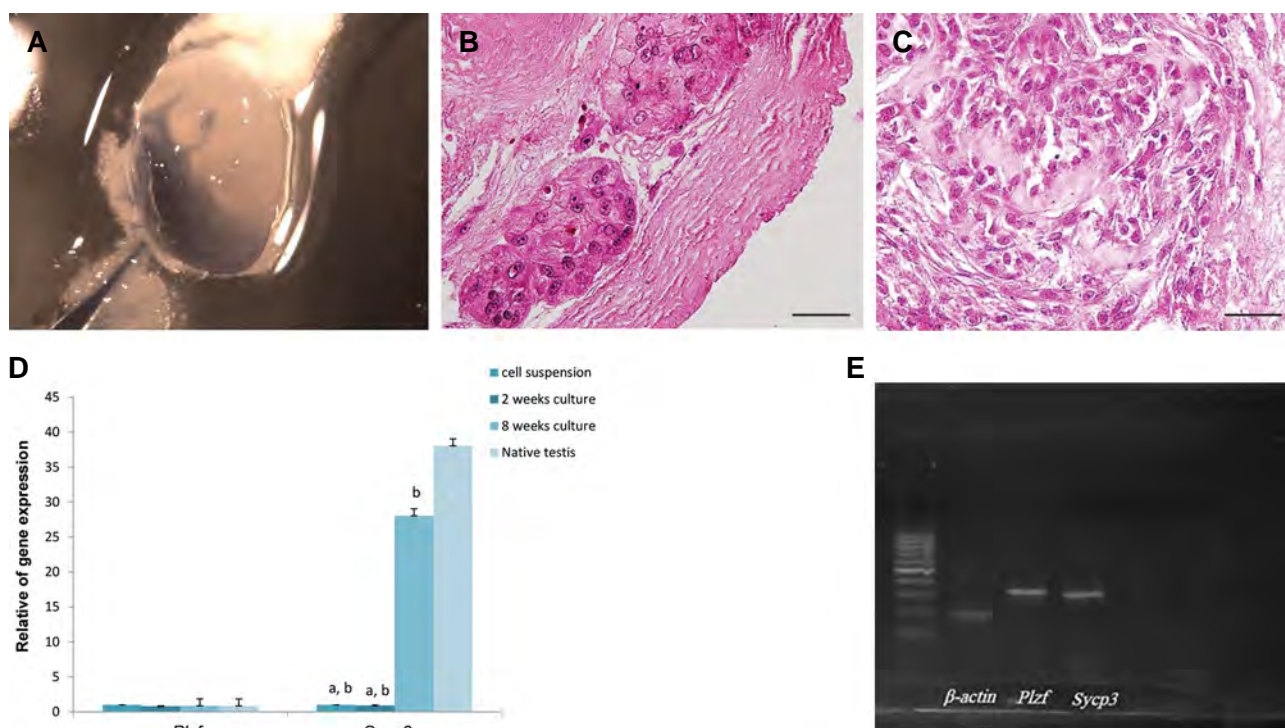


Fig.4: Characterization of cell injected scaffolds. **A.** Gross image of repopulated testicular scaffolds using *in vitro* transplantation (IVT) of spermatogonial stem cells, **B.** Haematoxylin-eosin images of the recellularized scaffolds after two weeks (scale bar: 20 μ m), **C.** Eight weeks of culturing. Representative image of decellularised scaffolds without IVT after eight weeks in culture (scale bar: 20 μ m), **D.** Relative gene expression of recellularized scaffolds after two and eight weeks of culture, and **E.** Bands of *Plzf* and *Sycp3* genes, and β -*actin* gene as the housekeeping control were obtained by real-time polymerase chain reaction (PCR). a; Indicated significant difference with samples cultured for eight weeks and b; Indicated significant difference with intact testis.

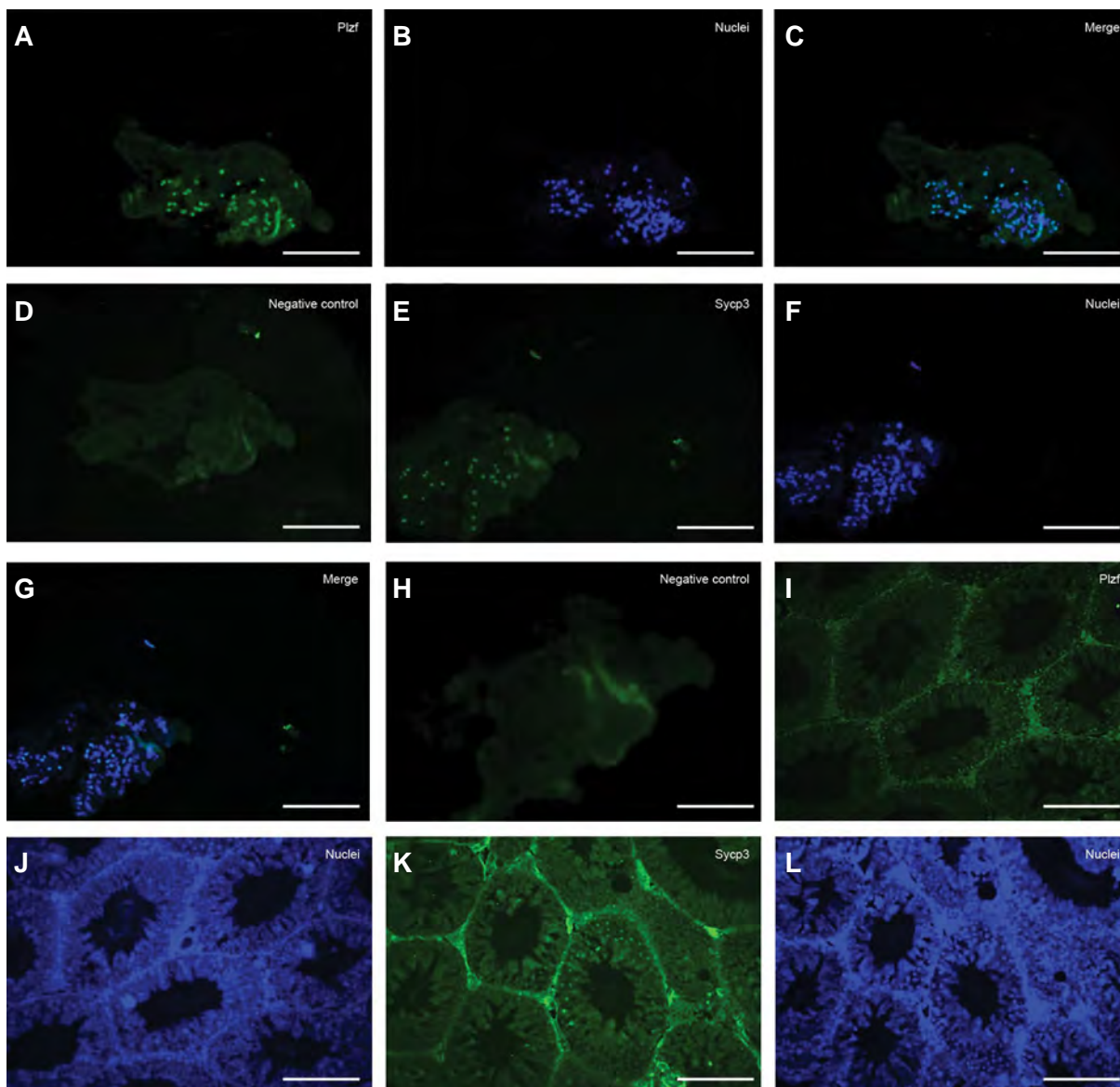


Fig.5: Immunohistochemistry (IHC) images of the cell-injected scaffolds and intact testes. **A-C.** IHC staining showed PLZF-positive cells in scaffolds cultured for eight weeks, **D.** Negative control of PLZF, **E-G.** SYCP3-positive cells in scaffolds cultured for eight weeks, **H.** Negative control of SYCP3, **I, J.** Positive control of PLZF, **K,** and **L.** SYCP3 in adult testis (scale bar: 50 μ m).

Discussion

Applications of ECM scaffolds are increasing for the establishment of artificial organ structures in order to mimic organ functions (22). This study investigated the use of decellularised whole testicular scaffold to support proliferation and differentiation of spermatogonial stem cells *in vitro*. Initially, murine whole testes were decellularised using SDS and Triton X-100. DNA content analyses demonstrated 98% cell removal, suggesting that our decellularisation method efficiently removes testicular cellular components. Our results were in line with other studies on SDS plus Triton X-100 application for tissue decellularisation in tendon-bone, small-diameter blood vessels and pericardium and cardiac tissues (13, 23-25). Preservation of ECM proteins is necessary in tissue engineering in order to facilitate interactions between cell and matrix (26). Main components of testicular ECM are

laminin, fibronectin, and collagens that were detected in testicular scaffolds using IHC. Baert et al. have reported that decellularisation of human testes by detergents could preserve the components of basement membrane including collagens, laminin, and fibronectin (12). Collagens are necessary for the maintenance of tissues structure, laminin is an important adhesion molecule, and fibronectin supports cell attachment and migration (27). So, these proteins are important factors for successful attachment of spermatogonial stem cells to the basement membrane of the seminiferous tubules (10). Cytotoxicity assay by MTT showed that decellularised testicular scaffolds had no harmful effects on MEF proliferative activity. The cells metabolized the MTT substrate, indicating that MEF cell mitochondria were functional on decellularised testicular scaffolds, which in turn resulted in a good overall cell viability and proliferation. Thus, the

decellularised testicular scaffolds were confirmed to be cell-compatible.

Subsequently, these scaffolds were recellularized by injection of spermatogonial stem cells via efferent ductuli to whole testicular scaffolds and were cultured on agarose gel for eight weeks in order to evaluate the differentiating potentials of spermatogonial stem cells. In the previous studies (9, 10) the cell suspension was seeded directly onto scaffolds, while in our study the cells were injected to rete testes and seminiferous tubules for facilitating attachment of the spermatogonial stem cells to the basal lamina, their colonization and differentiation. H&E staining showed that the injected cells resided on the basement membrane of the seminiferous tubule and interstitium after two weeks of culture. Organoid-like structures were seen in the samples cultured for eight-weeks. Baert et al. (9) reported natural testicular scaffolds could support the self-assembly of human testicular cells to organoid structures. So, injection of the cells into seminiferous tubules or seeding the cell on to the scaffolds results in development of a similar structure. In decellularised scaffolds without IVT, seminiferous tubules collapsed and no cells were seen on the scaffolds after eight weeks of culture. Injection of the cells to the seminiferous tubules resulted in cell proliferation and of secretion of ECM proteins. In another study in 2018, Vermeulen, et al. declared that seeding Sertoli cells onto testicular scaffolds could rise the proliferative activity of the Sertoli cells (10). They did not investigate the fate of spermatogonial stem cells in the presence of the scaffolds.

For identification of the nature of the observed cells in seminiferous tubules, cell-specific gene expression was evaluated over time. The expression of *Plzf* gene did not show any significant differences between two and eight weeks cultured samples. *PLZF* is a pluripotency marker that plays an important role in proliferation and self-renewal of spermatogonial stem cells (28). Baert et al. (29) reported that key markers of human spermatogonial stem cells, such as *Plzf*, *Uchl1*, and *Thy1*, were easily detected in the mRNA samples from spermatogonial stem cells, which had been cultured on testicular scaffolds. Pendergraft et al. (30) reported that *Plzf* expression remained unchanged in testicular organoid during the culture period. This could indicate that the spermatogonial stem cells pool in a scaffold is able to maintain the undifferentiated state for eight weeks in culture. Since differentiation of spermatogonial stem cells is a key aspect of normal spermatogenesis, we further evaluated *Sycp3* gene expression. The results showed a significant increase in samples that had been cultured for eight weeks compared to those cultured for two weeks. SYCP3 is a meiotic marker that elaborates in recombination and separation of chromosomes in meiotic division (31). Deletion of SYCP3 in mice causes problems in fertility. Also, lack of SYCP3 in males could induce apoptosis in spermatocytes and may prevent formation of synaptonemal complexes. Aarabi et al. (32) showed that the expression level of

testicular *sycp3* mRNA is correlated with the degree of spermatogenic failure. The expression of SYCP3 was not seen in patients with testicular atrophy, Sertoli cell-only syndrome, or arrest of spermatogonial stem cells. In the current study, spermatogonial stem cells could proliferate and initiate meiosis, but spermatocytes did not complete spermiogenesis to produce functional sperms.

In addition to transcripts level, immunostaining of samples confirmed the presence of spermatogonial stem cells expressing PLZF and spermatocyte cells expressing SYCP3 proteins in samples cultured for eight weeks. Taken together, these data indicate that our scaffold has the capacity to support spermatogonial stem cells attachment and differentiation through the spermatocyte formation stage. We could not find round spermatid or spermatozoa after eight weeks of culturing. This may be due to the cultivation system and the types of culture medium supplements. In the present study, the culture media were supplemented by several factors including LIF, BFGF, EGF, estradiol, progesterone, and glial cell line-derived neurotrophic factor (GDNF) to improve proliferation of spermatogonial stem cells and to induce their differentiation. From these factors, LIF, BFGF, and estradiol induce proliferation and lead to survival of spermatogonial stem cells in culture (33, 34). EGF activates differentiation of germ cells, but reduces the proliferation rate of spermatogonial stem cell (35). Progesterone stimulates early stages of spermatogenesis (36). GDNF has an important role in self-renewal and differentiation of germ cells (37). It seems that our supplemented medium with a variety of factors with different effects on proliferation and differentiation may have impaired the spermatogenesis process. Therefore, further studies should be conducted to focus on improving the culture system and culture medium. This could possibly be done by using a dynamic culture system or hydrogel developed from decellularised testicular ECM. Recently, growth factors have been successfully conjugated to biological or synthetic scaffolds. The cells that have interactions with the matrix could use these conjugated factors, so that they provide extremely localized signals to regulate the cell fate (38). Applications of growth factors conjugated to decellularised testicular scaffolds for induction of differentiation in spermatogonial stem cells could be considered in future studies.

Conclusion

Our decellularised testicular scaffolds were cell-compatible and did not have a harmful effect on MEF and spermatogonial stem cells viability. Recellularization of this scaffold using the IVT method could help spermatogonial stem cells to differentiate to produce the spermatocytes.

Acknowledgements

Financial support for this work was provided by the Tarbiat Modares University, Iran. The authors declare no conflict of interest in this project.

Authors' Contributions

N.M.Gh.; Performed the experiments, data acquisition, data analysis and interpretation and drafting the manuscript. M.M.; Was the conductor of the study, participated in study design and editing the manuscript and also participated in the finalization of the manuscript and approved the final draft. Z.M.; Participated in statistical analysis and editing the manuscript. All authors read and approved the final version of the manuscript.

References

- Huleihel M, Lunenfeld E. Regulation of spermatogenesis by paracrine/autocrine testicular factors. *Asian J Androl*. 2004; 6(3): 259-268.
- Kostereva N, Hofmann MC. Regulation of the spermatogonial stem cell niche. *Reprod Domest Anim*. 2008; 43 Suppl 2: 386-392.
- Hofmann MC. Gdnf signaling pathways within the mammalian spermatogonial stem cell niche. *Mol Cell Endocrinol*. 2008; 288(1-2): 95-103.
- Oatley JM, Reeves JJ, McLean DJ. Biological activity of cryopreserved bovine spermatogonial stem cells during in vitro culture. *Biol Reprod*. 2004; 71(3): 942-947.
- Lee JH, Kim HJ, Kim H, Lee SJ, Gye MC. In vitro spermatogenesis by three-dimensional culture of rat testicular cells in collagen gel matrix. *Biomaterials*. 2006; 27(14): 2845-2853.
- Badylak SF, Freytes DO, Gilbert TW. Extracellular matrix as a biological scaffold material: structure and function. *Acta Biomater*. 2009; 5(1): 1-13.
- Keane TJ, Saldin LT, Badylak SF. Decellularisation of mammalian tissues: preparing extracellular matrix bioscaffolds. *Characterisation and design of tissue scaffolds*: Elsevier; 2016; 75-103.
- Gilbert TW, Sellaro TL, Badylak SF. Decellularisation of tissues and organs. *Biomaterials*. 2006; 27(19): 3675-3683.
- Baert Y, Rombaut C, Goossens E. Scaffold-based and scaffold-free testicular organoids from primary human testicular cells. *Methods Mol Biol*. 2017 (ahead of print).
- Vermeulen M, Del Vento F, de Michele F, Poels J, Wyns C. Development of a cyto-compatible scaffold from pig immature testicular tissue allowing human sertoli cell attachment, proliferation and functionality. *Int J Mol Sci*. 2018; 19(1): pii: E227.
- Duisit J, Amiel H, Wüthrich T, Taddeo A, Dedriche A, Destoop V, et al. Perfusion-decellularisation of human ear grafts enables ECM-based scaffolds for auricular vascularized composite tissue engineering. *Acta Biomater*. 2018; 73: 339-354.
- Baert Y, Stukenborg JB, Landreh M, De Kock J, Jörnvall H, Söder O, et al. Derivation and characterization of a cyto-compatible scaffold from human testis. *Hum Reprod*. 2014; 30(2): 256-267.
- Gui L, Muto A, Chan SA, Breuer CK, Niklason LE. Development of decellularised human umbilical arteries as small-diameter vascular grafts. *Tissue Eng Part A*. 2009; 15(9): 2665-2676.
- Weymann A, Patil NP, Sabashnikov A, Jungebluth P, Korkmaz S, Li S, et al. Bioartificial heart: a human-sized porcine model-the way ahead. *PLoS One*. 2014; 9(11): e111591.
- Kajbafzadeh AM, Sabetkish N, Sabetkish S, Tavangar SM, Hossein Beigi RS, Talebi MA, et al. Lung tissue engineering and preservation of alveolar microstructure using a novel casting method. *Biotech Histochem*. 2015; 90(2): 111-123.
- Jozefczuk J, Drews K, Adjaye J. Preparation of mouse embryonic fibroblast cells suitable for culturing human embryonic and induced pluripotent stem cells. *J Vis Exp*. 2012; (64): pii: 3854.
- Fang NT, Xie SZ, Wang SM, Gao HY, Wu CG, Pan LF. Construction of tissue-engineered heart valves by using decellularised scaffolds and endothelial progenitor cells. *Chin Med J (Engl)*. 2007; 120(8): 696-702.
- Mirzapour T, Movahedin M, Tengku Ibrahim TA, Koruji M, Haron AW, Nowroozi MR, et al. Effects of basic fibroblast growth factor and leukaemia inhibitory factor on proliferation and short-term culture of human spermatogonial stem cells. *Andrologia*. 2012; 44 Suppl 1: 41-55.
- Ibtisham F, Wu J, Xiao M, An L, Banker Z, Nawab A, et al. Progress and future prospect of in vitro spermatogenesis. *Oncotarget*. 2017; 8(39): 66709-66727.
- Yokonishi T, Sato T, Katagiri K, Ogawa T. In vitro spermatogenesis using an organ culture technique. *Methods Mol Biol*. 2013; 927: 479-488.
- Alrahel A, Movahedin M, Mazaheri Z, Amidi F. Study of Tnp1, Tekt1, and Plzf genes expression during an in vitro three-dimensional neonatal male mice testis culture. *Iran Biomed J*. 2018; 22(4): 258-263.
- Crapo PM, Gilbert TW, Badylak SF. An overview of tissue and whole organ decellularisation processes. *Biomaterials*. 2011; 32(12): 3233-3243.
- Kasimir MT, Rieder E, Seebacher G, Silberhumer G, Wolner E, Weigel G, et al. Comparison of different decellularisation procedures of porcine heart valves. *Int J Artif Organs*. 2003; 26(5): 421-427.
- Gonçalves AC, Griffiths LG, Anthony RV, Orton EC. Decellularisation of bovine pericardium for tissue-engineering by targeted removal of xenoantigens. *J Heart Valve Dis*. 2005; 14(2): 212-217.
- Woods T, Gratzner PF. Effectiveness of three extraction techniques in the development of a decellularised bone-anterior cruciate ligament-bone graft. *Biomaterials*. 2005; 26(35): 7339-7349.
- Brown BN, Badylak SF. Extracellular matrix as an inductive scaffold for functional tissue reconstruction. *Transl Res*. 2014; 163(4): 268-285.
- Wierzbicka-Patynowski I, Schwarzbauer JE. The ins and outs of fibronectin matrix assembly. *J Cell Sci*. 2003; 116(Pt 16): 3269-3276.
- Hobbs RM, Seandel M, Falciatori I, Rafii S, Pandolfi PP. Plzf regulates germline progenitor self-renewal by opposing mTORC1. *Cell*. 2010; 142(3): 468-479.
- Baert Y, De Kock J, Alves-Lopes JP, Söder O, Stukenborg JB, Goossens E. Primary human testicular cells self-organize into organoids with testicular properties. *Stem Cell Reports*. 2017; 8(1): 30-38.
- Pendergraft SS, Sadri-Ardekani H, Atala A, Bishop CE. Three-dimensional testicular organoid: a novel tool for the study of human spermatogenesis and gonadotoxicity in vitro. *Biol Reprod*. 2017; 96(3): 720-732.
- Easley CA, Phillips BT, McGuire MM, Barringer JM, Valli H, Hermann BP, et al. Direct differentiation of human pluripotent stem cells into haploid spermatogenic cells. *Cell Rep*. 2012; 2(3): 440-446.
- Aarabi M, Modarressi MH, Soltanghorae H, Behjati R, Amirjannati N, Akhondi MM. Testicular expression of synaptonemal complex protein 3 (SYCP3) messenger ribonucleic acid in 110 patients with nonobstructive azoospermia. *Fertil Steril*. 2006; 86(2): 325-331.
- Sofikitis N, Giotitsas N, Tsounapi P, Baltogiannis D, Giannakis D, Pardalidis N. Hormonal regulation of spermatogenesis and spermiogenesis. *J Steroid Biochem Mol Biol*. 2008; 109(3-5): 323-330.
- Sirianni R, Chimento A, Ruggiero C, De Luca A, Lappano R, Andò S, et al. The novel estrogen receptor, G protein-coupled receptor 30, mediates the proliferative effects induced by 17beta-estradiol on mouse spermatogonial GC-1 cell line. *Endocrinology*. 2008; 149(10): 5043-5051.
- Yan YC, Sun YP, Zhang ML. Testis epidermal growth factor and spermatogenesis. *Arch Androl*. 1998; 40(2): 133-146.
- Chen SX, Bogerd J, Schoonen NE, Martijn J, de Waal PP, Schulz RW. A progestin (17alpha, 20beta-dihydroxy-4-pregnen-3-one) stimulates early stages of spermatogenesis in zebrafish. *Gen Comp Endocrinol*. 2013; 185: 1-9.
- Meng X, Lindahl M, Hyvönen ME, Parvinen M, de Rooij DG, Hess MW, et al. Regulation of cell fate decision of undifferentiated spermatogonia by GDNF. *Science*. 2000; 287(5457): 1489-1493.
- Lee K, Silva EA, Mooney DJ. Growth factor delivery-based tissue engineering: general approaches and a review of recent developments. *J R Soc Interface*. 2011; 8(55): 153-170.

The Use of β -Elemene to Enhance Radio Sensitization of A375 Human Melanoma Cells

Zahra Balavandi, M.Sc.^{1,2}, Ali Neshasteh-Riz, Ph.D.^{1,2*}, Fereshteh Koosha, Ph.D.^{1,3}, Samira Eynali, M.Sc.¹,

Mahmood Hoormand, Ph.D.⁴, Minoo Shahidi, Ph.D.⁵

1. Radiation Biology Research Center, Iran University of Medical Sciences, Tehran, Iran

2. Department of Radiation Sciences, School of Allied Medical Sciences, Iran University of Medical Sciences, Tehran, Iran

3. Department of Medical Physics and Biomedical Engineering, School of Medicine, Tehran University of Medical Sciences, Tehran, Iran

4. Department of Pharmacology, School of Medicine, Iran University of Medical Sciences, Tehran, Iran

5. Department of Hematology, School of Allied Medical Sciences, Iran University of Medical Sciences, Tehran, Iran

*Corresponding Address: P.O.Box: 1449614535, Radiation Biology Research Center, Iran University of Medical Sciences, Tehran, Iran
Email: neshastehriz@yahoo.com

Received: 27/August/2018, Accepted: 18/November/2018

Abstract

Objective: Melanoma is the most malignant and severe type of skin cancer. It is a tumor with a high risk of metastasis and resistant to conventional treatment methods (surgery, radiotherapy, and chemotherapy). β -elemene is the most active constituent of Curcuma wenyujin which is a non-cytotoxic antitumor drug, proved to be effective in different types of cancers. The study aimed to investigate the therapeutic effects of β -elemene in combination with radiotherapy on A375 human melanoma.

Materials and Methods: In this experimental study, human melanoma cells were grown in the monolayer culture model. The procedure of the treatment was performed by the addition of different concentrations of β -elemene to the cells. Then, the cells were exposed to 2 and 4 Gy X-ray in different incubation times (24, 48, and 72 hours). The MTT assay was used for the determination of the cell viability. To study the rate of apoptosis response to treatments, the Annexin V/PI assay was carried out.

Results: The results of the MTT assay showed β -elemene reduced the cell proliferation in dose- and time-dependent manners in cells exposed to radiation. Flow cytometry analysis indicated that β -elemene was effective in the induction of apoptosis. Furthermore, the combination treatment with radiation remarkably decreased the cells proliferation ability and also enhanced apoptosis. For example, cell viability in a group exposed to 40 μ g/ml of β -elemene was 80%, but combination treatment with 6 MV X beam at a dose of 2 Gy reduced the viability to 61%.

Conclusion: Our results showed that β -elemene reduced the proliferation of human melanoma cancer cell through apoptosis. Also, the results demonstrated that the radio sensitivity of A375 cell line was significantly enhanced by β -elemene. The findings of this study indicated the efficiency of β -elemene in treating melanoma cells and the necessity for further research in this field.

Keywords: Apoptosis, Beta-Elemene, Melanoma, X-ray

Cell Journal(yakhteh), Vol 21, No 4, January-March (Winter) 2020, Pages: 419-425

Citation: Balavandi Z, Neshasteh-Riz A, Koosha F, Eynali S, Hoormand M, Shahidi M. The use of β -Elemene to enhance radio sensitization of A375 human melanoma cells. Cell J. 2020; 21(4): 419-425. doi: 10.22074/cellj.2020.6326.

Introduction

Melanoma is the most malignant and severe skin cancer type. It is a tumor with a risk of high metastasis and accounts for 75 % of deaths associated with skin cancer (1). This type of skin cancer is rapidly growing in recent years, and this can be due to chronic exposure of skin to sun rays without the use of equipment for the protection against sunlight, which especially can lead to melanoma in Caucasians (2). Patients suffering from melanoma may undergo surgery and/or receive chemotherapeutic agents and radiotherapy or receive a combination of these treatments (3). In addition, metastasis of the tumor is a significant problem following surgery (4). Chemotherapy drugs are often used for the treatment of melanoma include cisplatin and dacarbazine. Despite the efficacy of these therapies, several adverse effects have been so far reported such as tumor resistance to medications and cytotoxicity such as ototoxicity, nephrotoxicity, and leucopenia (5). Radiotherapy can be applied following surgery and chemotherapy considering the depth of the

lesion and the severity of the disease. The irradiation could be performed by photon or electron. Usually, the dose range between 1.8 to 2 (Gy) could be employed per fraction. Melanoma tumors are among the most resistant cells to radiation (6). Radiosensitizer drugs have been developed to reduce the dose of radiation and the side effects of radiotherapy with the same outcomes (7).

Elemene is a compound extracted from Curcuma wenyujin which, for the first time, was used against cancer in China (8). β -elemene is the active component of Curcuma wenyujin that is a non-cytotoxic antitumor drug (9). Recent studies have shown that β -elemene may sensitize tumor cells to chemotherapy drugs such as cisplatin, taxanes, and paclitaxel (10-12). As reported in previous studies, treatment with β -elemene is useful for the treatment of leukemia, HCC, glioblastoma, breast, bladder, lung, gastric, prostate, ovarian, and liver cancers (13-16). The beneficial effect of β -elemene such as low toxicity, low side

effects, well tolerance by patients, high potency, and high synergistic effects with other anti-tumor drugs have made β-elemente a bona fide candidate for the treatment of various type of cancers. β-elemente also increases the immunogenicity of cancer cells, makes tumor tissues sensitive to irradiation, reduces the proliferation of cancer cells, and induces the process of apoptosis in resistant tumors.

In vitro and *in vivo* studies showed that β-elemente makes cancer cells prone to radiation by inactivation of the ataxia telangiectasia mutated (ATM) signaling pathway which decreases the repair rate of damaged DNA. The formation of double strand break (DSB) activates ATM kinase following radiation. β-elemente acts as an ATM inhibitor via the inhibition of phosphorylation of ATM after radiotherapy; so, it could cause increased the death rate by this way (13). Thus, β-elemente causes radiosensitization via a reduction in the repair of double strand break (DSB) or an increase in radiation-induced DNA damage (17). Furthermore, recent studies have shown that radiation can increase the mRNA/protein expression of survivin in tumor cells and also increase HIF-1α activity. It has been observed that tumors highly expressing survivin or HIF-1α are resistant to radiation. Previous studies have shown that β-elemente enhances radiosensitivity of tumors by the inhibition of the survivin and HIF-1α expression (18-21). It has been implicated that β-elemente induced radiosensitization is capable of the upregulation of and downregulation of Bcl-2 in cancer cells. It also activates caspase -7, caspase-9, and caspase -3, as well as inducing apoptosis in tumor cells and increasing the efficiency of radiotherapy (17).

So, the study aimed to analyze the inhibitory effect β-elemente alone or in combination with radiotherapy on the human melanoma cell line (A375) using MTT test and flow cytometry.

Materials and Methods

The procedure of the study was approved by the Ethics Committee of the Iran University of Medical Science (No. IR. IUMS.REC1395.9311581001).

Agents

β-elemente was purchased from Abcam (Abcam, USA). Dulbecco's modified Eagle's medium (DMEM) and penicillin/streptomycin solution were procured from Atocel (Austria). Trypsin-ethylene diamine tetra-acetic acid (EDTA) and fetal bovine serum (FBS) inactivated with heat was purchased from Biowest company (France). 3-(4,5-dimethylthiazol-2-yl)-2,5-diphenyltetrazolium bromide (MTT) and dimethyl sulfoxide (DMSO) were purchased from Merck (Germany) Annexin V/PI kit was purchased from Ebioscience company (CA).

Cell culture conditions

A375 human melanoma cell line was purchased from

the cellular bank of the Pasteur Institute of Iran (Iran) and then the cell culture was performed in standard conditions [37°C, 5% CO₂, 1% antibiotic solution (pen-strep), high glucose DMEM containing 10% FBS].

Cell proliferation assay

β-elemente cytotoxicity and viability of incubated cells in different concentrations of the β-elemente were evaluated using MTT assay. To perform this assay, cells were seeded at a density of 5000 cells/well (in 100 μl medium) into 96-well flat-bottomed microtiter plates at 24, 48, and 72 hours. During the incubation time, the medium was changed every other day. Then, the cells were incubated with different concentrations of β-elemente (0-220 μg/ml) for 24 -72 hours with eight replicates for each treatment. Subsequently, cells were washed with phosphate buffer saline (PBS) after the treatment, and the medium was discarded. Afterwards, 10 μl of MTT dye (5 mg/ml in PBS) was added to each well; then, the plate was incubated for 3-4 hours at 37 C with 5% CO₂. MTT-containing medium was removed, and formazan crystals dissolved by the addition of 100 μl DMSO to each well of the plate and kept in the dark place at 25°C for 15 minutes. Eventually, the absorbance of dissolved formazan was read at 570 nm using a microplate reader (DYNEX MRX, USA). The relative viability of A375 cells was described as the proportion of viable cells to untreated cells. The dose-response curves were plotted. The half maximal inhibitory concentration (IC₅₀) value for β-elemente was obtained from the dose-response curves by drawing log-linear regression and analyzed by the GraphPad Prism software version 6.01.

Irradiation

To perform radiotherapy, the A375 cell line was irradiated by using LINAC accelerator (Siemens, Germany), at the energy level of 6 MV at doses of 2 and 4 Gy. In order to reach the energy level of 6 MV, the distance between a radiation source and tissue surface should be 3cm. So, we placed 3 layers of Plexiglass (1 cm in diameter) under the plate and 5 layers (1 cm in diameter) above the plate. The irradiation process was applied in the front side at a distance of 100 cm from the bottom of the plate, and the radiation field size was 20×20 square centimeters. The monitor unit was calculated by the Core Plan Software in each irradiation process.

The combinatory effect of β-elemente and radiotherapy

To examine the combinatory effects of β-elemente and radiotherapy, A375 cells were cultivated in 96-well plates and incubated for 24 hours. After discarding the culture medium, β-elemente were added at the concentrations of 40 and 80 μg/ml to each well. Next, the cells were incubated for 24 hours. The radiation was delivered at doses of 2 and 4 Gy X-ray at the energy of 6 MV.

Apoptosis analysis by Flow cytometry

The rate of apoptosis was determined by Annexin V/PI-Fluorescein isothiocyanate (FITC). The cells were treated with different β -elemene concentrations (40, 80 $\mu\text{g/ml}$) for 24 hours and harvested by trypsinization after the treatment and centrifugation at 300 g for 5 minutes. After centrifuging, the cells were washed with 1X binding buffer and PBS. Then, the cells were suspended in 5 μl of Fluorochrome-conjugated and 1X binding buffer. Next, 100 μl of Annexin V was added into the cell suspension and incubated in a dark place for 20 minutes. The cells washed with 2 ml of binding buffer and resuspended in 200 μl of 1X binding buffer. Finally, 5 μl of propidium iodide (PI) staining solution was added to 200 μl cell suspension, and the samples were evaluated by flow cytometry (BD FACSCantoII, USA).

Statistical analysis

All the plotted data are shown as the mean \pm SD, and the tests were at least repeated three times. Analysis of variance analysis (ANOVA) was conducted to analyze the data, and the comparison was made among different groups by the SPSS software version 16. The graphs and curves were assessed by the GraphPad Prism software (version 6.01). To indicate the significance of differences, the $P < 0.05$ was statistically considered significant.

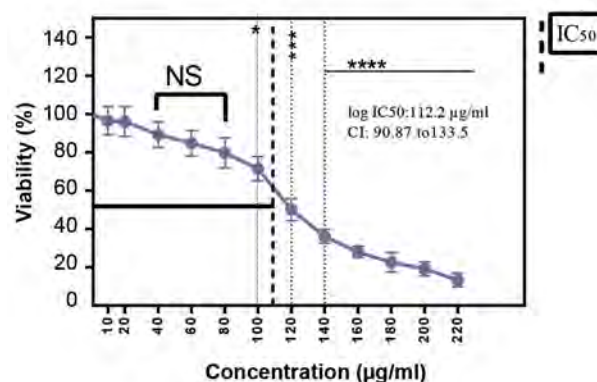
Results

Assessment of cell death and IC_{50} value of the drug following drug treatment using MTT assay

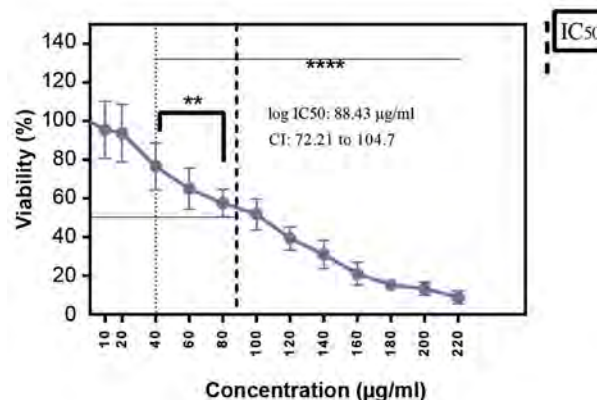
Cells were treated with various concentrations (0-220 $\mu\text{g/ml}$) of β -elemene and incubated for 24, 48 and 72 hours. Figure 1A shows the percentage of cells viability after the 24-hour treatment process. Upon increasing the concentrations of β -elemene from 10 to 80 $\mu\text{g/ml}$, the differences between cell viability do not significantly change. On the other hand, in a range of 100 to 220 $\mu\text{g/ml}$ β -elemene a significant reduction in the viability of the cells was observed. After a 48-hour incubation period, as shown in Figure 1B, in cells treated with 10 $\mu\text{g/ml}$ β -elemene, a slight reduction in the viability of cells was observed (non-significant). At a concentration range of 20 to 220 $\mu\text{g/ml}$, the viability of cells was remarkably reduced. Figure 1C shows the viability of cells after a 72-hour incubation period. At a concentration range of 40 to 160 $\mu\text{g/ml}$ β -elemene, the cell viability was reduced significantly. In cells treated with 180, 200, and 220 $\mu\text{g/ml}$ β -elemene, a slight increase in the viability of cells was observed. Also, no significant difference was observed at a concentration range of 10 and 20 $\mu\text{g/ml}$ β -elemene. All the treatment groups were compared with the control group (treatment-naive). Furthermore, the IC_{50} values for β -elemene, at three different time points in human melanoma were calculated based on the results obtained from the MTT assay results. IC_{50} values for β -elemene were 112.2 $\mu\text{g/ml}$, confidence interval (CI): 90.87-133.5,

88.43 $\mu\text{g/ml}$, CI: 90.87-133.5 and (42.06 $\mu\text{g/ml}$, CI: 6.460-77.65) at 24, 48, and 72 hours, respectively.

A



B



C

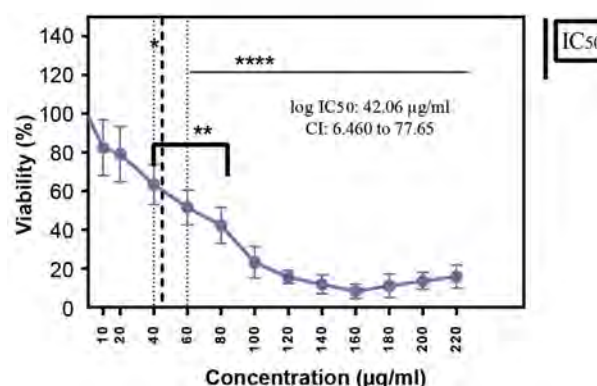


Fig.1: The growth rate of A375 cell line was inhibited by β -elemene. A375 cells were cultivated in 96-well plates at a density of 5×10^3 cells/well and treated with different concentrations of β -elemene in different time periods: **A.** 24, **B.** 48, and **C.** 72 hours. Cell proliferation was evaluated using the MTT assay. The IC_{50} value is a concentration of a drug that inhibits cell proliferation by 50% in comparison to the control. The data are shown as the means \pm SD of three independent experiments. Asterisks indicate significant differences. ****, $P < 0.0001$, ***, $P < 0.001$, **, $P < 0.01$, *, $P < 0.05$, NS; Non significant, IC_{50} : The half maximal inhibitory concentration, and CI; Confidence interval.

Figure 2 shows the comparison of all the mentioned groups in three different times (24 hours, 48 hours, 72 hours).

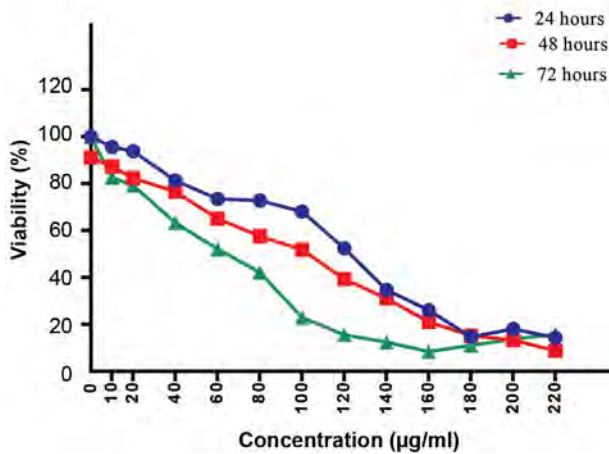


Fig.2: The capability of β-elemente to inhibit cell proliferation was measured by the MTT assay. The viability of cells was approximately decreased in dose- and time-dependent manners. The difference in the IC₅₀ value for β-elemente was observed among the different incubation times. A significant reduction was detected in the viability of treated cells in a 72 hours incubation time compared with 24 and 48 hour periods. The data are presented as the means ± SD of three independent experiments. IC₅₀: The half maximal inhibitory concentration.

Cell death evaluation in A-375 cell line, following the treatment with β-elemente and radiation using the MTT assay

To study the effects of β-elemente on radiotherapy, pretreating was performed on cells with two concentrations of β-elemente, namely 40 and 80 µg/ml for 24 hours. Then, cells were exposed to radiation at doses of 2 and 4 Gy. Considering Figure 3, groups treated with a combination of β-elemente and radiation, had a significant reduction in the viability compared with the groups treated with β-elemente alone. Combination therapy with β-elemente and radiotherapy significantly halted the proliferation of cancer cells compared with when each therapy was applied alone.

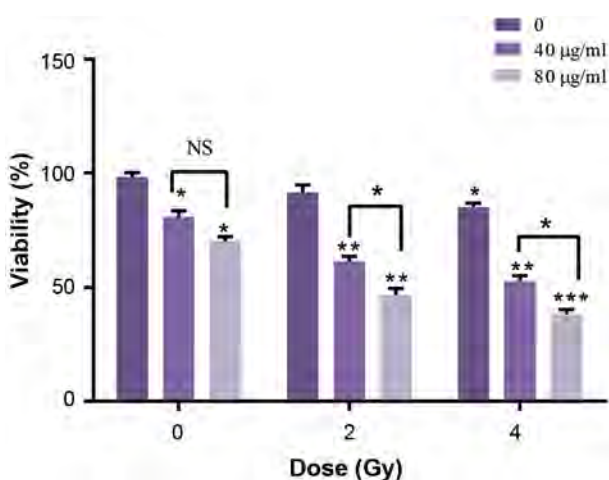
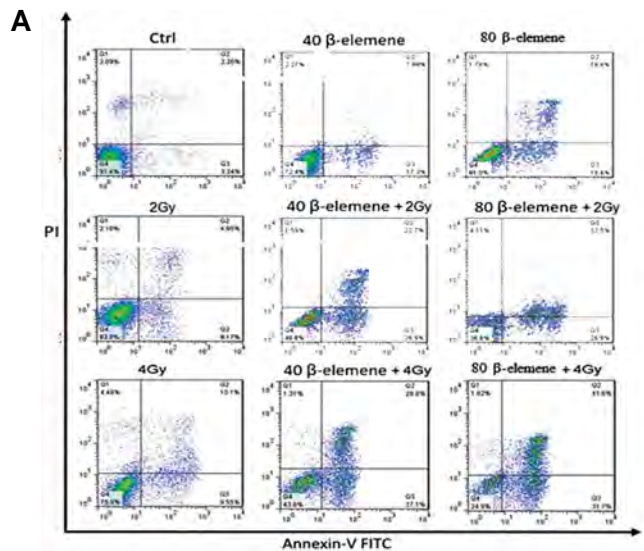


Fig.3: Cell proliferation was inhibited by β-elemente. β-elemente also increased the radiosensitivity of A375 cells. Comparison of the viability of A375 cells after the treatment with 40, 80 µg/ml of β-elemente. After 24 hours of incubation time, cells were exposed to 2 and 4 (Gy) of 6 MV X-ray; then, the viability of cells was measured using the MTT assay. All treated groups were compared with the control group (treatment-naive). The data are presented as the means ± SD of three independent experiments. Asterisks indicate significant difference. *, P<0.05, **, P<0.01, ***, P<0.001, and NS; Non significant.



Legend for Figure 4: 0 (dark purple), 40 µg/ml (medium purple), 80 µg/ml (light purple)

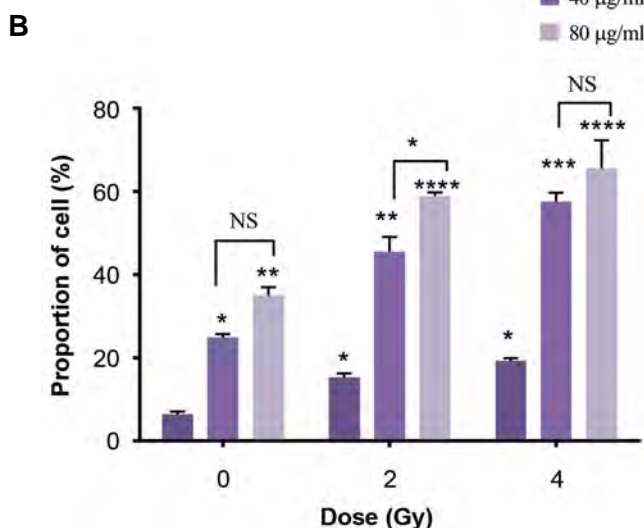


Fig.4: Annexin V-PI staining for the assessment of apoptosis following β-elemente and radiation therapy in A375 human melanoma cell line. The pretreated process on cancer cells was performed at two concentrations of β-elemente (40 and 80 µg/ml) for 24 hours. Then cells were exposed to 2 and 4 Gy irradiations in combination with β-elemente for 24 hours. **A.** Early apoptosis was evaluated by Annexin V+/PI- staining, and Annexin V+/PI+ staining was applied as a marker for the detection of cells in the late apoptosis phase and **B.** PI and Annexin V double staining results indicated the induction of apoptosis by β-elemente and enhanced radiation-induced apoptosis in human melanoma cancer cells. Cells were exposed to β-elemente at concentrations of 40 and 80 µg/ml along with 2 and 4 Gy irradiations. All the treatment groups were compared with the control group (no drug). The data are presented as the means ± SD of three independent experiments. Asterisks indicate significant differences. ****, P<0.0001, ***, P<0.001, **, P<0.01, *, P<0.05, and NS; Non significant.

The effect of β-elemente on apoptosis of A375 cell line

According to the results, β-elemente induces apoptosis and enhances the potency of the radiation driving A375 cancer cells to undergo apoptosis. Annexin V/PI staining was employed to detect the rate of apoptosis to show the effect of radiosensitization ability of β-elemente on A-375 cell line. Following the treatment with β-elemente, apparent morphological alterations were detected in cancer cells. Early apoptosis was examined via Annexin V+/PI- staining, while late apoptosis was monitored via Annexin V+/PI+ staining as

depicted in Figure 4A. The quantification of different modes of cell death following β -elemene and radiation exposure were shown in Figure 4B. The number of apoptotic cells in the groups treated with either β -elemene or radiation were significantly higher than the control group (no therapy, no radiation). Furthermore, a significantly higher apoptotic rate was observed in the groups treated with radiation and β -elemene at concentrations of 40 and 80 $\mu\text{g/ml}$ ($P < 0.01$, $P < 0.001$, $P < 0.0001$). The apoptotic rate was increased in parallel with an increment in the concentrations of β -elemene.

Discussion

Melanoma is the most malignant and serious type of skin cancer (22). Patients suffering from melanoma can undergo various forms of therapy including surgery, chemotherapy, and radiotherapy, as well as receiving a combination of these treatment methods. Since melanoma tumor cells are among the most resistant cells to radiation (23); therefore, we need to novel treatments to conquer the resistance of this cancer to radiation. Recently, researchers attempt to find new anticancer drugs which among them radio sensitizers showed hold a great promise for the treatment of melanoma. β -elemene, is a natural and traditional Chinese medicinal herb, indicating antitumor effects on many types of tumors with much fewer side effects (24). It has been demonstrated that β -elemene could inhibit the growth and development of some chemotherapy-resistant tumors, including ovarian, prostate, and glioblastoma (14, 25).

In this study, combination treatment with β -elemene and radiation was examined to enhance radio sensitization with 6 MV X-ray in A375 cell line. The advantage of combination therapy is to increase the efficiency of the treatment when compared with standard treatment procedures. The MTT assay showed that β -elemene could reduce the viability and inhibit the in-vitro growth of the human melanoma cell line in dose and time dependent manners. In the following step, after a 24-hour incubation period, a significant reduction in the viability was observed when β -elemene was applied at the concentrations range of 100 $\mu\text{g/ml}$ to 220 $\mu\text{g/ml}$, however, after a 48-hour incubation period, treatment with β -elemene at concentrations range of 20 $\mu\text{g/ml}$ to 220 $\mu\text{g/ml}$ reduced the viability of cells from 93 to 8%. The highest reduction rate of the cell viability was achieved at the concentrations range of 40 $\mu\text{g/ml}$ to 160 $\mu\text{g/ml}$ at a 72-hour incubation period. The trend of the reduction in the cell viability not only depends on the concentration of β -elemene but also depends on the incubation time. The IC_{50} values obtained from the effect of β -elemene on A375 cells were approximately 112.2, 88.43, 46.03 $\mu\text{g/ml}$ at 24, 48, and 72 hours, respectively. These data indicate that β -elemene vigorously decreases the viability of tumor cells. The statistical analysis of the data indicated a considerable reduction in the cells viability in the groups co-treated with β -elemene and radiation compared with those treated with β -elemene alone or the control group (no therapy).

The cell viability of the group treated with 40 $\mu\text{g/ml}$ of β -elemene was 80%, while in combination treatment at a dose of 2 Gy with 6 MV X-ray reduced the viability to 61%. The results of the current study are consistent with previous studies. For example, Lu et al. (26) investigated the effect of β -elemene on bladder tumor cells. They examined the cytotoxicity of β -elemene using the MTT method and observed β -elemene could inhibit the proliferation of T24 bladder carcinoma cells. Furthermore, Zhan et al. (27) evaluated the viability of human RCC 786-0 cell line after the treatment with different concentrations of β -elemene for 24, 48 or 72 hours. The MTT assay indicated that β -elemene inhibited the proliferation of 786-0 cells in dose and time depending manners.

In this research, we analyzed the effect of β -elemene on radiosensitivity of tumor cells to drive them to undergo apoptosis. The flow cytometry analysis indicates that β -elemene is effective to induce apoptosis. β -elemene induced apoptosis in A375 cell line was measured by Annexin V/PI staining. Treatment with either β -elemene or radiation could somewhat increase the number of apoptotic cells in a dose-dependent way, confirming the results obtained from the MTT assay. Also, the flow cytometry analysis demonstrated that β -elemene inhibits A375 cells proliferation and stimulates cell death by means of inducing apoptosis. The number of apoptotic cells by co-treatment with β -elemene and radiation were significantly higher than those undergone cell death by the radiation or β -elemene individually. For example, combination treatment with β -elemene (40 $\mu\text{g/ml}$) and radiation at a dose of 4 (Gy) resulted in a decrease in the cell survival by 57.5% in comparison with the control. The percentages of apoptotic cells in response to the treatment of cells with 40 $\mu\text{g/ml}$ β -elemene or exposure to 4Gy of X-ray were 25/29% and 19/65%, respectively.

Liu et al. (28) investigated the effect of β -elemene on stomach tumor cells using the flow cytometry method. They indicated a higher rate of apoptotic cells when incubated with β -elemene in comparison with the control group. They found that β -elemene interferes with the PI3K/Akt/mTOR/p70S6K1 pathways and causes apoptosis in tumor cells. Furthermore, the results of a study conducted by Dai et al. (29) showed that one of the important apoptotic pathways in tumors is the expression of Fas/FasL. β -elemene is capable of inducing apoptosis in HepG2 cancer cells thereby the increase in the expression of Fas/FasL.

Li et al. (30) and Pugazhenthii et al. (31) have shown that β -elemene could activate caspase-3 caspase-7, and caspase-9 and increase the ratio of Bax: Bcl-2, which is associated with the apoptosis of cancer cells. Also, Li et al. (32) observed that β -elemene makes NSCLC cells sensitive to cisplatin triggering the intrinsic apoptosis pathway which involves Bcl-2 family proteins and inhibitor of apoptosis proteins (IAPs). So, our data showed that β -elemene effectively enhanced radio sensitivity in A375 cell line. Similar results were obtained when the cells treated with 80 $\mu\text{g/ml}$ of β -elemene in combination

with 2 and 4 Gy of X-ray. Liu et al. (33) investigated the effect of alone and also in combination with radiation on glioblastoma cells (U87-MG) using colony formation. In the colony formation assay, in cells treated with both β-elemene and radiation, the colony formation ability was significantly reduced compared with the control group. As well, radiosensitivity was significantly enhanced following the treatment of the cells with β-elemene. Li et al. (34) examined radiosensitization of β-elemene in lung cancer cells (A549) by the comet assay and observed the same results. In general, β-elemene increases tumor radio sensitivity through two mechanisms; i. The induction of cell cycle arrest at the G2/M phase and ii. The activation of ATM kinase by the DSB formation following radiation. So, the process of radio sensitization is related to the enhancement in radiation-induced DNA damage or a decrease in the repair of DSB (35). However, the precise mechanism of action of this herb is still unknown.

Conclusion

Radiation and β-elemene are able to reduce the cell viability and increase apoptosis of melanoma cells. The cells viability was decreased by 23 and 30% for 2 and 4 Gy, respectively. Also, combination therapy with β-elemene and radiation resulted in an increased rate of apoptosis. The percentages of apoptotic cells treated with 40 μg/ml β-elemene and 4 Gy of X-ray alone were 25 and 19 %, respectively. The findings of this study indicated the efficiency of β-elemene in treating melanoma cells and showed the necessity of more research in this field.

Acknowledgements

This research was financially supported by a research grant (Grant No. 28597) from the Iran University of Medical Sciences (IUMS). We wish to thank all our colleagues in Asia Hospital and Research Institute of the Iran University of Medical Sciences. There is no conflict of interest in this study.

Authors' Contributions

Z.B.; Contributed to all experimental work, data collection, the evaluation of the data, drafting, and statistical analysis. F.K.; Contributed to the design and writing of the manuscript. A.N.-R.; Conducted and supervised the study design, data collection and evaluation, drafting, statistical analysis and was in charge of overall direction and planning. S.E.; Helped in data analysis and interpretation of them. M.H.; Contributed to performing experimental procedures. M.Sh.; Contributed to conception and design, perfumed data collection, all experimental work and drafting. All authors read and approved the final manuscript.

References

1. Le Gal K, Ibrahim MX, Wiel C, Sayin VI, Akula MK, Karlsson C, et al. Antioxidants can increase melanoma metastasis in mice. *Sci Transl Med.* 2015; 7(308): 308re8.
2. Karimi K, Lindgren TH, Koch CA, Brodell RT. Obesity as a risk fac-

- tor for malignant melanoma and non-melanoma skin cancer. *Rev Endocr Metab Disord.* 2016; 17(3): 389-403.
3. Spagnolo F, Ghiorzo P, Orgiano L, Pastorino L, Picasso V, Tornari E, et al. BRAF-mutant melanoma: treatment approaches, resistance mechanisms, and diagnostic strategies. *Onco Targets Ther.* 2015; 8: 157-168.
4. Stratigos A, Garbe C, Lebbe C, Malvehy J, del Marmol V, Pehamberger H, et al. Diagnosis and treatment of invasive squamous cell carcinoma of the skin: European consensus-based interdisciplinary guideline. *Eur J Cancer.* 2015; 51(14): 1989-2007.
5. Ferdosi S, Saffari M, Eskandarieh S, Raziye R, Moghaddam MG, Ghanadan A, et al. Melanoma in Iran: a retrospective 10-year study. *Asian Pac J Cancer Prev.* 2016; 17(6): 2751-2755.
6. Burmeister BH, Smithers BM, Davis S, Spry N, Johnson C, Krawitz H, et al. Radiation therapy following nodal surgery for melanoma: an analysis of late toxicity. *ANZ J Surg.* 2002; 72(5): 344-348.
7. Tong E, Xu Y, Li G, Zou K, Zou L. The effects of β-elemene on the expression of mTOR, HIF-1α, surviving in lung adenocarcinoma A549 cell. *Afr J Tradit Complement Altern Med.* 2013; 10(4): 18-23.
8. Khan MK, Khan N, Almasan A, Macklis R. Future of radiation therapy for malignant melanoma in an era of newer, more effective biological agents. *Onco Targets Ther.* 2011; 4: 137-148.
9. Grossmann KF, Margolin K. Long-term survival as a treatment benchmark in melanoma: latest results and clinical implications. *Ther Adv Med Oncol.* 2015; 7(3): 181-191.
10. Robbins KT, Clayman G, Levine PA, Medina J, Sessions R, Shaha A, et al. Neck dissection classification update: revisions proposed by the American Head and Neck Society and the American Academy of Otolaryngology-Head and Neck Surgery. *Arch Otolaryngol Head Neck Surg.* 2002; 128(7): 751-758.
11. Zhao J, Li QQ, Zou B, Wang G, Li X, Kim JE, et al. In vitro combination characterization of the new anticancer plant drug beta-elemene with taxanes against human lung carcinoma. *Int J Oncol.* 2007; 31(2): 241-252.
12. Strojjan P. Role of radiotherapy in melanoma management. *Radiother Oncol.* 2010; 44(1): 1-12.
13. Liu S, Zhou L, Zhao Y, Yuan Y. β-elemene enhances both radiosensitivity and chemosensitivity of glioblastoma cells through the inhibition of the ATM signaling pathway. *Oncol Rep.* 2015; 34(2): 943-951.
14. Li QQ, Lee RX, Liang H, Zhong Y, Reed E. Enhancement of cisplatin-induced apoptosis by β-elemene in resistant human ovarian cancer cells. *Med Oncol.* 2013; 30(1): 424.
15. Yu Z, Wang R, Xu L, Xie S, Dong J, Jing Y. β-Elemene piperazine derivatives induce apoptosis in human leukemia cells through downregulation of c-FLIP and generation of ROS. *PLoS One.* 2011; 6(1): e15843.
16. Yan B, Zhou Y, Feng S, Lv C, Xiu L, Zhang Y, et al. β-elemene-attenuated tumor angiogenesis by targeting Notch-1 in gastric cancer stem-like cells. *Evid Based Complement Alternat Med.* 2013; 2013: 268468.
17. Li LJ, Zhong LF, Jiang LP, Geng CY, Zou LJ. β-Elemene radiosensitizes lung cancer A549 cells by enhancing DNA damage and inhibiting DNA repair. *Phytother Res.* 2011; 25(7): 1095-1097.
18. Guan C, Liu W, Yue Y, Jin H, Wang X, Wang XJ. Inhibitory effect of β-elemene on human breast cancer cells. *Int J Clin Exp Pathol.* 2014; 7(7): 3948-3856.
19. Cai DY, Gao X, Wu XH, Hong TT. Synergistic effect of beta-elemene injection combined paclitaxel injection on human breast cancer MB-468 cells: an in vitro study. *Zhongguo Zhong Xi Yi Jie He Za Zhi.* 2013; 33(7): 978-982.
20. Zhang F, Xu L, Qu X, Zhao M, Jin B, Kang J, et al. Synergistic anti-tumor effect of β-elemene and etoposide is mediated via induction of cell apoptosis and cell cycle arrest in non-small cell lung carcinoma cells. *Mol Med Rep.* 2011; 4(6): 1189-1193.
21. Tan W, Lu J, Huang M, Li Y, Chen M, Wu G, et al. Anti-cancer natural products isolated from chinese medicinal herbs. *Chin Med.* 2011; 6(1): 27.
22. Robbins PF, Morgan RA, Feldman SA, Yang JC, Sherry RM, Dudley ME, et al. Tumor regression in patients with metastatic synovial cell sarcoma and melanoma using genetically engineered lymphocytes reactive with NY-ESO-1. *J Clin Oncol.* 2011; 29(7): 917-924.
23. Visvader JE, Lindeman GJ. Cancer stem cells in solid tumours: accumulating evidence and unresolved questions. *Nat Rev Cancer.* 2008; 8(10): 755-768.
24. Li QQ, Wang G, Huang F, Banda M, Reed E. Antineoplastic effect of beta-elemene on prostate cancer cells and other types of solid tumour cells. *J Pharm Pharmacol.* 2010; 62(8): 1018-1027.
25. Zhao YS, Zhu TZ, Chen YW, Yao YQ, Wu CM, Wei ZQ, et al.

- β -Elemene inhibits Hsp90/Raf-1 molecular complex inducing apoptosis of glioblastoma cells. *J Neurooncol.* 2012; 107(2): 307-314.
26. Lu X, Wang Y, Luo H, Qiu W, Han H, Chen X, et al. β -Elemene inhibits the proliferation of T24 bladder carcinoma cells through up-regulation of the expression of Smad4. *Mol Med Rep.* 2013; 7(2): 513-518.
 27. Zhan YH, Liu J, Qu XJ, Hou KZ, Wang KF, Liu YP, et al. β -Elemene induces apoptosis in human renal-cell carcinoma 786-0 cells through inhibition of MAPK/ERK and PI3K/Akt/mTOR signalling pathways. *Asian Pac J Cancer Prev.* 2012; 13(6): 2739-2744.
 28. Liu J, Zhang Y, Qu J, Xu L, Hou K, Zhang J, et al. β -Elemene-induced autophagy protects human gastric cancer cells from undergoing apoptosis. *BMC Cancer.* 2011; 11: 183.
 29. Dai ZJ, Tang W, Lu WF, Gao J, Kang HF, Ma XB, et al. Antiproliferative and apoptotic effects of β -elemene on human hepatoma HepG2 cells. *Cancer Cell Int.* 2013; 13(1): 27.
 30. Li CL, Chang L, Guo L, Zhao D, Liu HB, Wang QS, et al. β -elemene induces caspase-dependent apoptosis in human glioma cells in vitro through the upregulation of Bax and Fas/FasL and downregulation of Bcl-2. *Asian Pac J Cancer Prev.* 2014; 15(23): 10407-10412.
 31. Pugazhenti S, Nesterova A, Sable C, Heidenreich KA, Boxer LM, Heasley LE, et al. Akt/protein kinase B up-regulates Bcl-2 expression through cAMP-response element-binding protein. *J Biol Chem.* 2000; 275(15): 10761-10766.
 32. Li QQ, Wang G, Zhang M, Cuff CF, Huang L, Reed E. beta-el-emene, a novel plant-derived antineoplastic agent, increases cis-platin chemosensitivity of lung tumor cells by triggering apoptosis. *Oncol Rep.* 2009; 22(1): 161-170.
 33. Liu JS, Che XM, Chang S, Qiu GL, He SC, Fan L, et al. β -elemene enhances the radiosensitivity of gastric cancer cells by inhibiting Pak1 activation. *World J Gastroenterol.* 2015; 21(34): 9945-9956.
 34. Li G, Xie B, Li X, Chen Y, Xu Y, Xu-Welliver M, et al. Downregulation of peroxiredoxin-1 by β -elemene enhances the radiosensitivity of lung adenocarcinoma xenografts. *Oncol Rep.* 2015; 33(3): 1427-1433.
 35. Li G, Xie B, Li X, Chen Y, Wang Q, Xu Y, et al. Down-regulation of survivin and hypoxia-inducible factor-1 α by β -elemene enhances the radiosensitivity of lung adenocarcinoma xenograft. *Cancer Biother Radiopharm.* 2012; 27(1): 56-64.
-

Characterization and In Silico Analysis of The Structural Features of G-CSF Derived from Lysates of *Escherichia coli*

Sharareh Peymanfar, M.Sc.¹, Rasoul Roghanian, Ph.D.^{1*}, Kamran Ghaedi, Ph.D.¹, Sayed-Hamid Zarkesh-Esfahani, Ph.D.¹, Reza Yari, Ph.D.²

1. Department of Biology, Faculty of Science, University of Isfahan, Isfahan, Iran
2. Department of Biology, Borujerd Branch, Islamic Azad University, Borujerd, Iran

*Corresponding Address: P.O.Box: 81746, Department of Biology, Faculty of Science, University of Isfahan, Isfahan, Iran
Email: r.roghanian@sci.ui.ac.ir

Received: 3/July/2018, Accepted: 10/December/2018

Abstract

Objective: Granulocyte colony-stimulating factor (G-CSF) has a wide variety of functions including stimulation of hematopoiesis and proliferation of granulocyte progenitor cells. Recombinant human G-CSF (rh-G-CSF) is used for treatment of neutropenia in patients receiving chemotherapy. The mature bloodstream neutrophils express G-CSF receptor (G-CSFR), presenting a significant and specific mechanism for circulating G-CSF clearance. Computational studies are essential bioinformatics methods used for characterization of proteins with regard to their physicochemical properties and 3D configuration, as well as protein–ligand interactions for recombinant drugs. We formerly produced rh-G-CSF in *E. coli* and showed that the isolated protein had unacceptable biological activity in mice. In the present paper, we aimed to characterize the purified rh-G-CSF by analytical tests and developed an *in vivo* model by computational modelling of G-CSF.

Materials and Methods: In this experimental study, we analyzed the purified G-CSF using the analytical experiments. Then, the crystalline structure was extracted from Protein Data Bank (PDB) and molecular dynamics (MD) simulation was performed using Gromacs 5.1 package under an Amber force field. The importance of amino acid contents of G-CSF, to bind the respective receptor was also detected; moreover, the effect of dithiothreitol (DTT) used in G-CSF purification was studied.

Results: The results revealed that characteristics of the produced recombinant G-CSF were comparable with those of the standard G-CSF and the recombinant G-CSF with the residual amino acid was stable. Also, purification conditions (DTT and existence of extra cysteine) had a significant effect on the stability and functionality of the produced G-CSF.

Conclusion: Experimental and in silico analyses provided good information regarding the function and characteristics of our recombinant G-CSF which could be useful for industrial researches.

Keywords: Characterization, *E. coli*, Granulocyte Colony-Stimulating Factor

Cell Journal (Yakhteh), Vol 21, No 4, January–March (Winter) 2020, Pages: 426–432

Citation: Peymanfar Sh, Roghanian R, Ghaedi K, Zarkesh-Esfahani SH, Yari R. Characterization and in silico analysis of the structural features of G-CSF derived from lysates of *Escherichia coli*. Cell J. 2020; 21(4): 426-432. doi: 10.22074/cellj.2020.6158.

Introduction

The granulocyte colony stimulating factor (G-CSF) serves a directing role in the growth, differentiation, and motivation of neutrophils and their precursors in the immune system (1). Likewise, G-CSF has been effectively utilized in patients undergoing intensive chemotherapy; further, it might be utilized to recover the immune system in the patients with HIV, pneumonia, and febrile neutropenia (2-4). The recombinant human G-CSF (rh-G-CSF) was expressed in engineered *E. coli* and affirmed in chemotherapy-induced neutropenia by the U.S Food and Drug Administration (FDA) in 1991 for clinical usage (5).

Previous studies described various protocols for assessment of rh-G-CSF. These protocols used different chromatography columns and diverse detergents for purification of rh-G-CSF (6-8). Nowadays, purification of proteins fused to intein tags is an easy task. N-terminus or C-terminus of the target protein binds the intein tags. To achieve this purpose and also to double the expression of target protein, in our previous study, we linked 2 copies of *G-CSF* gene with 2 different intein sequences and attained target protein in two forms: G-CSF and G-CSF plus cysteine (9, 10).

Furthermore, since intein tags may interfere with

G-CSF binding to its receptor and therefore, disrupt its biological activity, it is necessary to simulate molecular dynamics (MD) to check the presence of these tags and examine their effect on G-CSF binding to G-CSFR. The receptor of hematopoietic cytokine G-CSF is a member of a family of proteins referred to as the "family of cytokine receptors" and characterized by the existence of a 200-residue ligand-binding module. Alternatively, it is required to assess the effect of purification process on the protein stability and its receptor binding. To answer this question, computational studies were used in the present research. It should be mentioned that such study has not been conducted on G-CSF protein so far. The use of computational tools for determination of a new protein structure represents the most actual alternative to the experimental procedures. As relates to characterization of physicochemical and structural properties of a protein, there is no doubt that in silico methods can resolve complications made by purification techniques (11-15).

Considering very different properties of commercially available rh-G-CSF proteins, we constructed a model of the isolated G-CSF and its G-CSFR. Previously, we produced G-CSF with intein tags and purified it using DTT and pH exchange. So, the present work was designed to identify

functional and structural changes, especially with respect to the extra amino acid residue of G-CSF, and intein tags as well as the presence of DTT in protein solution, and finally compare the results obtained for natural and purified G-CSF. We studied G-CSF characteristics, created our models with respect to the improved dynamic modelling of rh-G-CSF and studied the effect of DTT and the residual cysteine on G-CSF stability and function.

Materials and Methods

Designing the DNA fragment encompassing rh-G-

CSF coding sequence, intein, PelB, and intervening sequences of Trp operon

Two tandems of G-CSF sequences linked to inteins (CBD-Ssp DnaB and Mxe GryA-CBD) were described in a previous study. This fragment purchased from GENESCRIP T Company (USA) was acquired in the pUC57 vector located at 5' *MscI* and 3' *XhoI* (14). In the next step, this fragment was inserted into the pET22b vector at the same sites in the downstream of the pelB signal sequence (Fig.1A) (9).

Rh-G-CSF production and purification

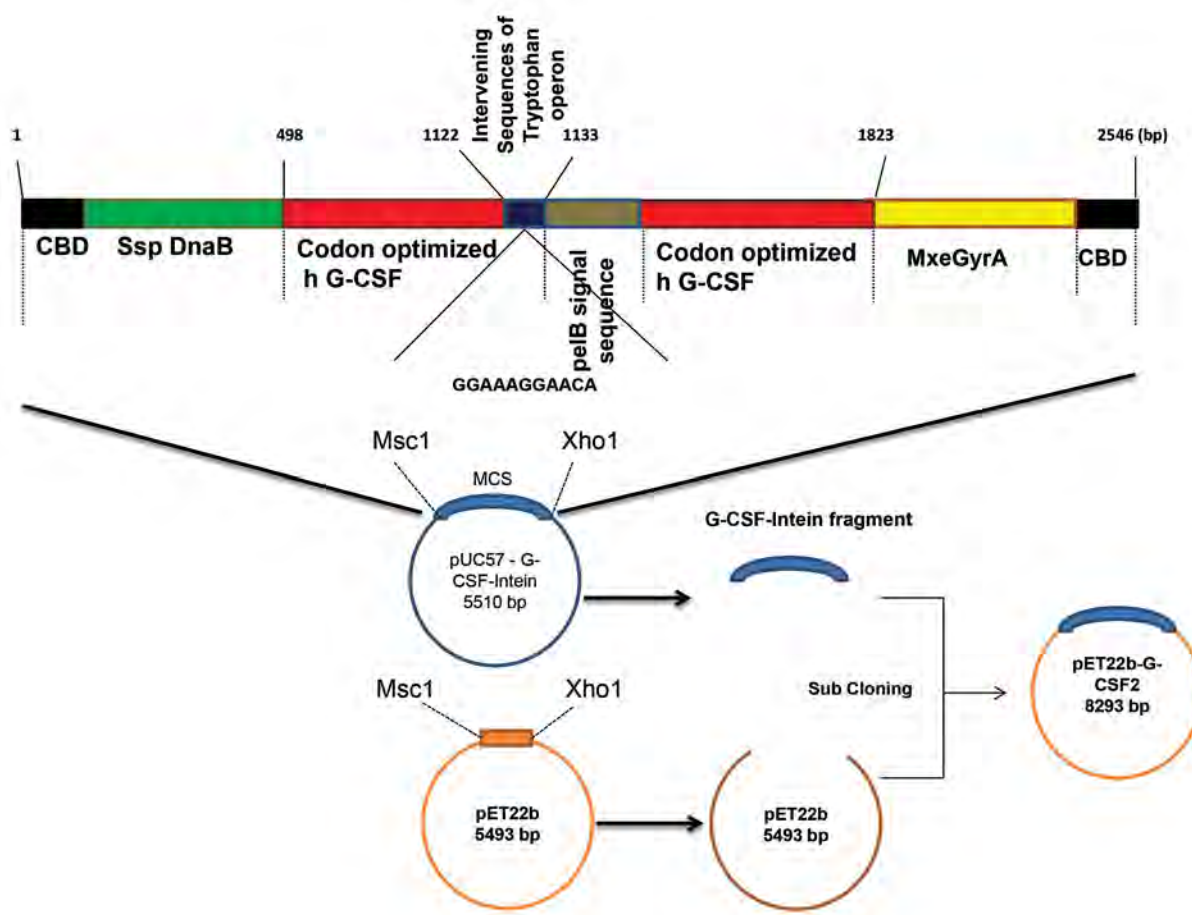
The cloning, expression and intein-mediated purification were performed in pET-22b (+) vector (9, 10, 16). Purification was performed according to the template

shown in Figure 1B (9).

Detection of *E. coli* host cell proteins

E. coli host cell proteins (HCP) were studied by an immunoenzymetric assay kit (Cygnus, USA) and an ELISA reader (Amersham, USA). According to the manufacturer's protocol, 25 μ L of each sample was loaded into each well. Next, 100 μ L of *E. coli* antibody conjugated to horseradish peroxidase (HRP, Abcam, UK) was pipetted into each well. Then, these wells were covered and incubated on a rotator at 400-600 rpm for 90 minutes at room temperature ($24 \pm 4^\circ\text{C}$). The content of each well was dumped into waste. The wells were blotted softly but firmly tapped over an absorbent paper to remove most of the residual liquid. The wells were filled generously to overflow with the diluted wash solution using a squirt bottle or pipetting in 350 μ L. Washing was repeated. From the bottom outside of the microtiter wells, any fluid residue that could interfere in the reading step, was wiped off. Then, 100 μ L of the 3,3',5,5'-tetramethylbenzidine (TMB) substrate was pipetted and incubation was performed at room temperature for 30 minutes. Finally, 100 μ L of the stop solution was pipetted. Absorbance was read at 450/650 nm. The microplate reader drew one standard curve and automatically calculated the amount of HCP in the purified protein (17).

A



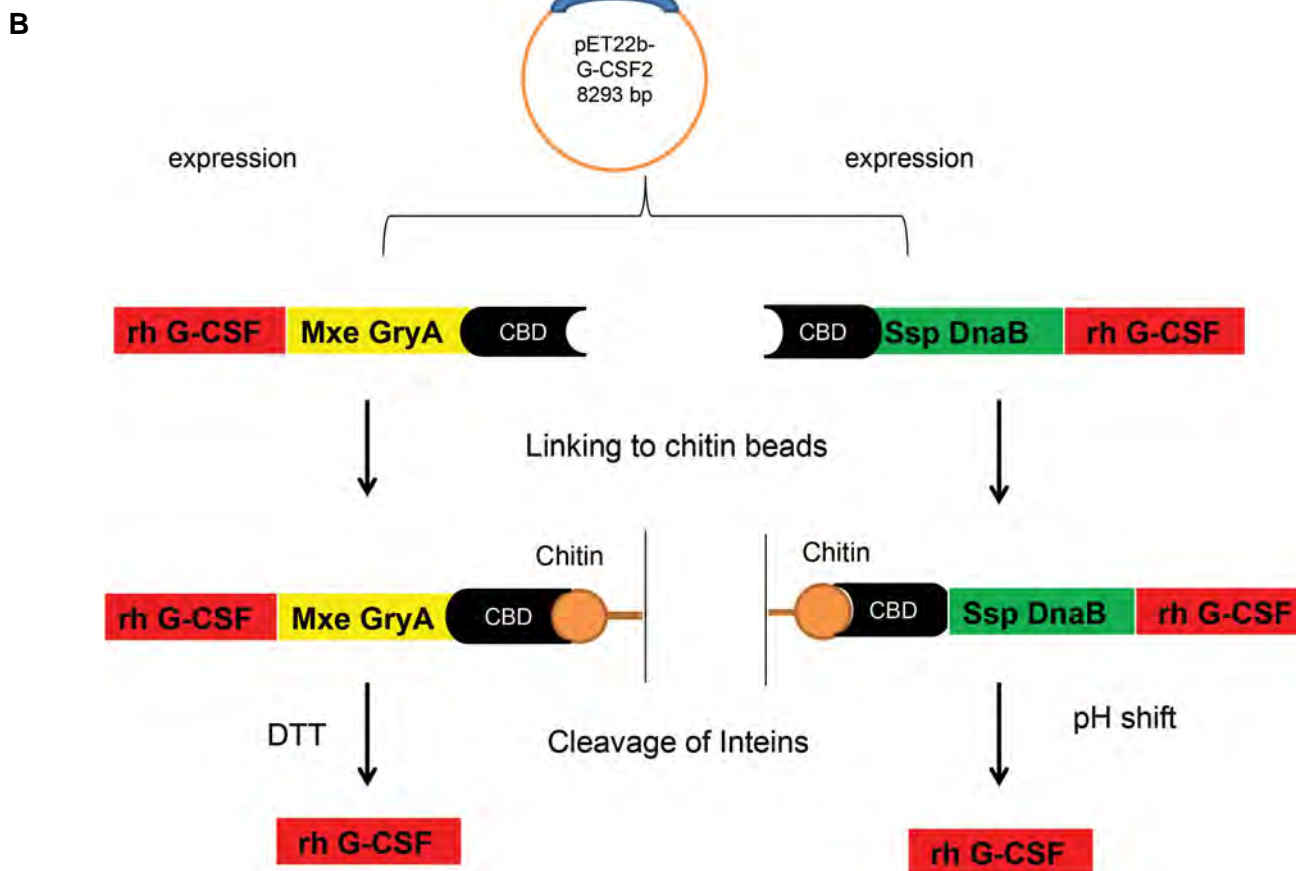


Fig.1: Overall schema of 2800 bp expression vector with *g-csf* gene and 2 different inteins genes, pelB signal sequence and intervening sequence. **A.** Schematic representation of the vector construction and the expression of the N-terminal fusion and C-terminal fusion proteins and **B.** In C-terminal fusion protein, intein2-CBD was fused to the C-terminus of h G-CSF, allowing the cleavage of h G-CSF from G-CSF-intein2 using DTT. In N-terminal fusion protein, CBD-intein1 was fused to the N-terminus of h G-CSF, allowing the cleavage of h G-CSF from intein1- G-CSF through a pH and temperature shift. G-CSF; Granulocyte colony-stimulating factor.

Measurement of bacterial endotoxin contamination

The amount of bacterial endotoxin was determined by the LAL kit (Lonza, Switzerland) and an ELISA reader (Amersham, USA). Carefully, 50 μ L of the purified protein was dispensed into suitable tubes that were endotoxin-free. These tubes were kept in a 37°C water bath. Blank tubes plus four endotoxin standards were run in duplicate. The blank tubes contained 50 μ L of the LAL reagent water instead of the sample. At the same time, to the reaction vessel, 50 μ L of LAL was added. Then, 100 μ L of the substrate solution was added to the tubes (pre-warmed to 37 \pm 1°C) after 10 minutes. After 16 minutes, 100 μ L of the stop reagent was added and mixed well. Absorbance of reaction in each tube was read at 405/410 nm by the ELISA reader using distilled water to adjust the photometer to the zero absorbance. The ELISA reader drew one standard curve and automatically calculated the amount of endotoxin in the purified protein (17).

Impurities with charges that were different from those of Filgrastim (Isoelectric focusing)

Isoelectric focusing (IEF) was performed using a pH 3-10 IEF gel (Invitrogen, Grand Island, NY) (17, 18).

The electrophoresis system (Multiphor II, Amersham, USA) was fitted out with a buffer tank, a cooling plate, an electrode holder, and electrophoresis (EPH)/IEF electrodes. Experiments were performed using 7-cm immobilized pH gradient (IPG) stripes (pH=3-10). The system worked at room temperature. The pH gradient was 4.5-8.0 and an isoelectric point (pI) calibration solution was prepared in the pI range of 2.5-6.5. The standard and the sample were put on the stripes. In this test, proteins were moving in the gel stripes and finally, the purified protein and standard protein were stopped at their pI. If there was any impurity in the purified protein, it would move in the gel and could be stopped at its pI. The Filgrastim standard was obtained from Pooyesh Darou Company (Iran).

Peptide mapping with RP-HPLC

Peptide map analysis is an important analytical technique widely used to verify protein primary structures. The method is capable of specifically detecting and quantifying structural alterations in the recombinant proteins, such as those derived from N-terminal blockage, oxidation, proteolysis, or amino acid substitutions. To identify the

structure and fundamental variations, RP-HPLC was used (17, 18). In this test, standard and sample proteins were digested by glutamyl endopeptidase for 18 hours at 37°C and then analyzed by HPLC. The HPLC system (Agilent, USA) included a system controller, a pump, a degasser, the auto-sampler, and a photodiode array (PDA) detector. The detector was set at 214 nm and the peak regions were integrated by computational analyses. Experiments were done using a C18 column (100× 2.1 mm, 5 µm particle size, with 300 Å pore size). The HPLC test was performed at 60°C, using acetonitrile as the mobile phase. The standard and the sample were at the concentration of 25 µg per 10 µL, and all determinations were carried out in triplicate. The flow rate was 0.2 mL/minutes.

Retrieval of protein sequences and 3D structures

The protein sequences of G-CSF and G-CSFR were achieved from UniProt (<http://www.uniprot.org/>). The protein sequences were retrieved in the FASTA format in order to be analyzed by the computational methods. Also, the crystal structure of G-CSF and G-CSFR from the PDB data storage site with the codes 1GNC and 2D9Q, was obtained; finally, it was used as the primary structure for the MD simulation. Likewise, sequences of inteins (Ssp DnaB and Mxe GryA) were obtained from InBase database (New England Biolabs Intein Database available at <http://www.inteins.com/>) and used in the MD Simulation (19-21).

Molecular dynamics simulation

MD simulation was performed by Gromacs 4.6.4 package using GROMOS96 (53a6) (19). In this test, effect of DTT (40 mM) and pH exchange was studied on the protein structure and stability and also the effect of extra cysteine on G-CSF stability and its GCSF-R binding was evaluated. The protein topology file for Gromacs was provided utilizing the program Topolbuild, developed by Bruce D. Ray. All systems were solvated by explicit solvents (TIP3P) and counter ions were added to neutralize each system. Next, the energy minimization (EM) was performed by the steepest descent algorithm at tolerance value of 100 kJ/mol.nm. Also, EM was followed by the equilibration with position restraint on the protein molecule for 0.5 ns using Constant temperature and volume (NVT) and Constant temperature and pressure (NPT) ensembles by standard coupling methods. Then, main runs were performed without any restraint on the protein molecule, trajectories were generated with a time interval of 0.01 ns, and frames were saved at every 0.01 ns. Particle mesh ewald (PME) summation was used to assess long-range Coulomb interactions (20). In the equilibration and subsequent production runs, the internal degrees of freedom of the solvent molecules were restrained by the SHAKE algorithm (21), and all bond lengths were restrained in the macromolecules via the LINCS algorithm (22).

All analyses were provided by Gromacs toolbox and the images were produced by PyMol (23) and LigPlot (24).

Results

Detection of *E. coli* host cell proteins in the purified rh-G-CSF solution

E. coli HCP were detected by the immunoenzymetric assay kit (Cygnus, USA). The results indicated that HCP was less than 100 ppm/dose and thus, they were in the permissible range (data not shown).

Bacterial endotoxins

The number of bacterial endotoxins was determined by the LAL kit (Lonza, Switzerland). The results showed that the amount of *E. coli* endotoxins was less than 2 IU/mg protein.

Impurities with charges that were different from those of Filgrastim (Isoelectric focusing)

IEF was performed using a pH=3-10 IEF gel. Filgrastim main band in the standard and purified sample was stopped at pH=6.1; also, no band was more intense than the chief one in the electropherogram attained with the reference solution (PDgrastim) (Fig.2).

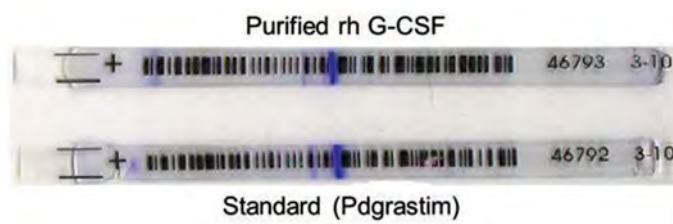


Fig.2: Isoelectric focusing of purified rh G-CSF and PDgrastim (standard) in the strips of pH=3-10. Both of the standard and purified proteins were stopped in pH=6.1 and no impurity or no band was found. G-CSF; Granulocyte colony-stimulating factor.

Peptide mapping

To confirm the protein structure and identify modifications, peptide mapping and RP-HPLC were done (18). The chromatogram attained with the reference solution was similar to that of the purified G-CSF. The chromatogram obtained with the test solution corresponded to that of the chromatogram achieved with the reference, but they were not exactly the same (Fig.3). This discrepancy could be due to the fact that the enzyme did not affect the purified protein or changed the amino acid content.

Molecular dynamic simulation

The crystal structure of proteins was attained from PDB. Visualization of the proteins model was done by Chimera (version 1.8). To determine the structural and

functional differences between G-CSF and cysteine-G-CSF and to find their differences in binding G-CSF-R, MD simulation studies were performed. The simulations were carried out for all of the mentioned structures, as mentioned in the Materials and Methods section, under explicit solvent conditions. The trajectory results obtained from MD simulation were evaluated for RMSD and RMSF.

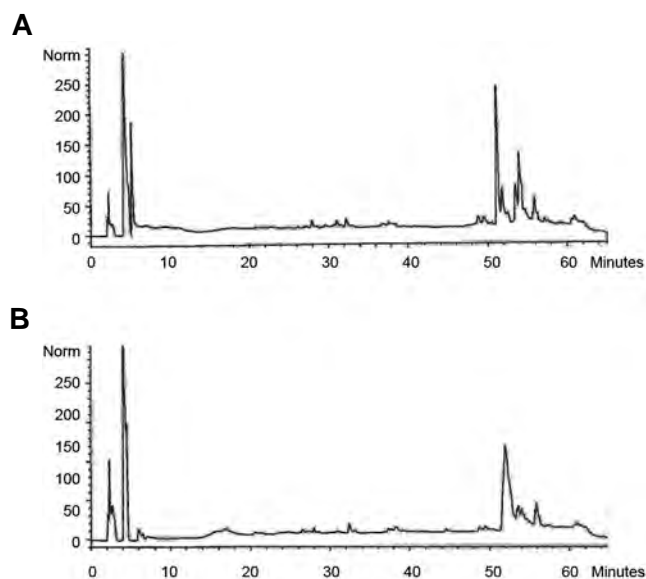


Fig.3: The reversed phase HPLC chromatogram for the Endopeptidase digest of purified rh G-CSF in comparison with standard rh G-CSF. **A.** Peptide map chromatograms of PDgrastim and **B.** Purified rh G-CSF. G-CSF; Granulocyte colony-stimulating factor.

The effect of dithiothreitol on the protein stability and receptor binding

The Figure 4A depicts the RMSD variations during the simulation of G-CSF protein in the presence and absence of DTT. As shown in Figure 4A, protein in the presence of DTT was more unstable and its RMSD was greater than that in the non-DTT state. Likewise, the RMSF graph showed that in the presence of DTT, the protein's flexibility was increased in certain regions (Fig.4B).

As shown in the RMSF diagram, in the residues 1 to 40, as well as 65 to 80, the presence of DTT led to a dramatic increase. As shown by the RMSD and RMSF diagrams, the presence of DTT increased protein flexibility. Additionally, the stability of the G-CSF protein, when bound to G-CSF-R, was monitored in the presence of DTT. For this reason, in this part, the RMSF diagram of the G-CSF protein was analyzed in the complex mode with G-CSFR in the presence of DTT (Fig.4C).

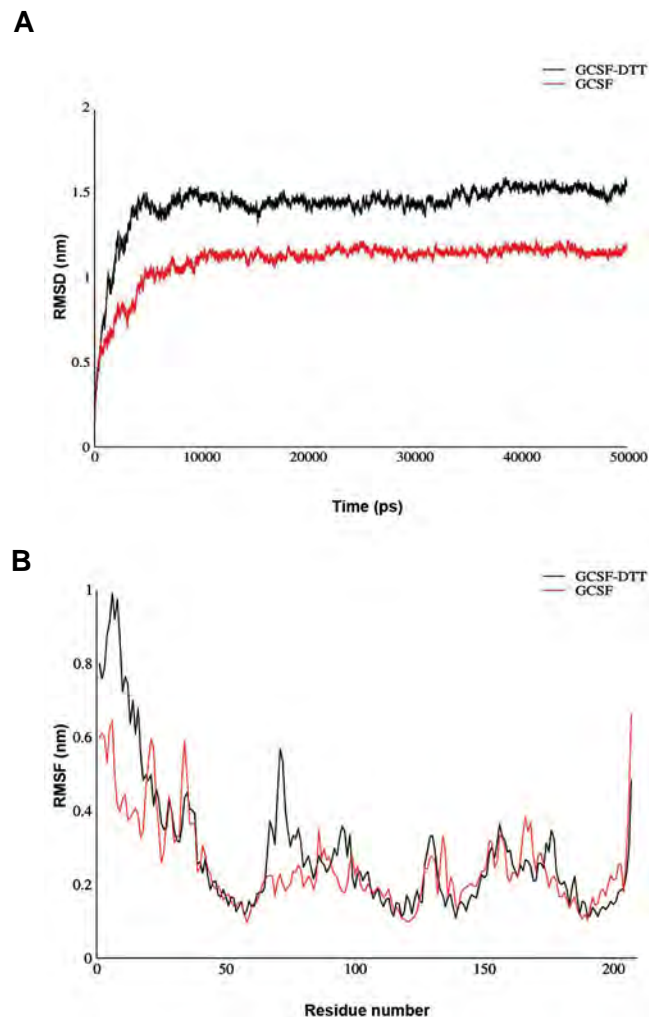
As shown in this diagram, DTT increased the protein's flexibility in all its amino acids. This increase

in flexibility could probably cause the G-CSF- G-CSFR complex to become unstable and reduce the binding affinity between the two proteins.

The effect of the residual cysteine on the protein stability and receptor binding

After G-CSF purification, it was possible to keep the extra cysteine in the N-terminal of G-CSF. Hence, to study the effect of this amino acid on the protein stability and receptor binding, we performed the computational analysis. The Figure 4D shows the variations of the RMSD associated with the natural G-CSF protein and the cysteine residue. As shown, the presence of cysteine residue in the protein significantly reduced the RMSD level and stabilized the protein over time.

The graph shows the flexibility of the residues for a natural and atypical protein (containing cysteine). As shown in the RMSF diagram, the total flexibility of the structure in the atypical state was reduced, as compared with the normal one, and this reduction was significant in the early amino acid sequence of the protein. Analysis of the two above-mentioned graphs shows that the presence of cysteine residues reduced the flexibility and stability of the G-CSF structure (Fig.4E).



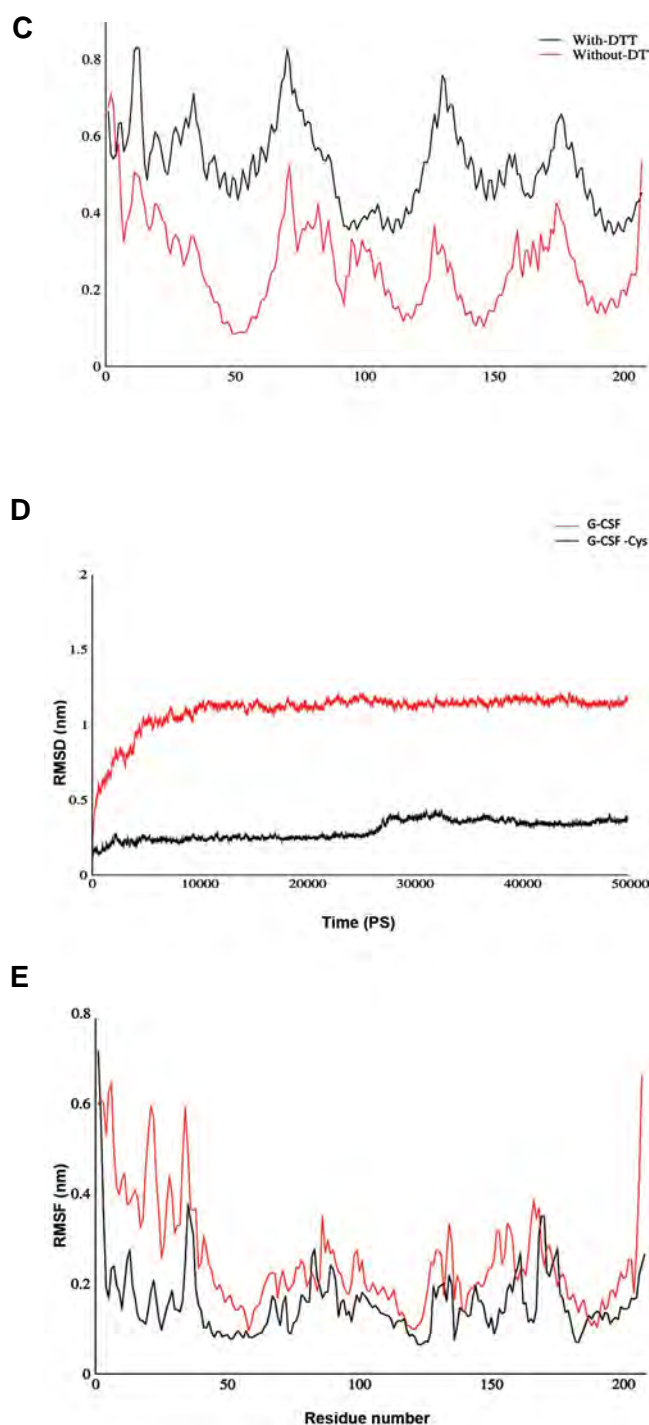


Fig.4: Results of molecular dynamic simulation of RMSF and RMSD diagram. **A.** Comparison of RMSD changes. The simulation of G-CSF protein in the presence and absence of DTT, **B.** Comparison of the RMSF diagram of G-CSF in the presence and absence of DTT, **C.** RMSF diagram of GCSF protein in complex with GCSFR in the presence of DTT, **D.** The RMSD variations associated with the natural GCSF protein and GCSF have Cysteine amino acid, and **E.** RMSF diagram shows flexible amount of single amino acids for normal and atypical protein (contains cysteine). RMSF; Root-mean-square fluctuation, RMSD; Root-mean-square deviation, G-CSF; Granulocyte colony stimulating factor, and DTT; Dithiothreitol.

Discussion

rh-G-CSF is widely used as a useful hematopoietic growth factor. Therefore, production of rh-G-CSF seems to be required. Hence, it was decided to analyze rh-G-CSF that had already been produced in *E. coli* with laboratory

and in silico methods. Formerly, we produced G-CSF linked to intein (9). The intein segments were preferably used for better expression and purification due to their low molecular weight, resulting in a high percentage of small G-CSF as fusion protein. Xie et al. (10) cloned OG2 antimicrobial peptide in the pTWIN1 vector with two different intein segments and achieved high-rate expression and production of the recombinant protein. They achieved purified proteins with extra cysteine in the N-terminal. We also implemented this procedure to purify rh-G-CSF with chitin beads, achieving G-CSF and cysteine-GCSF. Then, we analyzed the purified G-CSF for impurities using IEF and HCP determination tests, also the structure was analyzed using peptide mapping. Our results were comparable with those achieved by Kim et al. (18). This was because they could produce G-CSF in *E. coli* with good quality and no impurity. Additionally, we investigated the effect of DTT (used for purification) and extra cysteine on stability and function of G-CSF. The results displayed that the purified G-CSF had characteristics similar to those of the standard, and DTT reduced G-CSF stability and increased its flexibility. Also, our studies showed that the residual cysteine increased the stability and reduced flexibility; therefore, it might not affect receptor binding. The results of computational studies of this protein were shown to be consistent with those of laboratory studies and the biological activity of this protein. In this way, the presence or absence of cysteine could not have any important effect on the biological activity of protein. Comparison of GCSF and cysteine-GCSF results revealed that both of them were stable and probably had similar functionality. It was even imaginable that the modified protein had higher biological activity; we previously observed that cysteine-GCSF biological activity was higher than that of the standard G-CSF (9).

Conclusion

The information displayed here may be important to biopharmaceutical companies to produce new recombinant proteins using new techniques. Despite various applications of MD simulation in protein engineering, no similar research was done on this protein. Therefore, studying the structural dynamic properties of this protein under different conditions provided a new opportunity to study the stability and function of G-CSF.

Acknowledgements

This study was financially supported by the University of Isfahan, Iran. There is no conflict of interest and all authors support submission to this journal.

Authors' Contributions

S.P., K.G., R.R.; Participated in study conception. S.P., R.Y.; Performed experimental analyses, and data collection and evaluation as well as statistical analysis. All authors participated in interpretation of the data and drafting the manuscript. All authors approved the final

draft of manuscript prepared for submission and read the final manuscript.

References

- Jin H, Cantin GT, Maki S, Chew LC, Resnick SM, Ngai J, et al. Soluble periplasmic production of human granulocyte colony-stimulating factor (G-CSF) in *Pseudomonas fluorescens*. *Protein Expr Purif*. 2011; 78(1): 69-77.
- Dale D. Current management of chemotherapy-induced neutropenia: the role of colony-stimulating factors. *Semin Oncol*. 2003; 30(4 Suppl 13): 3-9.
- Nishii K, Xing XH, Shiragami N, Unno H. Production of rG-CSF by CHO cell in aggregate microbeads culture. *Cytotechnol*. 1994; 6(7): 435-439.
- Frampton JE, Yarker YE, Goa KL. Lenograstim. A review of its pharmacological properties and therapeutic efficacy in neutropenia and related clinical settings. *Drugs*. 1995; 49(5): 767-793.
- Souza L M, Boone T C, Gabrilove J, Lai P H, Zsebo K M, Murdock D C, et al. Recombinant human granulocyte colony-stimulating factor: effects on normal and leukemic myeloid cells. *Science*. 1986; 232(4746): 61-65.
- Guo C, Li Z, Shi Y, Xu M, Wise JG, Trommer WE, et al. Intein-mediated fusion expression, high efficient refolding, and one-step purification of gelonin toxin. *Protein Expr Purif*. 2004; 37(2): 361-367.
- Laemmli U K. Cleavage of structural protein during the assembly of head of bacteriophage T4. *Nature*. 1970; 227(5259): 680-685.
- Jeong K J, Lee SY. Secretory production of human granulocyte colony stimulating factor in *Escherichia coli*. *Protein Expr Purif*. 2001; 23(2): 311-318.
- Peymanfar P, Roghanian R, Ghaedi K, Sayed H, Yari R. Production and simple purification of recombinant human granulocyte colony-stimulating factor using the intein tag in *Escherichia coli*. *Int J Med Biotechnol Genetics*. 2016; 4(2): 40-46.
- Xie YG, Han EF, Luan Ch, Zhang HW, Feng J, Choi YJ, et al. High-yield soluble expression and simple purification of the antimicrobial peptide OG2 using the intein system in *Escherichia coli*. *Biomed Res Int*. 2013; 2013: 754319.
- Durrant JD, McCammon JA. Molecular dynamics simulations and drug discovery. *BMC Biol*. 2011; 9: 71.
- Hwang I, Park S. Computational design of protein therapeutics. *Drug Discov Today Technol*. 2008; 5(2-3): e43-e48.
- Hornak V, Abel R, Okur A, Strockbine B, Roitberg A, Simmerling C. Comparison of multiple amber force fields and development of improved protein backbone parameters. *Proteins*. 2006; 65(3): 712-725.
- Moore GL, Maranas CD. Computational challenges in combinatorial library design for protein engineering. *AIChE J*. 2004; 50(2): 262-272.
- Vinay Kumar C, Swetha RG, Anbarasu A, Ramaiah S. Computational analysis reveals the association of threonine 118 methionine mutation in PMP22 resulting in CMT-1A. *Adv Bioinformatics*. 2014.
- Peymanfar Sh, Roghanian R, Ghaedi K. Comparison of different methods of osmotic shocks for extraction of Human Granulocyte Colony Stimulating Factor produced in periplasm. *Biological Journal of Microorganism*. 2018; 26: 42-50.
- European Pharmacopoeia 6.3; Filgrastim concentrated solution. Strasbourg: Stationery Office. 2009.
- Kim CK, Lee CH, Lee SB, Oh JW. Simplified large-scale refolding, purification, and characterization of recombinant human granulocyte colony stimulating factor in *Escherichia coli*. *PLoS One*. 2013; 8(11): e80109.
- Case DA, Cheatham TE 3rd, Darden T, Gohlke H, Luo R, Merz KM Jr, et al. The amber bio molecular simulation programs. *J Comput Chem*. 2007; 26(16): 1668-1688.
- Essmann U, Perera L, Berkowitz ML. A smooth particle mesh Ewald method. *J Chem Phys*. 1995; 103(19): 8577-8593.
- Ryckaert JP, Ciccoti G, Berendsen HJC. Numerical integration of the cartesian equations of motion of a system with constraints: molecular dynamics of n-Alkanes. *J Comput Phys*. 1977; 23(3): 327-341.
- Hess B, Bekker H, Berendsen HJC, Fraaije JGEM. LINCS: a linear constraint solver for molecular simulations. *J Comp Chem*. 1997; 18: 1463-1472.
- DeLano WL. The PyMOL molecular graphics system. *Proteins Structure Function and Bioinformatics*. 2002; 30: 442-454.
- Wallace AC, Laskowski RA, Thornton JM. LIGPLOT: a program to generate schematic diagrams of protein-ligand interactions. *Protein Eng*. 1995; 8(2): 127-134.

Biosimilar Gene Therapy: Investigational Assessment of Secukinumab Gene Therapy

Ali Fallah, Ph.D.^{1,2}, Hajar Estiri, Ph.D.², Elizabeth Parrish, B.Sc.², Mansoureh Soleimani, Ph.D.³,

Sirous Zeinali, Ph.D.^{4*}, Azita Zadeh-Vakili, Ph.D.^{5*}

1. Department of Biotechnology, School of Advanced Technologies in Medicine, Shahid Beheshti University of Medical Sciences, Tehran, Iran

2. RNAx Ltd., London, UK

3. Cellular and Molecular Research Center, Iran University of Medical Sciences, Tehran, Iran

4. Molecular Medicine, Pasteur Institute of Iran, Tehran, Iran

5. Cellular and Molecular Endocrine Research Center, Research Institute for Endocrine Sciences, Shahid Beheshti University of Medical Sciences, Tehran, Iran

*Corresponding Addresses: Molecular Medicine, Pasteur Institute of Iran, Tehran, Iran

P.O.Box:19395-4763, Cellular and Molecular Endocrine Research Center, Research Institute for Endocrine Sciences, Shahid Beheshti University of Medical Sciences, Tehran, Iran

Emails: zeinali@pasteur.ac.ir, azitavakili@endocrine.ac.ir

Received: 19/August/2018, Accepted: 09/December/2018

Abstract

Objective: Tumor necrosis factor-alpha (TNF- α), checkpoint inhibitors, and interleukin-17 (IL-17) are critical targets in inflammation and autoimmune diseases. Monoclonal antibodies (mAbs) have a successful portfolio in the treatment of chronic diseases. With the current progress in stem cells and gene therapy technologies, there is the promise of replacing costly mAbs production in bioreactors with a more direct and cost-effective production method inside the patient's cells. In this paper we examine the results of an investigational assessment of secukinumab gene therapy.

Materials and Methods: In this experimental study, the DNA sequence of the heavy and light chains of secukinumab antibodies were cloned in a lentiviral vector. Human chorionic villous mesenchymal stem cells (CMSCs) were isolated and characterized. After lentiviral packaging and titration, part of the recombinant viruses was used for transduction of the CMSCs and the other part were applied for systemic gene therapy. The engineered stem cells and recombinant viruses were applied for *ex vivo* and *in vivo* gene therapy, respectively, in different groups of rat models. *In vitro* and *in vivo* secukinumab expression was confirmed with quantitative real-time polymerase chain reaction (qRT-PCR), western blot, and ELISA by considering the approved secukinumab as the standard reference.

Results: Cell differentiation assays and flow cytometry of standard biomarkers confirmed the multipotency of the CMSCs. Western blot and qRT-PCR confirmed *in vitro* gene expression of secukinumab at both the mRNA and protein level. ELISA testing of serum from treated rat models confirmed mAb overexpression for both *in vivo* and *ex vivo* gene therapies.

Conclusion: In this study, a lentiviral-mediated *ex vivo* and *in vivo* gene therapy was developed to provide a moderate dose of secukinumab in rat models. Biosimilar gene therapy is an attractive approach for the treatment of autoimmune disorders, cancers and other chronic diseases.

Keywords: Gene Therapy, Genetic Vectors, Monoclonal Antibody, Secukinumab, Stem Cells

Cell Journal (Yakhteh), Vol 21, No 4, January-March (Winter) 2020, Pages: 433-443

Citation: Fallah A, Estiri H, Parrish E, Soleimani M, Zeinali S, Zadeh-Vakili A. Biosimilar gene therapy: investigational assessment of secukinumab gene therapy. Cell J. 2020; 21(4): 433-443. doi: 10.22074/cellj.2020.6309.

Introduction

Autoimmune diseases comprise 81 clinically distinct conditions and affect approximately 2.7% of the male, and 6.4% of the female population globally. Psoriasis, celiac disease, Graves' disease, inflammatory bowel disease, multiple sclerosis, rheumatoid arthritis, systemic lupus erythematosus, and diabetes mellitus type 1 are some common autoimmune diseases. Diagnostics and categorization of autoimmune diseases are generally difficult, and it is expected that the percentage of the people affected with autoimmune diseases will increase. Autoimmune diseases have overlapping mechanisms with the same functional cells and molecular malfunctions (1).

T helper 17 (TH17) cells are a distinct subtype of CD4⁺ TH cells that produce interleukin-17 (IL-17) and play a critical role in the defense against fungal and bacterial extracellular pathogens. Furthermore, TH17 cells play

a core role in chronic inflammatory and autoimmune disorders, namely, multiple sclerosis, rheumatoid arthritis, psoriasis, asthma, and type 1 diabetes (2). IL-17 is a CD4⁺ T cell-derived cytokine that promotes inflammatory responses and is elevated in rheumatoid arthritis, asthma, multiple sclerosis, psoriasis, diabetes, and transplant rejection (3). IL-17 and IL-17Rs inhibitors have recently shown potential for universal targeting treatments to tackle autoimmune diseases (4).

Developing monoclonal antibodies (mAbs) against IL-17 and IL-17Rs are advantageous for the biopharma industry's fight against autoimmune diseases and cancer. Secukinumab (Cosentyx), Ixekizumab (Taltz), and Brodalumab (Siliq) are approved mAbs against IL-17 and IL-17R. A few molecules such as IL-17, checkpoint inhibitors, and tumor necrosis factor-alpha (TNF- α) are universal targets for a broad spectrum of cancers and

inflammatory and autoimmune diseases. Gene therapy based biosimilars of these universal molecules will provide more available and cost-effective solutions for long-lasting diseases. Approved secukinumab is employed to treat psoriasis, ankylosing spondylitis, and psoriatic arthritis. Developing a gene therapy based biosimilar of secukinumab provides a time and cost effective, universal therapy for disease with IL-17 pathogenicity.

In immunotherapy, neutralizing the antigen is an important step for reaching the desired therapeutic effects. A blocking antibody binds to its target molecule to directly interfere with the molecule's function or to modify a downstream cellular effect (4). Targeting mAbs to novel antigens in the body is complex. Thus, the mAb needs an effective therapeutic dose in order to be effective. Antibodies are large, complex proteins with expensive production, purification, formulation, storage and distribution processes. Improvement and cost reduction in the process of antibody production and distribution will dramatically contribute to a reduction in the cost of immunotherapy.

The integration of the DNA code of mAbs in cells will allow for transcription into mRNAs, and subsequently, the mRNA will produce a few thousand mAbs. This means that the patient's cells will be working as a bioreactor, therefore manufacturing, storage, transportation, and finally administration steps will be eliminated, or at least would be reduced with the natural production of proteins inside the human body. Introducing DNA code to patient's cells for providing intrinsic sources for the antibody is possible with gene therapy and RNA therapy (5, 6). A relatively equal number of antibodies are needed to eliminate antigens, and DNA or mRNA molecule of mAbs will eliminate a few thousand to a few million antigens with any mRNA or gene therapy. Thus, with signs of progress in gene therapy and RNA therapy platforms, in the near future, these technologies can reduce the cost of antibody-based immunotherapy.

Gene therapy strategies are applicable in *ex vivo* and *in vivo* formats. *In vivo* gene therapy involves the systemic injection of the viral or non-viral vectors into the blood or a local injection into tissues like muscles (7). *Ex vivo* gene therapy involves cell extraction, genetic engineering of the cells and transplantation of the manipulated cells back into the body. A current approved cell-based immunotherapy, the chimeric antigen receptor (CAR) T cells, mainly rely on lentivirus-mediated *ex vivo* gene therapies (8).

With emerging stem cell technologies in clinical applications, *ex vivo* gene therapy will evolve by providing gene products releasing from manipulated stem cells. In addition to providing gene products, the engineered cells will incorporate into normal and damaged tissues and will provide additional regenerative advantages (9). Pluripotent and multipotent stem cells are an excellent carrier for *ex vivo* gene therapy. Chorionic villi mesenchymal stem cells (CMSCs) are abundant and have an immunomodulatory capability, and a high rate of

division and differentiation make them unique carriers for *ex vivo* gene therapy (10).

There are several viral and non-viral gene transfer systems for *ex vivo* and *in vivo* gene therapies. Adeno associated viruses (AAVs) are a popular format for *in vivo* gene therapy and lentiviral vectors are widely used in *ex vivo* gene therapy. Lentiviral vector features include; integration, targeting, low immunogenicity, and large transgene carrying capacity, thus they are an ideal choice for *ex vivo* gene therapy. In many *ex vivo* gene therapies like CAR T cell immunotherapy, lentiviral vectors are the main gene transfer system (11).

Next-generation immunotherapies will play a critical role in reducing health care costs, in combination with a growing biosimilar market they will provide more cost-effective advanced therapies. A biosimilar drug is a biological medicine that is similar to a referenced and approved product and its clinical properties in terms of safety, purity and potency are the same as the reference drug. Biosimilar drugs offer less expensive treatment options for patients, therefore the shorter required time, lower-cost and high competition in biosimilar approval pathways would improve patients' access to life-saving drugs for serious diseases such as cancer and autoimmune diseases.

Autoimmune diseases affect the lives of patients from the emergence of the first symptoms till the end of their lives. Protein-based therapies have a 21-30-day half-life and create a huge financial burden for patients with short lasting effects. However, with RNA and gene therapy the drug can last from a few months to years and will provide a more cost-effective and painless solution (12).

In this study, *ex vivo* and *in vivo* secukinumab biosimilar gene therapy is investigated in rat models. As with protein-based biosimilars, similarity in DNA and protein sequences is key. The aim of this study is to present a proof of concept for replacing recombinant biosimilars with gene therapy based biosimilars. Considering the function of IL-17 in the initiation and progression of many autoimmune diseases, the secukinumab antibody was selected for this research. To the best of our knowledge, there are no clinical trials for biosimilar gene therapy. Hopefully, biosimilar mRNA and gene therapy can provide more options for the biosimilar industry that will lead to lower health care expenditures.

Materials and Methods

This study approved by The Local Ethics Committee of The Research Institute for Endocrine Sciences, Shahid Beheshti University of Medical Sciences (ir.sbm. endocrine.rec.1395.195).

Dual promoter lentiviral vector construct

In this experimental study, the secukinumab protein sequences were extracted from the patent (US7807155B2) and published data by the manufacturing company

(Novartis AG, Switzerland). The full DNA sequence of heavy and light chains (HC-LC) of secukinumab were synthesized as the human IgG1 κ antibody. The DNA sequence of HC and LC was separated by T2A self-cleavage peptide and Furin endopeptidase sequence. The secukinumab, T2A, and Furin DNA sequences were cloned after a cytomegalovirus (CMV) promoter in the single open reading frame (ORF). The vector pCDH-513B1 (System Bioscience, USA) in addition to the cloned secukinumab, expressed copGFP and a puromycin resistance gene under the control of EF1 promoter as a bicistronic mRNA (13). The transfer vector (pCDH-513B1) is a Tat-independent and 3rd generation lentiviral vector.

Recombinant lentivirus production, titration, and concentration

Inducible packaging cells (293SF-PacLV 29-6) were used for recombinant lentivirus production (14). The 293SF-PacLV cells express the CymR and rtTA2s-M2 regulators. The Rev and VSV-G genes were under the control of an inducible Tet (rtTA2S-M2) and Cumate (CymR) promoters respectively and Gag-Pol was under the control of the constitutive CMV promoter. The transfer vector was transfected after which packaging was induced with 1 μ g/ml doxycycline and 30 μ g/ml cumate. The transfer vector (21 μ g) was transfected with a CaPo₄ method with 2 \times 10⁶ 293SF-PacLV cells in a 10 cm plate. After 14-16 hours, the transfection rate was monitored by observing GFP intensity under a fluorescence microscope (Nikon, Japan). The transfection reagents were replaced with 12-15 ml of fresh culture medium with 10% fetal bovine serum (FBS, Gibco, USA), 1 μ g/ml doxycycline and 30 μ g/ml cumate. At the 3rd, 4th and 5th days after transfection, the supernatant was collected and replaced with fresh medium that contained an inducer. After incubation for at least 12 hours at 4°C, precipitation at 10% polyethylene glycol (PEG, Sigma, USA) was performed followed by centrifuging (4°C, 10000 g) in order to concentrate the recombinant viruses. Titration of the recombinant viruses was done with flow cytometry on both crude and concentrated viruses (15).

Chorionic villi mesenchymal stem cells isolation, expansion, and characterization

After an ethical committee approval and consent from the parents, human placenta tissue was obtained under sterile conditions (at Erfan Hospital, Iran). The transfer buffer contained penicillin-streptomycin (Pen-Strep, Gibco, USA) and amphotericin B (AmphB, Gibco, USA) and was used to avoid contamination in the transfer to the lab. The fresh sample was washed 3 times with FBS supplemented with Pen-Strep-AmphB. A small amount of the chorionic tissue from below the chorionic plate was dissected out. A tiny piece of villous tissue was washed 3 times with phosphate-buffered saline (PBS, Sigma, USA) containing Pen-Strep-AmphB. After mechanical digestion with surgical scissors and scalpel, trypsin (0.5%)

and collagenase type I (100 U/ μ L) were added to 3 ml of tissue-containing medium in a 15 mL centrifuge tube. This mixture was shaken for 30 minutes inside a 37°C incubator. The enzymes were inactivated with 500 μ L of FBS, mixed thoroughly with a pipette, and centrifuged at 1200 RPM at room temperature (RT) for 5 minutes. The supernatant was carefully discarded of, the depleted cells were suspended in fresh DMEM-F12 (Gibco, USA) medium with 10% FBS and were cultured in a T75 flask. After reaching 75-80 % confluence, the first passage was done with a 1:3 ratio. The main part (80%) of the extracted cells were frozen in DMEM medium containing 20% FBS and 10% dimethyl sulfoxide (DMSO, Invitrogen, USA) and stored in liquid nitrogen. Part of the cells (20%) were characterized based on morphology, cell division, and differentiation to adipogenic and osteogenic lineages.

Chorionic villi mesenchymal stem cells Flow cytometry analysis

Using cell surface biomarkers cells were analyzed. To confirm cells were CMSCs the use of CD73, CD90, CD44, and CD105 were regarded as specific mesenchymal stem cell markers, and CD34, CD11b were regarded as negative markers. A small part of the undifferentiated CMSCs (passage 3, 10⁵ cells) were checked using BD FACS Calibur flow cytometry (BD Biosciences, US) for the expression of CMSC surface markers using cell-specific antibodies. After the addition of the recommended concentration of antibodies, cells were incubated in the dark at the RT for 30-60 minutes; flow cytometry analysis was performed, and the data was analyzed using FlowJo (version 7.6.1) software.

CMSC differentiation, cells transduction, and cell proliferation assays

For adipogenic differentiation of CMSCs, cells were cultured in DMEM-F12 containing 10% FBS, 0.5 mM isobutylmethylxanthine (IBMX, Invitrogen, USA), dexamethasone (1 μ M, Invitrogen, USA), insulin (10 μ g/mL, Sigma, USA), and indomethacin (100 μ M, Sigma, USA). For osteocyte differentiation, cells were cultured in DMEM-F12 containing 10% FBS (Gibco, USA), dexamethasone (1 μ M), β -glycerol-phosphate (0.2 mM, Sigma, USA), and ascorbic acid 2-phosphate (50 μ g/ml, Sigma, USA).

CMSCs and Chinese hamster ovary (CHO) cells at 30% confluence were seeded in T75 flask in DMEM-F12 and supplied with 10% FBS. Recombinant lentiviral particles without secukinumab were used for the first group, while secukinumab expression particles were used in the second. The spinfection protocol (1500 rpm for 1.5 hours) was applied for CMSCs and CHO transduction with a multiplicity of infection (MOI) equal to 5. After 24 hours the virus-containing medium was replaced with fresh medium (DMEM-F12 with 10% FBS). After 72 hours cell viability and transduction efficiency were evaluated under an inverted light and fluorescence microscope (Nikon, Japan). For the purpose of selection, transduced

cells were treated with 1.5 µg/ml puromycin, 72 hours after transduction.

The cell viability was evaluated with an MTT assay after puromycin selection in both non-transduced cells, and those transduced with an MOI of 1, 5 and 10. About 7×10^3 cells were cultured per well, in 96 well plates. After 24 hours, MTT reagents were added and incubated for 4 hours. With the addition of DMSO, the MTT reaction was terminated. MTT was quantified by using absorbance readings via the microplate reader (BioTek, USA).

Quantitative polymerase chain reaction

Total RNA was extracted from transduced and non-transduced CMSCs and CHO cells using an mRNA extraction kit (Qiagen, Germany) according to the manufacturer's protocol. Real-time polymerase chain reaction (PCR) was carried out with 0.5 µg of extracted RNA and an SYBR Green-based master mix (Invitrogen, USA) in CFX96 Touch qRT-PCR machine (Bio-Rad, USA). Data was calculated as the ratio of mean threshold cycles of targeted human exogenous genes to human endogenous *GAPDH*. The specificity of the PCR product was assessed by verifying a single peak on the respective melting curve analysis.

Western blot and *in vitro* ELISA analysis

After transduction and selection of CMSCs and CHO cells, the supernatant from both types of cells were collected and purified using a protein A purification column. Purified, and unpurified supernatants, as well as concentrated lysates were resolved using sodium dodecyl sulfate-polyacrylamide gel electrophoresis (SDS-PAGE) and transferred to a nitrocellulose membrane. The membrane with transferred proteins was probed with a rabbit anti-human IgG antibody (Abcam, UK), washed, and incubated with a secondary HRP antibody goat anti-rabbit (Abcam, UK) conjugated with HRP for 30 minutes at RT. Subsequently, the membrane was washed 3 times with tris-buffered saline and Polysorbate 20 (TBS-T, BioRad, USA) and was incubated with enhanced chemiluminescence substrate for HRP for 1 minute. Finally, the membrane exposed to X-ray film for autoradiography. Part of the supernatant was collected from the CHO and CMSCs was transduced with recombinant viral particles to quantify *in vitro* mAbs expression. Supernatant samples were collected on days 7, 14, 21 and 30, and assayed using an ELISA kit (Abcam, UK).

Secukinumab

In vitro functional bioassay

The inducing effect of IL-17 on IL-6 production in human fibroblast was used in a functional bioassay of secukinumab. In this experiment, secukinumab was collected and purified from transduced CMSC cells. Cultured human dermal fibroblasts were incubated with IL-17A (15 ng/ml) in the presence of increasing concentrations of the secukinumab antibody. After 48 hours the production of IL-6 in these cells was quantified

using an ELISA kit (Abcam, UK) as an indicator of secukinumab functionality.

Intravenous delivery of transduced CMSCs and recombinant viruses

In this experimental study 50 adult female Wistar rats aged 6-8 weeks were purchased (Pasture Institute, Iran). Housing and handling of the rats were done based on standard animal laboratory protocols. Rats were divided into five groups that were injected with either PBS, recombinant GFP lentiviruses (rLV-GFP), recombinant secukinumab viruses (rLV-Secu), CMSC cells transduced with recombinant GFP lentiviruses (CMSC-rLV-GFP), or CMSC cells transduced with recombinant secukinumab lentiviruses (CMSC-rLV-Secu).

An intravenous injection of 2×10^6 genetic engineered cells per rat was used for *ex vivo* gene therapy. For *in vivo* gene therapy 3×10^8 VSV-G pseudo typed recombinant lentivirus particles were injected per rat. The cells and viruses were injected into the lateral tail veins of the female rats with an insulin syringe. Both gene therapy results were checked for two months and we collected blood from the rats on days 7, 15, 30, 45 and 60. Up to 1.5 ml of blood was collected from the Rats at each time point for serum separation. Rat serum was tested by quantitative ELISA using the anti-human IgG1 antibody kit (Abcam, UK).

Statistical analysis

Our research is an interventional study in a rat model. The data is expressed as mean values \pm SD. Student's t test was performed for survival data. $P \leq 0.05$ were to be used as the threshold for statistical significance in these study. The statistical analysis was carried out using SPSS version 25 (IBM SPSS Statistics for Windows, version 25.0. Armonk, NY: IBM Corp.).

Results

Construction of lentiviral-based bicistronic antibody expression vector

Secukinumab heavy and light chain DNA sequences were synthesized with a Furin proteolytic cleavage site, a GSG- linker motif, and a T2A self-cleavage peptide between two chains. The resulting single ORF was cloned using the pCDH513B lentiviral vector. Gene cloning was confirmed through sequencing and restriction enzyme digestion. The transfer vector had dual promoters to express secukinumab under the CMV promoter and GFP and puromycin under the human EF1a promoter. The lentiviral vector produces two mRNAs and four separate proteins total, after transduction. The footprint of T2A will be removed by means of the signal peptide and furine peptidase activity. Figure 1 shows a schematic illustration of the transfer vector, as well as the transcription, translation and mAb assembly process.

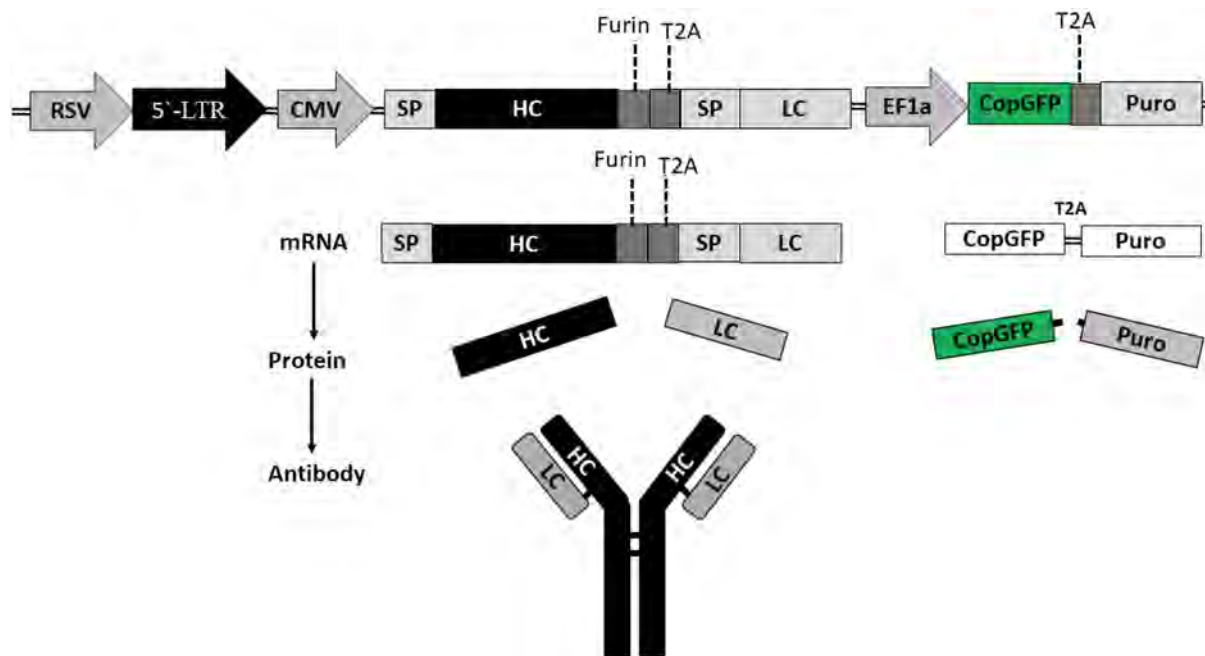


Fig.1: Transfer vector features and secukinumab transcription, translation and assembling. Schematic illustration of the third-generation lentiviral transfer vector with dual-promoter. This vector, after transduction, will express GFP and a puromycin selection marker. The recombinant lentiviral vector will produce two separate bicistronic mRNAs. This will lead to four proteins being produced after transduction. The secukinumab HC and LC proteins assemble as a human IgG1-Kapa antibody. RSV; Respiratory syncytial virus, CMV; Cytomegalovirus, SP; Signal peptide, LC; Light chain, and HC; Heavy chain.

Recombinant lentiviral production, concentration, and titration:

LV-SF9 cells were transfected with CaPO₄ resulting in 90-95% GFP positive cells (Fig.2A, B). Based on FACS titration, more than $5-6 \times 10^6$ recombinant particles were found in the crude supernatant. After virus concentration with PEG precipitation, the total titration reached to $2-3 \times 10^8$ particles/ml. LV-SF9 is a suspension culture adapted cell line that is developed for large scale lentiviral packaging. The Helper gene and envelope gene products will be made following the addition of the inducer to the culture medium and only the transfection of the transfer lentiviral vector is needed.

Stem cells isolation, characterization, and transduction

A MOI of 5 was applied for the transduction of CHO and CMSC cells, and about 65-70% transduction rate was confirmed by observation of GFP under a fluorescent microscope after 72 hours. Completely purified transduced CHO and CMSC cells was achieved by treating the cells with puromycin for selective culture (Fig.2C, D). The application of puromycin is important for preclinical uses as it leads to high purity of manipulated cells and for optimizing the dosage for gene therapy. GFP helped with visualization in every step from transfection, and transduction, to selection. Use of GFP and puromycin are not allowed for clinical applications but help for optimization in pre-clinical studies. CMSCs were isolated from fresh placenta chorionic villi tissue. After primary cell confluency of 80%, a large part of the cells (90%) were stored and a small part of the cells (10%) were treated for characterization. Isolated cells were confirmed

based on morphology (Fig.3Aa, b). Osteogenesis and adipogenesis through the differentiation of these cells were confirmed (Fig.3Ac, d). It is important that stem cells function as more than the carrier of genes and integrate into the host tissues. CMSCs in *ex vivo* gene therapy will be able to differentiation based on extrinsic signals that will be received after homing. Flow Cytometry analysis (Fig.3B) showed a high rate of cells positive for CD44, CD73, CD90, and CD105 specific markers and a low rate of cells with negative markers (CD34, CD11b). The results indicated the high purity of isolated CMSCs and demonstrated the efficacy of this protocol.

In vitro gene overexpression assessment at the mRNA level

To assess the amount of mAb gene expression, mRNA levels were measured using quantitative real-time polymerase chain reaction (qRT-PCR) for both CHO and CMSC cells. The qRT-PCR results confirmed the expression of secukinumab in CHO and CMSC cells but not in GFP-only transduced control cells. Based on results shown in (Fig.4A) transcription of secukinumab mRNA was dramatically increased in both CMSCs and CHO cells.

In vitro mAb expression, cell viability assay, and IL-17 bioassay

In vitro secukinumab expression at the protein level was confirmed with WB (Fig.4B). After the transduction of CHO cells and CMSCs, the viability of the CMSCs was checked using MTT assay (Fig.5A). These results clearly showed that transduction and mAb production didn't affect the physiological viability of CHO cells and CMSCs.

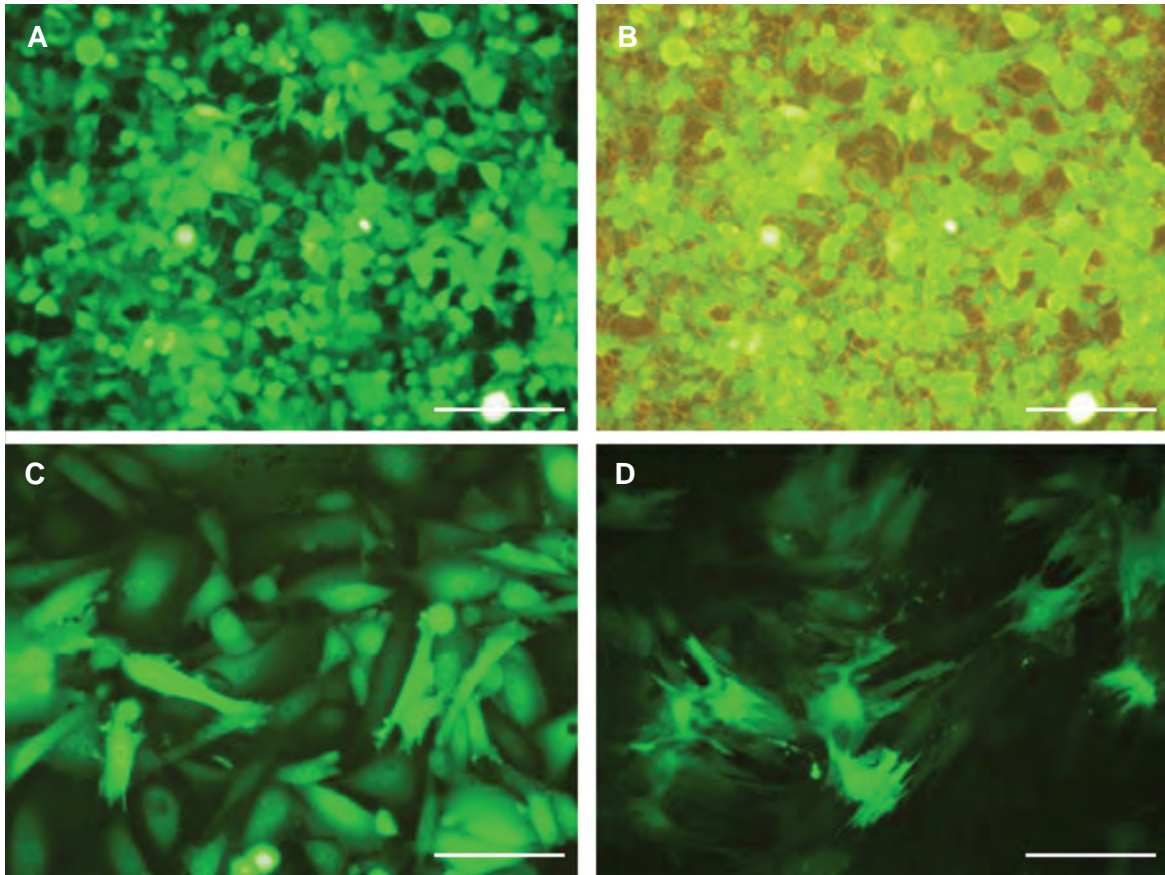
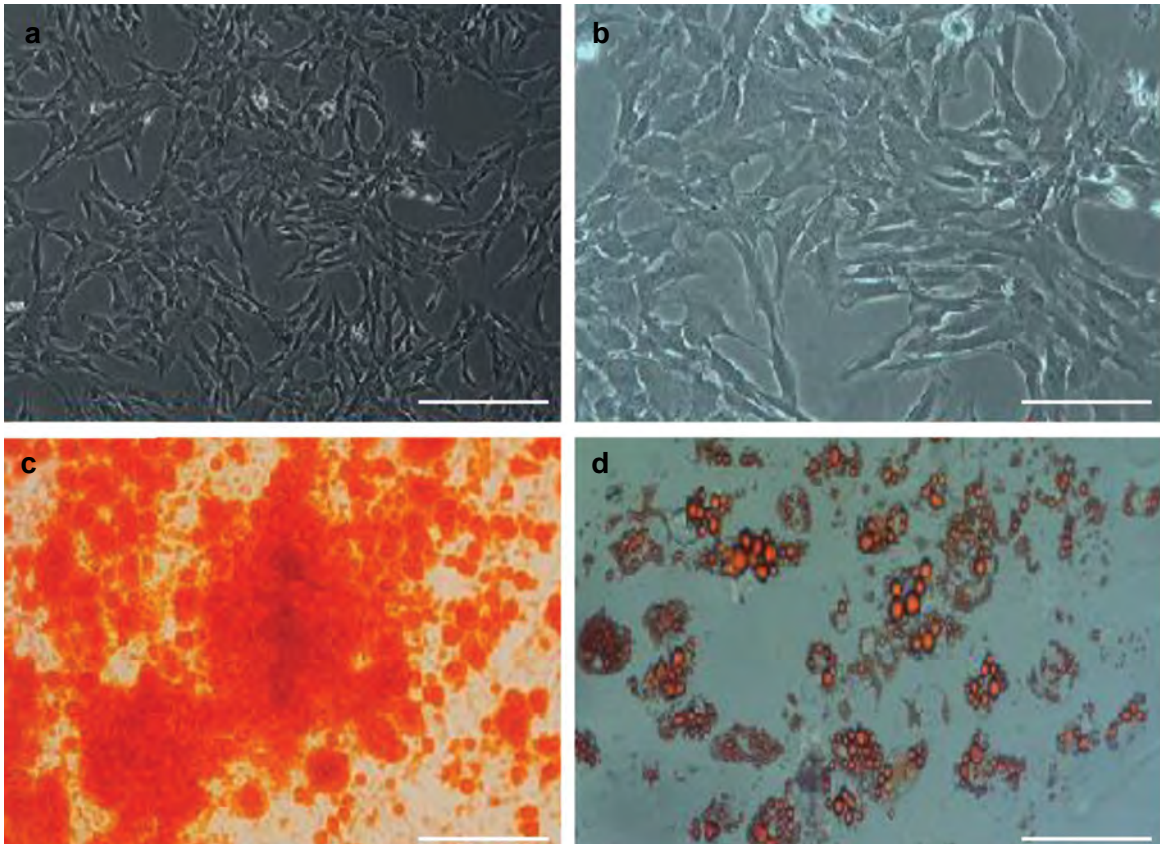


Fig.2: Cells transfection and transduction. **A, B.** The transfection efficiency of LV-SF9 packaging cell line with CaPo₄ protocol. Imaging of GFP-specific fluorescence with about 90- 95% transfection rate, **C.** Imaging of transduced CHO, and **D.** Imaging of transduced CMSC cells with secukinumab transfer vector that were selected with puromycin. Use of GFP helped with visualization during all transfection and transduction steps and puromycin was used for selection of transduced cells (scale bar: ×100). CHO; Chinese hamster ovary and CMSC; Human chorionic derived mesenchymal stem cells.

A



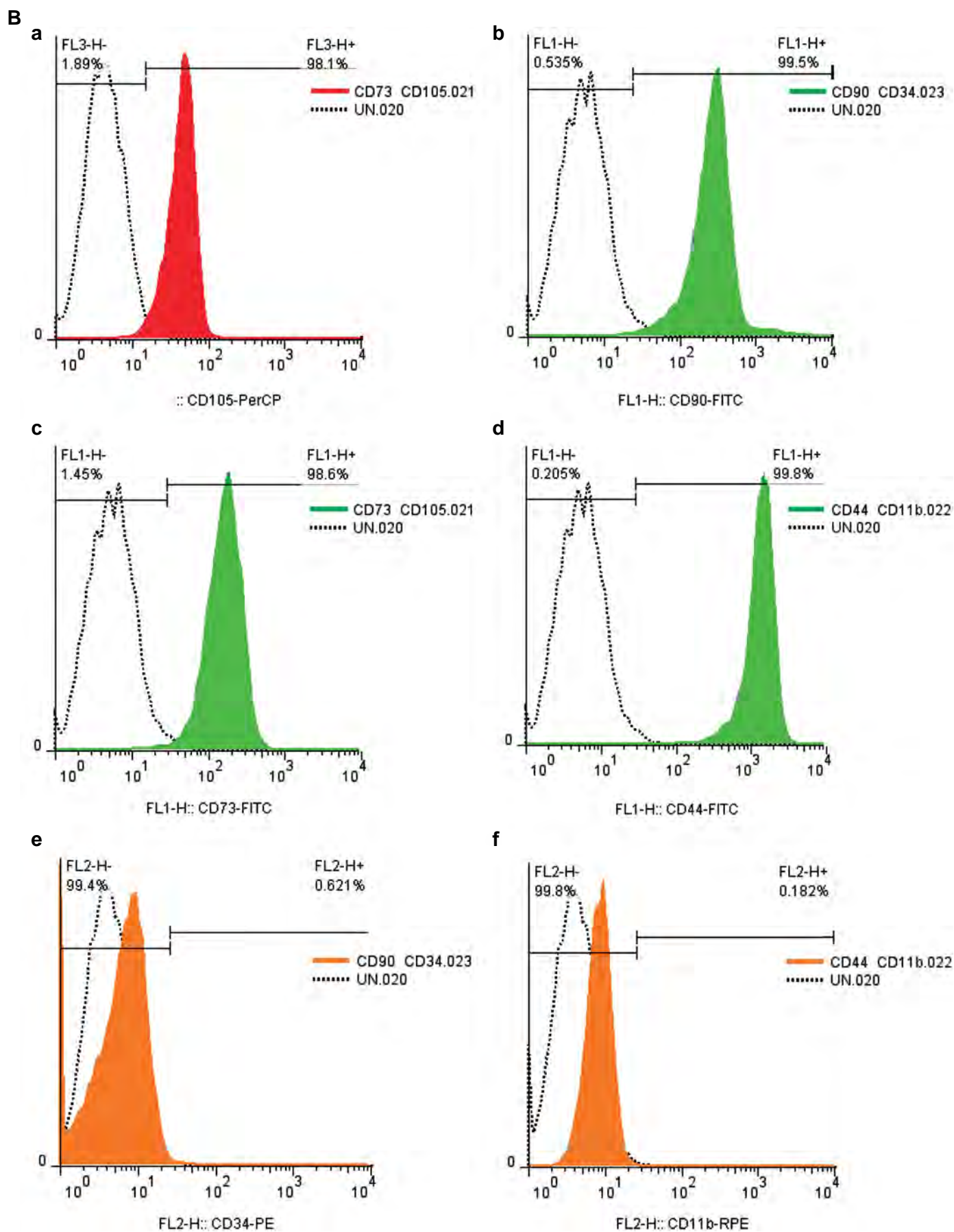


Fig.3: Human chorionic derived mesenchymal stem cells (CMSCs) cell morphology, differentiation and flow cytometry. **A.** Inverted microscope image of CMSCs with $\times 100$ magnification (a), and a $\times 200$ magnification (b). The mesenchymal morphology is clear in both figures, the CMSCs osteogenic (Alizarin Red) and adipogenic (Oil Red) fates (c, d) and **B.** Flow cytometry analysis results for CMSCs positive markers [CD44 (a), CD73 (b), CD90 (c), CD105 (d)], and negative markers [CD34 (e) and CD11b (f)].

Based on the fact that IL-17 induces IL-6 expression in human dermal fibroblasts, the ability of secukinumab to neutralize human IL-17A and inhibit IL-17A-induced IL-6 production was assessed. For the IL-17 bioassay, we applied ELISA as shown in Figure 5B. This result confirms that our secukinumab is fully functional and can bind successfully to IL-17A to inhibit this ligand from attaching to IL-17R.

The supernatant of transduced cells was collected 7 days after transduction and puromycin selection. These cells were used as the source of the secukinumab antibody protein expression tests. These results demonstrated that secukinumab mRNA translation, assembly, and secretion as kappa-IGg1 is correct and detectable by anti-human IgG1 Fc antibody in both solutions through ELISA (Fig.6A) and fixed on a membrane using WB (Fig.4B).

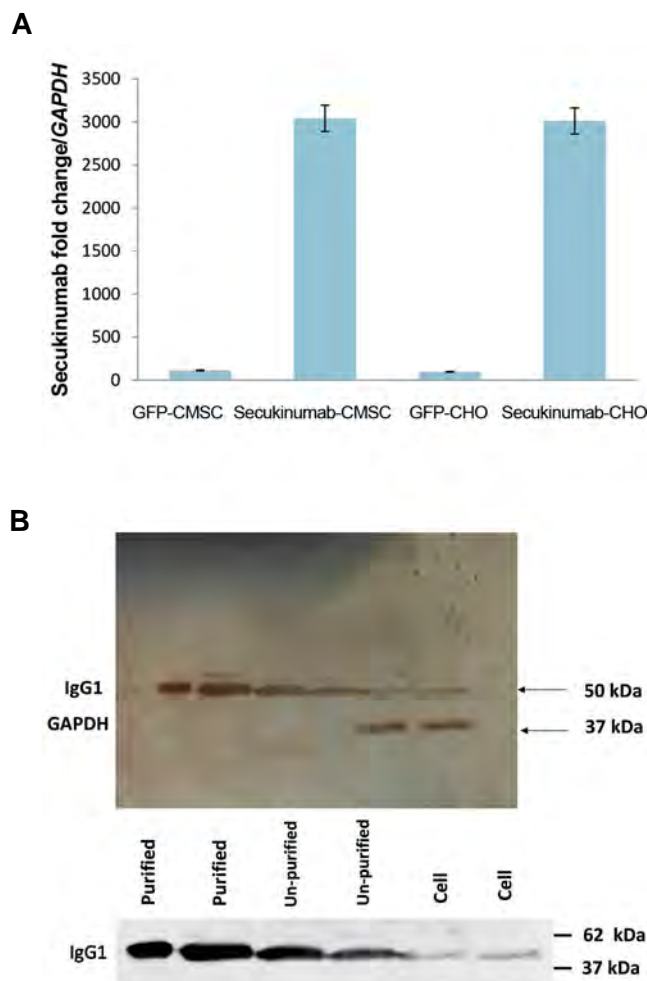


Fig.4: qRT-PCR and western blot. **A.** Comparison of secukinumab gene expression by qRT-PCR in CHO cells and CMSCs. Cells transduced with secukinumab transfer vector or GFP recombinant lentiviruses and **B.** WB test results from both CMSCs and CHO cells. Purified secukinumab with protein A from the supernatant of CMSCs (line 1) and CHO cells (line 2). Unpurified but concentrated supernatant secukinumab from CHO cells (line 3) and CMSCs (line 4). Concentrated lysate total protein from CHO cells (line 5) and CMSCs (line 6) for comparison with the control GAPDH protein. WB was done with the primary antibody against the FC domain of the HC of human IgG1. qRT-PCR; Quantitative real-time polymerase chain reaction, CHO; Chinese hamster ovary, WB; Western blot, CMSCs; Human chorionic derived mesenchymal stem cells, GFP; Green fluorescent protein, and HC; Heavy chain.

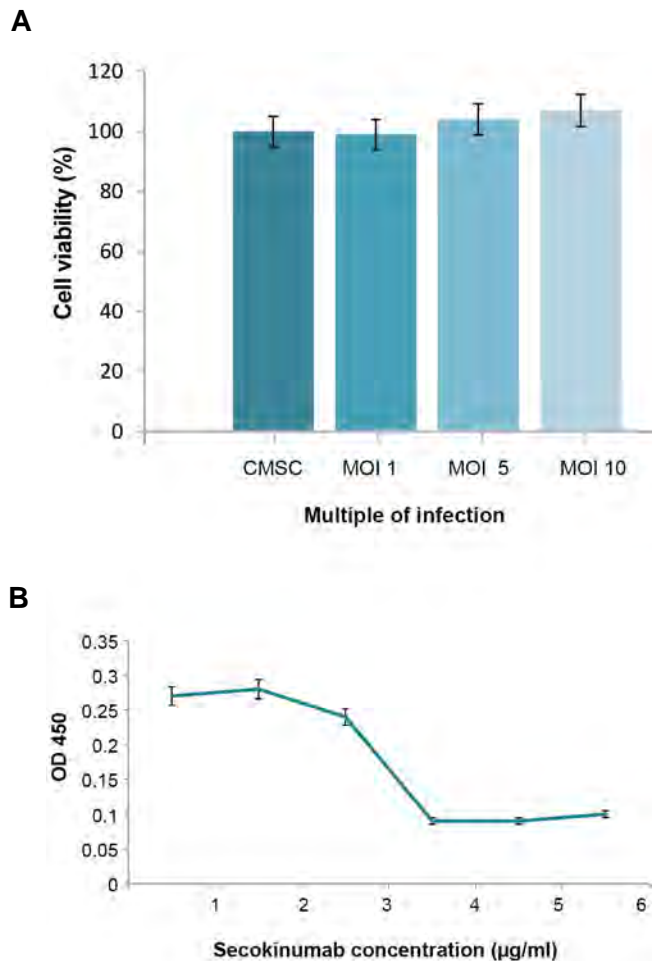


Fig.5: Cell viability MTT assay and secukinumab bioassay. **A.** MTT assay results for CMSCs before and after transduction with secukinumab transfer vector. As shown in the figure, transduction with an MOI of 1,5, or 10 has no significant effect on CMSC viability and **B.** ELISA test results of IL-6 on human primary dermal fibroblast in increasing concentrations of secukinumab in the presence of recombinant human interleukin-17A (15 ng/ml). After 72 hours reduced IL-6 secretions from fibroblasts confirmed the inhibitory activity of secukinumab on human IL-17. CMSCs; Human chorionic derived mesenchymal stem cells, MOI; Multiplicity of infection, and OD; Optical density.

Systemic gene therapy

Systemic administration of recombinant viruses and genetically engineered CMSCs in rats lead to secukinumab overexpression and its release in their bloodstream. Our evaluations confirmed that *ex vivo* gene therapy provided 2-3 µg secukinumab per ml of rat blood serum and *in vivo* gene therapy was shown to provide 3-4 µg/ml of serum (Fig.6B). Secukinumab epitope mapping revealed that this mAb cannot bind to mouse and rat IL-17. This is a big challenge in preclinical studies of secukinumab and other biosimilars. A few humanized animal models like TNF-alpha (GenOway, France) are available for the preclinical study of biosimilars. In the case of secukinumab, the model allows for an *in vivo* efficacy and safety assessment of anti-human IL-17A. With regards to this point, we only checked the bioavailability of secukinumab in the rat model in this study.

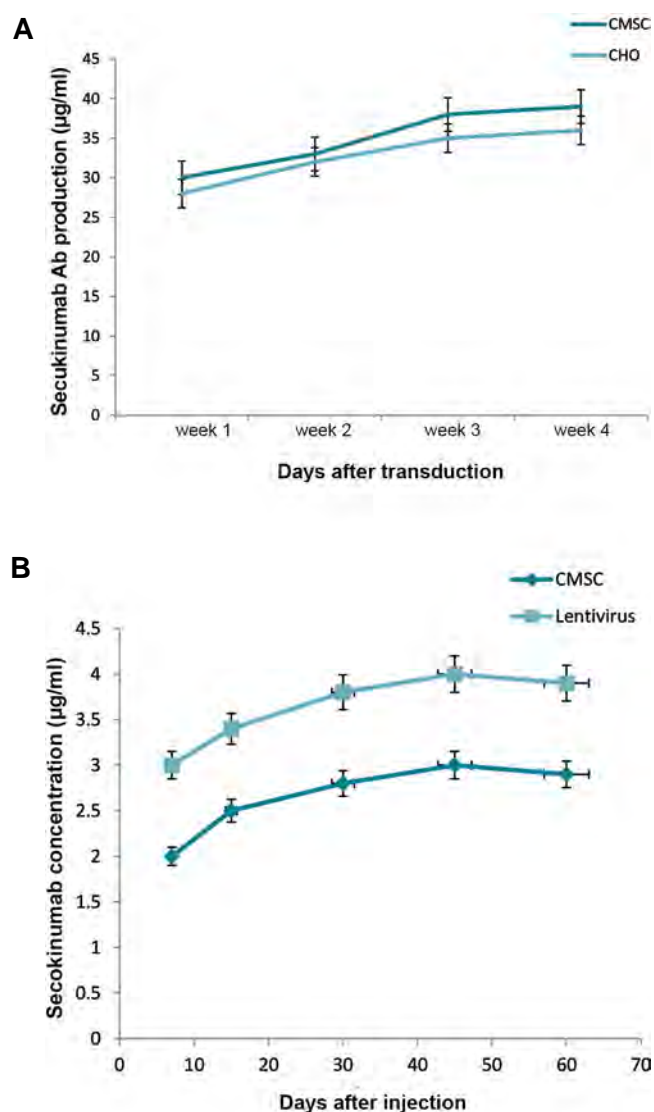


Fig.6: Secukinumab *in vitro* and *in vivo* ELISA. **A.** *In vitro* ELISA tests of secukinumab production from transduced CHO cells and CMSCs with the secukinumab transfer vector. Stem cells showed slightly higher mAbs production in comparison with CHO cells. Sampling was done 4 times a month and **B.** Rat serum ELISA results with five blood samples taken after treatment during the two-month duration. Secukinumab concentration resulting from *in vivo* lentivirus (orange) gene therapy is higher than CMSC-mediated *ex vivo* (blue) gene therapy. ELISA; Enzyme-linked immunosorbent assay, CHO; Chinese hamster ovary, and CMSCs; Human chorionic derived mesenchymal stem cells.

Discussion

In the present study we developed a novel therapeutic strategy involving the expression of a biosimilar antibody, secukinumab, through a lentivirus-based, stem cell therapy, and vector-mediated gene therapy in a rat model. We showed that lentivirus-mediated secukinumab expression is possible with relative therapeutic effects comparable to protein therapy both *in vitro* and *in vivo*.

Lentivirus vectors, with highly efficient *ex vivo* and *in vivo* transduction, provide excellent gene transfer systems. The enveloped lentiviruses used in this research allowed us to target any cell receptor with a natural or synthetic ligand. Incorporating the GFP reporter gene allowed for monitoring of all the steps of cell engineering; puromycin

provided absolute purity in the resulting engineered cells. For clinical applications, incorporating recombination systems like Cre-LoxP could allow us to remove both the fluorescent and puromycin DNA sequences after cell manipulation and before clinical administration. Inducible packaging cells with serum-free and sustainable cell culture conditions create a closer product to commercial gene therapy products (14).

CMSCs have a high *in vitro* differentiation potency and a high level of stem cell marker expression, as such they are applicable as the base for *ex vivo* gene therapy. The DNA sequence of mAbs was integrated into the genome of CMSCs, therefore homing and differentiation of these cells directly into the body can provide a long-lasting source of therapeutic proteins. CMSCs with their immunomodulatory properties and high proliferation rates are promising cellular resources for regenerative medicine. Based on our results, there is no significant difference between mAb production by CHO cells, the predominant host used to produce therapeutic proteins and CMSCs. A comparison of *in vitro* expression between CMSCs and CHO cells showed that CMSCs can produce a comparable amount, 30-40 µg/ml of secukinumab, in established cell lines using the same vectors and sequences.

When comparing ELISA tests of *ex vivo* and *in vivo* secukinumab gene therapy, CMSCs provide more stable expression at 2-3 µg/ml of secukinumab. In comparison, direct lentivirus injection and *in vivo* gene therapy provided 3-4 µg/ml of secukinumab but with more variation over time. *In vitro* and *in vivo* mAb expression assays showed that we could apply gene therapy for expression of sustainable recombinant proteins and mAb in the patient's body. Stem cells as a source of mAb production, with their tumor-tropic properties and unique ability to cross the blood-brain barrier (BBB), will be an alternative carrier for cancer and especially brain cancer treatment.

In vivo antibody gene therapy was first attempted by means of Adenoviruses. Several research papers showed stable *in vivo* expression of mAbs with a wide range of long-term concentrations ranging from 50 ng/ml to 40 µg/ml (16, 17). Another successful vector for mAb gene therapy is Adeno-associated virus (AAV) with a range of 10-400 µg/ml even 6 months after administration (18, 19). Non-viral vectors like naked DNA, plasmid, minicircle, and mRNA delivery are the alternative approaches and produce about 1-300 µg/ml mAbs based on delivery dosage, the frequency of administration and the nature of the nucleic acid (20).

With the current approval of lentivirus and CAR T cell products in the USA and the anticipated results in ongoing clinical trials, CAR T has emerged as a powerful viral gene therapy vector (11). Several mAb gene therapies with lentiviral vectors provide long-lasting mAbs titers in blood serum with a range of 1-3 µg/ml for more than 7 months. When comparing these preexisting study

data with our results, a single dose of our gene therapy provided a relatively high level of secukinumab in the rat serum (21, 22). AAVs are impressive gene therapy vectors, however, lentiviral vectors have more stable and steady expression and additionally provide a more reliable system for therapeutic use.

Ex vivo mAb gene therapy was successful in fibroblast *ex vivo* gene therapy, providing 1-2 µg/ml mAbs in the blood serum (23). The next experiment, with mesenchymal and neural stem cells, provided alternative approaches for *ex vivo* mAbs gene therapy allowing for about 1-5 µg/ml mAb in the serum (24, 25).

Like other mesenchymal stem cells, CMSCs with their immunomodulatory and cancer cell tropism provided a more efficient platform for *ex vivo* mAb gene therapy. The differentiation potential of this type of stem cell allows for integration and adoption of these cells in the cancer environment and long-term mAb expression that is critical for some cancers like breast cancer and gliomas. Approved secukinumab serum concentrations were 44.5 µg/mL for Cosentyx 300 mg and 22.2 µg/mL for Cosentyx 150 mg. In this case, a single administration of secukinumab via *ex vivo* and *in vivo* gene therapy resulted in a 3-4 µg/mL titration, that revealed these gene therapies need improved serum concentrations for human application (26). In comparison with the current recombinant protein therapy, gene therapy is a more durable and sustainable source of secukinumab treatment. Biosimilar secukinumab gene therapy resulted in significant and prolonged antibody expression with only a single dose. Based on the definition of a biosimilar i.e. a biological medicine that is an almost identical copy of an existing authorized biological medicine, we expected that secukinumab's biosimilar gene therapy would have the same clinical efficacy in comparison with the approved recombinant version.

Conclusion

The high cost in the development of advanced therapies for patients can be countered by novel approaches such as, biosimilars gene therapy and mRNA biosimilars therapeutics. These technologies can provide a cost-effective and reliable approach for both the public and private healthcare systems. Engineered CMSCs and recombinant viruses can be a source of sustained expression of mAbs *in vivo*. This study showed that both *in vivo* and *ex vivo* gene therapy are effective platforms for the production of therapeutic mAbs. The approval of *in vivo* gene therapies e.g. Glybera (alipogene tiparvovec), and *ex vivo* gene therapy e.g. Kymriah (tisagenlecleucel), allow for incorporation of novel gene therapies and play a vital role in the future of the healthcare systems.

Acknowledgements

This study was conducted as part of the thesis for obtaining a Ph.D. degree in molecular medicine at the School of Advanced Technologies in Medicine, Shahid

Beheshti University of Medical Sciences. This study was financially supported by Research Institute for Endocrine Sciences, Shahid Beheshti University of Medical Sciences. The authors declare no conflicts of interest regarding the publication of this paper.

Authors' Contributions

A.F., H.E., E.P., S.Z., A.Z.-V., M.S.; Contributed to conception and design, statistical analysis, interpretation of data, conclusion and drafting. A.F., H.E.; Conducted all experimental work and data collection. All authors performed editing and approving the final version of this manuscript for submission.

References

- Hayter SM, Cook MC. Updated assessment of the prevalence, spectrum and case definition of autoimmune disease. *Autoimmun Rev.* 2012; 11(10): 754-765.
- Wang L, Wang FS, Gershwin ME. Human autoimmune diseases: a comprehensive update. *J Intern Med.* 2015; 278(4): 369-395.
- Gaffen SL, Jain R, Garg AV, Cua DJ. The IL-23-IL-17 immune axis: from mechanisms to therapeutic testing. *Nat Rev Immunol.* 2014; 14(9): 585-600.
- Bartlett HS, Million RP. Targeting the IL-17-T(H)17 pathway. *Nat Rev Drug Discov.* 2015; 14(1): 11-12.
- Nelson AL, Dhimolea E, Reichert JM. Development trends for human monoclonal antibody therapeutics. *Nat Rev Drug Discov.* 2010; 9(10): 767-774.
- Schnepf BC, Johnson PR. Vector-mediated antibody gene transfer for infectious diseases. *Adv Exp Med Biol.* 2015; 848: 149-167.
- Pardi N, Scretto AJ, Shan X, Debonera F, Glover J, Yi Y, et al. Administration of nucleoside-modified mRNA encoding broadly neutralizing antibody protects humanized mice from HIV-1 challenge. *Nat Commun.* 2017; 8: 14630.
- Zheng D. Antibody gene therapy: an attractive approach for the treatment of cancers and other chronic diseases. *Cell Res.* 2007; 17(4): 303-306.
- Urba WJ, Longo DL. Redirecting T cells. *N Engl J Med.* 2011; 365(8): 754-757.
- Levy O, Zhao W, Mortensen LJ, Leblanc S, Tsang K, Fu M, et al. mRNA-engineered mesenchymal stem cells for targeted delivery of interleukin-10 to sites of inflammation. *Blood.* 2013; 122(14): e23-e32.
- Hosseini A, Estiri H, Akhavan Niaki H, Alizadeh A, Abdolhossein Zadeh B, Ghaderian SMH, et al. Multiple sclerosis gene therapy with recombinant viral vectors: overexpression of IL-4, leukemia inhibitory factor, and IL-10 in wharton's jelly stem cells used in EAE mice model. *Cell J.* 2017; 19(3): 361-374.
- Milone MC, O'Doherty U. Clinical use of lentiviral vectors. *Leukemia.* 2018; 32(7): 1529-1541.
- Mohammadzadeh A, Pourfathollah AA, Shahrokhi S, Fallah A, Tahoori MT, Amari A, et al. Evaluation of AD-MSC (adipose-derived mesenchymal stem cells) as a vehicle for IFN-β delivery in experimental autoimmune encephalomyelitis. *Clin Immunol.* 2016; 169: 98-106.
- Broussau S, Jabbour N, Lachapelle G, Durocher Y, Tom R, Transfiguracion J, et al. Inducible packaging cells for large-scale production of lentiviral vectors in serum-free suspension culture. *Mol Ther.* 2008; 16(3): 500-5007.
- Szulc J, Wiznerowicz M, Sauvain MO, Trono D, Aebischer P. A versatile tool for conditional gene expression and knockdown. *Nat Methods.* 2006; 3(2): 109-116.
- Arafat WO, Gómez-Navarro J, Buchsbaum DJ, Xiang J, Wang M, Casado E, et al. Effective single chain antibody (scFv) concentrations in vivo via adenoviral vector mediated expression of secretory scFv. *Gene Ther.* 2002; 9(4): 256-262.
- Jiang M, Shi W, Zhang Q, Wang X, Guo M, Cui Z, et al. Gene therapy using adenovirus-mediated full-length anti-HER-2 antibody for HER-2 Overexpression cancers. *Clin Cancer Res.* 2006; 12(20 Pt 1): 6179-6185.
- Fang J, Qian JJ, Yi S, Harding TC, Tu GH, VanRoey M, et al. Stable antibody expression at therapeutic levels using the 2A peptide. *Nat*

- Biotechnol. 2005; 23(5): 584-590.
19. Watanabe M, Boyer JL, Crystal RG. AAVrh.10-mediated genetic delivery of bevacizumab to the pleura to provide local anti-VEGF to suppress growth of metastatic lung tumors. *Gene Ther.* 2010; 17(8): 1042-1051.
 20. Pang X, Ma F, Zhang P, Zhong Y, Zhang J, Wang T, et al. Treatment of human B-cell lymphomas using minicircle DNA Vector expressing anti-CD3/CD20 in a mouse model. *Hum Gene Ther.* 2017; 28(2): 216-225.
 21. Li M, Wu Y, Qiu Y, Yao Z, Liu S, Liu Y, et al. 2A Peptide-based, lentivirus-mediated anti-death receptor 5 chimeric antibody expression prevents tumor growth in nude mice. *Mol Ther.* 2012; 20(1): 46-53.
 22. Lamikanra A, Myers KA, Ferris N, Mitrophanous KA, Carroll MW. In vivo evaluation of an EIAV vector for the systemic genetic delivery of therapeutic antibodies. *Gene Ther.* 2005; 12(12): 988-998.
 23. Noël D, Pelegrin M, Brockly F, Lund AH, Piechaczyk M. Sustained systemic delivery of monoclonal antibodies by genetically modified skin fibroblasts. *J Invest Dermatol.* 2000; 115(4): 740-745.
 24. Balyasnikova IV, Ferguson SD, Sengupta S, Han Y, Lesniak MS. Mesenchymal stem cells modified with a single-chain antibody against EGFRvIII successfully inhibit the growth of human xenograft malignant glioma. *PLoS One.* 2010; 5(3): e9750.
 25. Frank RT, Edmiston M, Kendall SE, Najbauer J, Cheung CW, Kassa T, et al. Neural stem cells as a novel platform for tumor-specific delivery of therapeutic antibodies. *PLoS One.* 2009; 4(12): e8314.
 26. Bruin G, Loesche C, Nyirady J, Sander O. Population pharmacokinetic modeling of secukinumab in patients with moderate to severe psoriasis. *J Clin Pharmacol.* 2017; 57(7): 876-885.
-

Repression of TGF- β Signaling in Breast Cancer Cells by miR-302/367 Cluster

Mona Ahmadelizadeh Khanehsar, M.Sc.^{1,2}, Moslem Hoseinbeyki, M.Sc.¹, Masoumeh Fakhri Taha, Ph.D.¹,

Arash Javeri, M.D., Ph.D.^{1*}

1. Department of Stem Cells and Regenerative Medicine, Institute for Medical Biotechnology, National Institute of Genetic Engineering and Biotechnology (NIGEB), Tehran, Iran
2. Department of Biology, Damghan Branch, Islamic Azad University, Damghan, Iran

*Corresponding Address: P.O. Box 14965-161, Department of Stem Cells and Regenerative Medicine, Institute for Medical Biotechnology, National Institute of Genetic Engineering and Biotechnology (NIGEB), Pajooheh Blvd., Tehran, Iran
Email: arashj@nigeb.ac.ir

Received: 7/July/2018, Accepted: 21/November/2018

Abstract

Objective: Epigenetic alterations of the malignantly transformed cells have increasingly been regarded as an important event in the carcinogenic development. Induction of some miRNAs such as miR-302/367 cluster has been shown to induce reprogramming of breast cancer cells and exert a tumor suppressive role by induction of mesenchymal to epithelial transition, apoptosis and a lower proliferation rate. Here, we aimed to investigate the impact of miR-302/367 overexpression on transforming growth factor- β (TGF- β) signaling and how this may contribute to tumor suppressive effects of miR-302/367 cluster.

Materials and Methods: In this experimental study, MDA-MB-231 and SK-BR-3 breast cancer cells were cultured and transfected with miR-302/367 expressing lentivector. The impact of miR-302/367 overexpression on several mediators of TGF- β signaling and cell cycle was assessed by quantitative real-time polymerase chain reaction (qPCR) and flow cytometry.

Results: Ectopic expression of miR-302/367 cluster downregulated expression of some downstream elements of TGF- β pathway in MDA-MB-231 and SK-BR-3 breast cancer cell lines. Overexpression of miR-302/367 cluster inhibited proliferation of the breast cancer cells by suppressing the S-phase of cell cycle which was in accordance with inhibition of TGF- β pathway.

Conclusion: TGF- β signaling is one of the key pathways in tumor progression and a general suppression of TGF- β mediators by the pleiotropically acting miR-302/367 cluster may be one of the important reasons for its anti-tumor effects in breast cancer cells.

Keywords: Breast Cancer, miR-302/367, Reprogramming, Transforming Growth Factor-Beta

Cell Journal (Yakhteh), Vol 21, No 4, January-March (Winter) 2020, Pages: 444-450

Citation: Ahmadelizadeh Khanehsar M, Hoseinbeyki M, Fakhri Taha M, Javeri A. Repression of TGF- β Signaling in breast cancer cells by miR-302/367 cluster. Cell J. 2020; 21(4): 444-450. doi: 10.22074/cellj.2020.6193.

Introduction

Despite recent advancements in the treatment of breast cancer, it still remains one of the leading causes of cancer deaths among women (1). Therefore, development of new therapeutic approaches for breast cancer is of the utmost importance. Reprogramming of somatic cells and generation of induced pluripotent stem (iPS) cells by some transcription factors including OCT3/4, SOX2, NANOG, KLF4, LIN28 and MYC (2, 3) demonstrated that the cell fate can be manipulated *in vitro*. Reprogramming is a process accompanied by distinct alterations in chromatin and transcriptional programs.

MiRNAs constitute a class of 17-24 bp small non-coding RNAs, involved in regulation of different biological processes and cancer-related cellular activities such as apoptosis, proliferation and invasion (4, 5). MiR-302/367 cluster possesses a coding sequence located in intron 8 of the *LARP7* gene and codes for 5 miRNAs including miR302a, miR302b, miR302c, miR302d, and miR367 which are highly expressed in embryonic stem cells (6-8), but their expression decline rapidly after differentiation (9). It was shown that miR-302/367 cluster can effectively

reprogram human and mouse somatic cells to iPS cells (10, 11). miR-302 is also able to reprogram human cancer cells to a human embryonic stem cell-like state with a slow cell cycle rate and dormant cell-like morphology (12, 13). Reprogramming by miR-302/367 cluster has shown tumor suppressive effects on different cancer cells, such as melanoma and colon cancer cells (14), cervical carcinoma cells (15) glioblastoma cells (16), prostate cancer cells (13), endometrial cancer cells (17) and breast cancer (18). The miR-302/367 cluster has been shown to induce reprogramming of somatic cells through multiple pathways, including MECP1/2 and AOF1/2 silencing, repression of suppressor *NR2F2* gene expression, and silencing RHOC and TGFBR11 (19).

Transforming growth factor- β (TGF- β) signaling pathway is one of the major players in malignant progression through multiple mechanisms which enhance tumor cell invasion, dissemination, and immune evasion (20, 21). In this study we aimed to investigate how overexpression of miR-302/367 cluster in breast cancer cells affects some of the main TGF- β signaling pathway mediators.

Materials and Methods

Cell lines and culture conditions

In this experimental study, human MDA-MB-231 and SK-BR-3 breast cancer cell lines were respectively purchased from Pasteur Institute and Iranian Biological Resource Center (IRBC), Iran. Both cell lines were cultured in Dulbecco's Modified Eagle's medium (DMEM) with 10% fetal bovine serum (FBS), 1% L-glutamine and 1% penicillin-streptomycin (all from Gibco™, Thermo Fisher Scientific, USA) at 5% CO₂ and 37°C. The culture medium was renewed every other day.

Transfection with miR-302/367 expressing vector

Transfection of MDA-MB-231 and SK-BR-3 were performed using either a TDH101PA-GP miR-302abcd/367 expressing Lentivector (System Biosciences, SBI, USA) or the same vector without the miR-302/367 cluster as the mock control type, using Lipofectamine® 2000 transfection reagent (Invitrogen, Thermo Fisher Scientific, USA) according to the manufacturer's protocol. 48 hours after transfection, transfected cells were selected by adding 1 mg/ml puromycin dihydrochloride (Bio Basic Inc., Canada) to the culture medium every other day up to the elimination of untransfected cells. Transfected cells were kept in culture condition for a two-week period.

Analysis of miRNA and gene expression by quantitative real time polymerase chain reaction

For analysis of miRNA expression, total RNA including

small RNA, was extracted from the cultured cells using RNX-Plus solution (Sinaclon, Iran) according to the manufacturer's protocol. Equal amounts of RNA were reverse transcribed into cDNA using BON-miR miRNA 1st-Strand cDNA Synthesis Kit (Stem Cell Technology Co., Iran).

For quantification of mRNAs, total RNA was extracted using the High Pure RNA Isolation Kit (Roche, Germany) according to the manufacturer's protocol. RNA quality and quantity were assessed using a NanoDrop™ 2000/2000c Spectrophotometer (Thermo Fisher Scientific, USA). Equal amount of total RNA from each group was reverse transcribed into cDNA using oligo-dT primers and RevertAid H Minus Reverse Transcriptase (Thermo Fisher Scientific). Assessment of miRNA and mRNA expression was performed, using FastStart SYBR Green Master (Roche, Germany) and specific primers for *miR-302a*, *miR-302b*, *miR-302c*, *miR-302d*, *miR-367* and other genes as mentioned in Table 1, on a Rotor-Gene 6000 (Corbett Research, Australia) real-time PCR instrument. *SNORD47* was selected as the internal reference gene for quantification of miRNAs. *GAPDH* and *B2M* were used as the internal reference genes for quantification of the mRNAs. Comparative analysis of gene expression between different groups was performed using REST 2009 software (Relative Expression Software Tool, Qiagen) based on a Pair Wise Reallocation Randomization Test (22). Four replicates of each group were included in the qPCR reactions.

Table 1: Primers used for quantitative real-time polymerase chain reaction

Target	Primer sequence (5'-3')	Size (bp)	Accession no.
<i>TGFBR2</i>	F: CCCATCCACTGAGACATATTAAT R: CATTCTTTCTCCATACAGCCAC	198	NM_001024847.2
<i>BUB1</i>	F: GAGTCAAATATGGAACGAAGAG R: GTCTTCATTTACCCATTGCTCA	207	NM_004336.4
<i>RHOC</i>	F: CCTGACAGCCTGGAAAACAT R: AACGGGCTCCTGCTTCATCT	153	NM_175744.4
<i>AKT1</i>	F: ACAAACGAGGGGAGTACATCAA R: TCTTCATCAGCTGGCACTGC	156	NM_005163.2
<i>MAPK1</i>	F: ATTCCAAGGGCTACACCAAGT R: GGATCCAAGAATACCCAAAATGT	136	NM_002745.4
<i>MAPK14</i>	F: TGGCTGTCGACTTGCTGGA R: CATAGGTCAGGCTTTTCCAAT	189	NM_001315.2
<i>SMAD3</i>	F: CATAATAACTTGGACCTGCAGC R: ACGCCTCTTCCGATGTGTCT	236	NM_005902.3
<i>B2M</i>	F: TCCAGCGTACTCCAAAGATTCA R: GTCAACTTCAATGTCCGATGGAT	113	NM_004048.2
<i>GAPDH</i>	F: TCACCATCTTCCAGGAGCGA R: CAAATGAGCCCCAGCCTTCT	116	NM_002046.5

Analysis of cell cycle by flow cytometry

At the end of transfection and cell culture period, the cells were harvested and fixed in 70% cold ethanol and DNA content was stained with propidium iodide (PI) solution. Four replicates of each group were used in this study. Cell cycle analysis was carried out using a FACSCalibur™ flow cytometer (BD Biosciences, USA). FlowJo vX.0.7 software (Tree Star Inc., USA) was used for analysis of the results. Comparison of the cell cycle G1, S and G2/M proportions was performed between the mock and miR-302/367 transfected group of each cell line, using unpaired t test.

Results

Overexpression of the miR-302/367 members in transfected cells

Antibiotic-based selection of the miR-302/367 transfected breast cancer cells caused producing a highly (>90%) GFP-expressing cells population (Fig.1A) which were used for the subsequent experiments. Quantification of the miR-302/367 expression in MDA-MB-231 cells showed upregulation of miR-302a, miR-302b, miR-302c, miR-302d and miR-367 by mean factors of 74, 946, 33, 145 and 25, respectively (Fig.1B). In SK-BR-3 cells, after miR-302/367 transfection, miR-302a, miR-302b, miR-

302c, miR-302d and miR-367 were upregulated by mean factors of 145, 1581, 20, 202 and 6, respectively (Fig.1B).

Regulation of TGF-β and MAPK pathway genes by miR-302/367 cluster

Firstly, we checked how transfection of the breast cancer cells with miR-302/367 cluster affects the expression of some key mediators of TGF-β and mitogen-activated protein kinase (MAPK) pathways at gene level. Quantitative real-time PCR showed that in the both MDA-MB-231 and SK-BR-3 cells, overexpression of miR-302/367 cluster downregulated *TGFBR2*, *BUB1*, *RHOC*, *AKT1*, *MAPK1*, *MAPK14* and *SMAD3* expression compared to the mock transfected cells (Fig.2).

Cell cycle arrest by overexpression of miR-302/367 cluster

At the end of culture period, transfected breast cancer cells with either miR-302/367 or mock vector were analyzed for the cell cycle phases, using PI staining and flow cytometry. In the miR-302/367 transfected MDA-MB-231 and SK-BR-3 cells, there was a marked decrease in the S-phase population, while the G2/M phase population was partially increased compared to the mock transfected group (Fig.3).

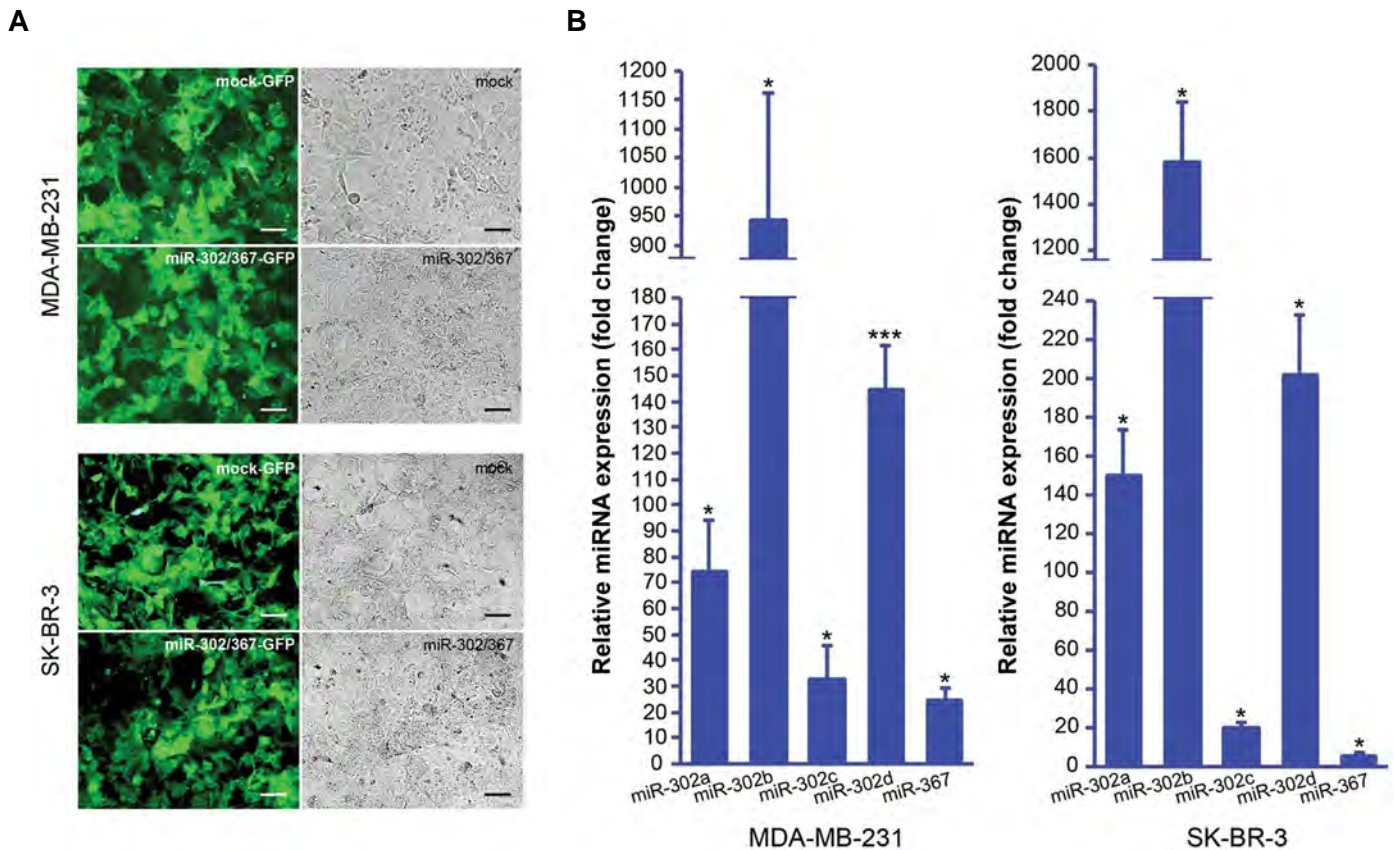


Fig.1: Ectopic expression of miR-302 cluster in the BC cells. **A.** Photomicrographs of the MDA-MB-231 and SK-BR-3 cells transfected with either miR-302/367 or mock vector. Transfected cells show GFP expression. Scale bar represents 50 μm and **B.** Assessment of miR-302/367 expression using quantitative real-time polymerase chain reaction (qPCR) in MDA-MB-231 cells (left) and SK-BR-3 cells (right) transfected with miR-302/367 vector. Fold changes are reflected on the vertical axis compared to the control group (transfected with mock vector) which has been normalized to 1. Analysis performed by REST 2009 software based on a Pair Wise Fixed Reallocation Randomisation Test© and significant P values (*, P<0.05, ***, P<0.001) are indicated on the chart. BC; Breast cancer and GFP; Green fluorescent protein.

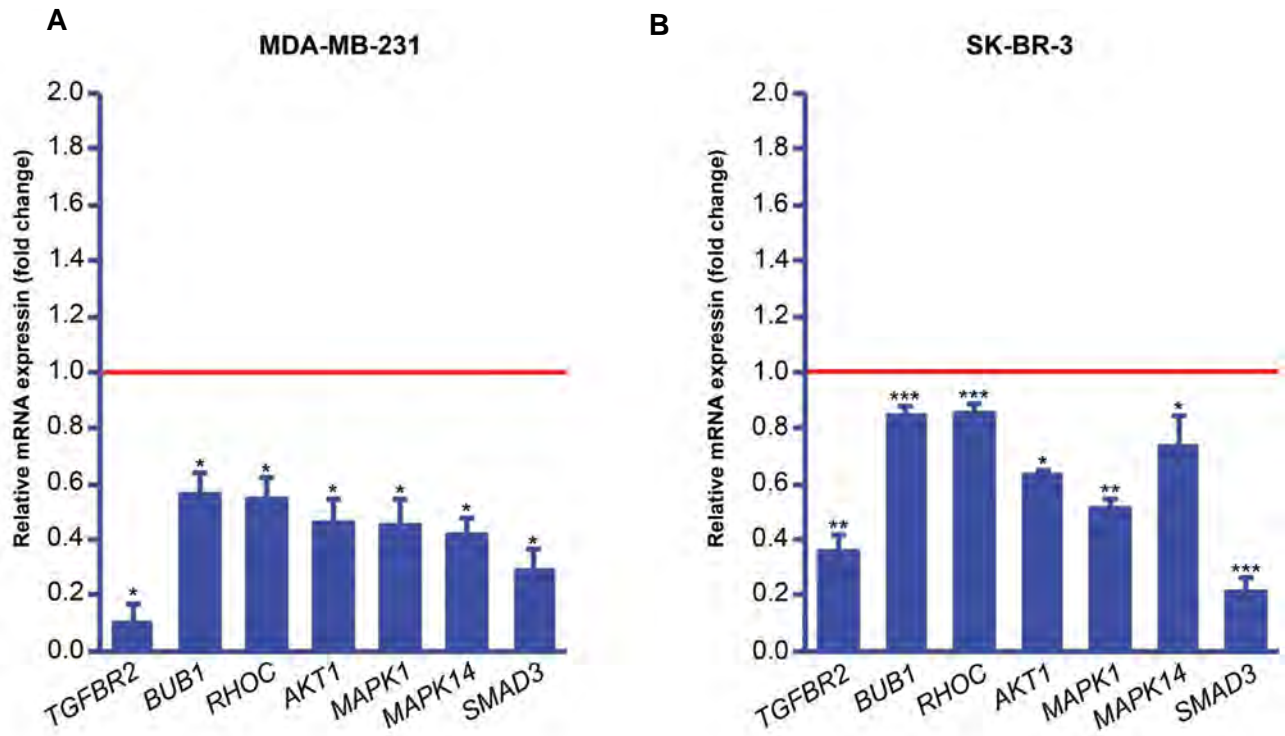


Fig.2: Expression analysis of some transforming growth factor-beta (TGF-β) mediators at mRNA level after transfection with miR-302/367 vector using quantitative real-time polymerase chain reaction (qPCR). Downregulation of TGF-β-related genes in **A.** MDA-MB-231 and **B.** SK-BR-3 cells. Red line represents expression level in the mock transfected group. P values were generated by REST 2009 software based on a Pair Wise Fixed Reallocation Randomisation Test©. Significant P values (*; P<0.05, **; P<0.01, ***; P<0.001) are reflected on the chart.

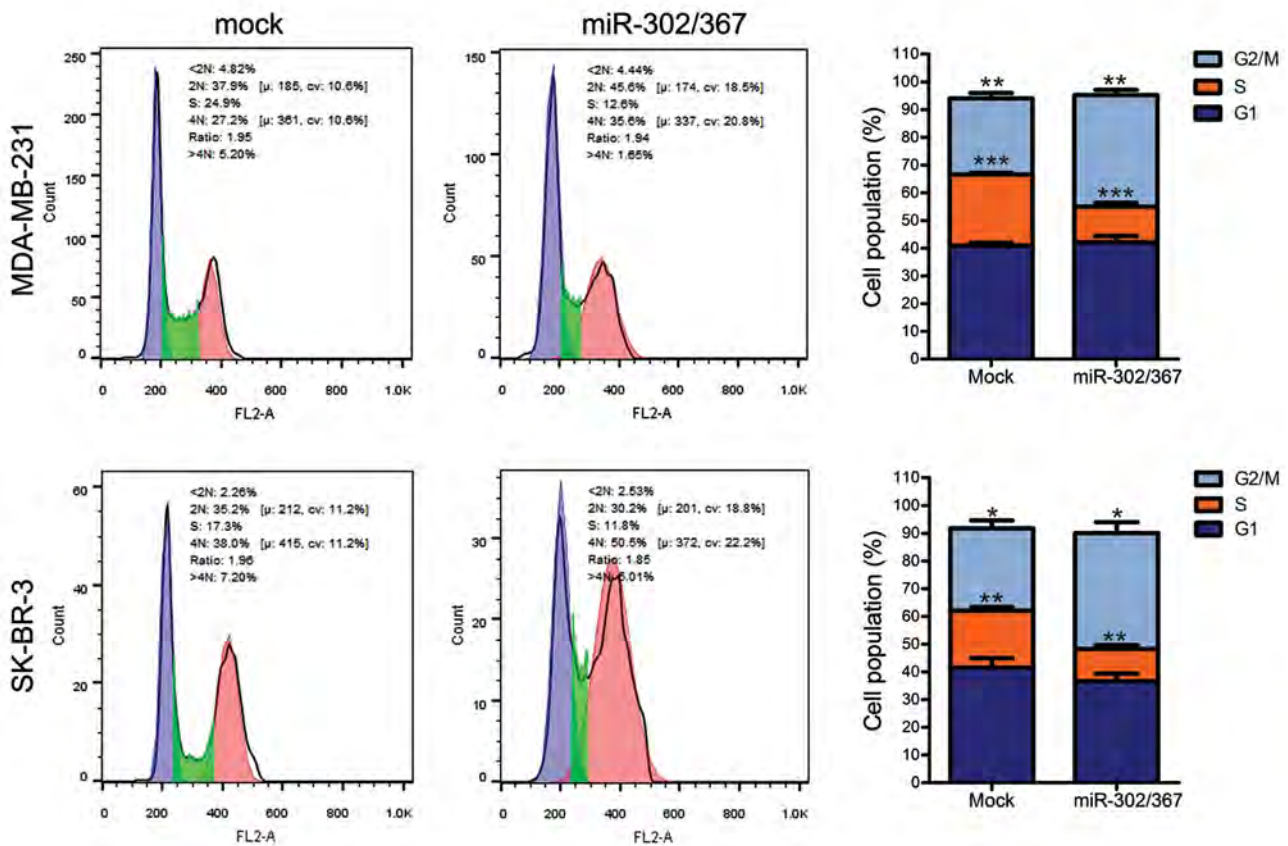


Fig.3: Flow cytometry analysis of cell cycle. There was a significant decrease in S-phase and a partial increase in G2/M-phase population of both MDA-MB-231 and SK-BR-3 cells, after overexpression of miR-302/367 cluster (unpaired t test, n=4, *, P<0.05, **, P<0.01 and ***, P<0.001).

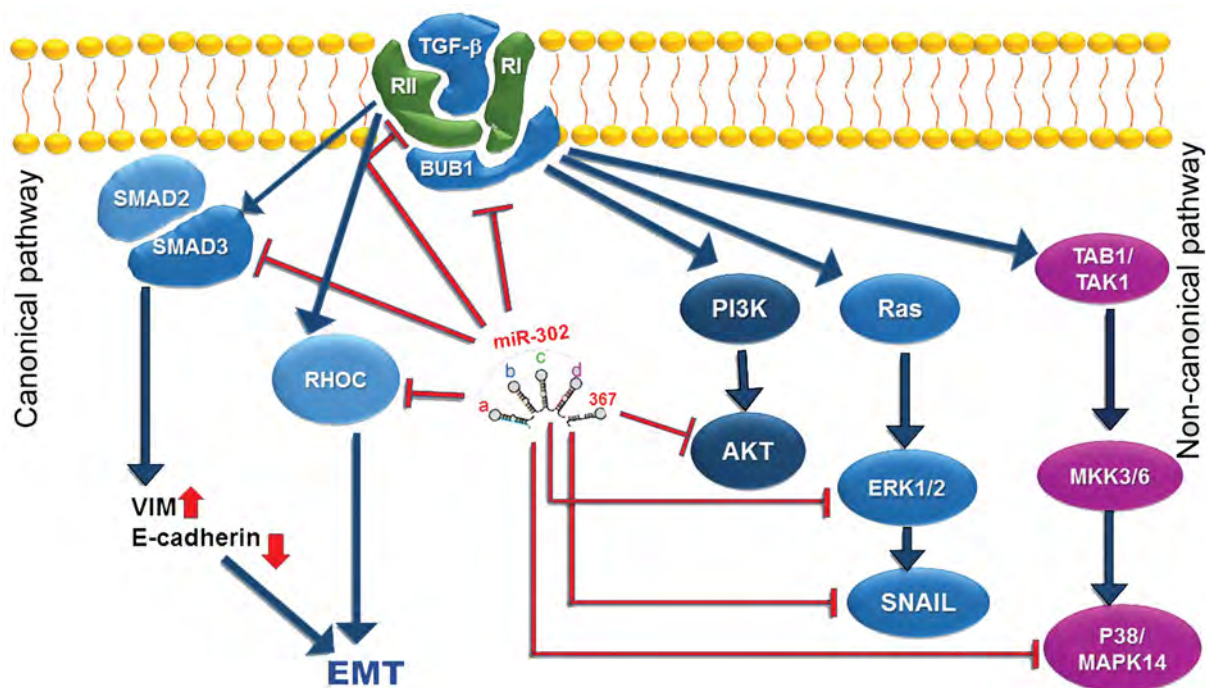


Fig.4: Interaction between miR-302/367 cluster and several mediators of transforming growth factor-beta (TGF- β) signaling in both canonical and non-canonical pathways. The inhibitory effect of miR-302/367 cluster is shown by the red lines.

Discussion

Genetic and epigenetic alterations contribute to cancer initiation and progression through affecting gene expression. While genetic mutations may lead to stable and irreversible alterations, transient and reversible changes are usually caused by epigenetic modifications (23). It has been shown that reprogramming of cancer cells by some pluripotency transcription factors or specific miRNAs, like miR-302/367 cluster, may lead to an embryonic stem cell-like state and less tumorigenicity (13, 24). We previously demonstrated upregulation of some pluripotency factors, including OCT4A, SOX2 and NANOG, by overexpression of miR-302/367 cluster in MDA-MB-231 and SK-BR-3 cells (18).

Accumulating evidence supports the function of miR-302 cluster as a tumor suppressor family which can alleviate tumorigenicity of cancer cells through reversal of epithelial to mesenchymal transition (EMT), induction of apoptosis and anti-proliferative effect (13-15). Previously, we demonstrated some anti-tumor effects of miR-302 cluster in melanoma, colon and breast cancer cells (14, 18). Among the pathways promoting EMT, several studies have reported that inhibition of TGF- β signaling induces somatic cell reprogramming (25, 26).

In this study, we investigated how overexpression of miR-302/367 cluster in MDA-MB-231 and SK-BR-3 breast cancer cells affects some mediators of TGF- β /MAPK/AKT signaling pathway at gene level. As shown, *TGFBR2* and *RHOC* are directly targeted by miR-302 cluster, subsequently facilitating human or mouse fibroblast reprogramming towards iPS cells (27,

28). In accordance with these studies, we found that overexpression of miR-302/367 in human breast cancer cells downregulates *TGFBR2* and *RHOC* expressions. TGF- β signaling has two canonical and non-canonical pathways (Fig.4). In the canonical or SMAD-dependent pathway, SMAD proteins play key regulatory roles among which SMAD2 and SMAD3 proteins are phosphorylated through activity of TGF- β and activin (29). While, in the non-canonical or SMAD-independent pathway, TGF- β activates phosphatidylinositol 3kinase (PI3K)/AKT and MAPK pathways (30). In the current study, expressions of *TGFBR2*, *BUB1*, *RHOC*, *AKT1*, *MAPK1*, *MAPK14* and *SMAD3* were significantly downregulated after overexpression of miR-302/367 cluster in the both cell lines. Previously, Cai et al. (15) reported that miR-302/367 directly targets *AKT1* and it suppresses proliferation of HeLa and SiHa cervical carcinoma cells. In the same study, *AKT1* protein level was decreased after miR-302/367 transfection, but *AKT1* gene expression was not significantly changed. In another study, Li et al. (31) demonstrated that miR-302abcd cluster upregulated OCT4 expression by targeting *AKT1* gene at its 3'-UTR. The same report also showed downregulation of *AKT1* at both gene and protein levels, following miR-302 transfection. Similarly, we showed that overexpression of miR-302/367 cluster in MDA-MB-231 and SK-BR-3 cells induces expression of *OCT4* gene (18) and downregulates expression of *AKT1*. Therefore, it seems that a mechanism, similar to that of previous reports, is applicable to breast cancer cells.

We also detected a significant downregulation of *SMAD3* expression following miR-302/367 transfection

of the breast cancer cells. Sustained activity of SMAD complexes in the nucleus is one of the key features of TGF- β signaling in cancer cells. It was reported that an interaction between FOXM1 and SMAD3 is critical for TGF- β -mediated gene expression. Thus, it promotes breast cancer cell invasion and metastasis (32).

BUB1 was also downregulated in the breast cancer cells after ectopic expression of *miR-302/367* cluster. BUB1 is a serine/threonine kinase playing a significant role in cell cycle regulation, chromosome cohesion (33), and it is a key mediator of TGF- β signaling. It has been shown that BUB1 promotes canonical and non-canonical TGF- β signaling and mediates TGF- β -dependent EMT, cell migration and invasion through interaction with both TGFBR1 and TGFBR2 (34). Here, for the first time, we are reporting downregulation of *BUB1* expression in breast cancer cells following overexpression of *miR-302/367* cluster. This provides further evidence regarding the significance of *miR-302/367* suppressive impact on TGF- β signaling through inhibition of both canonical and non-canonical pathways.

MAPK pathway is part of the non-SMAD pathways, activated by the TGF- β receptors (35). MAPK1, also known as ERK2, is encoded by *MAPK1* gene. The ERK1/2 pathway plays a pivotal role in regulation of cell proliferation, and it is known as a master regulator of G1 to S-phase progression (36, 37). Another player of the non-canonical TGF- β pathway, MAPK14/p38 α is encoded by *MAPK14* gene. MAPK14/p38 α is 50% identical to ERK2 and generally expressed in cell lines and tissues (36). There has been controversy regarding the role of p38 MAPKs in regulating cell proliferation and survival (38). This primarily depends on the cell type determining whether p38 MAPK induces progression or inhibition of G1/S transition through differential regulation of cyclin A or D levels, phosphorylation of RB protein (39, 40), and phosphorylation of p53 (40). In our study, ectopic expression of *miR-302/367* cluster in the breast cancer cells downregulated expression of all of the investigated TGF- β mediators, including *TGFBR2*, *BUB1*, *RHOC*, *AKT1*, *MAPK1*, *MAPK14* and *SMAD3*. These findings indicate a strong suppressive effect of *miR-302/367* cluster on the TGF- β signaling (Fig.4). In this study we report a lower proliferation rate and S-phase suppression of the breast cancer cells by overexpression of *miR-302/367*, confirming our previous report (18). This can be explained by suppression of *MAPK1* and *MAPK14* to some extent. Therefore, suppression of TGF- β mediators may provide a good reason behind the partial cell cycle arrest observed in the breast cancers, following overexpression of *miR-302/367* cluster.

Conclusion

Overexpression of *miR-302/367* cluster in human breast cancer cells resulted in a general suppressive effect on multiple mediators of TGF- β signaling and BUB1. This finding was accompanied by inhibition of cell proliferation. Previously, we reported anti-tumor

effects of either *miR-302bcad* or *miR-302bcad/367* clusters on melanoma, colon and breast cancer cells due to induction of apoptosis and suppression of proliferation and invasion. Current results are providing new evidence that suppression of TGF- β signaling at gene level may be one of the important reasons for anti-tumor effects of *miR-302/367* cluster in breast cancer cells.

Acknowledgements

There is no financial support and conflict of interest in this study.

Authors' Contributions

M.A.K.; Did the gene expression analysis and writing the draft. M.H.; Performed cell culture and transfection of the cells. M.F.T.; Gave technical assistance on the reprogramming process and contributed to writing the draft. A.J.; Designed the study, supervised the project, performed the cell cycle analysis and edited the manuscript draft. All authors read and approved the final manuscript.

References

- Torre LA, Bray F, Siegel RL, Ferlay J, Lortet-Tieulent J, Jemal A. Global cancer statistics, 2012. *CA Cancer J Clin*. 2015; 65(2): 87-108.
- Takahashi K, Yamanaka S. Induction of pluripotent stem cells from mouse embryonic and adult fibroblast cultures by defined factors. *Cell*. 2006; 126(4): 663-676.
- Yu J, Vodyanik MA, Smuga-Otto K, Antosiewicz-Bourget J, Frane JL, Tian S, et al. Induced pluripotent stem cell lines derived from human somatic cells. *Science*. 2007; 318(5858): 1917-1920.
- Bartel DP. MicroRNAs: genomics, biogenesis, mechanism, and function. *Cell*. 2004; 116(2): 281-297.
- Ma L, Weinberg RA. MicroRNAs in malignant progression. *Cell Cycle*. 2008; 7(5): 570-572.
- Pi J, Tao T, Zhuang T, Sun H, Chen X, Liu J, et al. A microRNA302-367-Erk1/2-Klf2-S1pr1 Pathway prevents tumor growth via restricting angiogenesis and improving vascular stability. *Circ Res*. 2017; 120(1): 85-98.
- Zhang Z, Hong Y, Xiang D, Zhu P, Wu E, Li W, et al. MicroRNA-302/367 cluster governs hESC self-renewal by dually regulating cell cycle and apoptosis pathways. *Stem Cell Reports*. 2015; 4(4): 645-657.
- Suh M-R, Lee Y, Kim JY, Kim S-K, Moon S-H, Lee JY, et al. Human embryonic stem cells express a unique set of microRNAs. *Dev Biol*. 2004; 270(2): 488-498.
- Kuo CH, Ying SY. Advances in microRNA-mediated reprogramming technology. *Stem Cells Int*. 2012; 2012: 823709.
- Anokye-Danso F, Trivedi CM, Juhr D, Gupta M, Cui Z, Tian Y, et al. Highly efficient miRNA-mediated reprogramming of mouse and human somatic cells to pluripotency. *Cell Stem Cell*. 2011; 8(4): 376-388.
- Galoian K, Qureshi A, D'Ippolito G, Schiller PC, Molinari M, Johnstone AL, et al. Epigenetic regulation of embryonic stem cell marker miR302C in human chondrosarcoma as determinant of anti-proliferative activity of proline-rich polypeptide 1. *Int J Oncol*. 2015; 47(2): 465-472.
- Lin SL, Chang DC, Ying SY, Leu D, Wu DT. MicroRNA miR-302 inhibits the tumorigenicity of human pluripotent stem cells by coordinate suppression of the CDK2 and CDK4/6 cell cycle pathways. *Cancer Res*. 2010; 70(22): 9473-9482.
- Lin SL, Chang DC, Chang-Lin S, Lin CH, Wu DT, Chen DT, et al. Mir-302 reprograms human skin cancer cells into a pluripotent ES-cell-like state. *RNA*. 2008; 14(10): 2115-2124.
- Maadi H, Moshtaghian A, Taha MF, Mowla SJ, Kazeroonian A, Haass NK, et al. Multimodal tumor suppression by miR-302 cluster in melanoma and colon cancer. *Int J Biochem Cell Biol*. 2016; 81(Pt A): 121-132.

15. Cai N, Wang YD, Zheng PS. The microRNA-302-367 cluster suppresses the proliferation of cervical carcinoma cells through the novel target AKT1. *RNA*. 2013; 19(1): 85-95.
16. Yang CM, Chiba T, Brill B, Delis N, von Manstein V, Vafaizadeh V, et al. Expression of the miR-302/367 cluster in glioblastoma cells suppresses tumorigenic gene expression patterns and abolishes transformation related phenotypes. *Int J Cancer*. 2015; 137(10): 2296-2309.
17. Yan GJ, Yu F, Wang B, Zhou HJ, Ge QY, Su J, et al. MicroRNA miR-302 inhibits the tumorigenicity of endometrial cancer cells by suppression of Cyclin D1 and CDK1. *Cancer Lett*. 2014; 345(1): 39-47.
18. Ramezankhani B, Taha MF, Javeri A. Vitamin C counteracts miR-302/367-induced reprogramming of human breast cancer cells and restores their invasive and proliferative capacity. *J Cell Physiol*. 2019; 234(3): 2672-2682.
19. Kuo CH, Deng JH, Deng Q, Ying SY. A novel role of miR-302/367 in reprogramming. *Biochem Biophys Res Commun*. 2012; 417(1): 11-16.
20. Miyazono K. Transforming growth factor-beta signaling in epithelial-mesenchymal transition and progression of cancer. *Proc Jpn Acad Ser B Phys Biol Sci*. 2009; 85(8): 314-323.
21. Meulmeester E, Ten Dijke P. The dynamic roles of TGF-beta in cancer. *J Pathol*. 2011; 223(2): 205-218.
22. Pfaffl MW, Horgan GW, Dempfle L. Relative expression software tool (REST©) for group-wise comparison and statistical analysis of relative expression results in real-time PCR. *Nucleic Acids Res*. 2002; 30(9): e36.
23. Nishikawa S, Ishii H, Haraguchi N, Kano Y, Fukusumi T, Ohta K, et al. microRNA-based cancer cell reprogramming technology. *Exp Ther Med*. 2012; 4(1): 8-14.
24. Miyoshi N, Ishii H, Nagai K, Hoshino H, Mimori K, Tanaka F, et al. Defined factors induce reprogramming of gastrointestinal cancer cells. *Proc Natl Acad Sci USA*. 2010; 107(1): 40-45.
25. Maherali N, Hochedlinger K. Tgfbeta signal inhibition cooperates in the induction of iPSCs and replaces Sox2 and cMyc. *Curr Biol*. 2009; 19(20): 1718-1723.
26. Lin T, Ambasudhan R, Yuan X, Li W, Hilcove S, Abujarour R, et al. A chemical platform for improved induction of human iPSCs. *Nat Methods*. 2009; 6(11): 805-808.
27. Liao B, Bao X, Liu L, Feng S, Zovoilis A, Liu W, et al. MicroRNA cluster 302-367 enhances somatic cell reprogramming by accelerating a mesenchymal-to-epithelial transition. *J Biol Chem*. 2011; 286(19): 17359-17364.
28. Subramanyam D, Lamouille S, Judson RL, Liu JY, Bucay N, Derynck R, et al. Multiple targets of miR-302 and miR-372 promote reprogramming of human fibroblasts to induced pluripotent stem cells. *Nat Biotechnol*. 2011; 29(5): 443-448.
29. Chaudhury A, Howe PH. The tale of transforming growth factor-beta (TGFbeta) signaling: a soigne enigma. *IUBMB Life*. 2009; 61(10): 929-939.
30. Chapnick DA, Warner L, Bernet J, Rao T, Liu X. Partners in crime: the TGFβ and MAPK pathways in cancer progression. *Cell Biosci*. 2011; 1: 42.
31. Li HL, Wei JF, Fan LY, Wang SH, Zhu L, Li TP, et al. miR-302 regulates pluripotency, teratoma formation and differentiation in stem cells via an AKT1/OCT4-dependent manner. *Cell Death Dis*. 2016; 7: e2078.
32. Xue J, Lin X, Chiu WT, Chen YH, Yu G, Liu M, et al. Sustained activation of SMAD3/SMAD4 by FOXM1 promotes TGF-beta-dependent cancer metastasis. *J Clin Invest*. 2014; 124(2): 564-579.
33. Johnson VL, Scott MI, Holt SV, Hussein D, Taylor SS. Bub1 is required for kinetochore localization of BubR1, Cenp-E, Cenp-F and Mad2, and chromosome congression. *J Cell Sci*. 2004; 117(Pt 8): 1577-1589.
34. Nyati S, Schinske-Sebolt K, Pitchiaya S, Chekhovskiy K, Chator A, Chaudhry N, et al. The kinase activity of the Ser/Thr kinase BUB1 promotes TGF-β signaling. *Sci Signal*. 2015; 8(358): ra1.
35. Zhang YE. Non-smad signaling pathways of the TGF-beta family. *Cold Spring Harb Perspect Biol*. 2017; 9(2). pii: a022129.
36. Cargnello M, Roux PP. Activation and function of the MAPKs and their substrates, the MAPK-activated protein kinases. *Microbiol Mol Biol Rev*. 2011; 75(1): 50-83.
37. Meloche S, Pouyssegur J. The ERK1/2 mitogen-activated protein kinase pathway as a master regulator of the G1- to S-phase transition. *Oncogene*. 2007; 26(22): 3227-3239.
38. Cuenda A, Rousseau S. p38 MAP-kinases pathway regulation, function and role in human diseases. *Biochim Biophys Acta*. 2007; 1773(8): 1358-1375.
39. Brancho D, Tanaka N, Jaeschke A, Ventura JJ, Kelkar N, Tanaka Y, et al. Mechanism of p38 MAP kinase activation in vivo. *Genes Dev*. 2003; 17(16): 1969-1978.
40. Ambrosino C, Nebreda AR. Cell cycle regulation by p38 MAP kinases. *Biol Cell*. 2001; 93(1-2): 47-51.

CD44 Gene rs8193 C Allele Is Significantly Enriched in Gastric Cancer Patients

Roya Mokhtarian, M.Sc.¹, Hossein Tabatabaeian, Ph.D.^{2,3}, Pardis Saadatmand, M.Sc.⁴, Mansoureh Azadeh, M.Sc.⁴,
Negar Balmeh, M.Sc.¹, Bagher Yakhchali, Ph.D.⁵, Kamran Ghaedi, Ph.D.^{3,6*}

1. Division of Cellular and Molecular Biology, Department of Biology, NourDanesh Institute of Higher Education, Meymeh, Iran

2. Department of Biochemistry, Yong Loo Lin School of Medicine, National University of Singapore, Singapore

3. Department of Biology, Faculty of Sciences, University of Isfahan, Isfahan, Iran

4. ZistFanavari Novin Biotechnology Institute, Isfahan, Iran

5. Institute of Industrial and Environmental Biotechnology, National Institute of Genetic Engineering and Biotechnology Institute, Tehran, Iran

6. Department of Cellular Biotechnology, Cell Science Research Center, Royan Institute for Biotechnology, ACECR, Isfahan, Iran

*Corresponding Address: P.O.Box: 816513-1378, Department of Cellular Biotechnology, Cell Science Research Center, Royan Institute for Biotechnology, ACECR, Isfahan, Iran
Email: kamranghaedi@royaninstitute.org

Received: 18/September/2018, Accepted: 23/February/2019

Abstract

Objective: Gastric cancer is a multifactorial disease. In addition to environmental factors, many genes are involved in this malignancy. One of the genes associated with gastric cancer is *CD44* gene and its polymorphisms. *CD44* gene plays role in regulating cell survival, growth and mobility. The single nucleotide polymorphism (SNP) rs8193, located in the *CD44* gene, has not been studied in gastric cancer patients of the Iranian population. The present study aims to study this polymorphism in 86 gastric cancer patients and 96 healthy individuals.

Materials and Methods: In this cross-sectional case-control study, rs8193 polymorphism was genotyped by allele specific primer polymerase chain reaction (ASP-PCR) technique. The obtained data were statistically analyzed. To find the potential mechanism of action, rs8193 was bioinformatically investigated.

Results: rs8193 C allele played a risk factor role for gastric cancer. Patients carrying this allele were more susceptible to have gastric cancer, with lymph node spread. On the other hand, rs8193 T allele, a protective factor, was associated with a higher chance of accumulation in the lower stages of cancer. C allele might impose its effect via destabilizing *CD44* and miR-570 interaction.

Conclusion: rs8193 is statistically associated with the risk of malignancy, lymph node spread and stage of gastric cancer in Iranian population.

Keywords: *CD44*, Gastric Cancer, miR-570

Cell Journal (Yakhteh), Vol 21, No 4, January-March (Winter) 2020, Pages: 451-458

Citation: Mokhtarian R, Tabatabaeian H, Saadatmand P, Azadeh M, Balmeh N, Yakhchali B, Ghaedi K. *CD44* gene rs8193 C allele is significantly enriched in gastric cancer patients. Cell J. 2020; 21(4): 451-458. doi: 10.22074/cellj.2020.6389.

Introduction

Gastric cancer is one of the most prevalent and leading causes of cancer death (1). Several factors such as race, ethnicity, sex, age, genetic and environmental factors are associated with this malignancy. The International Agency for Research on Cancer reported *Helicobacter pylori* (*H. pylori*) infection as the potential risk factor for gastric adenocarcinoma and described it as a group 1 carcinogen (2). The key genes involved in the development of cancer include the oncogenes and tumor suppressor genes, contributing to DNA repair and apoptosis mechanisms, among which *K-Ras*, *Myc* and *CD44* are the most important genes that have been proven to be associated with gastrointestinal cancers (3).

From the cytogenetic point of view, *CD44* gene is located on chromosome 11p13 (4). This gene encodes various protein isoforms generated by alternative processing and post-translation modifications. *CD44* and its processed isoforms are central mediators

of cellular behaviors, such as cell survival, growth and mobility. Interest in the study of *CD44* was boosted when *CD44v6* was confirmed to induce complete metastasis in non-metastatic cancer of the rat pancreatic cells. It has increasingly been shown that *CD44v6* is expressed from gastric precancerous lesions to advanced carcinoma, while role of *CD44* in tumorigenesis still remains controversial (5).

Almost all cell-signaling pathways are regulated by microRNAs (miRNAs) and consistently physiological phenotypes of stomach cells are regulated by these small non-coding RNAs. Some of these miRNAs target the oncogenes, known as tumor suppressor miRNAs (tsmiRs), while the others modulate expression of tumor suppressor genes and known as oncomiRs (6-10). In addition, evidences demonstrate the regulatory effect of miRNAs during carcinogenesis, through modulating cell proliferation, migration, invasion and anti-apoptotic properties (11-13).

CD44 is one of the genes tightly correlated with

gastric cancer (14). The association of miRNA-related single nucleotide polymorphism (SNP) rs8193, located within 3'UTR of *CD44* gene, has not been studied in gastric cancer of Iranian population. Therefore, in this study, we aimed to investigate frequency of different rs8193 alleles in Iranian population. We further conducted in silico study in order to have a predicted vision on a mechanism of action, whereby different rs8193 alleles can alter the carcinogenic impact of *CD44* gene.

Materials and Methods

Compliance with ethical standards

All procedures performed in this study including human participants and ethical considerations were on the basis of the Ministry of Health and Medical Education of Iran

and the 1964 Helsinki declaration. The study protocol was approved by the Nourdanesh Institute of Higher Education in Meymeh, Iran. Informed consent was obtained from all participants involved in this study.

Study subjects

In this cross-sectional case-control study, 5 ml of peripheral blood samples were taken from 86 gastric cancer patients and 96 healthy controls in Seyed-al-Shohada Hospital, Isfahan, Iran. All participants were selected randomly and analyzed in advance (Fig.1). To prevent clotting, the blood samples were transferred into tubes containing 1 ml EDTA at a concentration of 0.5 M, and then stored at -20°C until testing. The presence of *H. pylori* infection was qualitatively evaluated by an expert pathologist.

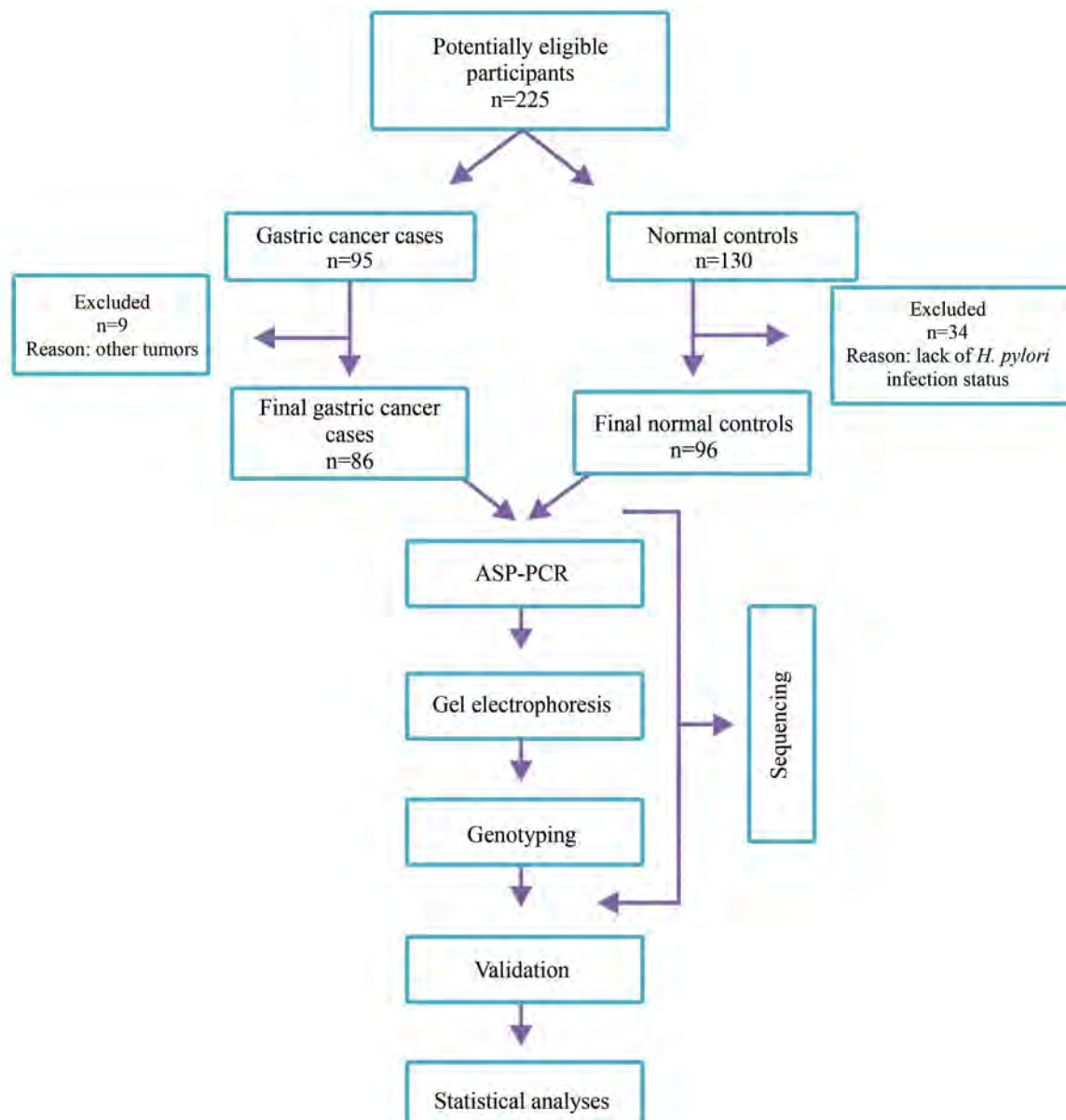


Fig.1: STARD diagram reporting flow of participants. ASP-PCR; Allele-specific primer polymerase chain reaction.

DNA extraction and primer designing

In this study, the PrimePrep Genomic DNA Isolation Kit from Blood (GeNetBio, Korea) was used for DNA extraction according to the manufacturer's instructions. In addition, allele-specific primer polymerase chain reaction (ASP-PCR) method was applied to examine the SNP genotypes. Three primers, including wild-type forward, SNP forward and common reverse primer, were designed in accordance with the WASP site at <http://bioinfo.biotech.or.th/WASP> (Table 1) and they were ordered from Bioneer Company (Korea).

Table 1: Primer sequences utilized for ASP-PCR

Primer	Sequence (5'-3')
Wild-type forward	CCTAATCCCTGGGCACTGC
SNP forward	CATAGCCTAATCCCTGGGCATTAT
Common reverse	ATACATTGTAGGGACCCAGACAGTG

ASP-PCR; Allele-specific primer polymerase chain reaction and SNP; Single nucleotide polymorphism.

The primer-specific binding sites were confirmed by BLAST assay. The primers were designed to align 3' terminal of both wild-type forward and SNP forward primers with the SNP site. A mismatch nucleotide was also designed at -2 and -4 nucleotide regions in order to minimize possibility of non-specific annealing, as described by Assad Samani et al. (15).

Genotyping by allele-specific primer polymerase chain reaction

ASP-PCR was performed in a final volume of 25 μ l, as previously described (16, 17), including 4 μ l DNA template, 2.5 μ l of 10X PCR buffer (Bioron, Germany), 0.75 μ l $MgCl_2$ (50 mM), 1 μ l dNTP mix (10 mM, both from Bioron, Germany), 1 μ l wild-type forward primer (10 μ M), 1 μ l SNP forward primer (10 μ M), 1 μ l reverse primer (10 μ M), 0.25 μ l Taq DNA polymerase (5 U/ μ l, Bioron, Germany), and 14.5 μ l distilled H_2O .

Gradient temperature and $MgCl_2$ was used to optimize the ASP-PCR conditions. The best-optimized conditions are as follows: hot start 95°C for 5 minutes, 35 cycles including denaturation at 94°C for 20 seconds, annealing at 58.5°C for 50 seconds, extension at 72°C for 50 seconds, and the final extension at 72°C for 10 minutes. PCR products were analyzed by 2% agarose gel electrophoresis and RedSafe Nucleic Acid Staining Solution (iNTRON, Hong Kong), in order to determine the genotypes. Dissimilar to tetra-primer ARMS-PCR, as a multiplex-based method

(18), reactions were performed in two separate vials in ASP-PCR technique. Some random samples from both groups were sequenced and the outcomes confirmed the accuracy of genotyping performed by ASP-PCR technique.

Statistical analysis

The univariate (Chi-square test and Fisher's exact test) and multivariate (Multivariate logistic regression) analyses were performed using SPSS software (version 19, SPSS Inc., USA). For all tests, $P < 0.05$ was considered statistically significant.

Data sources

Interaction analysis between miRNA and SNP rs8193, located in *CD44* 3'UTR of respective mRNA, was performed by miRNASNP database V2.0 to identify the potential miRNAs with capability of targeting 3'UTR of *CD44* transcripts. This database was also used to predict the effect of different rs8193 alleles on the binding affinity of miRNA570 to *CD44* transcript, as well as modulation in Gibbs free energy (ΔG) of binding reaction (19, 20).

Single nucleotide polymorphism data

Critical information on rs8193, such as the minor allele frequency (MAF) as well as upstream and downstream sequences of this SNP, was obtained from the NCBI database (<http://www.ncbi.nlm.nih.gov>).

Signaling system enrichment analysis

A possible target of rs8193 associated with miRNA570 was obtained using miRWalk V2.0 database (21). Finally, the database for annotation, visualization and integrated discovery (DAVID) V6.7 was used for cell signaling enrichment analyses (22, 23).

Results

Genotyping the rs8193 position in control and gastric cancer samples

Due to almost similarity of the fragment sizes, two separate ASP-PCRs were performed: one with wild-type forward and reverse primers and the other with SNP forward and reverse primers. Using agarose gel electrophoresis, two bands of 335 and 340 bp in heterozygous (CT) individuals, one band of 335 bp in homozygous dominant (CC) and one band of 340 bp in homozygous recessive (TT) was observed. Control samples with two bands of 335 and 340 bp, relating respectively to C and T alleles, demonstrated CT genotype. Control samples with only 335 bp band represented CC genotype, and control samples with only 340 bp revealed TT genotype (Fig.2A). Some samples were sequenced to validate the efficacy of the ASP-PCR. The outcomes of sequencing were totally consistent with the ASP-PCR findings, confirming the efficacy of the ASP-PCR method.

rs8193 C allele associates with the risk of gastric cancer

To study association of different rs8193 genotypes with risk of the gastric cancer, we studied the samples in two ways. First, we considered allele T as the risk variant. Therefore, the samples were analyzed as CC compared to CT+TT (recessive model). The statistical outcomes revealed no significant association (Pearson chi-square test, $P=0.122$). However, categorizing CC+CT samples, as dominant model compared to TT, showed a significant association (Pearson chi-square test, $P<0.001$). This outcome indicated that harboring allele C has increased the risk of gastric cancer with odds ratio (OR) of 3.429 [95% confidence interval (CI): 1.768-6.647]. Univariate association study between the patients carrying C allele and the incidence of gastric cancer is shown in Table 2.

To evaluate the significance of rs8193 C allele risk in the studied gastric cancer patients, we incorporated confounder factors into the regression model. These factors consist of blood groups, smoking status and *H. pylori* infection (Table 3). Based on the univariate analysis (Table 2), *H. pylori* infection and harboring C allele at the rs8193 position were both associated with gastric cancer outcome. Although statistical analysis showed that *H. pylori* infection had higher significance to associate with the gastric cancer outcome, benefiting from the multivariate logistic regression. Study the effect of rs8193 in the context of other confounders revealed that rs8193 C allele was still associated with the increased risk of gastric cancer with OR: 2.888 (95% CI: 1.430-5.835, $P=0.003$). Wald

value for *H. pylori* was 16.707; while it was 8.742 for carrying C allele, showing the higher significance of *H. pylori* infection to contribute to the gastric cancer outcome. As both *H. pylori* infection and rs8193 C allele were significantly important to have the gastric cancer outcome, we performed a chi-square test in order to know if rs8193 is associated with risk of *H. pylori* infection. Among 24 TT samples, 12 were *H. pylori* positive and 12 samples were negative. Among 144 C allele carriers, 119 cases did not show *H. pylori* infection and 91 samples showed *H. pylori* infection. Chi-square test revealed that there is no association between *H. pylori* infection and rs8193 C allele; therefore, rs8193 C allele does not correlate with the risk of *H. pylori*-mediated gastric cancer ($P=0.534$). Taken together, these data strongly suggest that the C allele carriers at rs8193 position are genetically predisposed to gastric cancer.

Based on the available clinicopathological characteristics of the gastric cancer patients, we investigated if having C allele at rs8193 position would associate with distal metastasis, lymph node spread and stage of gastric cancer. Among different conditions, statistical analyses demonstrated that the patients who carried C allele associated with higher chance of having regional lymph node spread with OR: 4.896 (95% CI: 1.985-12.076, $P<0.001$, Table 4). Moreover, these patients were less likely to have stage I gastric cancer, (OR: 0.241, 95% CI: 0.084-0.688, $P=0.011$), as C allele-carriers are more accumulated in the groups with higher stages. Clinically, these findings support the prognostic importance of rs8193 C allele in gastric cancer.

Table 2: Univariate comparison of the controls and cases

Variable	Cancer n=168 n (%)	Controls n=66 n (%)	OR (95% CI)	P value*
Smoking			-	0.748
No	75 (44.64)	31 (46.97)		
Yes	93 (55.36)	35 (53.03)		
<i>H. pylori</i> infection			4.704 (2.388-9.268)	< 0.001
No	78 (46.43)	53 (80.30)		
Yes	90 (53.57)	13 (19.70)		
Blood group A			-	0.926
No	108 (64.29)	42 (63.64)		
Yes	60 (35.71)	24 (36.36)		
Carrying C allele at rs8193 position			3.429 (1.768-6.647)	< 0.001
No	24 (14.29)	24 (36.36)		
Yes	144 (85.71)	42 (63.64)		

*; Chi-square test, OR; Odds ratio, and CI; Confidence interval.

Table 3: Multivariate logistic regression comparison of the controls and cases

Variable	Cancer	Controls	OR (95% CI)	P value*
	n=168	n=66		
Smoking			-	0.786
No	75	31		
Yes	93	35		
<i>H. pylori</i> infection			4.223 (2.116-8.425)	<0.001
No	78	53		
Yes	90	13		
Blood group A			-	0.957
No	108	42		
Yes	60	24		
Carrying C allele at rs8193 position			2.888 (1.430-5.835)	0.003
No	24	24		
Yes	144	42		

*; Multivariate logistic regression. Smoking (No), *H. pylori* infection (No), blood group A (No) and carrying C allele at rs8193 position (No) were considered as references of cancer outcom, OR; Odds ratio, and CI; Confidence interval.

Table 4: Association of rs8193 C allele harboring patients with gastric cancer characteristics

Characteristic	rs8193 genotype		OR (95% CI)	P value
	TT	CC+CT		
	n=24 n (%)	n=144 n (%)		
Distal metastasis				0.899*
No	13 (54.17)	80 (55.56)		
Yes	11 (45.83)	64 (44.44)		
Regional lymph node spread			4.896 (1.985-12.076)	<0.001*
No	13 (54.17)	28 (19.44)		
Yes	11 (45.83)	116 (80.56)		
Stage			0.241 (0.084-0.688)	0.011**
I	7 (29.17)	13 (9.03)		
II, III and IV	17 (70.83)	131 (90.97)		
II	2 (8.33)	30 (20.83)	-	0.254**
I, III and IV	22 (91.67)	114 (79.19)		
III	6 (25)	48 (33.33)	-	0.487**
I, II and IV	18 (75)	96 (66.67)		
IV	9 (37.50)	53 (36.81)	-	0.998**
I, II and III	15 (62.50)	91 (63.19)		

*; Chi-square test, **; Fisher's exact test, OR; Odds ratio, and CI; Confidence interval.

Potential role of rs8193 in modulating interaction of *CD44* mRNA with miRNAs

As rs8193 is located in the 3'UTR of *CD44* gene, we postulated that this SNP may impose its effect through altering interaction of *CD44* mRNA with miRNAs. Using miRNASNP online database, exploring potential of the different rs8193 alleles demonstrated disrupting role of C allele, with regards to the interaction between *CD44* mRNA and *miR-570*. Indeed, C allele, which is shown

to be a risk factor in this study, could result in higher expression of *CD44*, due to the lower binding affinity of *miR-570* to it. On the other hand, rs8193 T allele, as a protective factor, can strengthen the interaction and therefore reduce the *CD44* expression level (Fig.2B). This finding is supported by the changes in ΔG values of *miR-570:CD44* interaction. This interaction could be stable ($\Delta G=-13.70$) when T is positioned, while it is unstable when C is replaced ($\Delta G=0$).

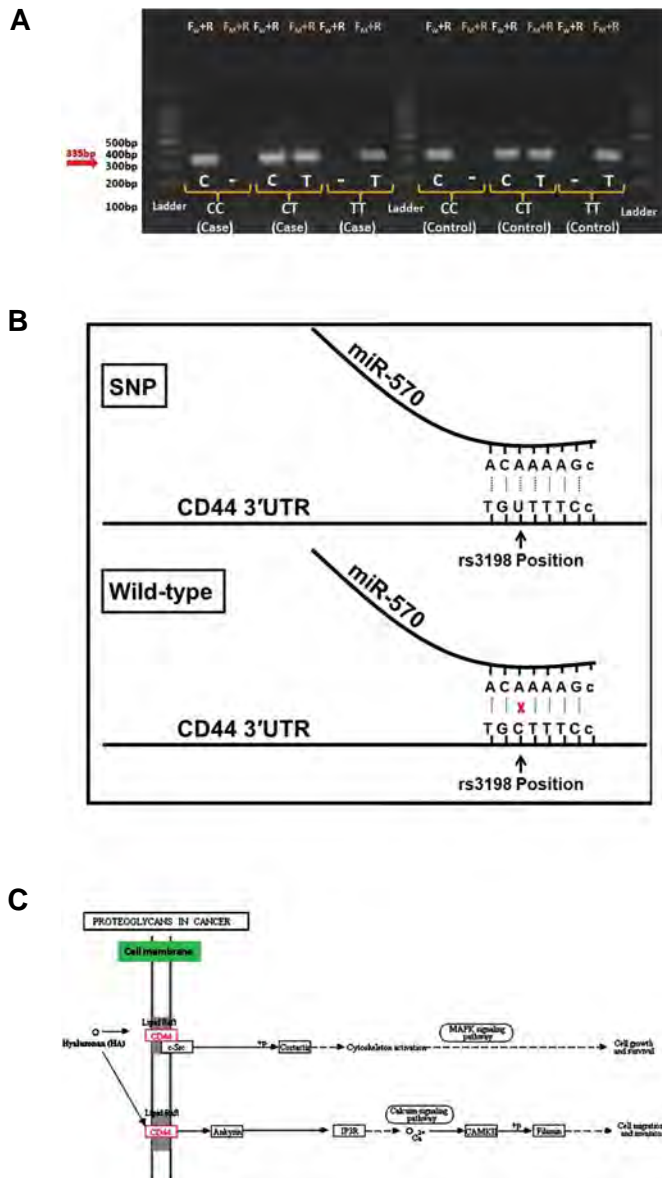


Fig. 2: Molecular characteristics of rs3198 position and genotyping of the samples. **A.** Optimized ASP-PCR followed by gel electrophoresis, **B.** The schematic view of allele T and C effect on the interaction between miR-570 and *CD44* mRNA at rs3198 position, and **C.** Enrichment analysis of miR-570 and its importance in targeting *CD44*.

Study the targetome of *miR-570* in miRWalk database further showed *CD44* as one of the high-score predicted genes, with the score 6 out of 7 integrated algorithms used (Table S1) (See Supplementary Online Information at www.celljournal.org). Moreover, enrichment analysis of *miR-570* targetome in DAVID tool suggested *CD44* as a putative target in gastric carcinogenesis. As shown in Figure 2C, activity of the *CD44* along with proteoglycan hyaluronan (HA) in MAPK signaling pathway is associated with growth and survival of tumor cells [$P=1.5 \times 10^{-6}$, false discovery rate (FDR) correction=0.0002]. Moreover, this interaction can result in cellular invasion and migration via calcium signaling pathway ($P=5.5 \times 10^{-7}$, FDR correction=0.0001). Albeit the *in silico* studies are required to be validated by the biochemical assays, these data are quite compatible with the outcomes of our study, showing that C allele is the risk factor. Rs8193 C allele,

indeed, can attenuate the interaction between *miR-570* and *CD44* mRNA, which in turn, enhances the expression and oncogenic effect of *CD44* in gastric cells.

Discussion

Late diagnosis, complexity of treatment and prevention are the main concerns of gastric cancer. These issues are tightly related to the multifactorial nature of this disease. Therefore, early detection of gastric cancer is highly necessary in order to control it. Along with the environmental parameters like *H. pylori* infection, genetic factors including gene expression profile and cancer biomarkers, such as SNPs, have a crucial role to better predict early diagnosis of gastric cancer (17).

In this study, we genotyped the rs8193 position in control and gastric cancer samples. Although the main cause of gastric cancer in the studied population was *H. pylori* infection, rs8193 C allele was shown to be associated with higher risk of gastric cancer, in both univariate and multivariate logistic regression models. Clinically, rs8193 C allele also associated with the enhanced risk of regional lymph node spread and lower chance of categorization in the gastric cancer stage I. In order to have an improved vision of rs8193 potential, it is highly recommended to study this SNP in a larger population with more patients' demographics, such as age, sex, alcohol consumption status, occupation, etc.

CD44, as a type 1 of single-pass transmembrane protein, is an important adhesive molecule for the extracellular matrix. It acts as a cell surface receptor of hyaluronic acid, and interferes with various biological processes such as cell adhesion, cell migration and cancer metastasis. In addition, *CD44* gene may increase the risk of tumor recurrence in a variety of cancers (24).

In order to find the potential role of rs8193 C allele in increasing chance of gastric cancer, *in silico* studies were recruited. Regarding that rs8193 is located within *CD44* 3'UTR, alteration in miRNA binding affinity could be the main mechanism of action for different rs8193 alleles. Based on the investigations, rs8193 C allele can attenuate the interaction between *miR-570* and *CD44* mRNA, which may result in the higher expression of *CD44* oncogene. Interestingly, Mumbreakar et al. (25) have shown that rs8193 can alter the expression of *CD44*, based on the HapMap database results. Moreover, functional SNP dataset (F-SN) indicated that rs8193 might change the affinity of transcription factors to the *CD44* promoter, due to a distant conformational effect. Taken together, they have also concluded that rs8193 is important for regulating expression of *CD44*. These data strongly confirm the *in silico* outcomes obtained from our study.

Enrichment analysis of *miR-570* targetome further revealed that this small non-coding RNA can target *CD44*, imposing its oncogenic role through MAPK and calcium signaling pathways. Therefore, rs8193 C allele, associated with higher risk of gastric cancer, might destabilize *CD44* and *miR-570* interaction. This, in turn, results in higher expression and

oncogenic impact of CD44. These mechanistic postulations are highly needed to be validated by luciferase reporter assay, Quantitative real time polymerase chain reaction (qRT-PCR) and western blot methods, which were out of the amenities of this study.

Albeit this proposed model can describe the potential mechanism of action by which rs8193 allele C can impose its oncogenic effect in gastric cancer, *in vitro* CD44 3'UTR luciferase assay with two alleles T and C and in the presence and absence of miR-570 mimic, is strongly recommended in order to validate the ability of miR-570 to differentially target CD44 mRNA. Furthermore, CD44 protein expression could be evaluated by western blot, immunohistochemistry (IHC) or ELISA in the samples with T and C alleles to understand if the CD44 expression is truly altered in samples with different genotypes, in the presence of miR-570 mimics or related inhibitors.

The polymorphisms affecting interaction affinity of miR-570 with its target genes have been reported in gastric cancer. Previous studies have shown that polymorphisms in the binding site of miR-570 to the *B7-H1* and *CD274* genes associates with the risk of gastric cancer and it might involve in human cancers (26, 27). Moreover, another study found that miR-570-3p is one of the diagnostic biomarkers for asthma and it is a potential pro-inflammatory miRNA. This miRNA up-regulates various types of cytokines as well as chemokines (CCL4, CCL5, TNF α and IL-6) and increases their induction by TNF α . It also has an inhibitory effect to suppress up-regulation of other cytokines (CCL2 and IL-8) by TNF α (28).

Evidences show that the other CD44 SNPs could also contribute to cancer. Studies showed that the polymorphisms in CD44 play a substantial role in the development of breast (29) and bladder cancers (30) in the northern Indian population and they may be important as a molecular prognostic markers. Moreover, CD44 haplotypes have been shown to significantly associate with the increased incidence of gastric cancer in Chinese patients (24). Furthermore, there is a significant relationship between the CD44 rs187115 and liver cancer (31).

Another investigation demonstrated that various SNPs of CD44 gene, including rs8193, have a significant association with gastric cancer in the Chinese population. According to this study, there was a significant association between rs8193 TT genotype (reported as a protective genotype in our study) and higher chance for lower tumor size or lower serosal invasion (32).

Collecting findings of the current and other studies have shown the importance of rs8193 in cancer, especially gastric malignancy. Further studies in a larger scale with taking the advantage of validation of the proposed miR-570-mediated mechanistic effect of rs8193 on the expression of CD44 can more clarify the significance of different rs8193 alleles in cancer.

Conclusion

An SNP located within 3'UTR of CD44, rs8193,

statistically associate with the risk of lymph node spread and stage of gastric cancer in Iranian population. In this study, rs8193 C allele has been introduced as a risk allele. This allele associates with higher risk of gastric cancer. Distribution of C allele is also enriched in the patients with regional lymph node metastasis. On the other hand, T allele plays role, as a protective allele, and it is statistically enriched in the gastric cancer patients with lower stage.

Acknowledgements

We would like to sincerely appreciate the blood donors and the staff of Zist-fanavari Novin Biotechnology Institute (Iran) for their comprehensive assistance in collecting the samples and related information. There is no financial support and conflict of interest in this study.

Authors' Contributions

R.M., H.T., K.G.; Conceived the experiments and designed the manuscript. R.M., N.B., P.S., M.A., B.Y.; Conducted molecular experiments as well as analysis and contributed extensively in interpretation of the data and conclusion. All authors performed editing and approving the final version of this manuscript.

References

1. Garay J, Piazuelo MB, Majumdar S, Li L, Trillo-Tinoco J, Del Valle L, et al. The homing receptor CD44 is involved in the progression of precancerous gastric lesions in patients infected with *Helicobacter pylori* and in development of mucous metaplasia in mice. *Cancer Lett.* 2016; 371(1): 90-98.
2. Baroudi O, Benammar-Elgaaied A. Involvement of genetic factors and lifestyle on the occurrence of colorectal and gastric cancer. *Crit Rev Oncol Hematol.* 2016; 107: 72-81.
3. Croce CM. *Oncogenes and Cancer.* N Engl J Med. 2008; 358(5): 502-511
4. Cooper DL, Dougherty G, Harn HJ, Jackson S, Baptist EW, Byers J, et al. The complex CD44 transcriptional unit: alternative splicing of three internal exons generates the epithelial form of CD44. *Biochem Biophys Res Commun.* 1992; 182(2): 569-578.
5. Branco da Cunha C, Klumpers DD, Koshy ST, Weaver JC, Chaudhuri O, Seruca R, et al. CD44 alternative splicing in gastric cancer cells is regulated by culture dimensionality and matrix stiffness. *Biomaterials.* 2016; 98: 152-162.
6. Dehghan Z, Sadeghi S, Tabatabaeian H, Ghaedi K, Azadeh M, Fazilati M, et al. ESR1 single nucleotide polymorphism rs1062577 (c.*3804T>A) alters the susceptibility of breast cancer risk in Iranian population. *Gene.* 2017; 611: 9-14.
7. Zabihi N, Sadeghi S, Tabatabaeian H, Ghaedi K, Azadeh M, Fazilati M. The association between rs1972820 and the risk of breast cancer in Isfahan population. *J Cancer Res Ther.* 2017; 13(1): 26-32.
8. Salimi Z, Sadeghi S, Tabatabaeian H, Ghaedi K, Fazilati M. rs11895168 C allele and the increased risk of breast cancer in Isfahan population. *Breast.* 2016; 28: 89-94.
9. Rouigari M, Dehbashi M, Tabatabaeian H, Ghaedi K, Mohammadynejad P, Azadeh M. Evaluation of the expression level and hormone receptor association of miR-126 in breast cancer. *Indian J Clin Biochem.* 2018: 1-7.
10. Mansouri Bidkani M, Tabatabaeian H, Parsafar S, Ghanei N, Fazilati M, Ghaedi K. ErbB4 receptor polymorphism 2368A>C and risk of breast cancer. *Breast.* 2018; 42: 157-163.
11. Noormohammad M, Sadeghi S, Tabatabaeian H, Ghaedi K, Talebi A, Azadeh M, et al. Upregulation of miR-222 in both *Helicobacter pylori*-infected and noninfected gastric cancer patients. *J Genet.* 2016; 95(4): 991-995.
12. Adami B, Tabatabaeian H, Ghaedi K, Talebi A, Azadeh M, Dehdashtian E. miR-146a is deregulated in gastric cancer. *J Cancer Res Ther.* 2018 (ahead of print).
13. Garzon R, Calin GA, Croce CM. MicroRNAs in cancer. *Annu Rev*

- Med. 2009; 60: 167-179.
14. Wakamatsu Y, Sakamoto N, Oo HZ, Naito Y, Uraoka N, Anami K, et al. Expression of cancer stem cell markers ALDH1, CD44 and CD133 in primary tumor and lymph node metastasis of gastric cancer. *Pathol Int.* 2012; 62(2): 112-119.
 15. Assad Samani L, Javadirad SM, Parsafar S, Tabatabaeian H, Ghaedi K, Azadeh M. TP53 rs1625895 is related to breast cancer incidence and early death in Iranian population. *Indian J Clin Biochem.* 2018; 1-5.
 16. Moradi B, Tabatabaeian H, Sadeghi S, Azadeh M, Ghaedi K. HER4 rs1595065 3'UTR variant is a possible risk factor for HER2 Positivity among breast cancer patients. *Thrita.* 2016; 5(4): e42195.
 17. Nabatchian F, Rahimi Naiini M, Moradi A, Tabatabaeian H, Hoghoughi N, Azadeh M, et al. miR-581-related single nucleotide polymorphism, rs2641726, located in MUC4 gene, is associated with gastric cancer incidence. *Indian J Clin Biochem.* 2018: 1-5.
 18. Honardoost MA, Tabatabaeian H, Akbari M, Salehi M. Investigation of sensitivity, specificity and accuracy of Tetra primer ARMS PCR method in comparison with conventional ARMS PCR, based on sequencing technique outcomes in IVS-II-I genotyping of beta thalassemia patients. *Gene.* 2014; 549(1): 1-6.
 19. Gong J, Tong Y, Zhang HM, Wang K, Hu T, Shan G, et al. Genome-wide identification of SNPs in microRNA genes and the SNP effects on microRNA target binding and biogenesis. *Hum Mutat.* 2012; 33(1): 254-263.
 20. Tabatabaian M, Mesrian Tanha H, Tabatabaeian H, Sadeghi S, Ghaedi K, Mohamadynejad P. ErbB4 3'-UTR variant (c.* 3622A>G) is associated with ER/PR negativity and advanced breast cancer. *Indian J Clin Biochem.* 1-6.
 21. Dweep H, Gretz N. miRWalk2. 0: a comprehensive atlas of microRNA-target interactions. *Nat Methods.* 2015; 12(8): 697.
 22. Huang da W, Sherman BT, Lempicki RA. Bioinformatics enrichment tools: paths toward the comprehensive functional analysis of large gene lists. *Nucleic Acids Res.* 2009; 37(1): 1-13.
 23. Noormohammad M, Khatami M, Tabatabaeian H, Ghaedi K, Talebi A, Heidari MM. In-silico investigation of Mir-222 in H. Pylori-associated gastric cancer. *Iranian Journal of Public Health.* 2014; 43(Suppl 2): 23.
 24. Verma A, Kapoor R, Mittal RD. Cluster of differentiation 44 (CD44) gene variants: a putative cancer stem cell marker in risk prediction of bladder cancer in north Indian population. *Indian J Clin Biochem.* 2017; 32(1): 74-83.
 25. Mumbreakar KD, Bola Sadashiva SR, Kabekkodu SP, Fernandes DJ, Vadhira BM, Suga T, et al. Genetic variants in CD44 and MAT1A confer susceptibility to acute skin reaction in breast cancer patients undergoing radiation therapy. *Int J Radiat Oncol Biol Phys.* 2017; 97(1): 118-127.
 26. Wang W, Li F, Mao Y, Zhou H, Sun J, Li R, et al. A miR-570 binding site polymorphism in the B7-H1 gene is associated with the risk of gastric adenocarcinoma. *Hum Genet.* 2013; 132(6): 641-648.
 27. Wang W, Sun J, Li F, Li R, Gu Y, Liu C, et al. A frequent somatic mutation in CD274 3'-UTR leads to protein over-expression in gastric cancer by disrupting miR-570 binding. *Hum Mutat.* 2012; 33(3): 480-484.
 28. Roff AN, Craig TJ, August A, Stellato C, Ishmael FT. MicroRNA-570-3p regulates HuR and cytokine expression in airway epithelial cells. *Am J Clin Exp Immunol.* 2014; 3(2): 68-83.
 29. Tulsyan S, Agarwal G, Lal P, Agrawal S, Mittal RD, Mittal B. CD44 gene polymorphisms in breast cancer risk and prognosis: a study in North Indian population. *PLoS One.* 2013; 8(8): e71073.
 30. Sharma KL, Yadav A, Gupta A, Tulsayan S, Kumar V, Misra S, et al. Association of genetic variants of cancer stem cell gene CD44 haplotypes with gallbladder cancer susceptibility in North Indian population. *Tumour Biol.* 2014; 35(3): 2583-2589.
 31. Chou YE, Hsieh MJ, Chiou HL, Lee HL, Yang SF, Chen TY. CD44 gene polymorphisms on hepatocellular carcinoma susceptibility and clinicopathologic features. *Biomed Res Int.* 2014; 2014: 231474
 32. Qiu Y, Hu Y, Zhang Z-Y, Ye L, Xu F-H, Schneider ME, et al. Genetic association of osteopontin (OPN) and its receptor CD44 genes with susceptibility to Chinese gastric cancer patients. *J Cancer Res Clin Oncol.* 2014; 140(12): 2143-2156.

Regulatory Network Analysis to Reveal Important miRNAs and Genes in Non-Small Cell Lung Cancer

Xingni Zhou, M.M.^{1#}, Zhenghua Zhang, M.M.^{2#}, Xiaohua Liang, M.D.^{1*}

1. Department of Oncology, Huashan Hospital of Fudan University, Shanghai, China

2. Department of Clinical Oncology, Jing'an District Centre Hospital of Shanghai (Huashan Hospital, Fudan University, Jing'an Branch), Shanghai, China

#The first two authors equally contributed to this work.

*Corresponding Address: Department of Oncology, Huashan Hospital of Fudan University, No.12 the Middle Wu Lu Mu Qi Road, Shanghai, China

Email: Liangxiaohuahh@163.com

Received: 1/August/2018, Accepted: 1/December/2018

Abstract

Objective: Lung cancer has high incidence and mortality rate, and non-small cell lung cancer (NSCLC) takes up approximately 85% of lung cancer cases. This study is aimed to reveal miRNAs and genes involved in the mechanisms of NSCLC.

Materials and Methods: In this retrospective study, GSE21933 (21 NSCLC samples and 21 normal samples), GSE27262 (25 NSCLC samples and 25 normal samples), GSE43458 (40 NSCLC samples and 30 normal samples) and GSE74706 (18 NSCLC samples and 18 normal samples) were searched from gene expression omnibus (GEO) database. The differentially expressed genes (DEGs) were screened from the four microarray datasets using MetaDE package, and then conducted with functional annotation using DAVID tool. Afterwards, protein-protein interaction (PPI) network and module analyses were carried out using Cytoscape software. Based on miR2Disease and Mirwalk2 databases, microRNAs (miRNAs)-DEG pairs were selected. Finally, Cytoscape software was applied to construct miRNA-DEG regulatory network.

Results: Totally, 727 DEGs (382 up-regulated and 345 down-regulated) had the same expression trends in all of the four microarray datasets. In the PPI network, TP53 and FOS could interact with each other and they were among the top 10 nodes. Besides, five network modules were found. After construction of the miRNA-gene network, top 10 miRNAs (such as *hsa-miR-16-5p*, *hsa-let-7b-5p*, *hsa-miR-15a-5p*, *hsa-miR-15b-5p*, *hsa-let-7a-5p* and *hsa-miR-34a-5p*) and genes (such as *HMGA1*, *BTG2*, *SOD2* and *TP53*) were selected.

Conclusion: These miRNAs and genes might contribute to the pathogenesis of NSCLC.

Keywords: Meta-Analysis, microRNA, Non-Small Cell Lung Cancer, Protein Interaction, Regulatory Network

Cell Journal(yakhteh), Vol 21, No 4, January-March (Winter) 2020, Pages: 459-466

Citation: Zhou X, Zhang Zh, Liang X. Regulatory network analysis to reveal important miRNAs and genes in non-small cell lung cancer. Cell J. 2020; 21(4): 459-466. doi: 10.22074/cellj.2020.6281.

Introduction

Lung cancer is a common tumor which has globally high incidence and mortality rate with 1.82 million newly diagnosed cases and 1.56 million death cases in 2012 (1). Lung cancer is comprised of small cell lung cancer (SCLC) and non-SCLC (NSCLC), among which NSCLC takes up approximately 85% of lung cancer cases (2). Tobacco smoking is the primary inducement for lung cancer, and other risk factors are air-pollution, radon, asbestos and chemical exposure (3). NSCLC mainly contains squamous cell carcinoma, adenocarcinoma and large cell carcinoma, while nearly half of NSCLC cases are non-squamous cell carcinoma (4). NSCLC is less sensitive to chemotherapy in comparison to SCLC, and it is usually treated by surgical resection (5). Therefore, investigating pathogenesis of NSCLC is of great significance.

Previous study found that fibroblast growth factor

receptor 1 (*FGFR1*) amplification is common in NSCLC and it might be utilized as a therapeutic target for inhibiting tumor cell growth (6, 7). Overexpressed lysine specific demethylase 1 (*LSD1*) can lead to poor prognosis of NSCLC patients, which also enhances cell proliferation, invasion and migration (8). Transcriptional co-activation with PDZ-binding motif (*TAZ*) is found to be an oncogene and plays a tumorigenic role in NSCLC, and thus *TAZ* serves as a potential diagnostic, therapeutic and prognostic target for the disease (9). *microRNA-21* (*miR-21*) is up-regulated in NSCLC tissues in comparison with normal tissues, which can negatively regulate phosphatase and tensin homolog (*PTEN*) expression. It contributes to the growth and invasion of tumor cells (10). *miR-451* expression is significantly related to pathological stage, tumor differentiation and lymph-node metastasis, and it mediates the survival of NSCLC

patients via down-regulating ras-related protein 14 (*RAB14*) (11). Although the above genes and miRNAs are considered to be correlated with NSCLC, the mechanisms of the disease have not been studied and reported comprehensively.

Meta-analysis for multiple datasets can improve statistical ability and identify more reliable differentially expressed genes (DEGs) (12, 13). In the current study, several microarray data of NSCLC were downloaded and conducted with meta-analysis. Subsequently, enrichment analysis and network analysis were carried out to select the key genes and miRNAs for NSCLC. Ultimately, it was concluded that the identified genes and miRNAs might be involved in the mechanisms of NSCLC and they may serve as promising targets for treatment of the disease.

Materials and Methods

Expression profile data

In this retrospective study, the expression profiles involving both NSCLC and normal samples were searched from gene expression omnibus (GEO) database (<http://www.ncbi.nlm.nih.gov/geo/>). Finally, the raw data and platform annotation files under GSE21933 (21 NSCLC and 21 normal samples; platform: GPL6254 Phalanx Human OneArray), GSE27262 (25 NSCLC and 25 normal samples; platform: GPL570 [HG-U133_Plus_2] Affymetrix Human Genome U133 Plus 2.0 Array), GSE43458 (40 NSCLC and 30 normal samples; platform: GPL6244 [HuGene-1_0-st] Affymetrix Human Gene 1.0 ST Array) and GSE74706 (18 NSCLC and 18 normal samples; platform: GPL13497 Agilent-026652 Whole Human Genome Microarray 4x44K v2) were extracted.

Data preprocessing

For the raw data, background correction and normalization were conducted by the Affy package of R software (<http://www.bioconductor.org/packages/release/bioc/html/affy.html>) (14). Combined with the platform annotation files, probe IDs were transformed into gene symbols and the probes which have no matching gene symbols were removed. Expression value of the gene matched with many probes was acquired by calculating the average value of the probes.

Meta-analysis

Using the MetaDE package in R software (<https://cran.r-project.org/web/packages/MetaDE/>) (15), DEGs were screened from the four microarray datasets. In detail, heterogeneity test was carried out for the expression values of each gene under different experimental platforms. The $\tau^2=0$ (estimated amount

of residual heterogeneity) and $Q_{pval}>0.05$ (P values for the test of heterogeneity) were the cut-off criteria of homogeneous data set. Then, differential expression analysis was conducted for NSCLC and normal samples. Using Benjamini-Hochberg method (16), the P values were corrected to obtain false discovery rates (FDRs). Genes with $\tau^2=0$, $Q_{pval}>0.05$ and $FDR<0.05$ were defined as DEGs. Furthermore, \log_2 fold change (FC) values of the DEGs were calculated. The DEGs with $\log_2FC>0$ in all of the four datasets were up-regulated genes in NSCLC samples, and the DEGs with $\log_2FC<0$ in all of the four datasets were down-regulated genes.

Enrichment analysis

Gene ontology (GO; <http://www.geneontology.org>) describes the purposes of gene products from molecular function (MF), biological process (BP), and cellular component (CC) aspects (17). The Kyoto Encyclopedia of Genes and Genomes (KEGG; <http://www.genome.ad.jp/kegg>) is a reference database for annotating genes or proteins (18). Based on the database for annotation, visualization and integrated discovery (DAVID; <https://david.ncifcrf.gov/>, version 6.8) tool, GO and KEGG analyses for the selected DEGs were conducted. The terms involving two or more genes and having $P<0.05$ were considered significant results.

Protein-protein interaction network construction

Search tool for the retrieval of interacting genes (STRING; <http://string-db.org/>, version 10.0) integrates the protein-protein interactions (PPIs) of various organisms. With medium confidence > 4 , as the threshold, PPIs were predicted for the DEGs using the STRING database (19). Next, PPI network was built by Cytoscape software (<http://www.cytoscape.org>, version 3.2.0). Moreover, degree centrality of the network nodes was analyzed, and those with higher degrees were taken as key nodes. Additionally, molecular complex detection (MCODE) plug-in in Cytoscape software (20) was applied for module analysis to identify the significant modules.

Construction of miRNA-DEG regulatory network

The miR2Disease (<http://www.mir2disease.org/>) is a database, containing dysregulated miRNAs implicated in multiple diseases. The miRNAs related to NSCLC were searched from miR2Disease database (21). Then, the verified targets of the NSCLC-associated miRNAs were obtained from Mirwalk2 database (<http://zmf.umm.uni-heidelberg.de/mirwalk2>) (22). Through getting the intersection of the targets and the DEGs, the miRNA-DEG regulatory relationships were selected. Finally, miRNA-gene regulatory network was built using Cytoscape software (20).

Results

Meta-analysis and enrichment analysis

There were a total of 749 dysregulated genes in NSCLC, compared to normal samples. Among these genes, 727 DEGs (382 up-regulated and 345 down-regulated) had the same expression trends in all of the four microarray datasets. The DEGs were enriched in multiple GO and KEGG terms, indicating the potential functions of the DEGs. Top five terms involving the up-regulated and down-regulated genes are respectively shown in Figure 1A and 1B.

Protein-protein interaction network analysis

A PPI network was built for the identified DEGs, involving 606 nodes and 2246 edges (Fig.S1) (See Supplementary Online Information at www.celljournal.org). After arranging the node degrees in descending order, tumor protein p53 (TP53, up, degree=109), mitogen-activated protein kinase 3 (MAPK3, down, degree=55), RNA polymerase II subunit B (POLR2B, up, degree=50), FBJ osteosarcoma oncogene (FOS, down, degree=49), integrin alpha 2 (ITGA2, up, degree=48), mechanistic target of rapamycin kinase (MTOR, up, degree=46), early growth response 1 (EGR1, down, degree=39), eukaryotic elongation factor 2 (EEF2, down, degree=34), ISG15 ubiquitin-like modifier (ISG15, up, degree=33), and ABL proto-oncogene 1 (ABL1, down, degree=33) were among the top 10 nodes. Importantly, TP53 could interact with

FOS in the PPI network, suggesting that TP53 might act in NSCLC via interacting with FOS.

Besides, five significant network modules (module a: 13 nodes and 77 edges; module b: 35 nodes and 110 edges; module c: six nodes and 15 edges; module d: six nodes and 15 edges; module e: 22 nodes and 45 edges) were selected (Fig.2). KEGG pathway enrichment analysis was conducted for the nodes in each module. Especially, Spliceosome (module a, $P=1.53E-05$), HTLV-I infection (module b, $P=4.62E-04$), Basal transcription (module c, $P=1.24E-04$), Ribosome (module d, $P=1.44E-07$), and Epstein-Barr virus (module e, $P=9.95E-04$) were enriched for the module nodes (Table 1).

Construction of miRNA-DEG regulatory network

From miR2Disease database, a total of 27 NSCLC-associated miRNAs was obtained. There were 15421 verified miRNA-target interactions, involving 27 miRNA in Mirwalk2 database. After selecting miRNA-DEG pairs, miRNA-gene regulatory network (involving 358 nodes and 658 edges) was visualized (Fig.S2) (See Supplementary Online Information at www.celljournal.org). According to node degrees, top 10 miRNAs (such as *hsa-miR-16-5p*, *hsa-let-7b-5p*, *hsa-miR-15a-5p*, *hsa-miR-15b-5p*, *hsa-let-7a-5p* and *hsa-miR-34a-5p*) and genes (such as high mobility group AT-hook 1, *HMGAI*; BTG family, member 2, *BTG2*; superoxide dismutase 2, *SOD2*; and *TP53*) were selected and listed in Table 2, while they might be critical for development of NSCLC (Fig.3).

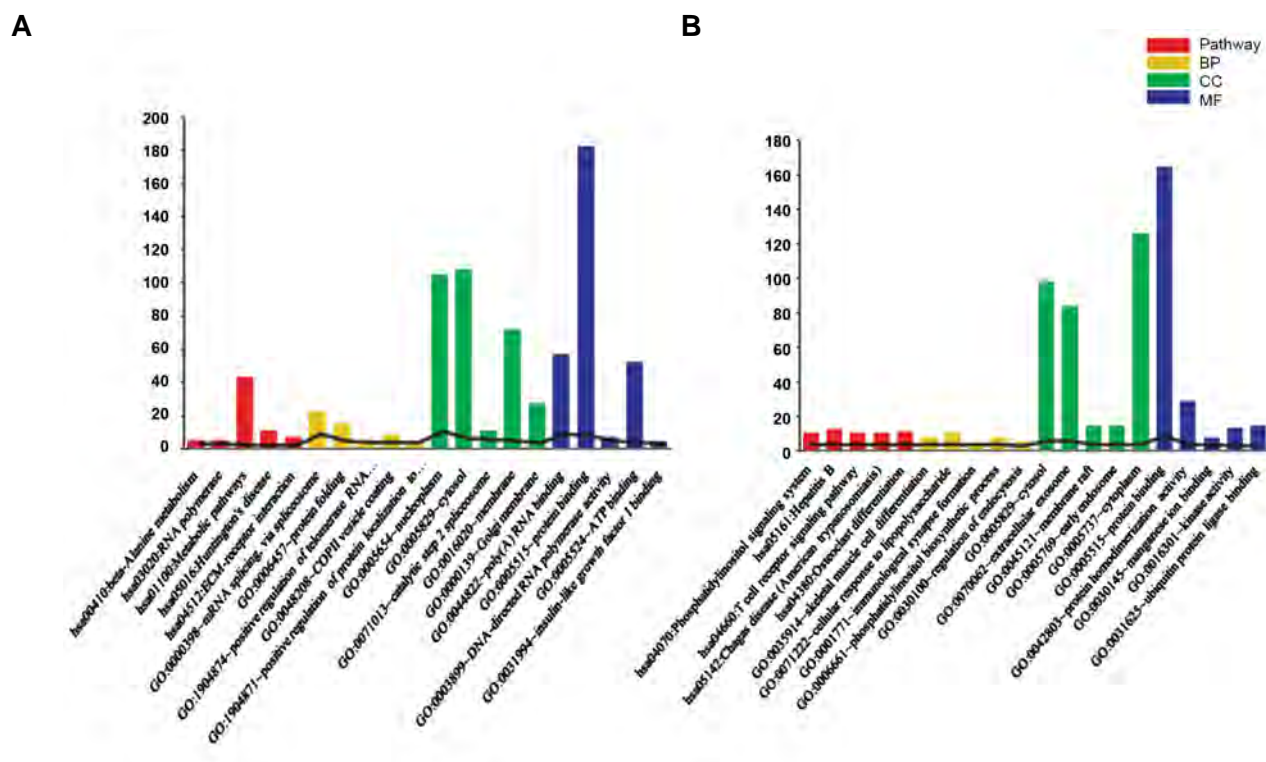


Fig.1: The results of enrichment analysis for the differentially expressed genes. **A.** Top five terms enriched for the up-regulated genes and **B.** Top five terms enriched for the down-regulated genes. The horizontal and vertical axes represent name of the enriched term and number of the genes involved in each term, respectively. BP; Biological process, CC; Cellular component, and MF; Molecular function.

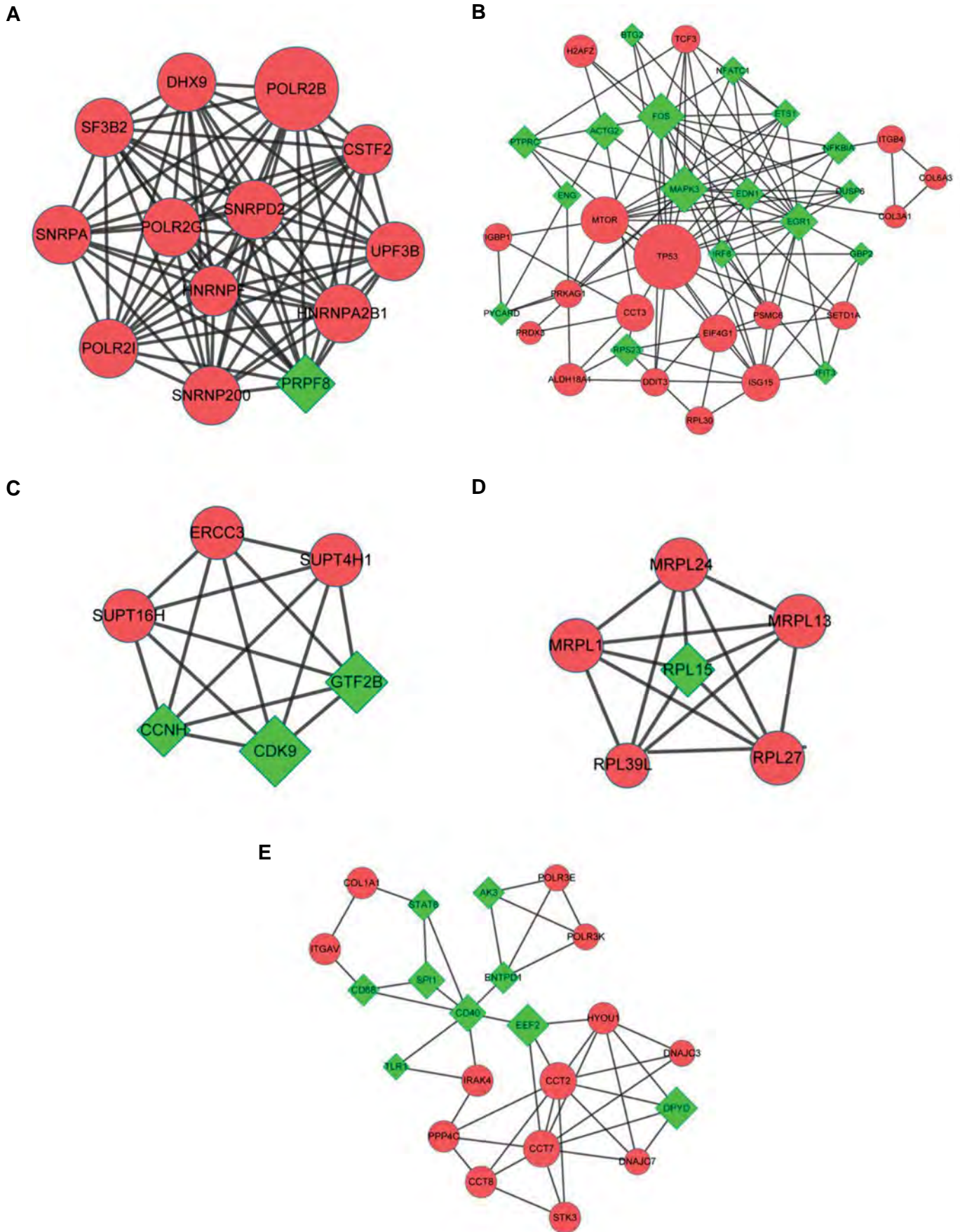


Fig.2: The significant modules identified from protein-protein interaction (PPI) network. **A.** The significant module a, **B.** The significant module b, **C.** The significant module c, **D.** The significant module d, and **E.** The significant module e. Red circles and green prismatic represent up-regulated genes and down-regulated genes, respectively.

Table 1: Pathways enriched for the nodes in module a, b, c, d and e

Module	Pathway ID	Pathway name	Count	P value	Genes
a	hsa03040	Spliceosome	5	1.53E-05	<i>PRPF8, SNRNP200, SNRPA, SNRPD2, SF3B2</i>
	hsa03020	RNA polymerase	3	7.33E-04	<i>POLR2G, POLR2I, POLR2B</i>
	hsa00240	Pyrimidine metabolism	3	7.54E-03	<i>POLR2G, POLR2I, POLR2B</i>
	hsa00230	Purine metabolism	3	2.06E-02	<i>POLR2G, POLR2I, POLR2B</i>
	hsa05169	Epstein-Barr virus infection	3	2.38E-02	<i>POLR2G, POLR2I, POLR2B</i>
	hsa05016	Huntington's disease	3	2.43E-02	<i>POLR2G, POLR2I, POLR2B</i>
b	hsa05166	HTLV-1 infection	7	4.62E-04	<i>EGRI, FOS, ETS1, TP53, NFKBIA, TCF3, NFATC1</i>
	hsa04660	T cell receptor signaling pathway	5	7.24E-04	<i>PTPRC, FOS, MAPK3, NFKBIA, NFATC1</i>
	hsa05161	Hepatitis B	5	2.57E-03	<i>FOS, MAPK3, TP53, NFKBIA, NFATC1</i>
	hsa04662	B cell receptor signaling pathway	4	2.61E-03	<i>FOS, MAPK3, NFKBIA, NFATC1</i>
	hsa04010	MAPK signaling pathway	6	3.22E-03	<i>FOS, MAPK3, TP53, DDIT3, NFATC1, DUSP6</i>
	hsa05133	Pertussis	4	3.31E-03	<i>FOS, IRF8, MAPK3, PYCARD</i>
	hsa05215	Prostate cancer	4	5.19E-03	<i>MAPK3, TP53, NFKBIA, MTOR</i>
	hsa04668	TNF signaling pathway	4	8.70E-03	<i>FOS, MAPK3, EDNI, NFKBIA</i>
	hsa04151	PI3K-Akt signaling pathway	6	1.15E-02	<i>MAPK3, COL3A1, COL6A3, TP53, ITGB4, MTOR</i>
	hsa04380	Osteoclast differentiation	4	1.54E-02	<i>FOS, MAPK3, NFKBIA, NFATC1</i>
	hsa04621	NOD-like receptor signaling pathway	3	2.06E-02	<i>MAPK3, PYCARD, NFKBIA</i>
	hsa04921	Oxytocin signaling pathway	4	2.53E-02	<i>FOS, PRKAG1, MAPK3, NFATC1</i>
	hsa05210	Colorectal cancer	3	2.58E-02	<i>FOS, MAPK3, TP53</i>
	hsa05230	Central carbon metabolism in cancer	3	2.73E-02	<i>MAPK3, TP53, MTOR</i>
	hsa05214	Glioma	3	2.81E-02	<i>MAPK3, TP53, MTOR</i>
	hsa04920	Adipocytokine signaling pathway	3	3.23E-02	<i>PRKAG1, NFKBIA, MTOR</i>
	hsa05140	Leishmaniasis	3	3.31E-02	<i>FOS, MAPK3, NFKBIA</i>
	hsa05220	Chronic myeloid leukemia	3	3.40E-02	<i>MAPK3, TP53, NFKBIA</i>
	hsa05132	Salmonella infection	3	4.40E-02	<i>FOS, MAPK3, PYCARD</i>
	hsa04024	cAMP signaling pathway	4	4.49E-02	<i>FOS, MAPK3, NFKBIA, NFATC1</i>
hsa04512	ECM-receptor interaction	3	4.79E-02	<i>COL3A1, COL6A3, ITGB4</i>	
hsa04510	Focal adhesion	4	4.95E-02	<i>MAPK3, COL3A1, COL6A3, ITGB4</i>	
c	hsa03022	Basal transcription factors	3	1.24E-04	<i>CCNH, ERCC3, GTF2B</i>
	hsa03420	Nucleotide excision repair	2	2.03E-02	<i>CCNH, ERCC3</i>
d	hsa03010	Ribosome	5	1.44E-07	<i>MRPL24, MRPL1, MRPL13, RPL15, RPL27</i>
e	hsa05169	Epstein-Barr virus infection	5	9.95E-04	<i>POLR3K, SPI1, CD40, ENTPD1, POLR3E</i>
	hsa00240	Pyrimidine metabolism	4	1.93E-03	<i>POLR3K, DPYD, ENTPD1, POLR3E</i>
	hsa00230	Purine metabolism	4	8.49E-03	<i>POLR3K, AK3, ENTPD1, POLR3E</i>
	hsa04620	Toll-like receptor signaling pathway	3	2.73E-02	<i>IRAK4, TLR1, CD40</i>

ID; Identification, HTLV; Human T-lymphotropic virus type 1, TNF; Tumour-necrosis factor, NOD; Nucleotide oligomerization domain, and ECM; Extracellular matrix.

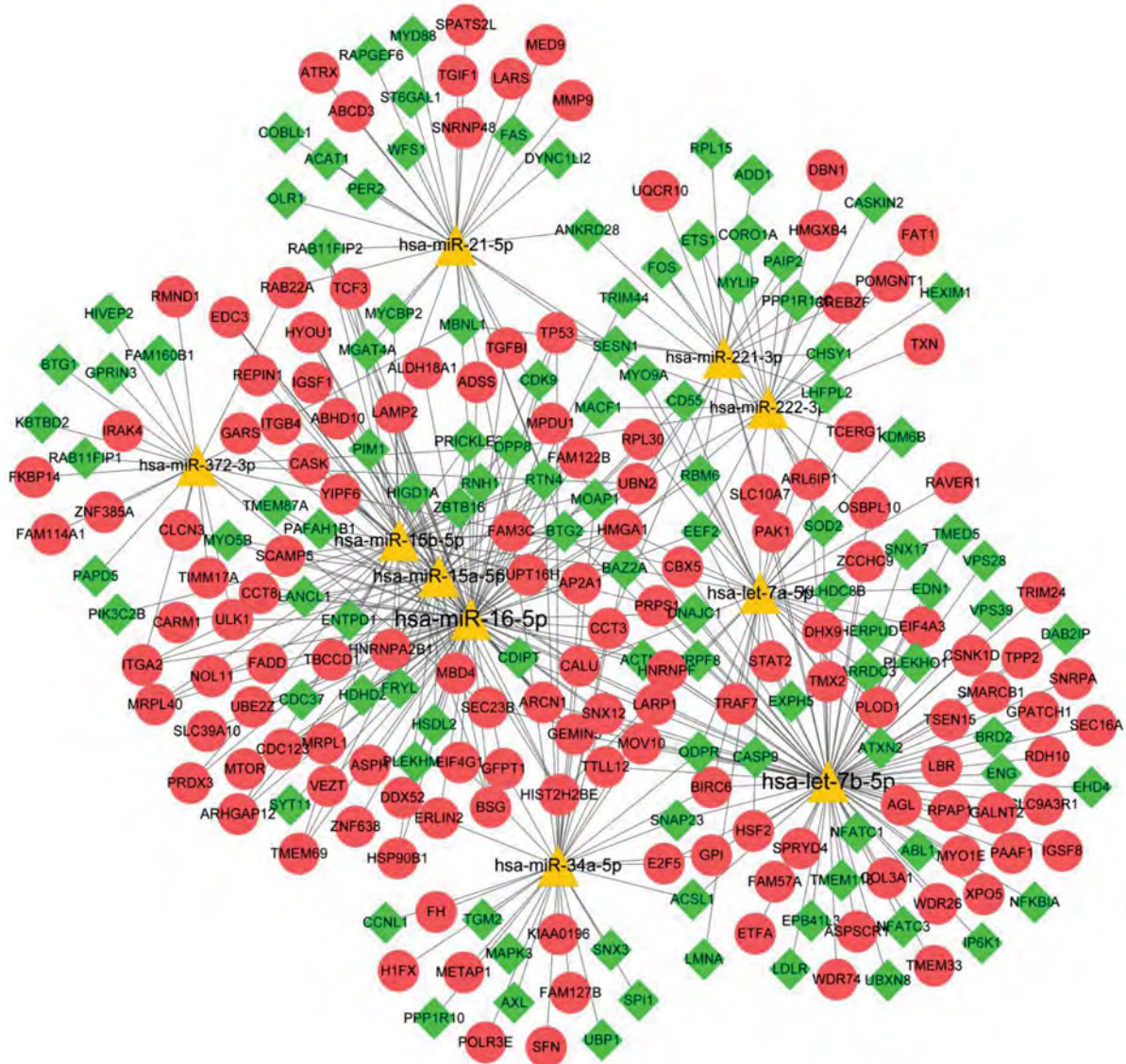


Fig.3: miRNAs-gene regulatory network containing the top 10 miRNAs. Red circles, green prismatic and yellow triangles represent up-regulated genes, down-regulated genes and miRNAs, respectively.

Table 2: Top 10 miRNAs and genes in the miRNA-gene regulatory network

miRNA	Degree	Gene	Degree
<i>hsa-miR-16-5p</i>	89	<i>HMGAI</i>	11
<i>hsa-let-7b-5p</i>	84	<i>BAZZA</i>	9
<i>hsa-miR-15a-5p</i>	44	<i>CALU</i>	9
<i>hsa-miR-15b-5p</i>	41	<i>BTG2</i>	8
<i>hsa-let-7a-5p</i>	40	<i>SOD2</i>	8
<i>hsa-miR-34a-5p</i>	37	<i>TP53</i>	7
<i>hsa-miR-21-5p</i>	33	<i>UBN2</i>	7
<i>hsa-miR-222-3p</i>	24	<i>CBX5</i>	6
<i>hsa-miR-221-3p</i>	23	<i>ITGA2</i>	6
<i>hsa-miR-372-3p</i>	23	<i>SLC10A7</i>	6

Discussion

To investigate the pathogenesis of lung tumorigenesis, Lo et al. (23) identify the differential and common chromosomal imbalance regions among Asian and Caucasian patients with lung cancer through analyzing the microarray dataset GSE21933. Using the dataset GSE27262, Wei et al. (24) explored the roles of protein arginine methyltransferase 5 (*PRMT5*) in the oncogenesis of lung cancer, and revealed cell-transforming activity of *PRMT5* and relevant mechanisms. Kabbout et al. (25) deposited and analyzed the microarray dataset GSE43458 to investigate the functions of *ETS2* in development of lung cancer, finding that *ETS2* acts as a tumor suppressor in NSCLC by suppressing *MET* proto-oncogene. Via analyzing the expression profile GSE74706, Marwitz et al. (26) found that reduced bone morphogenetic protein and activin membrane-bound inhibitor (*BAMBI*) contributes to the invasiveness of NSCLC and TGF- β signaling serves a candidate target for treating the disease. Nevertheless, the above studies have not conducted comprehensive bioinformatics analyses to identify the molecular mechanisms of NSCLC. In the present study, various bioinformatics methods were utilized to select the key genes and miRNAs for NSCLC. In the PPI network, TP53 and FOS were among the top 10 nodes. From the miRNA-gene regulatory network, the top 10 miRNAs (such as *hsa-miR-16-5p*, *hsa-let-7b-5p*, *hsa-miR-15a-5p*, *hsa-miR-15b-5p*, *hsa-let-7a-5p* and *hsa-miR-34a-5p*) and genes (such as *HMGA1*, *BTG2*, *SOD2* and *TP53*) were selected.

As a pivotal inhibitor of tumor-suppressor *p53*, up-regulated *iASPP* (inhibitory member of the apoptosis-stimulating protein of p53 family) mediates tumor cell proliferation and motility, and it serves as a promising target for treatment of lung cancer (27). Tumor suppressor *miR-34a* regulates some molecules involved in cell survival pathways, and *p53/miR-34a* regulatory axis may play important roles in sensitizing NSCLC cells (28). Through c-Fos/c-Jun pathway, interleukin γ (IL γ -)/IL γ -R enhance vascular endothelial growth factor-D (*VEGF-D*) expression and contribute to lymphangiogenesis in lung cancer (29). Via increasing protein expression of c-Fos and adaptor protein complex 1 (AP-1)/DNA binding, fibronectin (*FN*) promotes matrix metalloproteinase-9 (*MMP-9*) expression and accelerates NSCLC cell invasion and metastasis (30). TP53 could interact with FOS in the PPI network, suggesting that *TP53* and *FOS* might be involved in the pathogenesis of NSCLC through interacting with each other.

HMGA1 has higher expression in NSCLC tissues in comparison with normal lung tissues, which functions in development and prognosis of NSCLC (31). *HMGA1* was found to play a critical role in transformation through up-regulating *MMP-2* in large-cell lung carcinoma (32). *BTG2* overexpression may inhibit *MMP-1*, *MMP-2* and cyclin D1 (*CCND1*) expression in lung cancer A549 cell line, and it also has potential of suppressing tumor

cell proliferation, growth and invasiveness (33, 34). By promoting oxidative stress and *SOD2* protein expression, simvastatin suppresses proliferation of lung A549 cells (35). These declared that *HMGA1*, *BTG2* and *SOD2* might play critical roles in the mechanisms of NSCLC.

Co-regulated *miR-15a/16* and *miR-34a* can synergistically arrest the cell cycle of NSCLC in an Rb-dependent manner (36). Down-regulated *let-7b* and *miR-126* may have anti-angiogenic effect and they significantly contribute to poor survival in the patients with lung cancer (37, 38). Overexpression of *miR-15b* can promote the cisplatin chemoresistance of lung adenocarcinoma cells by inhibiting the expression of phosphatidylethanolamine-binding protein 4 (*PEBP4*) (39). *Let-7a* is down-regulated in NSCLC tissues, NSCLC cells and NSCLC blood samples, indicating that *let-7a* may be used as a serologic marker for the disease (40). Therefore, *hsa-miR-16-5p*, *hsa-let-7b-5p*, *hsa-miR-15a-5p*, *hsa-miR-15b-5p*, *hsa-let-7a-5p* and *hsa-miR-34a-5p* might also function in NSCLC via targeting the DEGs.

Conclusion

727 DEGs had similar expression trends in all of the four microarray datasets. Besides, several miRNAs (including *hsa-miR-16-5p*, *hsa-let-7b-5p*, *hsa-miR-15a-5p*, *hsa-miR-15b-5p*, *hsa-let-7a-5p* and *hsa-miR-34a-5p*) and genes (including *HMGA1*, *BTG2*, *SOD2*, *FOS* and *TP53*) might associate with the pathogenesis of NSCLC and they might be applied for targeted therapy of NSCLC. However, no experimental research has been performed to confirm our results. Thus, more in-depth studies should be designed and implemented in the future.

Acknowledgement

There is no financial support and conflict of interest in this study.

Authors' Contributions

X.Z.; Contributed to the design of the research, acquisition of data, analysis and interpretation of data, statistical analysis and drafting the manuscript. Z.Z.; Contributed to the analysis and interpretation of data and statistical analysis. X.L.; Helped to draft this manuscript, analysis and interpretation of data and were responsible for overall supervision. All authors read and approved the final manuscript.

References

1. Ferlay J, Shin H, Bray F, Forman D, Mathers C, Parkin D, et al. GLOBOCAN 2008, Cancer Incidence and Mortality Worldwide: IARC Cancer Base No. 10. International Journal of Cancer Journal International Du Cancer. 2012; 136(5): E359–E86.
2. Ettinger DS, Wood DE, Akerley W, Bazhenova LA, Borghaei H, Camidge DR, et al. NCCN guidelines insights: non-small cell lung cancer, version 4. 2016. J Natl Compr Canc Netw. 2016; 14(3): 255-264.
3. Liu X, Conner H, Kobayashi T, Kim H, Wen F, Abe S, et al. Cigarette smoke extract induces DNA damage but not apoptosis in human bronchial epithelial cells. Am J Respir Cell Mol Biol. 2005; 33(2): 121-129.

4. Chen Z, Fillmore CM, Hammerman PS, Kim CF, Wong KK. Non-small-cell lung cancers: a heterogeneous set of diseases. *Nat Rev Cancer*. 2014; 14(8): 535-546.
5. Herbst RS, Morgensztern D, Boshoff C. The biology and management of non-small cell lung cancer. *Nature*. 2018; 553(7689): 446-454.
6. Dutt A, Ramos AH, Hammerman PS, Mermel C, Cho J, Sharifnia T, et al. Inhibitor-sensitive FGFR1 Amplification in human non-small cell lung cancer. *PLoS One*. 2011; 6(6): e20351.
7. Cihoric N, Savic S, Schneider S, Ackermann I, Bichselnaef M, Schmid RA, et al. Prognostic role of FGFR1 amplification in early-stage non-small cell lung cancer. *Br J Cancer*. 2014; 110(12): 2914-2922.
8. Lv T, Yuan D, Miao X, Lv Y, Zhan P, Shen X, et al. Over-expression of LSD1 promotes proliferation, migration and invasion in non-small cell lung cancer. *PLoS One*. 2012; 7(4): e35065.
9. Zhou Z, Hao Y, Liu N, Raptis L, Tsao MS, Yang X. TAZ is a novel oncogene in non-small cell lung cancer. *Oncogene*. 2011; 30(18): 2181-2186.
10. Zhang JG, Wang JJ, Zhao F, Liu Q, Jiang K, Yang GH. MicroRNA-21 (miR-21) represses tumor suppressor PTEN and promotes growth and invasion in non-small cell lung cancer (NSCLC). *Clin Chim Acta*. 2010; 411(11-12): 846-852.
11. Wang R, Wang ZX, Yang JS, Pan X, De W, Chen LB. MicroRNA-451 functions as a tumor suppressor in human non-small cell lung cancer by targeting ras-related protein 14 (RAB14). *Oncogene*. 2011; 30(23): 2644-2658.
12. Hong F, Breitling R. A comparison of meta-analysis methods for detecting differentially expressed genes in microarray experiments. *Bioinformatics*. 2008; 24(3): 374-382.
13. Tseng GC, Ghosh D, Feingold E. Comprehensive literature review and statistical considerations for microarray meta-analysis. *Nucleic Acids Res*. 2012; 40(9): 3785-3799.
14. Gautier L, Cope L, Bolstad BM, Irizarry RA. *affy*--analysis of Affymetrix GeneChip data at the probe level. *Bioinformatics*. 2004; 20(3): 307-315.
15. Wang X, Kang DD, Shen K, Song C, Lu S, Chang LC, et al. An R package suite for microarray meta-analysis in quality control, differentially expressed gene analysis and pathway enrichment detection. *Bioinformatics*. 2012; 28(19): 2534-2536.
16. Moldvay J, Fábíán K, Jäckel M, Németh Z, Bogos K, Furák J, et al. Claudin-1 protein expression is a good prognostic factor in non-small cell lung cancer, but only in squamous cell carcinoma cases. *Pathol Oncol Res*. 2017; 23(1): 151-156.
17. Liu W, Liu J, Rajapakse JC. Gene ontology enrichment improves performances of functional similarity of genes. *Sci Rep*. 2018; 8(1): 12100.
18. Kanehisa M, Goto S. KEGG: kyoto encyclopedia of genes and genomes. *N Nucleic Acids Res*. 2000; 28(1): 27-30.
19. Franceschini A, Szklarczyk D, Frankild S, Kuhn M, Simonovic M, Roth A, et al. STRING v9. 1: protein-protein interaction networks, with increased coverage and integration. *Nucleic Acids Res*. 2013; 41(Database issue): D808-D815.
20. Saito R, Smoot ME, Ono K, Ruscheinski J, Wang PL, Lotia S, et al. A travel guide to cytoscape plugins. *Nat Methods*. 2012; 9(11): 1069-1076.
21. Jiang Q, Wang Y, Hao Y, Juan L, Teng M, Zhang X, et al. miR2D-isease: a manually curated database for microRNA deregulation in human disease. *Nucleic Acids Res*. 2009; 37(Database issue): D98-D104.
22. Dweep H, Gretz N. miRWalk2.0: a comprehensive atlas of microRNA-target interactions. *Nat Methods*. 2015; 12(8): 697.
23. Lo FY, Chang JW, Chang IS, Chen YJ, Hsu HS, Huang SF, et al. The database of chromosome imbalance regions and genes re-sided in lung cancer from Asian and Caucasian identified by array-comparative genomic hybridization. *BMC Cancer*. 2012; 12: 235.
24. Wei TY, Juan CC, Hisa JY, Su LJ, Lee YC, Chou HY, et al. Protein arginine methyltransferase 5 is a potential oncoprotein that upregulates G1 cyclins/cyclin-dependent kinases and the phosphoinositide 3-kinase/AKT signaling cascade. *Cancer Sci*. 2012; 103(9): 1640-1650.
25. Kabbout M, Garcia MM, Fujimoto J, Liu DD, Woods D, Chow CW, et al. ETS2 mediated tumor suppressive function and MET oncogene inhibition in human non-small cell lung cancer. *Clin Cancer Res*. 2013; 19(13): 3383-3395.
26. Marwitz S, Depner S, Dvornikov D, Merkle R, Szczygiel M, Müller-Decker K, et al. Downregulation of the TGF- β pseudoreceptor BAMBI in non-small cell lung cancer enhances TGF- β signaling and invasion. *Cancer Res*. 2016; 76(13): 3785-3801.
27. Chen J, Xie F, Zhang L, Jiang WG. iASPP is over-expressed in human non-small cell lung cancer and regulates the proliferation of lung cancer cells through a p53 associated pathway. *BMC Cancer*. 2010; 10: 694.
28. Chakraborty S, Mazumdar M, Mukherjee S, Bhattacharjee P, Adhikary A, Manna A, et al. Restoration of p53/miR-34a regulatory axis decreases survival advantage and ensures Bax-dependent apoptosis of non-small cell lung carcinoma cells. *FEBS Lett*. 2014; 588(4): 549-559.
29. Ming J, Zhang Q, Qiu X, Wang E. Interleukin 7/interleukin 7 receptor induce c-Fos/c-Jun-dependent vascular endothelial growth factor-D up-regulation: A mechanism of lymphangiogenesis in lung cancer. *Eur J Cancer*. 2009; 45(5): 866-873.
30. Han S, Ritzenthaler JD, Sitaraman SV, Roman J. Fibronectin increases matrix metalloproteinase 9 expression through activation of c-Fos via extracellular-regulated kinase and phosphatidylinositol 3-kinase pathways in human lung carcinoma cells. *J Biol Chem*. 2006; 281(40): 29614-29624.
31. Zhang Z, Wang Q, Chen F, Liu J. Elevated expression of HMGA1 correlates with the malignant status and prognosis of non-small cell lung cancer. *Tumour Biol*. 2015; 36(2): 1213-1219.
32. Hillion J, Wood LJ, Mukherjee M, Bhattacharya R, Di Cello F, Kowalski J, et al. Upregulation of MMP-2 by HMGA1 promotes transformation in undifferentiated, large-cell lung cancer. *Mol Cancer Res*. 2009; 7(11): 1803-1812.
33. Wei S, Hao C, Li X, Zhao H, Chen J, Zhou Q. Effects of BTG2 on proliferation inhibition and anti-invasion in human lung cancer cells. *Tumour Biol*. 2012; 33(4): 1223-1230.
34. Sun Q, Hang M, Guo X, Shao W, Zeng G. Expression and significance of miRNA-21 and BTG2 in lung cancer. *Tumour Biol*. 2013; 34(6): 4017-4026.
35. Li Y, Fu J, Yuan X, Hu C. Simvastatin inhibits the proliferation of A549 lung cancer cells through oxidative stress and up-regulation of SOD2. *Pharmazie*. 2014; 69(8): 610-614.
36. Bandi N, Vassella E. miR-34a and miR-15a/16 are co-regulated in non-small cell lung cancer and control cell cycle progression in a synergistic and Rb-dependent manner. *Mol Cancer*. 2011; 10: 55.
37. Jusufović E, Rijavec M, Keser D, Korošec P, Sodja E, Iljazović E, et al. let-7b and miR-126 are down-regulated in tumor tissue and correlate with microvessel density and survival outcomes in non-small-cell lung cancer. *PLoS One*. 2012; 7(9): e45577.
38. Trang P, Medina PP, Wiggins JF, Ruffino L, Kelnar K, Omotola M, et al. Regression of murine lung tumors by the let-7 microRNA. *Oncogene*. 2010; 29(11): 1580.
39. Zhao Z, Zhang L, Yao Q, Tao Z. miR-15b regulates cisplatin resistance and metastasis by targeting PEBP4 in human lung adenocarcinoma cells. *Cancer Gene Ther*. 2015; 22(3): 108-114.
40. Jeong HC, Kim EK, Lee JH, Lee JM, Yoo HN, Kim JK. Aberrant expression of let-7a miRNA in the blood of non-small cell lung cancer patients. *Mol Med Rep*. 2011; 4(2): 383-387.

Down-Regulation of *miR-200c* and Up-Regulation of *miR-30c* Target both Stemness and Metastasis Genes in Breast Cancer

Mahsa Rahimi, M.Sc.^{1,2}, Ali Sharifi-Zarchi, Ph.D.², Nosratollah Zarghami, Ph.D.¹, Lobat Geranpayeh, MD.³, Marzieh Ebrahimi, Ph.D.^{2*}, Effat Alizadeh, Ph.D.^{4*}

1. Department of Medical Biotechnology, Faculty of Advanced Medical Sciences, Tabriz University of Medical Sciences, Tabriz, Iran
2. Department of Stem Cells and Developmental Biology, Cell Science Research Center, Royan Institute for Stem Cell Biology and Technology, ACECR, Tehran, Iran
3. Department of Surgery, Sina Hospital, Tehran University of Medical Sciences, Tehran, Iran
4. Drug Applied Research Center, Tabriz University of Medical Sciences, Tabriz, Iran

*Corresponding Addresses: P.O. Box 16635-148, Department of Stem Cells and Developmental Biology, Cell Science Research Center, Royan Institute for Stem Cell Biology and Technology, ACECR, Tehran, Iran
P.O.Box: 5166653431, Drug Applied Research Center, Tabriz University of Medical Sciences, Tabriz, Iran
Emails: mebrahimi@royaninstitute.org, alizadehe@tbzmed.ac.ir

Received: 27/October/2018, Accepted: 27/September/2018

Abstract

Objective: microRNAs (miRNAs) play important role in progression of tumorigenesis. They can target self-renewal and epithelial-mesenchymal transition (EMT) abilities in tumor cells, especially in cancer stem cells (CSCs). The objective of this study was to implement data mining to identify important miRNAs for targeting both self-renewal and EMT. We also aimed to evaluate these factors in mammospheres as model of breast cancer stem cells (BCSCs) and metastatic tumor tissues.

Materials and Methods: In this experimental study, mammospheres were derived from MCF-7 cells and characterized for the CSCs properties. Then expression pattern of the selected miRNAs in spheroids were evaluated, using the breast tumor cells obtained from seven patients. Correlation of miRNAs with self-renewal and EMT candidate genes were assessed in mammospheres and metastatic tumors.

Results: The results showed that mammospheres represented more colonogenic and spheroid formation potential than MCF-7 cells ($P < 0.05$). Additionally, they had enhanced migration and invasive capabilities. Our computational analyses determined that *miR-200c* and *miR-30c* could be candidates for targeting both stemness and EMT pathways. Expression level of *miR-200c* was reduced, while *miR-30c* expression level was enhanced in mammospheres, similar to the breast tumor tissues isolated from three patients with grade II/III who received neo-adjuvant treatment. Expression level of putative stem cell markers (*OCT4*, *SOX2*, *c-MYC*) and EMT-related genes (*SNAIL1*, *CDH2*, *TWIST1/2*) were also significantly increased in mammospheres and three indicated patients ($P < 0.05$).

Conclusion: Simultaneous down-regulation and up-regulation of respectively *miR-200c* and *miR-30c* might be signature of BCSC enrichment in patients post neo-adjuvant therapy. Therefore, targeting both *miR-200c* and *miR-30c* could be useful for developing new therapeutic approaches, against BCSCs.

Keywords: Metastasis, *miR-200c*, *miR-30c*, Self-Renewal, Spheroid

Cell Journal (Yakhteh), Vol 21, No 4, January-March (Winter) 2020, Pages: 467-478

Citation: Rahimi M, Sharifi-Zarchi A, Zarghami N, Geranpayeh L, Ebrahimi M, Alizadeh E. Down-regulation of *miR-200c* and Up-regulation of *miR-30c* target both stemness and metastasis genes in breast cancer. Cell J. 2020; 21(4): 467-478. doi: 10.22074/cellj.2020.6406.

Introduction

Breast cancer is the second-most prevalent cancer between females worldwide (1) and effective treatment of breast cancer is faced to a number of hurdles including resistance to therapies, metastasis and recurrence (2). There are several evidences regarding the heterogeneity of breast cancer cell population, initiated from a very slight subset of cells named cancer stem cells (CSCs) (3). CSCs with self-renewal capacity are responsible for initiation of tumorigenesis in immunodeficient models (4) as well as maintenance and clinical outcomes of treatments (5). Although CSCs play central role from clinical points of view, molecular mechanisms and pathways involved in their survival and maintenance has not fully been identified (6). Increasing our knowledge in the field of tumor biology could consequently lead to suggestion of effective diagnostic and prognostic methods,

as well as more impressive treatment for breast cancer. Moreover, recent progress has highlighted the important role of microRNAs (miRNAs) in regulating stemness and metastasis of CSCs. In this way, several miRNAs are known to be differentially expressed in CSCs or normal stem cells, part of which has been studied in targeting genes and networks involved in cancer stemness properties (7). On the other hand, the regulatory role of miRNAs has been defined in epithelial-mesenchymal transition (EMT), as an important process through tumor progression (8). Although it is known that miRNAs could contribute to tumorigenesis as tumor suppressors or oncogenes (9, 10), the role of miRNAs targeting both self-renewal and EMT pathways in breast CSCs (BCSCs) has largely been remained unknown.

Recently, with regards to the new technologies innovation, data mining and bioinformatics approaches have tremendously been developed in the field of

genomic analysis large-scale endeavors created useful databases. We hypothesized that identification of common miRNAs targeting stemness-EMT network will improve our understanding of CSCs in metastatic breast cancer. To date, several investigations have been performed to find deregulated miRNA expression during EMT and metastasis of breast cancer or BCSCs. In this study, our approach is systematic analysis of combined clinical and molecular data to find common miRNAs deregulated in mammospheres, as BCSCs model, and metastatic breast cancer. To reach that, we integrated candidate miRNA expression profiles with their target mRNA gene expression data obtained from the same samples. In summary, our findings resulted to understand the important role of *miR-200c* and *miR-30c* in maintenance of stemness as well as EMT process in BCSCs. Therefore, we suggested that down-regulation of *miR-200c* combined with increasing level of *miR-30c* may be a signature of BCSCs enrichment in patients post neo-adjuvant therapy. These miRNAs may have potential to extent into both diagnostic filed, as biomarker, and therapeutic approach for BCSCs in patients who are under chemotherapy.

Materials and Methods

In this experimental study, breast cancer tissues were collected between January 2017 and January 2018, upon the approval of Farmanieh Hospital and Sina Oncologic Hospital (both from Tehran, Iran) according to local authorities. All contributors signed a written informed consent form to participate in this study. All procedures performed in studies including human patient involvements were in accordance with the ethical standards that approved by Tabriz University of Medical Sciences (5/D/25333) and Royan Institute Ethical Committee (IR.ACECR.ROYAN.REC.1396.229), as well as the 1964 Helsinki declaration and its later amendments or comparable ethical standards. Patients histopathological information, including tumor size and depth of invasion, lymph-vascular and perineural invasion, grade and clinical tumor/node/metastasis, were recorded and pathologically staged using the tumor-nodes-metastasis (TNM) staging method (11). Informed consent was obtained from all participants included in the present study in Sina and Farmanieh hospitals, Tehran, Iran.

Seven female breast cancer patients who underwent surgery at Farmanieh Hospital and Sina Oncologic Hospital were included in this research. The inclusion criteria for selection of female patients were 25 years of age and older, from all ethnicity. Breast cancer malignancy was confirmed based on histopathological examination and immunohistochemical studies of estrogen receptor (ER) and progesterone receptor (PR) expressions, performed on surgical resection tissue samples of the tumors based on the standard methods. Three samples were undergoing

neo-adjuvant therapy before sampling. Normal adjacent biopsies, as negative controls, were collected from all seven patients. For sampling, surgeon removed the tumors and small part of them was cut for cultivation, which transferred to phosphate buffer saline (PBS) containing penicillin/streptomycin and the reminding part of tissues were fixed for pathological evaluation. Adjacent breast tissues or the areas around tumor sites were removed and transferred to transferring media (PBS containing penicillin/streptomycin) in the separate tube. Later on, these samples are called as normal tissues in the present study.

Literature mining and computational analysis

First we performed a systematic literature review on PubMed and COREMINE website using the following keywords: "breast cancer tissue, stem cell, self-renewal, stemness, miRNA, metastasis or EMT". The studies with incomplete data were excluded from this analysis, providing that: i. The papers are review articles or letters, ii. Studies with insufficient or inaccessible data, and iii. Studies that are not related to CSCs and homo-sapiens. We also excluded nine articles, due to limitation to access to their full texts. Moreover, miRNA expression profiles were searched with the same keywords on NCBI GEO database. In overall, we found the most frequent miRNAs targeting the stemness and metastasis genes. Then, we used miRNA target prediction tools including TargetScan (12) and miRWalk (13), to find target genes of each candidate miRNA. We only preserved the target genes with at least two-fold expression change and $P < 0.05$, between human breast cancer versus human normal breast (the first group) and mammosphere versus MCF-7 adherent culture (the second group). Custom R scripts were used to rank miRNAs for targeting at least three stemness and two metastasis genes. Subsequently, we computed differential expression fold-changes and P values (using two-sided Student's t test) between breast cancers vs. normal breast (as the first group) and also mammospheres vs. MCF-7 adherent culture (as the second group). Enricher (14) and GO functional enrichment analysis on KEGG 2017 pathways were used to identify pathways and biological functions that were affected by the target genes of each miRNAs.

Cell line and monolayer culture

MCF-7 is an estrogen-dependent human breast adenocarcinoma cell line that was purchased from Iranian Biological Resource Center (IBRC), Iran. The cells were cultured in Dulbecco's Modified Eagle Medium (DMEM, Gibco, USA) supplemented with 10% heat inactivated fetal bovine serum (FBS, Invitrogen, USA), 1% non-essential amino acid (NEAA), 2 mM L-glutamine and 1% penicillin/streptomycin (all from Life Technologies, USA) at 37°C and 5% CO₂ using standard cell culture incubator.

Formation of spheroid cultures from MCF-7

The standard tissue culture plates were covered with

poly 2- hydroxyethyl methacrylate (poly-HEMA) preventing cell attachment to plate surface. Subsequently, the monolayer MCF-7 cells were enzymatically detached into single cells suspension with trypsin (Gibco, USA) and harvested. 2×10^4 single cells were seeded at low attachment plate, in serum-free DMEM medium enriched with 20 ng/ml epidermal growth factor (EGF, Royan Institute, Iran), 20 ng/ml basic fibroblast growth factor (bFGF, Royan Institute, Iran), 2% B27 (Gibco, USA) and 2 mM L-Glutamine (Life Technologies, USA). The media was refreshed every 48 hours and mammospheres were formed after 14 days.

Mammosphere-forming efficiency assay

When the spheroids reached to about 50 μm diameters, they were accumulated by gentle centrifugation at 1000 rpm for 5 minutes, and then were enzymatically separated with trypsin. About 2×10^4 cells were plated into poly-HEMA coated six-well plates in 2000 μl of serum-free DMEM medium per well. Mammosphere-forming efficiency (MFE) was calculated by dividing the number of mammospheres, which are greater than 60 μm or larger in size in the cells seeding density per well using a microscope fitted with magnitude. All experiments on each generation of mammospheres were performed in triplicates.

Colony-forming test

To compare colony forming capacity of the adherent cells and mammospheres, 200 cells of each group were counted and re-plated in a complete medium containing DMEM supplemented with 10% FBS, 1% NEAA, 2 mM L-glutamine and 1% penicillin/streptomycin in six-well-plates. After 10 days, cell colonies were fixed with 4% paraformaldehyde, and stained with 0.05% crystal violet (Sigma, USA). Ultimately, the round shape colonies with more than 400 μm diameter were counted using an inverted microscope (Japan Microscope brand, Japan).

Transmembrane migration and invasion assay

Adherent cells and mammospheres were grown up to 80% confluence. Then adherent cells were starved in serum-free medium the day before assay. The next day, the cells were dissociated into single cells with trypsin, counted and added at 1×10^5 cells/well density onto the top chambers of trans-well inserts of 8 μm pore size filter (BD, USA) coated with 0.5 mg/ml Matrigel (BD, USA) in a six-well plate. DMEM containing 10% of FBS was added to the bottom of chambers and the cells were then cultured for 24 hours at 37°C in a 5% humidified CO₂ incubator. Finally, the cells on the top surface of filter were removed from filter surface by using a cotton-swab, and cells at the bottom of filter were then fixed with 4% paraformaldehyde (Merk, Germany), stained with 0.05% crystal violet (Sigma, USA) for 30 minutes. Very carefully, to avoid washing off the fixed cells, the membrane was dipped

into distilled water to remove the excess crystal violet. Trans-well membrane was next allowed to dry.

The cells were observed using an inverted microscope with either $\times 4$ or $\times 10$ objective lens and number of the cells were quantified in different fields of view to get an average sum of cells invaded through the membrane and attached to the underside of membrane. For migration assay, all steps were carried out similar to those in the invasion assay, except the matrigel coating. All experiments were performed in triplicates.

Determining percent of invasion=

$$\frac{\text{Mean number of cells invading through matrigel matrix-coated membrane}}{\text{Mean number of cells migrating through uncoated membrane}} \times 100$$

Quantitative real time polymerase chain reaction analysis of gene expression

Tumor and normal breast tissue fragments ($< 3 \times 3$ mm) were snap frozen in liquid nitrogen and homogenized with a ceramic pestle in TRIzol Reagent (Invitrogen, USA). Total RNAs with the aim of small RNA retentions were extracted from the adherent cells (as control groups) and mammospheres (as experimental groups) using TRIzol reagent, according to the manufacturer's instructions. The concentration and purity of extracted RNA were determined by UV absorbance at 260 and 280 nm (260/280 nm) in spectrophotometer. The integrity of RNA samples was checked by gel electrophoresis. 2 μg total RNA was subjected to generate complementary DNA using cDNA synthesis kit (TaKaRa, Japan), according to the manufacturer's instructions. Expression level of stemness and metastasis genes was evaluated by Applied Biosystems real-time PCR Instrument (ABI, Thermo Fisher, USA) in 10 μl reactions containing 2.5 μl SYBR Green PCR mix (TaKaRa, Japan) and 1 μl of each primer with 5 pmol/ μl concentration. Specific human primers -including stemness related genes (*OCT4*, *SOX2*, *NANOG*, *c-MYC* and *KLF4*) and metastasis related genes (*CDH1*, *CDH2*, *SNAIL1*, *TWIST1*, *TWIST2* and *ZEB1*) were used (Table S1) (See Supplementary Online Information at www.celljournal.org). PCR program was incubated at 95°C for 10 minutes, 40 cycles of denaturation at 95°C for 10 seconds, annealing at 60°C for 20 seconds and elongation at 72°C for 20 seconds. A final melting curve analysis from 65°C to 95°C was performed and the relative levels of expression were analyzed using $2^{-\Delta\Delta C_t}$ values. *β -Actin* was used as house-keeping gene.

miRNA expression profiling

miRNA expression levels were studied by performing SYBR Green qRT-PCR. In brief, 1 μg total RNA containing miRNAs was poly adenylated by poly (A) polymerase and reverse transcribed to cDNA using reverse transcriptase enzyme first strand cDNA synthesis reaction, provided from Parsgenome miR-Amp kit (Parsgenome,

Iran) according to the manufacturer's instructions. Each reaction was performed in a final volume of 10 μ l, containing diluted cDNA and PCR master mix, and all reactions were run in triplicates. qRT-PCR reaction was performed using Applied Biosystems Real-Time PCR Instruments according to the manufacturer's protocol. Expression levels of miRNA were normalized against internal controls U6, as a housekeeping control.

Statistical analysis

In vitro characterization of MCF-7 cell mammosphere and primary breast cancer tissue are presented as the mean \pm SD of at least three different experiments. Two-tailed Student's t test and analysis of variance (ANOVA) were performed to evaluate the difference between the mean values. The Spearman's rank correlation test was used to evaluate miRNA and mRNA correlation. A two-tailed analysis with $P < 0.05$ was considered statistically significant for all experiments.

For functional enrichment analysis, target genes of the selected miRNAs were submitted to Enrichr database. Subsequently, biological process, cellular component and molecular function were analyzed by Gene Ontology (GO) and pathways analysis was applied by KEGG 2017 ($P < 0.05$).

Results

Computational analysis to identify common miRNA in stemness and EMT network

A total of 328 articles were yielded after the literature reviews, finally limited to 142 papers due to our exclusion criteria (mentioned in the method section). Full-text reviews were resulted in proposing 56 candidate miRNAs that have key role in BCSCs: 24 up-regulated and 32 down-regulated molecules. Among them, we chose *miR-200c* and *miR-30c* targeting at least three stemness and two EMT genes (Fig.1).

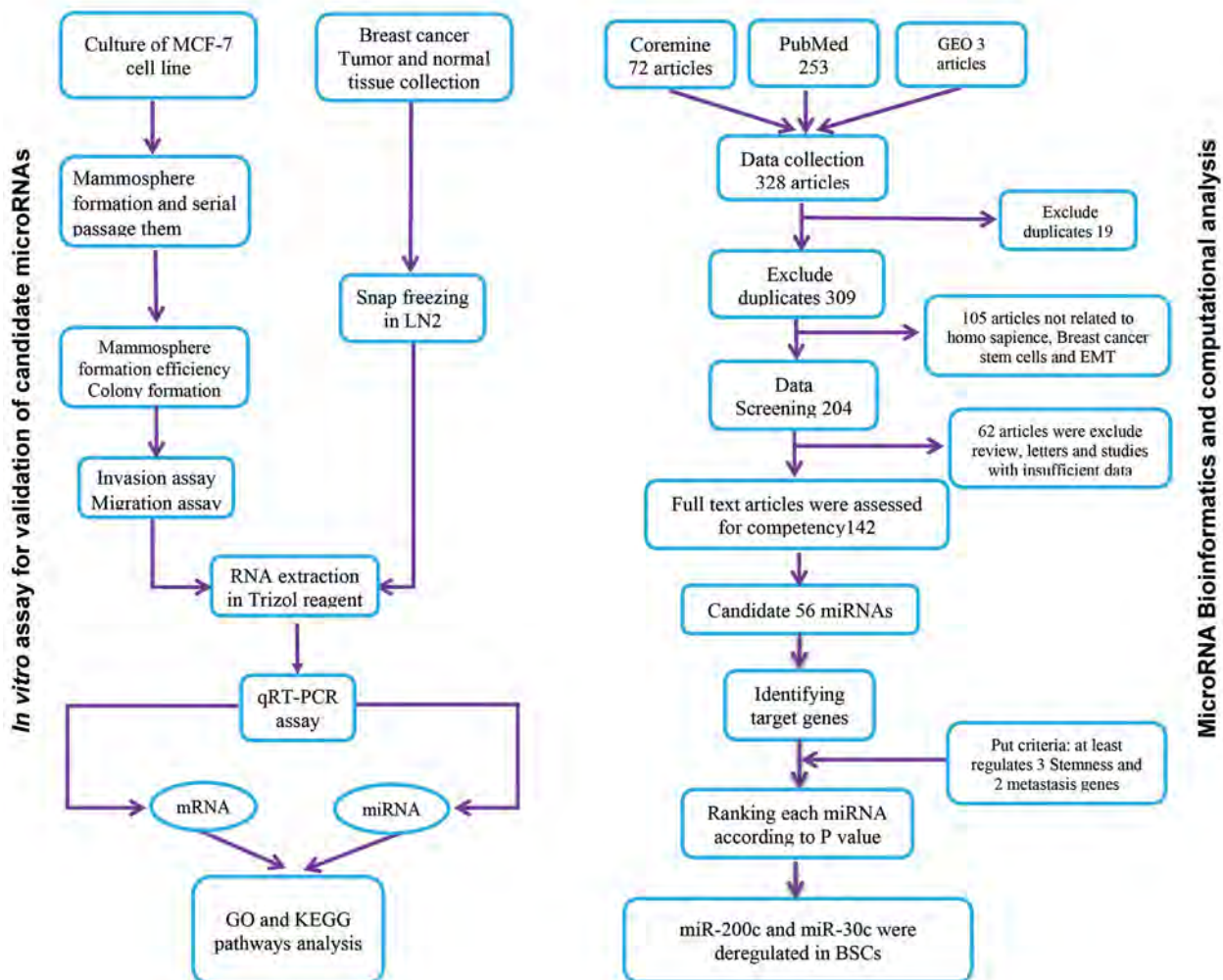


Fig.1: Flowchart of studies represent systematic analysis to find miRNAs targeting both self-renewal and EMT pathways. EMT; Epithelial-mesenchymal transition, qRT-PCR; Quantitative real time polymerase chain reaction, GO; Gene ontology, KEGG; Kyoto Encyclopedia of genes and genomes-genomenet, GEO; Gene expression omnibus, and BSCs; Breast cancer stem cells.

Mammospheres derived from MCF-7 as a model of breast cancer stem cells

MCF-7 cells were grown similar to adherent epithelial-like monolayer cells in culture (Fig.2A). Under serum-free and low-attachment conditions, MCF-7 cells grew into 3D non-linkage mammospheres within 24-48 hours, in comparison with their 2D adherent culture. Shape and appearance of spheres are solid and tightly packed in rounded margin, but we observed the mammospheres form looser and less rounded spheres over passages (Fig.2B-D). The secondary spheres were subsequently cultured up to three passages and MFE was calculated based on their size ($> 60 \mu\text{m}$, Fig.2E). The spheroid cells indicated about two folds increase ($P<0.05$) in MFE during three passages (Fig.2E). The results showed that MCF-7 cell-derived mammospheres had more colonogenic potential up to 5.5 fold. Indeed, the number as well as size of colonies was dominantly increased in mammospheres, in comparison with adherent cells ($P<0.05$, Fig.2F).

Mammospheres revealed increased ability of migration and invasion

The migratory capability of mammospheres was increased (about 1.7 fold). However, invasiveness potential of the isolated cells from mammospheres was significantly increased (about 3.35 fold), in comparison with adherent cells (Fig.2G, H).

Patients' demography

Seven female breast cancer patients (mean age of 48 ± 8.04 years) were included in the study after signing written informed consent. The clinicopathological data of all patients has been shown in Table 1. All tumors were classified as invasive ductal carcinoma (IDC). Immunohistochemical study of ER and PR expressions were performed on surgical resection tissue samples of the tumors based on the standard methods. Three samples

were positive for ER, PR and HER2 and four patients were undergoing neo-adjuvant therapy before sampling.

Expression of *miR-200c-3p* and *miR-30c-5p* in tumor/normal tissues and mammospheres/adherent cells

Findings showed that *miR-200c* was decreased in mammospheres, compared to parental MCF-7 cells ($P=0.0025$, Fig.3A, Right). Furthermore, this expression was down-regulated in breast cancers with metastatic conditions (patients I, II and V, Fig.3A, Left). In contrast, expression of *miR-30c* was overexpressed in mammospheres, compared to adherent cells ($P=0.0011$), and it was also up-regulated in three of patients with grade II/III who received neo-adjuvant therapy (Fig.3A).

Gene expression in tumor/normal tissues and mammospheres/adherent cells

In the next step, expression level of stemness related genes (*OCT4*, *SOX2*, *KLF4*, *c-MYC* and *NANOG*) and EMT transcription factors (*CDH1*, *CDH2*, *SNAIL1*, *TWIST1*, *TWIST2* and *ZEB1*) were evaluated in all tumor samples and mammospheres. Interestingly, expression level of *OCT4*, *SOX2* and *c-MYC* was significantly increased in mammospheres and three malignant breast tumors who were under neo-adjuvant therapy (patients I, II and V, Fig.3B, C). *KLF4* was down-regulated in both tumor samples and mammospheres. Meanwhile, expression of *NANOG* was not changed in mammospheres, but it was down-regulated in tumors (Fig.3B). Among EMT-related genes, *CDH2*, *SNAIL1*, *TWIST1/2* and *ZEB1* were also overexpressed in mammospheres. However, tumors differentially expressed EMT related genes. Expression of *CDH2*, *SNAIL1* and *ZEB1* were up-regulated in three malignant breast tumors (patients I, II and V), but the others were down-regulated (Fig.3D, E). This demonstrates that signature of self-renewal related gene expressions and some EMT genes in malignant breast tumor of patients who underwent neo-adjuvant therapy are similar to that of mammospheres, as BCSC model.

Table 1: Clinicopathological features of breast cancer patients

Patients	Age (Y)	Histological subtype	Ki-67	Grade	ER status	PR status	HER2 status	Metastasis	Neo-adjuvant
Case I	56	IDC	>10%	III	>80%	>80%	Negative	Yes	Yes
Case II	51	IDC	>30%	III	60%	20%	30%	Yes	Yes
Case III	45	IDC	NA	I	NA	NA	NA	No	Yes
Case IV	50	IDC	NA	NA	NA	NA	NA	No	NA
Case V	39	IDC	>50%	II	>80%	>80%	>30%	Yes	Yes
Case VI	58	IDC	NA	I	NA	NA	NA	No	No
Case VII	37	IDC	NA	I	NA	NA	NA	No	No

IDC; Invasive ductal carcinoma, ER; Estrogen receptor, PR; Progesterone receptor, and NA; Not available.

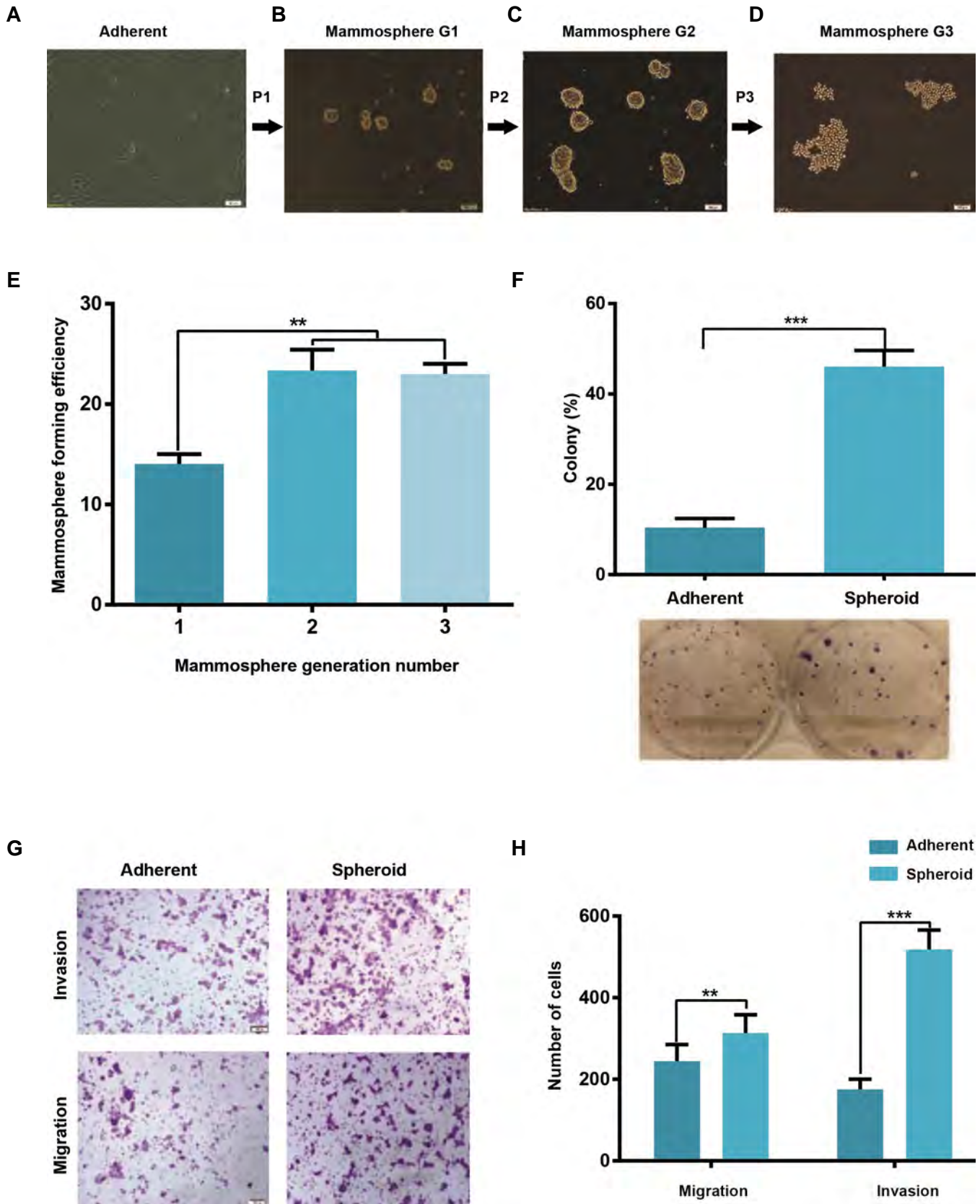


Fig.2: Colony and mammosphere formation abilities in MCF-7 and mammospheres. **A.** Parental cells cultured in 2D monolayer condition (magnification: $\times 4$, scale bar: 100 μm), **B-D.** Serial mammospheres derived from the first generation of mammospheres (up to passage 3) showing progressive loss of cell cohesion and formed loose spheroid (magnification: $\times 20$, scale bar: 100 μm), **E.** Mammosphere forming efficacy (MFE) was calculated from the first to third generation. Data are based on the mean percentages of the formed spheres quantity within a culture relative to the initial cell seeding number (mean \pm SD, $n=3$), **F.** The percentage of colonies increased in cells derived from mammospheres and MCF-7 monolayer. Left panel shows crystal violet stained cells, passing through the matrigel coated filter insert (as invasive cells) or uncoated filter insert (as migratory cells), and **H.** Quantification of migratory and invasive cells in adherent vs. mammosphere cells. Mammospheres revealed higher migration and invasion rate than their parental cells. Bars indicated mean \pm SD of three independent experiments. **, $P<0.01$ and ***, $P<0.001$.

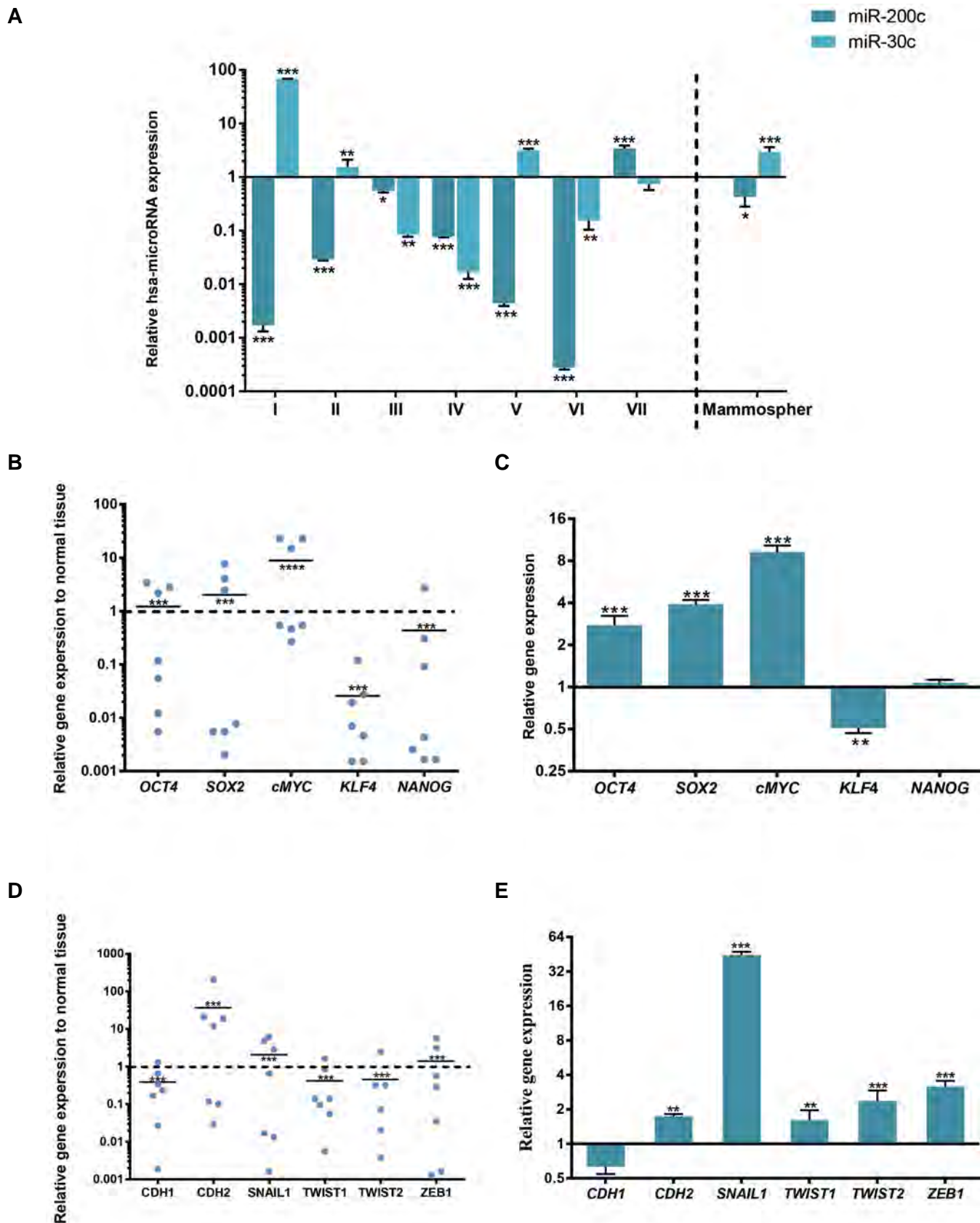


Fig.3: Expression level of miRNAs and genes. Expression levels of *miR-200c* and *miR-30c* as well as stemness and metastasis genes in human breast cancer versus normal breast (the first group), and mammospheres versus MCF-7 adherent cells (the second group) were determined by quantitative real time polymerase chain reaction (qRT-PCR). **A.** Expression of each miRNA was normalized to the levels of U6. Each cell line represents $n \geq 3$ and tumor represents $n \geq 1$. **B, C.** Scatter plot of stemness and metastasis gene expression levels in breast cancer and normal breast tissues (control). The line represents mean value, **D**, and **E.** Expression level of stemness and metastasis genes in mammospheres related to adherent cells (control), determined by qRT-PCR. β -Actin was used as the housekeeping gene. Statistically significant difference was determined by paired t test with GraphPad Prism 6 software. Bars indicated mean \pm SEM.

Correlation of *miR-200c* and *miR-30c* with stemness and EMT genes, and with overall survival of breast invasive carcinoma

In next step, correlation of *miR-200c* and *miR-30c* with stemness and metastasis gene expressions were assessed in both mammospheres and tumor tissues. As shown in Table 2, *miR-200c* was negatively correlated to *SOX2* and *KLF4* stemness genes, as well as *SNAIL* and *TWIST1* EMT genes. However, expression of *miR-30c* strongly displayed positive correlation with expression of most stemness related genes “*OCT4*, *SOX2*, *KLF4* and *NANOG*” and all EMT related genes. Moreover, *miR-200c* had negative correlation with *miR-30c* (R=-0.8, P=0.04). All aforementioned data indicates discriminatory potential of *miR-30c* and *miR-200c* to target both EMT and self-renewal pathways in BCSCs and malignant breast tumors.

Target genes and pathways analyses for *miR-200c-3p* and *miR-30c-5p*

In order to recognize the potential miRNA efficacy for breast cancer tracing, we predicted target genes of *miR-200c-3p* and *miR-30c-5p*. They were listed to GO annotation dataset for analysis of molecular function, biological processes and cellular component by Enricher. The result was sorted based on *p*-value. The lowest P value

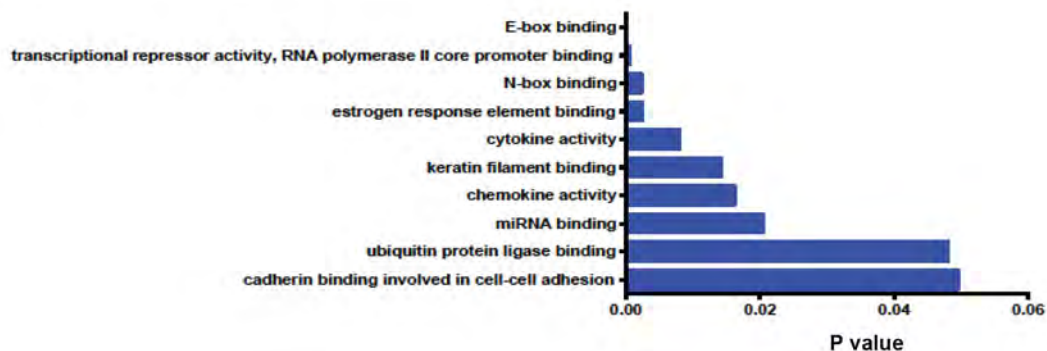
is related to more specific term. GO analysis showed that targeted genes of the differentially expressed miRNAs were enriched in the molecular functions of E-box binding, DNA binding, N-box binding, estrogen response element binding, cadherin binding involved in cell-cell adhesion and miRNA binding (Fig.4A). The biological process of these genes included cell-cell adhesion, stem cell proliferation process, cell cycle, angiogenesis and EMT process (Fig.4B). In terms of cellular component, most of the genes belong to the nucleolus and cytoplasmic organelles (Fig.4C). Finally, KEGG pathway analysis also showed similar results, in terms of the number of genes involved in the adhesion junction, pathways in cancer, MAPK signaling pathway, Wnt signaling pathway, PI3K-AKT signaling pathway, HIF-1 signaling pathway, TGF-beta signaling pathway, as well as the signaling pathways regulating pluripotency of stem cells, P53 signaling pathway and cell cycle (Fig.4D). Additionally, using PROGmiR (14), we were able to create a significant diagnostic plot between the expression level of individual *miR-200c* and *miR-30c*, and overall survival rate of the patients. Actually, simultaneous deregulation of *miR-200c* and *miR-30c* could significantly reduce the survival rate of breast invasive carcinoma cells via up-regulation of *OCT4*, *SOX2*, *c-MYC*, *SNAIL*, *ZEB1*, *CDH2* and down-regulation of *CDH1* (P=0.02, Fig.4E).

Table 2: Spearman’s rho for stemness and epithelial-mesenchymal transition (EMT) genes

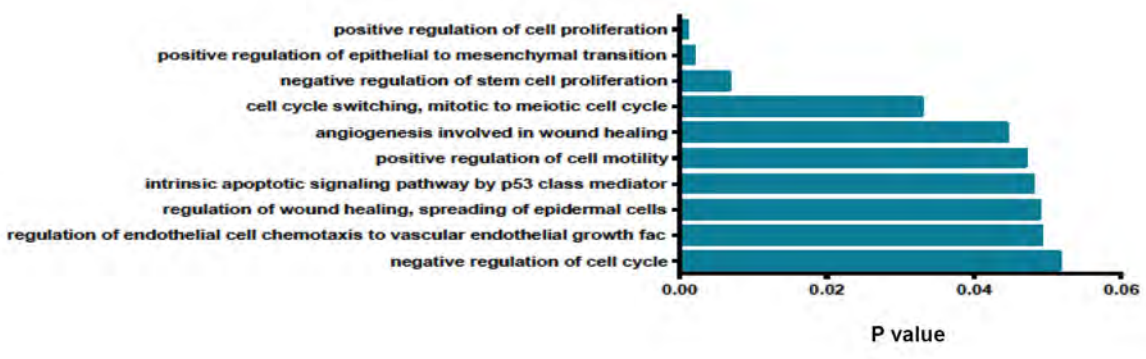
miR name	<i>OCT4</i>	<i>SOX2</i>	<i>c-MYC</i>	<i>KLF4</i>	<i>NANOG</i>	<i>CDH1</i>	<i>CDH2</i>	<i>SNAIL1</i>	<i>TWIST1</i>	<i>TWIST2</i>	<i>ZEB1</i>
<i>miR-200c</i>	R=-0.4	R=-0.94***	R=-0.5	R=-0.93***	R=-0.4	R=0.9**	R=-0.4	R=-0.6**	R=-0.8**	R=-0.4	R=0.5
	P=0.4	P=0.005	P=0.08	P=0.0006	P=0.39	P=0.01	P=0.39	P=0.01	P=0.01	P=0.32	P=0.28
<i>miR-30c</i>	R=0.85***	R=0.95***	R=-0.3	R=0.71**	R=0.9***	R=0.5*	R=0.74***	R=0.87***	R=0.92***	R=0.82***	R=0.83***
	P=0.000	P=0.003	P=0.29	P=0.004	P<0.001	P=0.04	P=0.002	P=0.001	P=2.9E-06	P=0.0002	P=0.0001

*, P<0.05, **, P<0.01, and ***, P<0.001.

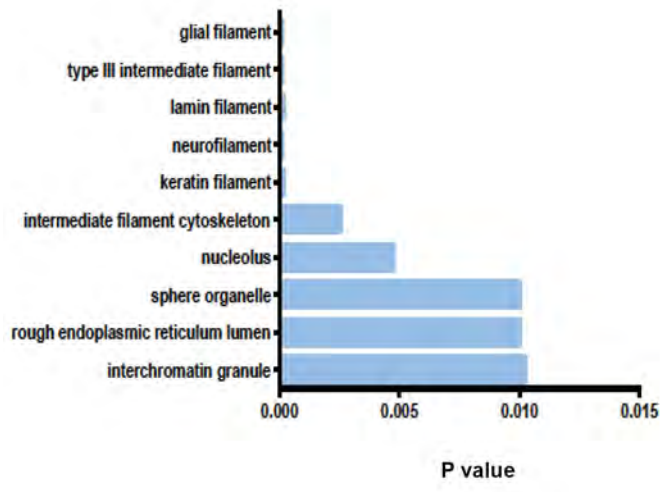
A



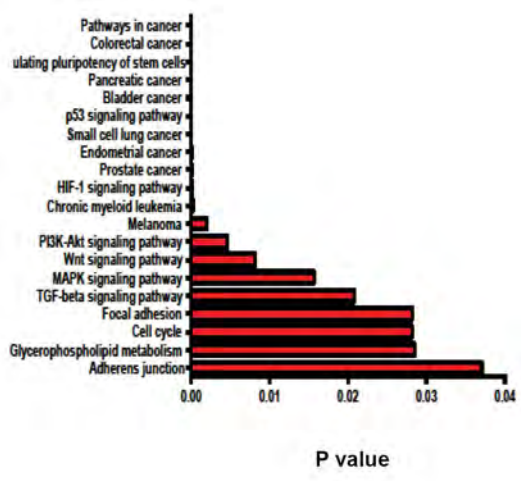
B



C



D



E

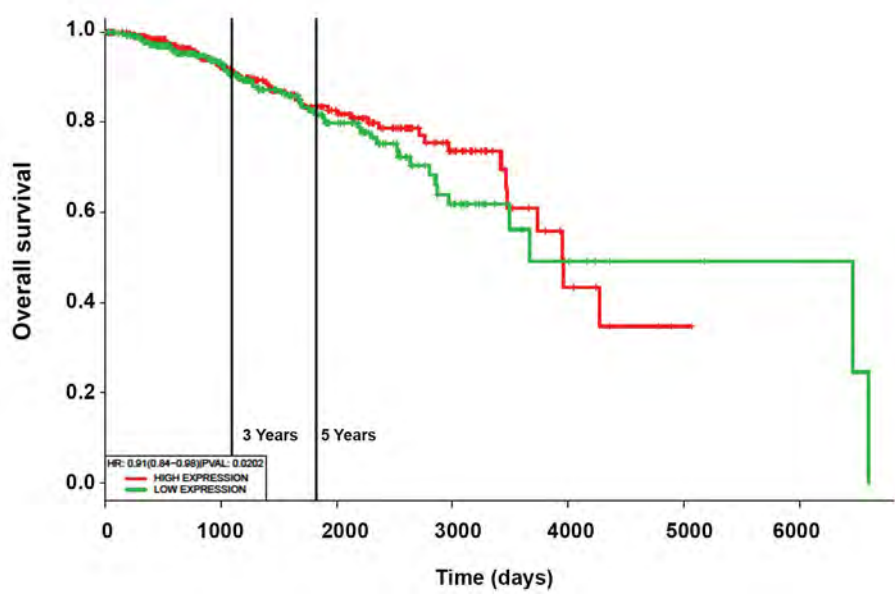


Fig.4: Gene ontology (GO), KEGG Pathway analysis using Enrichr and diagnostic plots creation with PROGmiR. **A.** Molecular function of stemness and epithelial-mesenchymal transition (EMT) regulated genes through the differentially expressed miRNAs, **B.** Biological process, **C.** Cellular component of these genes. Only the top ten enriched GO terms are represented, **D.** KEGG pathways with their P values. The most significant pathways bear the smallest P value listed from top to down, and **E.** Kaplan-Meier survival curve analysis was associated with overall survival in patients' breast invasive carcinoma cells. The patients were stratified into high-risk and low-risk groups according to median of each miRNA.

Discussion

This study evaluates expression of miRNAs targeting both stemness and metastasis pathways in BCSCs. To provide BCSC model, we used MCF-7 derived mammospheres representing higher ability to sphere and colony formations, compared to their parental cells, as well as more invasion and migration capabilities. Our data are in agreement with the previous studies (15, 16) that observed MCF-7 derived mammospheres contain highest CSCs population (17, 18) with CD44⁺/CD24⁻ phenotype (19, 20). Although, we did not evaluate tumorigenicity of the mammospheres *in vivo*, but adequate studies have determined tumorigenic ability of the cells originated from MCF-7-mammospheres in less than 1000 cell per injection (21).

To specify miRNAs involved in both stemness and metastasis regulation, systematic analysis was done using the important genes contributed to both pathways. The results implicated that *has-miR-200c-3p* and *has-miR-30c-5p* could potentially regulate these pathways. These miRNAs have been identified in different studies to control major transcription factors of EMT and induce metastasis (22, 23). It has also been reported that *miR-200c* controls BCSC functions (24, 25). Meanwhile, few studies implicated the role of *miR-30c* in BCSCs. Interestingly, the mammospheres of this study had similar expression pattern of *miR-200c* and *miR-30c* to three patients (I, II and V); these patients were at grade III/II and received neo-adjuvant therapy before sample collection. They showed significant down-regulation of *miR-200c* and up-regulation of *miR-30c*; however, *miR-200c* and *miR-30c* expression were both down-regulated in patients number six and four, among seven patients. Thus, by considering this similarity, we figured out the expression level of stemness related genes in mammospheres as well as all tissue samples. Impressively, expression of *OCT4*, *SOX2* and *c-MYC* was up-regulated in mammospheres and the same three previous patients (I, II and IV). *KLF4* expression, as another stemness related gene, was diminished in mammospheres and most of the tumor tissues, and *NANOG* was just significantly down-regulated in patient samples, but not in mammospheres. Moreover, transcription of *miR-30c* displayed positive correlation with *OCT4*, *SOX2*, *KLF4* and *NANOG* expressions. In addition, *miR-200c* had negative correlation with expression of *SOX2* and *KLF4*. Indeed, *miR-200c* significantly exhibited negative correlation with *miR-30c*. Similar to our data, *miR-200c* clusters (*miR-200c-141*, *miR-200b-200a-429* and *miR-183-96-182*) have been reported to be down-regulated in isolated BCSCs from eleven human breast cancers tissues, normal mammary stem cells (26, 27) and carcinoma cells (28). Furthermore, lower expression of *miR-200c* in patients could be considered as a prognostic factor of breast cancer metastasis, since its down-regulation associates with poor survival rate. Up-regulation of this miRNA correlates with inhibition of cell proliferation and regulates cancer stem cell functions (29-31). In addition, *miR-200c* plays

an important role in inhibiting proliferation of breast cancer cells by targeting the stemness related genes such as *NANOG*, *SOX2* and *KLF4* that are located in down-stream of *miR-200c*. It also inhibits tumor growth, differentiation and self-replication of CSCs by targeting *TUBB3* and as a result it would be involved in restoring sensitivity to microtubule-targeting drugs (32).

In this study, *miR-30c* represents stronger correlation with most of the stemness related genes. This miRNA has previously been reported as a breast cancer prognostic biomarker (33) and its expression is various among different breast cancer subtypes. Higher *miR-30c* expression level was reported in luminal-A tumors and low *miR-30c* expression level was observed in basal-like tumors (34). In fact, few evidences are available representing effect of *miR-30c* in regulation of stemness, with mainly focus on EMT regulation. In one study, Yu et al. (35) showed down-regulation of *miR-30* family, exclusively *miR-30e*, interferes with tumor beginning BCSCs (in mammospheres as well as primary BCSCs acquired from breast cancer patients) through up-regulation of ubiquitin-conjugating enzyme 9 (*Ubc9*) and integrin b3 (*ITGB3*). This up-regulation results in reduced self-renewal and anti-apoptotic features of BCSCs. Overexpression of *miR-30a* considerably decreased the sphere creation capability of MCF-7 cells, while deterrence of *miR-30a* intensely enhanced the number of mammospheres in the human breast cancer cell line, MCF-7 (36).

Consistent with other studies, the present study demonstrated correlation of *miR-200c* and *miR-30c* with expression of important EMT transcription factors (*SNAI1*, *TWIST* and *ZEB1*), in tumors and mammospheres. *miR-200c* not only is a malignancy biomarker, but also promote metastasis in poor metastatic cells *in vivo*, presence of which in serum of metastatic breast cancer patients can be indicated for brain metastases (37). *miR-200c* maintains cells in an epithelial state condition, via the regulation of mesenchymal genes such as *CDH2*, *SNAI1*, *SNAI2*, *TWIST1*, *TWIST2* and *ZEB1* (27). *miR-30c* contributes to miRNA-cytoskeleton regulation network and its target genes (*i.e.* *VIM*, *TWF1*, and *IL-11*) represent invasion, EMT and chemo-resistance molecular mechanisms (35). In treatment of breast cancer cells, *miR-200c* was also reported to induce apoptosis (38) and sensitize the cells to chemotherapy, radiotherapy and trastuzumab using therapy. Down-regulation of this molecule is known as marker for drug resistance in female genital tumors, such as ovarian, cervical and breast cancers (39).

We further employed bioinformatics tools to find out the target genes and pathways of *miR-200c* and *miR-30c* coordinating stemness and metastasis. Pathway analysis indicated that these genes considerably associate with "adherens junction pathway", "pathways involved in cancer", "MAPK signaling pathway", "Wnt signaling pathway", "PI3K-Akt signaling pathway", "regulating pluripotency of stem cells", "P53 signaling pathway", "TGFβ signaling pathway" and "HIF-1 signaling".

All of these pathways have been reported to be related to several cellular activities including proliferation, migration, invasion, cell cycle, regulation of ER signaling in cancer and CSCs. Adherens junction pathways are also of the major mechanisms presented in stem cells, where raising documents have illustrated that remodeling of the cytoskeletal proteins could characterize stem cell destiny (40). To the best of our knowledge, this is the first experiment comparing mammospheres as BCSCs model with signature pattern of metastatic patients (pre or post neo-adjuvant therapy). Because of similarity of *miR-200c* and *miR-30c* expression levels in mammospheres and some of our patients (I, II and V), we suggest that combination of these miRNAs might predict outcome of adjuvant therapy or metastasis in patients. Down-regulation of *miR-200c* and up-regulation of *miR-30c* suggest that metastatic breast tumors and mammospheres are similar and they contribute to communal molecular mechanisms regulating stem cell functions such as self-renewal, proliferation, EMT and resistance to drug.

Conclusion

The present study demonstrates that down-regulation of *miR-200c* and up-regulation of *miR-30c* promote BCSC features toward malignant breast tumors, leading to their resistance to neo-adjuvant therapy. These findings suggest a signature to predict metastasis post chemotherapy in breast cancer patients. However, further experiments are required in this regard.

Acknowledgements

This study was supported by the grant from Tabriz University of Medical Sciences (grant number: 95/2-1/6), Royan Institute, and the Iranian Council of Stem Cell Research and Technology (95000099.ICSCR). The authors have no conflict of interest in this study.

Authors' Contributions

M.E.; Participated in study design, interpretation of data, drafting and statistical analysis. E.A.; Contributed extensively in interpretation of the data, drafting and statistical analysis and the conclusion. M.R.; Contributed to all experimental work, data collection and evaluation and statistical analysis. A.Sh.-Z.; Conducted statistical and bioinformatics analysis. N.Z.; Participated in study design, drafting and approved the final version of this manuscript for submission. L.G.; Performed sample collection and prepared breast cancer tumor for molecular analysis to this component of the manuscript. All authors read and approved the final manuscript.

References

1. Torre LA, Bray F, Siegel RL, Ferlay J, Lortet-Tieulent J, Jemal A. Global cancer statistics, 2012. *CA Cancer J Clin*. 2015; 65(2): 87-108.
2. Owens TW, Naylor MJ. Breast cancer stem cells. *Front Physiol*. 2013; 4: 225.
3. Velasco-Velázquez MA, Popov VM, Lisanti MP, Pestell RG. The role of breast cancer stem cells in metastasis and therapeutic im-
4. Al-Hajj M, Wicha MS, Benito-Hernandez A, Morrison SJ, Clarke MF. Prospective identification of tumorigenic breast cancer cells. *Proc Natl Acad Sci USA*. 2003; 100(7): 3983-3988.
5. Bozorgi A, Khazaei M, Khazaei MR. New findings on breast cancer stem cells: a review. *J Breast Cancer*. 2015; 18(4): 303-312.
6. Dragu DL, Necula LG, Bleotu C, Diaconu CC, Chivu-Economescu M. Therapies targeting cancer stem cells: current trends and future challenges. *World J Stem Cells*. 2015;7(9): 1185-1201.
7. Garofalo M, Croce CM. Role of microRNAs in maintaining cancer stem cells. *Adv Drug Deliv Rev*. 2015; 81: 53-61.
8. Hayes J, Peruzzi PP, Lawler S. MicroRNAs in cancer: biomarkers, functions and therapy. *Trends Mol Med*. 2014; 20(8): 460-469.
9. Croce CM. Causes and consequences of microRNA dysregulation in cancer. *Nat Rev Genet*. 2009; 10(10): 704-714.
10. Humphries B, Yang C. The microRNA-200 family: small molecules with novel roles in cancer development, progression and therapy. *Oncotarget*. 2015; 6(9): 6472-6498.
11. Wittekind C, Compton CC, Greene FL, Sobin LH. TNM residual tumor classification revisited. *Cancer*. 2002; 94(9): 2511-2516.
12. Lewis BP, Burge CB, Bartel DP. Conserved seed pairing, often flanked by adenosines, indicates that thousands of human genes are microRNA targets. *Cell*. 2005; 120(1): 15-20.
13. Dweep H, Gretz N. miRWalk2.0: a comprehensive atlas of microRNA-target interactions. *Nat Methods*. 2015; 12(8): 697.
14. Kuleshov MV, Jones MR, Rouillard AD, Fernandez NF, Duan Q, Wang Z, et al. Enrichr: a comprehensive gene set enrichment analysis web server 2016 update. *Nucleic Acids Res*. 2016; 44(W1): W90-W97.
15. Gaziel-Sovran A, Segura MF, Di Micco R, Collins MK, Hanniford D, Vega-Saenz de Miera E, et al. miR-30b/30d regulation of GalNAc transferases enhances invasion and immunosuppression during metastasis. *Cancer Cell*. 2011; 20(1): 104-118.
16. Elson-Schwab I, Lorentzen A, Marshall CJ. MicroRNA-200 family members differentially regulate morphological plasticity and mode of melanoma cell invasion. *PLoS One*. 2010; 5(10): pii: e13176.
17. Akrap N, Andersson D, Bom E, Gregersson P, Ståhlberg A, Landberg G. Identification of distinct breast cancer stem cell populations based on single-cell analyses of functionally enriched stem and progenitor pools. *Stem Cell Reports*. 2016; 6(1): 121-136.
18. Wang R, Lv Q, Meng W, Tan Q, Zhang S, Mo X, et al. Comparison of mammosphere formation from breast cancer cell lines and primary breast tumors. *J Thorac Dis*. 2014; 6(6): 829-837.
19. Rosen JM, Jordan CT. The increasing complexity of the cancer stem cell paradigm. *Science*. 2009; 324(5935): 1670-1673.
20. Cioce M, Gherardi S, Viglietto G, Strano S, Blandino G, Muti P, et al. Mammosphere-forming cells from breast cancer cell lines as a tool for the identification of CSC-like and early progenitor-targeting drugs. *Cell Cycle*. 2010; 9(14): 2878-2887.
21. Ivascu A, Kubbies M. Diversity of cell-mediated adhesions in breast cancer spheroids. *Int J Oncol*. 2007; 31(6): 1403-1413.
22. Li X, Roslan S, Johnstone CN, Wright JA, Bracken CP, Anderson M, et al. MiR-200 can repress breast cancer metastasis through ZEB1-independent but moesin-dependent pathways. *Oncogene*. 2014; 33(31): 4077-4088.
23. Dobson JR, Taipaleenmäki H, Hu YJ, Hong D, van Wijnen AJ, Stein JL, et al. hsa-mir-30c promotes the invasive phenotype of metastatic breast cancer cells by targeting NOV/CCN3. *Cancer Cell Int*. 2014; 14: 73.
24. Wang G, Guo X, Hong W, Liu Q, Wei T, Lu C, et al. Critical regulation of miR-200/ZEB2 pathway in Oct4/Sox2-induced mesenchymal-to-epithelial transition and induced pluripotent stem cell generation. *Proc Natl Acad Sci USA*. 2013; 110(8): 2858-2863.
25. Lim YY, Wright JA, Attema JL, Gregory PA, Bert AG, Smith E, et al. Epigenetic modulation of the miR-200 family is associated with transition to a breast cancer stem-cell-like state. *J Cell Sci*. 2013; 126(Pt 10): 2256-2266.
26. Shimono Y, Zabala M, Cho RW, Lobo N, Dalerba P, Qian D, et al. Downregulation of miRNA-200c links breast cancer stem cells with normal stem cells. *Cell*. 2009; 138(3): 592-603.
27. Zaravinos A. The regulatory role of microRNAs in EMT and cancer. *J Oncol*. 2015; 2015: 865816.
28. Wu D, Ji N, Zhang L, Zhang L. Differential expression of miR-200c in breast cancer stem cells. *Int J Clin Exp Pathol*. 2017; 10(9): 10085-10091.
29. Song C, Liu LZ, Pei XQ, Liu X, Yang L, Ye F, et al. miR-200c inhibits breast cancer proliferation by targeting KRAS. *Oncotarget*. 2015; 6(33): 34968-34978.
30. Feng ZM, Qiu J, Chen XW, Liao RX, Liao XY, Zhang LP, et al. Es-

- sential role of miR-200c in regulating self-renewal of breast cancer stem cells and their counterparts of mammary epithelium. *BMC Cancer*. 2015; 15: 645.
31. Knezevic J, Pfefferle AD, Petrovic I, Greene SB, Perou CM, Rosen JM. Expression of miR-200c in claudin-low breast cancer alters stem cell functionality, enhances chemosensitivity and reduces metastatic potential. *Oncogene*. 2015; 34(49): 5997-6006.
 32. Cochrane DR, Spoelstra NS, Howe EN, Nordeen SK, Richer JK. MicroRNA-200c mitigates invasiveness and restores sensitivity to microtubule-targeting chemotherapeutic agents. *Mol Cancer Ther*. 2009; 8(5): 1055-1066.
 33. Bockhorn J, Dalton R, Nwachukwu C, Huang S, Prat A, Yee K, et al. MicroRNA-30c inhibits human breast tumour chemotherapy resistance by regulating TWF1 and IL-11. *Nat Commun*. 2013; 4: 1393.
 34. Bockhorn J, Yee K, Chang YF, Prat A, Huo D, Nwachukwu C, et al. MicroRNA-30c targets cytoskeleton genes involved in breast cancer cell invasion. *Breast Cancer Res Treat*. 2013; 137(2): 373-382.
 35. Yu F, Deng H, Yao H, Liu Q, Su F, Song E. Mir-30 reduction maintains self-renewal and inhibits apoptosis in breast tumor-initiating cells. *Oncogene*. 2010; 29(29): 4194-204.
 36. Yu RMC, Cheah YK. The roles of miRNAs in human breast cancer and canine mammary tumor. *Applied Cancer Research*. 2017; 37(1): 37.
 37. Le MT, Hamar P, Guo C, Basar E, Perdigão-Henriques R, Balaj L, et al. miR-200-containing extracellular vesicles promote breast cancer cell metastasis. *J Clin Invest*. 2014; 124(12): 5109-5128.
 38. Howe EN, Cochrane DR, Cittelly DM, Richer JK. miR-200c targets a NF- κ B up-regulated TrkB/NTF3 autocrine signaling loop to enhance anoikis sensitivity in triple negative breast cancer. *PLoS One*. 2012; 7(11): e49987.
 39. Cochrane DR, Cittelly DM, Howe EN, Spoelstra NS, McKinsey EL, LaPara K, et al. MicroRNAs link estrogen receptor alpha status and Dicer levels in breast cancer. *Horm Cancer*. 2010; 1(6): 306-319.
 40. Boraas LC, Guidry JB, Pineda ET, Ahsan T. Cytoskeletal expression and remodeling in pluripotent stem cells. *PLoS One*. 2016; 11(1): e0145084.
-

Chitosan Hydrogel Supports Integrity of Ovarian Follicles during *In Vitro* Culture: A Preliminary of A Novel Biomaterial for Three Dimensional Culture of Ovarian Follicles

Fatemeh Hassani, M.Sc.¹, Bita Ebrahimi, Ph.D.², Ashraf Moini, Ph.D.^{3,4}, Ali Ghiaseddin, Ph.D.⁵, Mahshid Bazrafkan, Ph.D.¹, Gholamreza Hassanzadeh, Ph.D.^{1*}, Mojtaba Rezazadeh Valojerdi, Ph.D.^{2,6*}

1. Department of Anatomy, School of Medicine, Tehran University of Medical Sciences, Tehran, Iran

2. Department of Embryology, Reproductive Biomedicine Research Center, Royan Institute for Reproductive Biomedicine, ACECR, Tehran, Iran

3. Department of Gynecology and Obstetrics, Roointan-Arash Maternity Hospital, Tehran University of Medical Sciences, Tehran, Iran

4. Department of Endocrinology and Female Infertility, Reproductive Biomedicine Research Center, Royan Institute for Reproductive Biomedicine, ACECR, Tehran, Iran

5. Biomedical Engineering Group, Faculty of Chemical Engineering, Tarbiat Modares University, Tehran, Iran

6. Department of Anatomy, Faculty of Medical Science, Tarbiat Modares University, Tehran, Iran

*Corresponding Addresses: P.O.Box: 14115-111, Department of Anatomy, School of Medicine, Tehran University of Medical Sciences, Tehran, Iran

P.O.Box: 16635-148, Department of Embryology, Reproductive Biomedicine Research Center, Royan Institute for Reproductive Biomedicine, ACECR, Tehran, Iran

P.O. Box: 14115-111, Department of Anatomy, Faculty of Medical Science, Tarbiat Modares University, Tehran, Iran

Emails: hassanzadeh@tums.ac.ir, mr_valojerdi@royaninstitute.org, mr_valojerdi@modares.ac.ir

Received: 20/September/2018, Accepted: 18/November/2018

Abstract

Objective: Testing novel biomaterials for the three dimensional (3D) culture of ovarian follicles may ultimately lead to a culture model which can support the integrity of follicles during *in vitro* culture (IVC). The present study reports the first application of a chitosan (CS) hydrogel in culturing mouse preantral follicles.

Materials and Methods: In this interventional experiment study, CS hydrogels with the concentrations of 0.5, 1, and 1.5% were first tested for fourier transform infrared spectroscopy (FT-IR), Compressive Strength, viscosity, degradation, swelling ratio, 3-(4,5-dimethylthiazol-2-yl)-2,5-diphenyltetrazolium bromide (MTT) cytotoxicity and live/dead assay. Thereafter, mouse ovarian follicles were encapsulated in optimum concentration of CS (1%) and compared with those in alginate hydrogel. The follicular morphology, quality of matured oocyte and steroid secretion in both CS and alginate were assessed by enzyme-linked immunosorbent assay (ELISA). The expression of folliculogenesis, endocrine, and apoptotic related genes was also evaluated by quantitative real-time polymerase chain reaction (qRT-PCR) and compared with day that in 0.

Results: The rates of survival, and diameter of the follicles, secretion of estradiol, normal appearance of meiotic spindle and chromosome alignment were all higher in CS group compared with those in alginate group ($P \leq 0.05$). The expression of *Cyp19a1* and *Lhcgr* in CS group was significantly higher than that of the alginate group ($P \leq 0.05$).

Conclusion: The results showed that CS is a permissive hydrogel and has a beneficial effect on encapsulation of ovarian follicle and its further development during 3D culture.

Keywords: Alginate, Chitosan, Hydrogel, Ovarian Follicle

Cell Journal (Yakhteh), Vol 21, No 4, January-March (Winter) 2020, Pages: 479-493

Citation: Hassani F, Ebrahimi B, Moini A, Ghiaseddin A, Bazrafkan M, Hassanzadeh GH, Valojerdi MR. Chitosan hydrogel supports integrity of ovarian follicles during *in vitro* culture: a preliminary of a novel biomaterial for three dimensional culture of ovarian follicles. Cell J. 2020; 21(4): 479-493. doi: 10.22074/cellj.2020.6393.

Introduction

More patients have survived thanks to the developments in cancer treatment; however, chemotherapy and/or radiation, for instance, can produce acute or chronic ovarian insufficiency. Nonetheless, fertility in at risk for premature ovarian failure (POF) and young women can be preserved in a number of ways (1). Recording over 70 live births, ovarian tissue transplantation has shown to be a successful procedure for fertility restoration among adults (2). Notwithstanding, for cases which incur a risk of reimplantation of malignant cells, cryopreserved ovarian tissue transplantation is not a safe method. Individual follicle culture (IVC) can be a good alternative for transplantation, which can be cultured through two-dimensional (2D) or three-dimensional (3D) systems. Eppig and Schroeder's pioneering work led to the first live

mouse offspring from *in vitro* matured (IVM) follicles grown on collagen gels (3).

In the conventional 2D culture systems, ovarian stromal cells move from around the oocyte and spread on the culture vessel surface and thereby interfering with stromal cell-oocyte interaction (4). The chief impediment to the procedures of IVM in this system has been the ineffectiveness of oocyte development. Hardly 2D culture system can preserve the follicle 3D architecture and the complex interaction between the components of the somatic cell and the oocyte that is required for nuclear and cytoplasmic maturation. Also, a critical element for the transport of particular amino acids to the oocyte and sharing of paracrine factors is the gap junctions between the oocyte and its surrounding granulosa cells. Likewise,

oocyte-derived secretions contributes to the regulation of metabolic processes and proliferation of granulosa cells (3). A great many recent studies have attempted to design 3D culture systems through application of hydrogel biomaterials which can grant biomechanical and biochemical support to ovarian follicle cultures (5). Some researchers have used various hydrogel materials, such as agarose (6), alginate (7) collagen (8) and hyaluronic acid (9) for 3D encapsulation of isolated follicles in different animal models. Alginate has proved the most appropriate biomaterial in various animal species for its positive results with follicles (10). Although there are some data affirming follicle culture in alginate and morphologically normal oocyte production, a new study has argued that the meiotic spindle assembly might suffer from disturbance due to the lower developmental competence of oocytes obtained from the alginate system (11). This fascinating finding give grounds for the time spent on the quest for a fundamentally different biomaterial for the 3D culture. Chitin, as a biomaterial commonly found in insect and crustacean exoskeletons and fungi cell walls, is the second most abundant natural polymer which can be used as a scaffold for culturing follicles. Chitin application is generally carried out using its deacetylated form, chitosan (CS), which is composed of glucosamine and N-acetyl glucosamine linked in a β manner (12-14). Crucial elements for describing the characteristics of CS are degree of deacetylation and molecular weight, which vary depending on source and process of production (13). CS has been widely used in biomedical applications within the two past decades for its suitability for cell in growth, biodegradability, osteoconduction, porous structure, intrinsic antibacterial nature, and biocompatibility (15). On that account, CS has been used extensively, for instance, in cartilage tissue engineering (16), wound healing (17), drug delivery system (18) and orthopedic applications (15). The present study reports the first application of a CS hydrogel in culturing mouse preantral follicles.

Materials and Methods

In this interventional experiment study, the Ethical guidelines set by Royan Institute was considered during all stages of the experiment (IR.ACECR.ROYAN.REC.1395.197).

Preparation of chitosan hydrogels

Three CS solutions (medium molecular weight, 75-85% deacetylated, Sigma Aldrich, USA); 0.5, 1 and 1.5% (w/v) were prepared through dissolution of CS powder in acetic acid 1% (w/v) in phosphate-buffered saline (PBS, Gibco, USA) at room temperature and magnetic stirring for 5 hours at 150 rpm. The pH of solutions was adjusted to be around 6.8-6.9 by adding NaOH (10 N, Merck, Germany) to the stirring solution. To change the phase from solution to gel (pH=7.2-7.4), NaOH solution (0.075 N) was added at pH=6.8 after dripping of CS solutions in microtiter wells.

Scanning electron microscopy

To investigate the pore structure of the CS gels, the samples were immersed (0.5, 1, and 1.5%) in 4% glutaraldehyde in PBS at 37°C, removed after 1-day, washed with PBS and frozen at -80°C followed by lyophilization (Zibrus technology GmbH, Germany) for 72 hours. Having gold nanoparticle sputtered on the samples' surfaces and scanned at an accelerating voltage of 20 kV using scanning electron microscopy (SEM, Seron, Korea), pore diameter of the dried hydrogels was obtained via image analysis using Image J software (version 1.44 p national institute of health).

Fourier transform infrared spectroscopy

The chemical bonds linking the CS and other chemicals were analyzed using Fourier transform infrared (FT-IR) spectroscopy analysis, an account of which was given in the hydrogel preparation process. In brief, the samples were dried in a vacuum oven for 72 hours (BINDER GmbH, Germany), grinded and mixed with potassium bromide for 1:100, then prepared a compressed disk with the thickness of 1mm. The FT-IR spectra in a wavelength range of 4000-400 cm^{-1} were acquired applying an FT-IR spectrometer (Thermo Nicolet, USA).

Compressive strength of hydrogel

In order to determine the elastic modulus, a compression test was applied to the cylindrically-shaped samples. The hydrogel samples were prepared based on the aforementioned method and were then tested between two compression plates under a rate of 5 mm per minute at room temperature (n=3) in a compressibility study instrument (Santam, Iran). The stress-strain curve was drawn and Young's modulus calculated to demonstrate the mechanical strength of the samples.

Hydrogel degradation

The hydrogel degradation rates were measured by preparing 500 μl precursor CS solutions in 2 mL Eppendorf tubes. After the gelation process was complete, 1 ml of the DMEM medium was loaded in each tube. The tubes were incubated in a shaker incubator at 100 rpm and were subsequently sampled at 0, 0.25, 0.5, 1, 2, 4, 8, 16, 32, 64, 128, 256 hours (n=3 per time point). The medium was changed every 48 hours (1 ml was removed and then replaced with a fresh medium). One ml of the medium was taken from the tubes and the gels were then frozen at -80°C. The samples were lyophilized along with each other for 72 hours and were weighed, and the weight loss rate was recorded.

Swelling studies

Through immersing lyophilized CS samples in PBS at 37°C, swelling rate of hydrogels was determined. The sample weights were recorded at particular intervals (n=3 per time point) until no weight change was observed. Afterwards, towel papers were used to blot the swollen

samples and were immediately weighted. The swelling ratios (Q) were determined as a percentage of the swollen gel weight increment, with the dry polymer weight serving as the reference.

Viscosity of hydrogel precursor solutions

CS samples in solution phase were transported and measured volumetrically. Workability of sol phase of samples was studied by measuring the viscosity of CS precursor solutions (0.5, 1, and 1.5%) at 30°C (n=3) using viscometer (Brookfield, DV-III Ultra, USA).

MTT cytotoxicity assay

The hydrogel samples from 100 µl of three different precursor solutions were prepared in each well of 96 well plates and an approximate number of 100000 human bone marrow mesenchymal stem cells (hBMMSCs), provided by Royan Institute, were seeded on the surface of each hydrogel sample. The samples were incubated in Dulbecco's Modified Eagle's medium (DMEM, Gibco, USA) and supplemented with 10% fetal bovine serum (FBS) under standard cell culture conditions in 96 micro-well. Then hydrogel cytotoxicity and proliferation were investigated by MTT-assay (Gibco, USA) after 0, 1, 3, 5, 10 days of incubation (n=3 per time point). The culture medium was changed every other day.

Live/dead assay

The proliferation potential and cell viability were studied via live/dead assay by applying acridine orange (AO) staining (Sigma-Aldrich, Germany). Images were captured with inverted fluorescent microscope (Nikon, Japan). It is noteworthy that double stranded DNA with AO emits green light, whereas single stranded DNA reveals dead cells and RNA becomes orange to red with AO.

Alginate hydrogel preparation

Sodium alginate (Sigma, USA) was dissolved in deionized water to a concentration of 1% (w/v). Then, to remove organic impurities and to improve the purity of alginate, it was purified with activated charcoal (0.5 g charcoal/g alginate). After treatment with charcoal, the sterile alginate solution was filtered through 0.22 µm filters, then diluted with 1×PBS at the rate of 0.7% (4, 19).

Animals and ovarian follicle isolation

Twelve-day-old female Naval Medical Research Institute (NMRI) mice were obtained from Royan Institute animal house. They were kept in a controlled temperature (-20- to -25°C) and light-controlled environment (12 hour light: 12 hour dark). Mice were sacrificed by cervical dislocation; ovaries were isolated and early prenatal follicles were mechanically dissected from the ovaries utilizing 28 gauge needles. Isolated follicles were immersed in α -minimal essential medium (α -MEM, Gibco, USA) supplemented with FBS (5 mg/ml) at 37°C in 5% CO₂ in air. Only follicles with 100-130

µm diameter, intact and visible immature centrally located oocyte round were selected for further experiment. Prior to encapsulation, individual follicles were maintained in α -MEM, 5% FBS at 37°C, 5% CO₂ for 45 minutes.

Follicle encapsulation and culture in chitosan and alginate hydrogel

First, 5 µL beads of alginate were placed on a petri dish (Falcon, USA) and individual preantral follicles were inserted into the beads. After that calcium bath [140 mM NaCl (Sigma, USA) and 50 mM CaCl₂·2H₂O (Sigma, USA)] was added to 5 µL beads of alginate solution containing preantral follicle for 3 minutes. For CS groups (0.5, 1, and 1.5%), NaOH solution (0.075 N) was added at pH=6.8. to change solution state to gel (pH=7.2-7.4). First, 5 µL beads of CS were placed on a petri dish (Falcon, USA), having already been neutralized with 0.5 µL of NaOH solution (0.075 N) and washed three times by PBS⁻ and α -MEM. Then 3 µL of solution CS were placed on a petri dish; one follicle plunged into the bead; follicle was removed from CS solution by pipette pasture and then was put on in the center of neutralized CS bead that plunged in α -MEM (follicle embedding). CS solution was cross-linked with OH sodium bicarbonate in culture medium. Finally, each bead was cultured in 96 wells containing 100 µL of culture medium and was incubated at 37°C and 5% CO₂ for 13 days. Every 3-4 days, 40 µl of culture medium was exchanged with fresh medium.

In vitro maturation of preantral follicles and ovulation induction

A total of 187 follicles were divided into, alginate (93 follicles, 6 replicates) and CS (94 follicles, 6 replicates) groups. Encapsulated follicles in 2 groups including alginate 0.7% and CS 1% were cultured individually in a 96-well plate (TPP, Switzerland) for 13 days. Culture medium was composed of α -MEM supplemented with 5% FBS, 5 mg/ml insulin, 5 mg/ml transferrin and 5 ng/ml sodium selenite (ITS, Gibco, UK), 10 mIU/ml recombinant-follicle stimulating hormone (r-FSH, Merk, Germany). An inverted microscope with transmitted light and phase objectives (Nikon TI) was utilized to assess follicle survival and diameter (ImageJ software). Those follicles which no longer had their oocytes surrounded by a granulosa cell layers or their granulosa cells had become dark and fragmented and their follicles had decreased in size were considered to be dead. Diameter of the follicles was assessed on days 6 and 13 of the culture. IVM oocytes were induced on day 13 of culture by adding 2.25 IU/ml human chorionic gonadotropin (hCG). After 16-18 hours, maturation was assessed through an inverted microscope by presence of the first polar body. A treatment was carried out for denudation of the oocytes from the surrounding cumulus cells with 0.3% hyaluronidase (Sigma-Aldrich, St. Louis, MO) and gentle aspiration via a polished drawn glass pipette. The

oocytes were checked to see whether they had germinal vesicle breakdown (GVBD) for the cases where germinal vesicle was not in sight. The oocytes were categorized as metaphase II (MII) if there was a polar body in the perivitelline space; shrunken or fragmented oocytes were categorized as degenerated (DG). In this phase, CS 1% was determined to be an optimum concentration. Thus, all assessments for CS 1% were compared with alginate 0.7%.

Immunocytochemistry

MII oocytes from the *in vitro*-cultured follicles and also *in vivo* oocytes (from adult mice) as a control were obtained and fixed in 4% paraformaldehyde at room temperature for 1 hour, permeabilized in PBS with 0.1% Triton X-100 and 0.3% bovine serum albumin (BSA) for 15 minutes, and blocked in PBS comprising of 0.01% Tween 20 and 0.3% BSA. The oocytes were incubated in anti-tubulin for visualization of the spindle: fluorescein isothiocyanate (anti-tubulin: FITC; 1:150; Abcam, USA) for 1 hour, and cortical granules (CGs) were detected with rhodamine-conjugated Lens culinaris agglutinin (1:200; Vector Laboratories, USA) during incubation with anti-tubulin: FITC. At the end, DNA was stained by 1 $\mu\text{g}/\text{mL}$ 4',6-diamidino-2-phenylindole (DAPI, Sigma, St. Louis, MO, USA) for 5 minutes. Images were taken using a fluorescence microscope (Eclipse 50i, Nikon, Japan).

Hormone assays

Androstenedione, 17 β -estradiol and progesterone were measured in conditioned media collected on follicle culture (day 1 and 13) using commercially available radioimmunoassay kits (ELISA kit, BT Lab, China). The condition media obtained from each time point of the specific cultures were pooled together (15-20 samples pooled per measurement). The sensitivities for the androstenedione, estradiol and progesterone assays were 0.1 ng/ml, 10 ng/ml and 0.1 ng/ml, respectively.

Gene expression and RNA extraction

To evaluate gene expression, follicles in the experimental and control groups were collected in four replicates: on day 0 (control group, 20-30 preantral follicles in each replicate), and day 13 (experimental groups, 15-20 antral follicles in each replicate) of culture, pooled in Cell Reagent RNA Protect (RNeasy kit, Qiagen, Germany) and stored at -70°C until RNA extraction. Total RNA was extracted from each of the separated follicular pools using an RNeasy Micro Kit (Qiagen, Germany) according to the manufacturer's instructions. cDNA was also synthesized using Revert Aid H Minus First Strand cDNA Synthesis Kit (Takara, Otsu, Shiga, Japan) and random hexamers according to the manufacturer's instructions.

Quantitative real-time polymerase chain reaction

mRNA was extracted and cDNA was synthesized, and was then amplified using master mix which was composed of specific oligonucleotides and TAKARA SYBR Green (Takara, Otsu, Shiga, Japan). Oligonucleotide primers used are listed in Table 1. Samples were analyzed for gene expression of folliculogenesis *Ggf9*, *Bmp15*, *Zp3*, *Cx37*, *Cx43*, *Bmp4* and *Bmp7*, endocrine genes *Lhcgr*, *Cyp11a1*, *Cyp17a1*, *Cyp19a1* and *Fshr*, as well as for apoptotic genes such as *Bax*, *Casp3*, *Bcl2*, and *P53* (Table 1). *Gapdh* was considered as the housekeeping gene. Data was representative of four independent experiments.

Statistical analysis

The statistical analysis was carried out using SPSS version 16 (SPSS Inc., Chicago, IL, USA). All experiments were performed with three independent biological replicates, and the data, with the exception of meiotic competence and hormone assays, were analyzed using one-way ANOVA, followed by Tukey's test. The meiotic competence and hormone assay data were analyzed using t test. Differences were considered significant at $P < 0.05$.

Results

Scanning electron microscopy analysis

Figures 1A show that the 0.5% and 1% CS samples were porous with almost homogeneous porosity which made sheet format of solid fibers. The sheets distance is about 25 μm which creates enough room for cell nests. In higher concentration of CS 1.5%, in hydrogel, the fibril solid content is much higher which, as it can be seen, there is no free space between in the layers. Moreover, in high resolution images, Figure 1B, the nano-pores about 300 nm are visible at 1% and 0.5% of CS where, high concentration of CS at 1.5% prevents the formation of these pores.

Fourier transform infrared spectroscopy analysis

As it was described in our previous article (20), FT-IR spectra in Figure 1C show stretching vibration of C—H at 663. There are peaks for hydroxy groups and N—H group stretching. Peak bend on 517, 643, 851 and 1093 cm^{-1} are showing presence of PO_4^{3-} which means successful gelation using ionic gelation process in the phosphate buffer. Peaks decreasing at $\sim 1090 \text{ cm}^{-1}$ and C—H bands with the centrality of $\sim 2880 \text{ cm}^{-1}$ reveal the presence of CH_3COONa made of NaOH reaction with acetic acid.

Mechanical strength and elastic modulus of hydrogels

The compressibility strength of the hydrogels in the three concentrations is shown in Figure 1D. The average peaks of stress for each concentration, 0.5, 1, 1.5% samples, at breaking point were 6.2, 10.3 and 15.5 kPa, respectively. The strain, length gradient over initial characteristics length, was 53.5, 51.4 and 52.6% for 0.5%, 1% and 1.5%; also, Young's modulus of the three samples was 30.8, 19.8, and 10.3 kPa, respectively.

Table 1: Primer sequences used for real-time polymerase chain reaction analysis

Gene	Primer sequence (5'-3')	Product length (bp)	Accession number
<i>Gdf9</i>	F: CAAACCCAGCAGAAGTCAC R: AAGAGGCAGAGTTGTTCAGAG	194	NM_008110.2
<i>Bmp15</i>	F: AAATGGTGAGGCTGGTAA R: TGAAGTTGATGGCGGTAA	148	NM_009757
<i>Zp3</i>	F: CTTGTGGATGGTCTATCTGAG R: GTGATGTAGAGCGTATTTCTG	125	NM_011776.1
<i>Gja4 (Cx37)</i>	F: CGACGAGCAGTCGGATTT R: AGATGACATGGCCCAGGTAG	155	NM_008120.3
<i>Gja1(Cx43)</i>	F: TAAGTGAAAGAGAGGTGCCCAGA R: GGTTGTTGAGTGTTACAGCGAAAAG	200	NM_010288.3
<i>Bmp4</i>	F: GGTCGTTTTATTATGCCAAGTCC R: ATGCTGCTGAGGTTGAAGAGG	417	NM_001316360.1
<i>Bmp7</i>	F: CTATGCTGCCTACTACTGTGAG R: GTTGATGAAGTGAACCAGTGTC	103	NM_007557.3
<i>Trp53 (p53)</i>	F: AACTTACCAGGGCAACTATG R: TGTGCTGTGACTTCTTGTAG	203	NM_001127233.1
<i>Casp3</i>	F: AAAGACCATACATGGGAGC R: CGAGATGACATTCCAGTGCT	138	NM_001284409.1
<i>Bax</i>	F: TTGCTACAGGGTTTCATCCAG R: CCAGTTGAAGTTGCCATCAG	246	NM_007527.3
<i>Bcl2</i>	F: GCCTTCTTTGAGTTCGGT R: ATATAGTCCACAAAGGCATCC	162	NM_009741.5
<i>Fshr</i>	F: ACGCCATTGAACTGAGATTTG R: GAACACATCTGCCTCTATTACC	134	NM_013523.3
<i>Lhcgr</i>	F: AAGCACAGTTAGAGAAGCGA R: GGTCAGGAGAACAAAGAGGA	244	NM_013582.3
<i>Cyp11a1</i>	F: TCCTTTGAGTCCATCAGCAG R: GTCCTTCCAGGTCTTAGTTCT	180	NM_001346787.1
<i>Cyp17a1</i>	F: AGAAGTGCTCGTGAAGAAGG R: TTGGCTTCCCTGACATATCATCT	201	NM_007809.3
<i>Cyp19a1</i>	F: ATGTCGGTCACTCTGTACTTC R: TTTATGTCTCTGTCACCCACAAC	107	NM_001348171.1
<i>Gapdh</i>	F: GACTTCAACAGCAACTCCCAC R: TCCACCACCCTGTTGCTGTA	125	NM_001289726.1

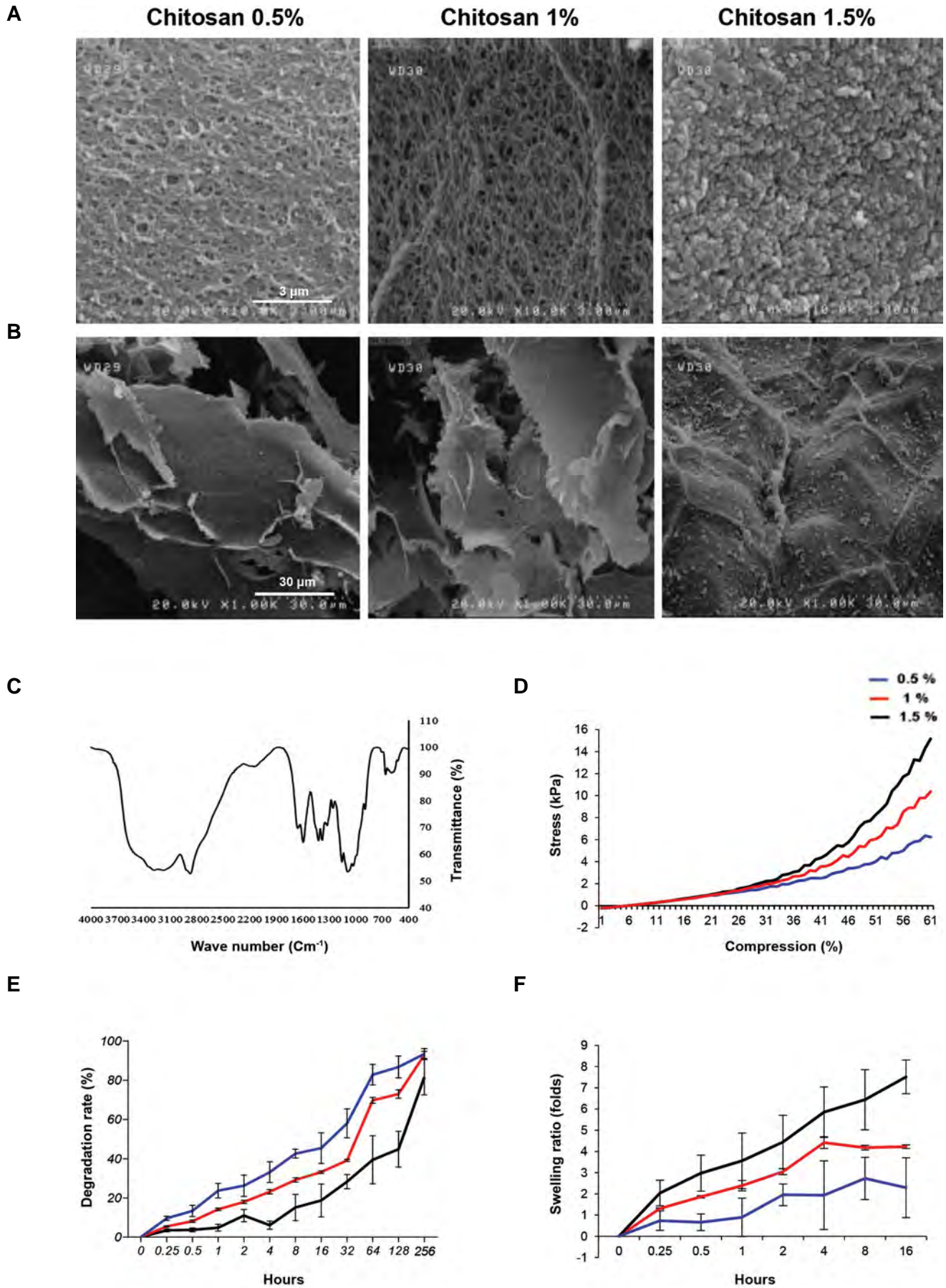


Fig.1: Mechanical and structural assessment of chitosan hydrogels. **A, B.** The scanning electron microscopy (SEM) images of morphology and porosity of chitosan hydrogels (scale bars A: 3 μ m, B: 30 μ m), **C.** FTIR spectra of chitosan hydrogels, **D.** Compressive strength of chitosan hydrogels, **E.** Degradation rate of the chitosan hydrogels, and **F.** Swelling ratio of the prepared chitosan hydrogels.

Hydrogel degradation

Figure 1E presents weight losses in the samples in DMEM over time. The three hydrogels could lose weight in the DMEM solution because of the solvent penetration and the growing swelling pressure on the mechanical strength arising from physical cross-linking points in the polymeric network. This resulted in a gradual decline in the structural integrity of the ionically and physically cross-linked hydrogels, leading to disintegration and collapse of the hydrogels in the media. In addition, due to modest and progressive drop of ambient pH to 6.5 and the hydrogels weight loss, there was a simultaneous transition of the gel-sol. Figure 1E shows the gradual weight loss of the samples in the early hours due to gel structure integrity. As could be seen in the figure, there was a steady increase in the gel-sol transition and rate disruption and after 20 days, with the 0.5% sample losing more than 90% of its weight. The two other samples reflected a similar case as well. The more weight loss of the 0.5% sample was affirmed by the mechanical strength test, samples morphology, and porosity.

Swelling ratio

According to Figure 1F, swelling ratio for 0.5 and 1% samples was high; however, it gradually decreased. The maximum swelling for the two concentrations is about 10 hours, but in 1.5% hydrogel even after 16 hours there is an increasing trend in the volume of hydrogel which could be attributed to high mechanical strength of the higher concentrations. The equilibrium swelling ratios for the two concentrations were 360 and 415, respectively after around 10 hours.

Viscosity of chitosan solutions

The viscosity of hydrogel precursor solutions was 12.5 and 20 cp for 0.5 and 1% samples, respectively. Whereas the parameter was not measurable for 1.5% sample due to its high viscosity which resembled a solid scaffold. The 1% sample had a higher viscosity for presence of more mineral salt in the precursor solution. On the whole, the results suggest that the viscosity of the 1% sample suited the *in situ* gel formation as follicle seeds during sol-gel transformation.

Cytotoxicity of hydrogels

Figure 2A shows the cytotoxic effect of hydrogels on hBMSCs which were seeded on their surface via MTT-assay for 10 days. The survival of cells is reported in terms of optical density (OD) at 570 nm. These results show that the hydrogels were non-toxic for hBMSCs, and biocompatible for 31, 45 and 36% cell growth during this time for the samples. The OD and proliferation of cells seeded on 1% sample were more than what were observed for the other samples. It could be explained by considering the fact that 1% sample contained culture medium more than 1.5% sample and it has more available surface for cell proliferation rather than 0.5% sample. With respect to time standard and given that 75% of the primary cells

survived after the MTT test, it can be said that all the hydrogels were biocompatible and non-toxic.

Cell viability

The viability rates for the hBMSCs, which were cultured in the 1% sample on days 1, 7 and 14, were 90.76, 95.45, and 94.97, and in the 1.5% sample 87.5, 95.04, and 91.30, accordingly. There was no significant difference regarding the number of viable cells of the two samples; however, there was a significant difference between the samples for the dead cells ($P < 0.05$) on the 14th day of culturing (Fig.2B). Figure 2C presents the results for AO staining concerning hBMSCs which was used to fill the hydrogel samples after 1, 7 and 14 days since cell culture was initiated. As the figures show, the majority of the cells were alive and fully dispersed and stretched in the hydrogels. There were remarkable survival rates for live/dead staining.

Biocompatibility and testing of chitosan concentrations for follicle culture

When NaOH was added to CS 0.5%, gel form did not compose that was because of the low viscosity. In addition, the severe stiffness of CS 1.5%, did not allow encapsulation. No obvious sign of cytotoxicity such as oocyte extrusion and cellular degeneration could be noticed after 24 hour of culturing. CS supported the *in vitro* follicular growth and granulosa cell proliferation for 13 days. Encapsulated follicles in 1% concentrations of CS continued to follicular diameter increase during the growth phase and they retained their spherical morphology (Fig.3A). As Figures 3B and 3C depict, survival rate was significantly lower in alginate compared to CS 1%. In addition, antral cavity formation was higher in CS 1% than alginate group but it was not significant.

Characterization of follicle growth and oocyte meiotic competence in chitosan hydrogel

Typical morphology of preantral follicles and oocytes after 3D culture in CS hydrogel is shown in Figure 3A, CS embedded secondary follicles maintained their 3D spheroid architecture throughout IVC. An intact basal lamina with a thecal cell layer was typically observed (Fig.3A, day 13). The diameter of the follicles in CS was significantly higher than that in alginate by day 6 and day 13 (day 6: 192 ± 18.81 versus 177.5 ± 7.37 μm , day 13: 392.25 ± 40.7 versus 332.3 ± 26.3 μm , respectively) (Fig.3D).

After 13 days of culture, follicles were separated from alginate, CS groups, and induced with hCG for 16-18 hours. Oocyte quality produced from engineered follicles in the CS and, alginate hydrogels was measured by their ability to continue meiosis, as shown by GVBD and MII oocytes (Fig.3A). MII rate was higher in the CS 1% than the alginate group (43.08 versus 26.3%); however, no significant difference in the MII rate was found among the two groups (Fig.3E). Oocytes from alginate 0.7% showed significantly higher GV (34.2 versus 7.6%) and lower GVBD (31.57 versus 47.63) rate than the CS group ($P < 0.05$) (Fig.3F, G).

Steroid secretion

Ovarian hormones including estradiol, androstenedione, and progesterone were secreted by the theca and granulosa cells throughout the follicle development. At the end of the culture, follicles in CS 1% group secreted significantly more estradiol compared to alginate group

(Fig.3H) ($P < 0.05$), and Progesterone levels increased, but this increase was not significant (Fig.3I). In CS 1%, androstenedione level decreased on day 13 compared to alginate but was not significant (Fig.3J). In two groups all hormones increased non-significantly throughout the culture period and in the meantime of culture, progesterone decreased slightly in alginate group.

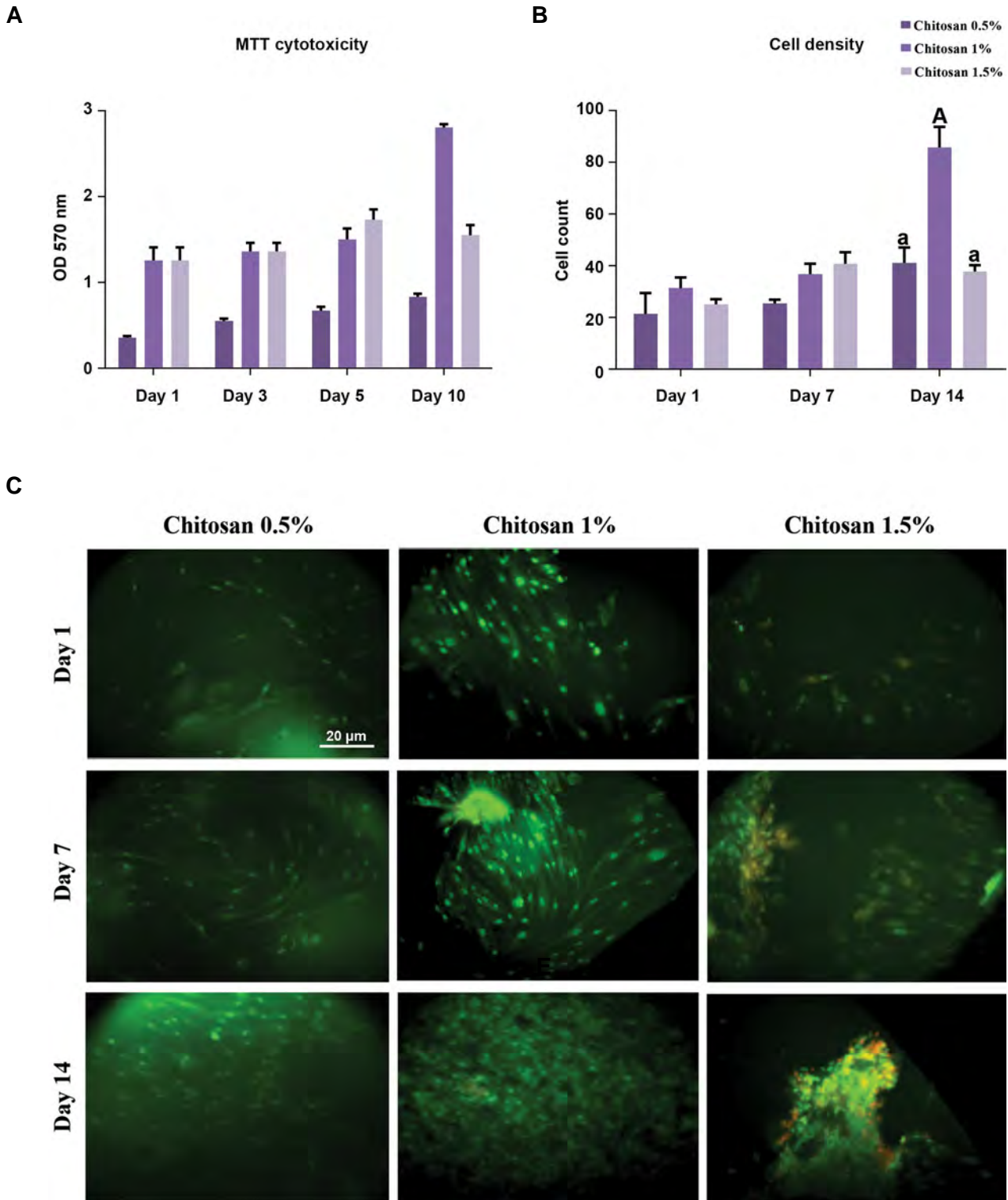


Fig.2: Hydrogel cytotoxicity and viability of hBMNCs were investigated by MTT-assay and acridine orange staining respectively. **A.** MTT-assay, **B** and **C.** Viability of cells was performed by live/dead staining acridine orange after 1, 7 and 14 days of cell culture (scale bar: 20 µm). The data were analyzed using ANOVA test. Capital letters versus same small letters (A with a) indicated significant difference ($P < 0.05$). hBMNCs; human bone marrow mesenchymal stem cells and OD; Optical density.

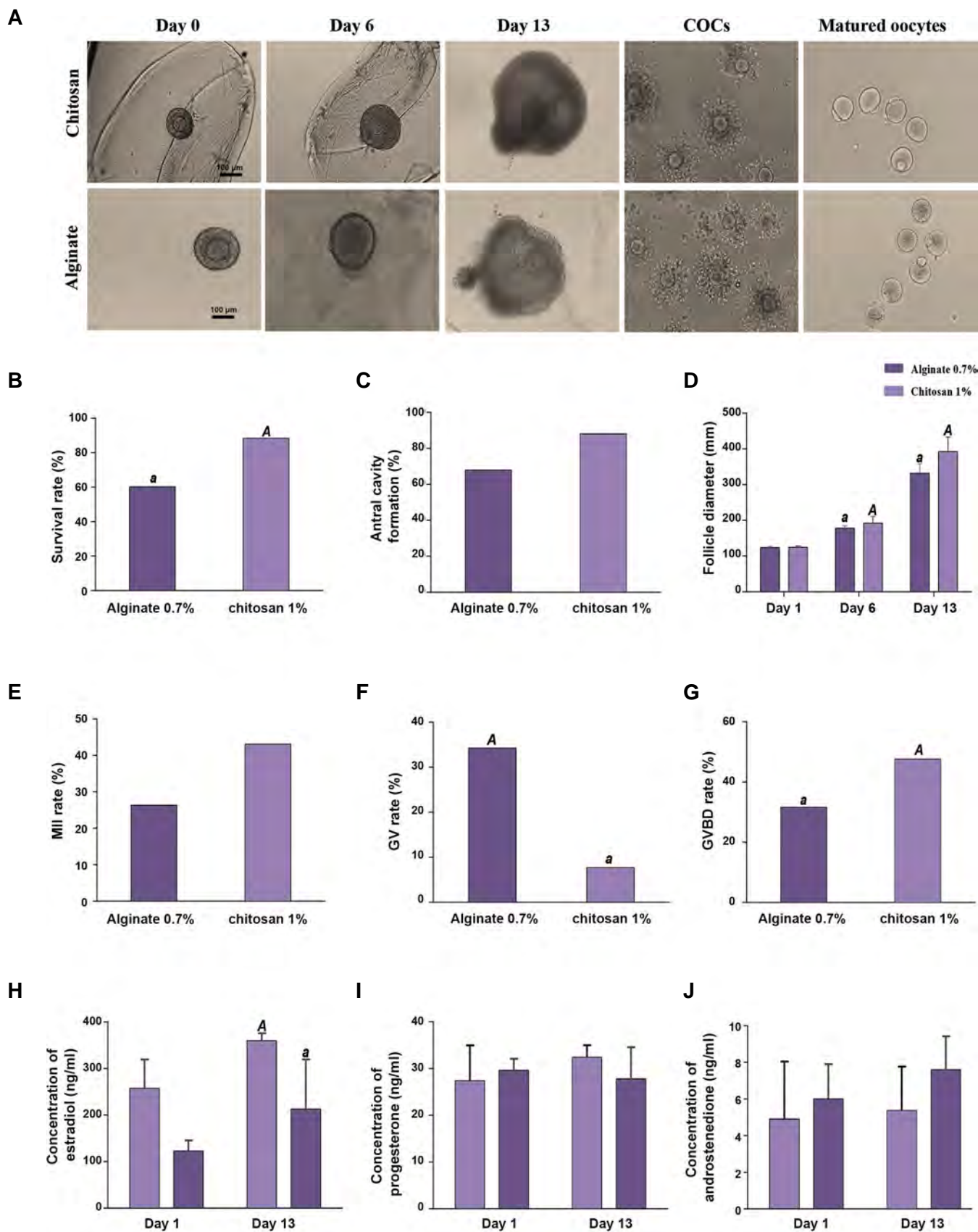


Fig.3: Morphology of follicles from day 1 to day 13, meiotic competence and hormone secretion. **A.** Morphology of preantral follicles was embedded in 1% chitosan (scale bar: 100 μ m) and alginate hydrogel (scale bar: 100 μ m) from day 0 to day 13. **B.** Survival rate, **C.** Antral formation rate, **D.** Follicle diameter, **E.** MII, **F.** GV, **G.** GVBD rate, **H.** I, and **J.** Estradiol, progesterone, and androstenedione secretion into the culture medium. As the graph depicts, estradiol and progesterone increased on day 13 in follicles from chitosan 1% when compared with alginate however, estradiol was significantly higher than alginate. The data were analyzed using t test. Capital letters versus same small letters (A with a) indicated significant difference ($P < 0.05$). Day 0; An early secondary follicle, Day 6; Eccentric oocyte movement within the follicle, Day 13; Antral cavity formation is clearly visible, COC; Cumulus-oocyte complex, MII; Metaphase II, GV; Germinal vesicle, and GVBD; Germinal vesicle breakdown.

Gene expression analysis

Folliculogenesis genes

The expression of seven genes involved in folliculogenesis such as *Ggf9*, *Bmp15*, *Zp3*, *Cx3*, *Cx43*, *Bmp4* and *Bmp7* were assessed. In CS and alginate groups, these genes had similar patterns of expression relative to day 0 as a control group. In CS and alginate hydrogel, the expression of all folliculogenesis genes, with the exception of *Cx43*, decreased significantly from preantral to antral stage with a fold change of at least 16 ($P < 0.05$, Fig.4A). *Cx43* had 2-3 fold increased expression in CS and alginate groups, relative to the control one ($P < 0.05$).

Endocrine-related genes

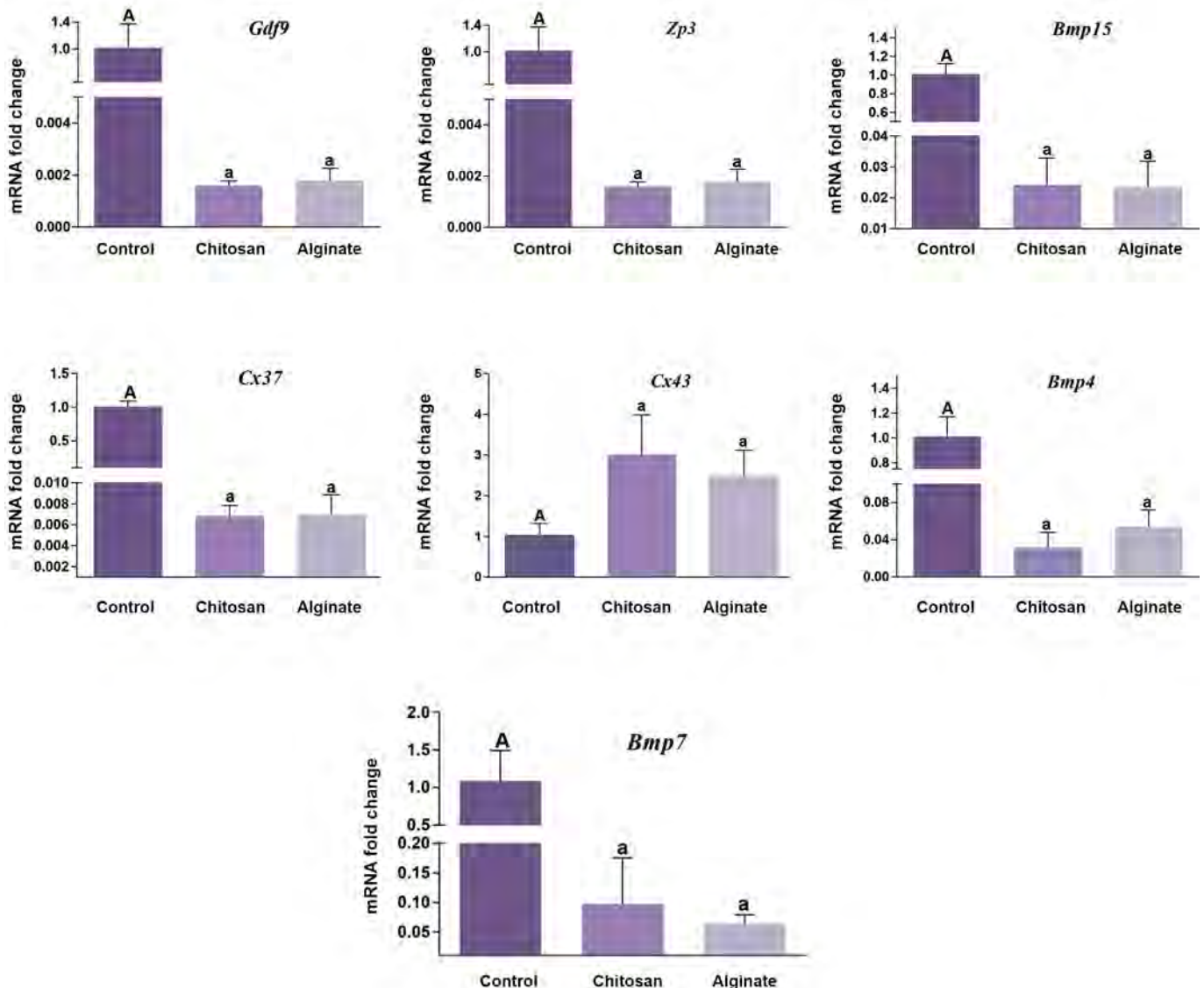
The expression of five genes involved in endocrine such as mRNA encoding aromatase *Cyp19a1*, *Cyp11a1*, *Cyp17a1*, the FSH receptor (*Fshr*), *Lhcgr* was assessed. In CS and alginate groups, five endocrine genes had similar patterns of expression relative to day 0 as a control group. In CS and alginate hydrogel, all endocrine-related

genes expression, with the exception of *Fshr*, increased from preantral to antral stage with a fold change of at least 3 ($P < 0.05$, Fig.4B). However, *Lhcgr*, *Cyp11a1*, and *Cyp19* expression levels during *in vitro* culture (IVC) in CS were higher than alginate. The expression of *Cyp19a1* (1.51 fold) and *Lhcgr* (1.82 fold) had significantly increased in the CS group relative to alginate. *Fshr* had 0.5 fold decreased expression in CS which was significant compared to alginate ($P < 0.05$).

Apoptotic-related genes

The expression of four genes involved in apoptosis such as mRNA encoding *Bax*, *Bcl2*, *Casp3*, *P53*, and ratio of *Bax/Bcl2* was assessed. In CS and alginate groups, these genes had similar patterns of expression relative to day 0 as a control group. In CS and alginate hydrogel, the expression of *P53*, *Bcl2*, decreased significantly from preantral to antral stage with a fold change of at least 1.5 ($P < 0.05$, Fig.4C). *Bax* and *Casp3* and *Bax/Bcl2* had 3 fold increased significantly expression in CS and alginate groups, relative to control group ($P < 0.05$).

A



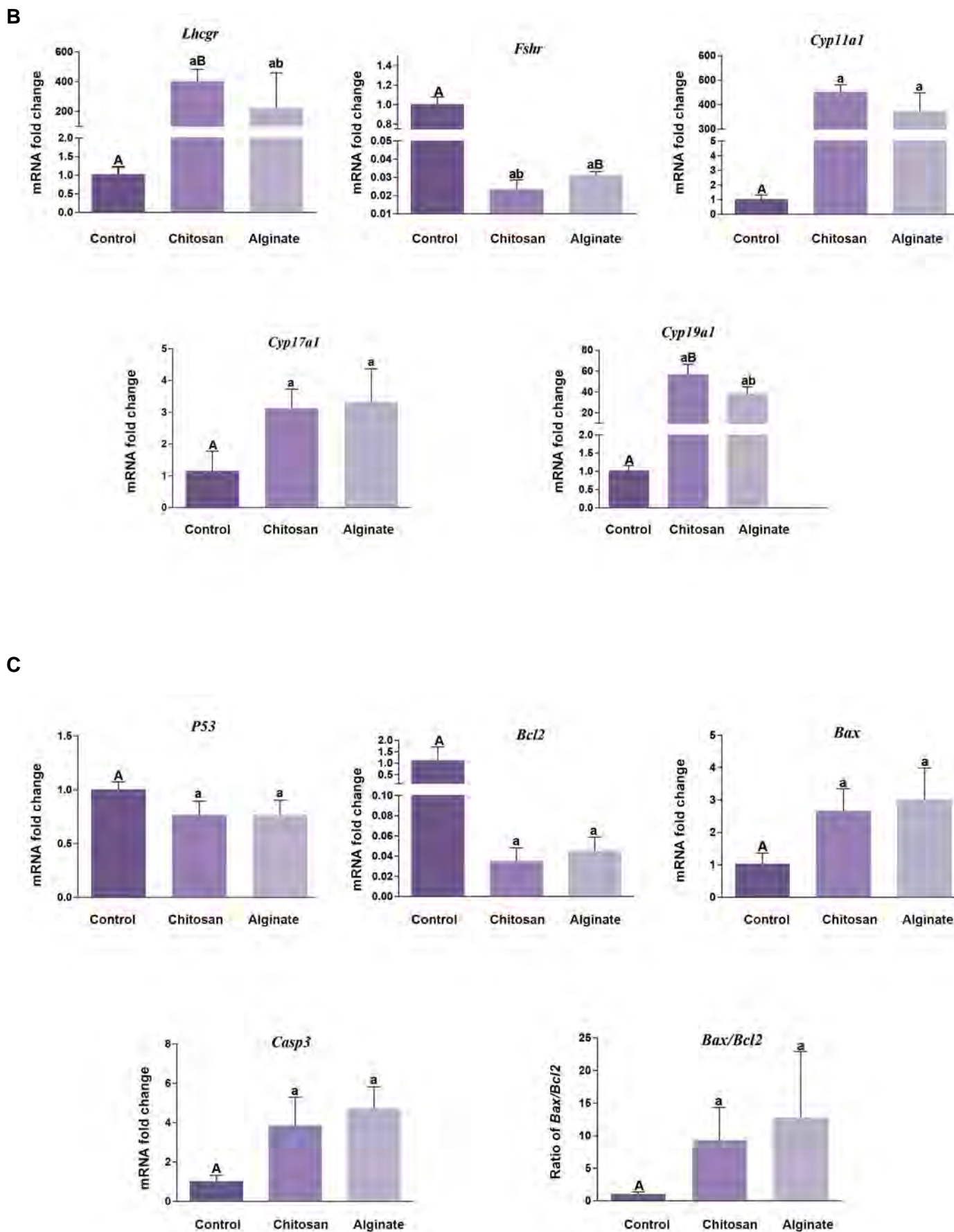


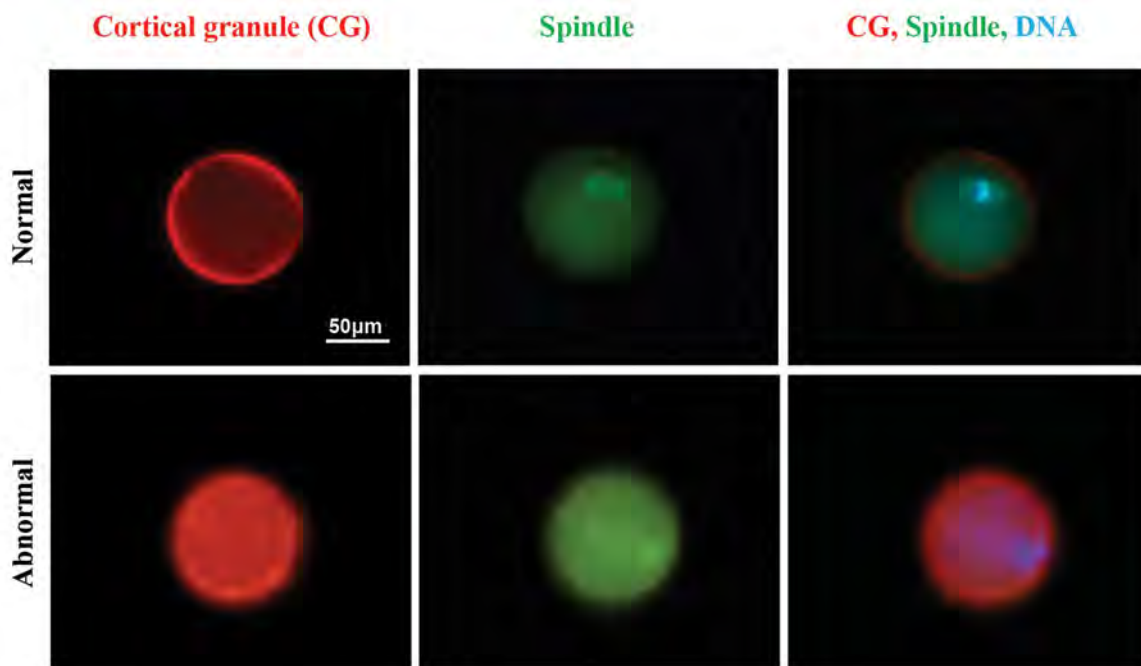
Fig.4: Gene expression analysis. **A.** Expression levels of folliculogenesis genes (*Gdf9*, *Zp3*, *Bmp4*, *7*, *15*, *Cx37* and *Cx43*), **B.** Expression levels of endocrine genes (*Lhcgr*, *Fshr*, *Cyp11a1*, *Cyp17a1*, *Cyp19a1*), and **C.** Expression levels of apoptotic genes (*P53*, *Bcl2*, *Bax*, and *Casp3*). *GAPDH* was regarded as the internal control. Data were analyzed using the one way ANOVA. Capital letters versus same small letters (A with a, B with b) indicated significant difference ($P < 0.05$).

Spindle and chromosome alignment, cortical granule formation

The weakened developmental competence of the *in vitro* follicle culture derived oocytes, could pose problems in chromosome alignment on the spindle and spindle formation (Fig.5A). Oocytes from alginate hydrogel group showed 42.1% of spindle disorganization and 47.36% of them had at least one chromosome located outside of the metaphase plate, which was significantly higher than *in vivo* MII oocyte as a control group and CS hydrogel, in which only 10% of spindle disorganization and 5% of chromosomes misalignment were seen in control group ($P < 0.05$). In

CS hydrogel, 16.6% of MII oocytes had a disorganized spindle and 20.83% had at least one chromosome located outside of the metaphase plate, which was not significantly higher than those of control group (Fig.5B). Cortical granules, the secretory granules found in CG exocytosis and oocytes play a role in inducing zona pellucida blocking to avert polyspermy (21). While CGs in the control group display a uniform cortical distribution in the MII oocytes (Fig.5A), CGs present in MII oocytes derived from *in vitro* cultured follicles in alginate and CS hydrogel were clumped and did not display a uniform cortical distribution (94.73 and 95.8%, respectively) and this was significantly higher than control group (5%) ($P < 0.05$, Fig.5A, B).

A



B

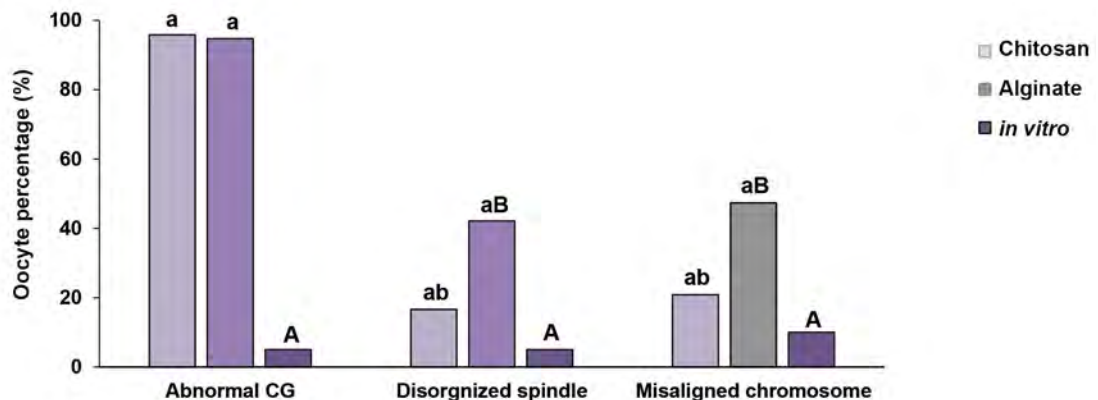


Fig.5: Spindle organization, chromosome alignment and cortical granule (CG) formation. **A.** MII oocytes were obtained from the ovaries of NMRI mice following culturing in the alginate and chitosan hydrogels. They were fixed and stained for DNA (DAPI, blue), tubulin (green) and analyzed for chromosome alignment and spindle organization. These oocytes were compared with oocytes which developed *in vivo* and were then matured *in vitro* (scale bar: 50 µm) and **B.** The experiment was performed three times, and at least 20 oocytes were analyzed for each group. Data were analyzed using ANOVA test. Capital letters versus same small letters (A with a, B with b) indicated significant difference ($P < 0.05$).

Discussion

This study aimed to elucidate the first application of a CS hydrogel to the 3D culture of ovarian follicles. To obtain optimal concentration of CS, 0.5, 1, and 1.5% (W/V) were used for ovarian follicular culture. FTIR tests confirmed the chemical stability of this type of in situ gel formation according to a study conducted by (20). It is supposed that the microstructure and swelling properties of scaffolds have significant effect on cell penetration, proliferation, and function in tissue engineering (22). The average pore size of scaffolds decreased by the increase in the hydrogel concentration. CS 1% showed homogeneously distributed pores and higher degradation ratio compared to CS 1.5%. On the whole, the swelling ratio of scaffold could be attributed both to the microstructure and hydrophilic nature of scaffold (23). The high hydrophilicity of CS may also have contributed to the high degradation of this hydrogel. Scaffold also was needed to have sufficient rigidity to maintain the 3D structure of the follicle and to coordinate follicle development. Antrum formation and steroidogenesis are two aspects of this developmental process which are affected by the scaffold (4). The elasticity of the CS hydrogels was altered by making adjustments in the concentration of the solution. The results of our study revealed that CS 1% was an optimum concentration for ovarian follicular culture. The higher swelling ratio of 0.5% sample and SEM images compared with that of 1% sample can be attributed to its weak mechanical strength.

The investigations demonstrated that varying the matrix physical properties would change the microenvironment from permissive to nonpermissive for follicular culture. The mechanical properties of the matrix and the hydrogel elasticity are two crucial elements that can directly influence the phenotype and function of the *in vitro*-cultured ovarian follicles (24-26). In this study, the elastic modulus for CS 1% was 19.8 kPa. M. Xu et al. (24), suggested that Matrices with a shear modulus of less than 250 Pa are considered as permissive since a large percentage of follicles cultured in these matrices survive and increase in diameter; develop an antrum; have a steroidogenic profile similar to that of follicles *in vivo*, and produce MII stage oocytes. On the other hand, matrices with a shear modulus greater than 500 Pa are considered as nonpermissive since they decrease the rate of antrum growth and formation, as well as alter steroid production, thereby decreasing the oocyte quality. Based on these studies and results obtained in our study, CS is a permissive hydrogel because its shear modulus is less than 250 Pa and lesser than alginate 0.7% (203 pa). Antral cavity formation, survival and MII rate, diameter of follicles on day 6 and day 13 are higher in CS 1% than in alginate 0.7%.

In hormone production, 17 β -estradiol hormone is produced by the mature ovarian follicle and maintains oocytes in the ovary (24, 27). At the end of the culture, follicles from CS1% secreted more estradiol compared with those in alginate. Our data showed that immature

ovarian follicles progress to mature form and secrete 17 β -estradiol hormone. The expression of genes associated with steroidogenesis and antrum formation was also explored to find out their patterns as a function of the matrix properties.

Time and matrix conditions were regarded as two factors affecting the variation in the detected levels (26). Thus, the expression of the following genes related to steroidogenesis during day 0 and day 13 of follicle culture and culture in two different matrix conditions, alginate 0.7% and CS 1%, was examined. In both groups, the folliculogenesis, endocrine, and apoptotic genes, had similar patterns of expression relative to the control group. *Cyp19a1* and *Lhcgr* had increased expression levels within the CS follicles compared with alginate. During development, *in vivo*, follicles demonstrated increasing *Cyp19a1*, which is responsible for the conversion of androstenedione to estradiol expression as they mature and approach ovulation (28, 29). As the mature follicles approach ovulation, there is expression of *in vivo*, *Lhcgr* in the mature follicles. The follicle is capable to respond to the LH surge for the upregulation of LHCGR, which results in ovulation, granulosa cell luteinization, and cumulus mucification (30). Consequently, expression of *Lhcgr* throughout the IVC is an indication of follicle maturity. The upregulation of *Lhcgr* in the permissive follicle culture took place on Day 6 of culture, which was in harmony with the timing of antrum development and follicle differentiation. In contrast to *Lhcgr*, *Fshr* was expressed in both mature and immature granulosa cells (31), with a stabilized expression level during the follicle development at the mRNA and protein levels (32, 33). In the same line with these *in vivo* observations, the *Fshr* expression did not undergo any alterations throughout the culturing, but in this study *Fshr* expression was downregulated in CS and alginate groups relative to control group. Also this gene had 0.5 fold reduced expression in CS compared with alginate. Thus, it can be concluded that in the last stage of follicular growth (preovulatory), the follicle would grow to its maximum and do not require *Fshr* gene expression, but on the other hand, for ovulation, the gene expression of *Lhcgr* should be high. *Gdf9* and *Bmp15* (Tgfb super family) are two oocyte-secreted proteins which are present in all follicular stages (34). Expression levels of the aforementioned genes decreased during 12 days of culture (35). Also in this study expression patterns of *Gdf9* and *Bmp15* were similar to those found in previous study (36). *ZP3* and *Bmp4*, 7 were essential in the follicular development and had an expression pattern similar to that in *Bmp15* and *Gdf9* in this study (37). This transcript decline could be translated into the rise in the protein synthesis at the end of the follicle culture, which could be regarded as a proof for a better growth of the follicles in the 3D culture system (36).

Forces were generated by follicles in 3D matrices as a result of outward force exerted by the growing follicle on its surrounding matrix, which was reciprocated by

the surrounding matrix at a magnitude depending on the stiffness of the matrix and the force exerted by the follicle. The resulting increased pressure on the follicle may account for the apoptosis and/or the decreased proliferation rates of follicle cells (38).

Apoptosis is a dynamic process which might occur during IVC of follicles. Apoptosis, a kind of programmed cell death, has been associated with a range of processes which deal with normal functions of the follicular and ovary development, including atresia and corpus luteum regression (39). Ratio of *Bax/Bcl2* in alginate group was higher than that in CS group, but this difference was not significant. This result demonstrated that stiffness of CS 1% was more suitable for 3D culture of preantral follicle to antral than alginate 0.7% hydrogel.

According to the results obtained in this study, CS system supports nuclear maturation, alignment of chromosomes, and organization of spindle; however, alginate system could not support them. Both of the systems, alginate and CS, could not support the cytoplasmic maturation. In the control group, CGs displayed a uniform cortical distribution, but they were clumped in CS and alginate groups. Thus, CG biogenesis/localization appeared to be impaired in these oocytes. The results of this study also confirmed the findings reported regarding the fact that in alginate hydrogel there might be some disturbance in meiotic spindle assembly and cortical granules (11).

The primary reason accounting for the low efficacy of IVM in assisted reproduction would be inadequacies of the culture media used. The evidence shows nuclear maturation in human oocytes is properly supported by the culture systems, but these systems cannot produce oocytes with cytoplasmic maturation, consequently, reducing the potential for embryo development (40). Therefore, the replacement of the matrix may not be an appropriate solution for improving cytoplasmic maturity. Changing the environment or adding growth factors alongside using combined hydrogels would be more efficient alternatives.

Conclusion

As the results of this study indicated, CS was a permissive hydrogel. This biomaterial supports integrity of follicles, survival and development, including phenotypic maintenance, hormone production, normal gene expression, maturation and ovulation during 3D culture system.

Acknowledgements

The authors would like to acknowledge M.R. Dalman for reading and editing the manuscript, M. Mohammadi for statistical analysis and E. Abedheydari for molecular technical support. Royan Institute (Grant Number, 94000162) financially supported this study. In addition, Tehran University of Medical science (grant number: 29496). The authors declare that there is no conflict of interest.

Authors' Contributions

F.H.; Contributed to all experimental work, data statistical analysis, and interpretation of data. B.E., A.M.; Drafted the manuscript and statistical analysis. A.G.; Participated in performing the experiments and drafting the manuscript. M.B.; Helped in the molecular experiment. M.R.V., G.H.; Contributed to conception, design, and responsible for overall supervision. All authors read and approved the final manuscript.

References

- Wallace WH, Kelsey TW, Anderson RA. Fertility preservation in pre-pubertal girls with cancer: the role of ovarian tissue cryopreservation. *Fertil Steril*. 2016; 105(1): 6-12.
- Silber S. Ovarian tissue cryopreservation and transplantation: scientific implications. *J Assist Reprod Genet*. 2016; 33(12): 1595-1603.
- Eppig JJ, Schroeder AC. Capacity of mouse oocytes from preantral follicles to undergo embryogenesis and development to live young after growth, maturation, and fertilization in vitro. *Biol Reprod*. 1989; 41(2): 268-276.
- West ER, Xu M, Woodruff TK, Shea LD. Physical properties of alginate hydrogels and their effects on in vitro follicle development. *Biomaterials*. 2007; 28(30): 4439-4448.
- Shikanov A, Smith RM, Xu M, Woodruff TK, Shea LD. Hydrogel network design using multifunctional macromers to coordinate tissue maturation in ovarian follicle culture. *Biomaterials*. 2011; 32(10): 2524-2531.
- Amorim CA, Rondina D, Lucci CM, Giorgetti A, de Figueiredo JR, Gonçalves PB. Cryopreservation of sheep primordial follicles. *Reprod Domest Anim*. 2007; 42(1): 53-57.
- Pangas SA, Saudye H, Shea LD, Woodruff TK. Novel approach for the three-dimensional culture of granulosa cell-oocyte complexes. *Tissue Eng*. 2003; 9(5): 1013-1021.
- Sharma GT, Dubey PK, Meur SK. Survival and developmental competence of buffalo preantral follicles using three-dimensional collagen gel culture system. *Anim Reprod Sci*. 2009; 114(1-3): 115-124.
- Desai N, Abdelhafez F, Calabro A, Falcone T. Three dimensional culture of fresh and vitrified mouse pre-antral follicles in a hyaluronan-based hydrogel: a preliminary investigation of a novel biomaterial for in vitro follicle maturation. *Reprod Biol Endocrinol*. 2012; 10(1): 29.
- Kreeger PK, Deck JW, Woodruff TK, Shea LD. The in vitro regulation of ovarian follicle development using alginate-extracellular matrix gels. *Biomaterials*. 2006; 27(5): 714-723.
- Mainigi MA, Ord T, Schultz RM. Meiotic and developmental competence in mice are compromised following follicle development in vitro using an alginate-based culture system. *Biol Reprod*. 2011; 85(2): 269-276.
- Felt O, Furrer P, Mayer J, Plazonnet B, Buri P, Gurny R. Topical use of chitosan in ophthalmology: tolerance assessment and evaluation of precorneal retention. *Int J Pharm*. 1999; 180(2): 185-193.
- Kumar MN, Muzzarelli RA, Muzzarelli C, Sashiwa H, Domb AJ. Chitosan chemistry and pharmaceutical perspectives. *Chem Rev*. 2004; 104(12): 6017-6084.
- Kim IY, Seo SJ, Moon HS, Yoo MK, Park IY, Kim BC, et al. Chitosan and its derivatives for tissue engineering applications. *Bio-technol Adv*. 2008; 26(1): 1-21.
- Di Martino A, Sittlinger M, Risbud MV. Chitosan: a versatile biopolymer for orthopaedic tissue-engineering. *Biomaterials*. 2005; 26(30): 5983-5990.
- Suh JK, Matthew HW. Application of chitosan-based polysaccharide biomaterials in cartilage tissue engineering: a review. *Biomaterials*. 2000; 21(24): 2589-2598.
- Ueno H, Mori T, Fujinaga T. Topical formulations and wound healing applications of chitosan. *Adv Drug Deliv Rev*. 2001; 52(2): 105-115.
- Elmizadeh H, Khanmohammadi M, Ghasemi K, Hassanzadeh G, Nassiri-Asl M, Garmarudi AB. Preparation and optimization of chitosan nanoparticles and magnetic chitosan nanoparticles as delivery systems using Box-Behnken statistical design. *J Pharm Biomed Anal*. 2013; 80: 141-146.
- Asgari F, Valojerdi MR, Ebrahimi B, Fatehi R. Three dimensional in vitro culture of preantral follicles following slow-freezing and vitrifi-

- cation of mouse ovarian tissue. *Cryobiology*. 2015; 71(3): 529-536.
20. Ghiaseddin A, Pouri H, Soleimani M, Vasheghani-Farahani E, Ahmadi Tafti H, Hashemi-Najafabadi S. Cell laden hydrogel construct on-a-chip for mimicry of cardiac tissue in-vitro study. *Biochem Biophys Res Commun*. 2017; 484(2): 225-230.
 21. Ducibella T, Kurasawa S, Duffy P, Kopf GS, Schultz RM. Regulation of the polyspermy block in the mouse egg: maturation-dependent differences in cortical granule exocytosis and zona pellucida modifications induced by inositol 1, 4, 5-trisphosphate and an activator of protein kinase C. *Biol Reprod*. 1993; 48(6): 1251-1257.
 22. Zhu Y, Liu T, Song K, Jiang B, Ma X, Cui Z. Collagen-chitosan polymer as a scaffold for the proliferation of human adipose tissue-derived stem cells. *J Mater Sci Mater Med*. 2009; 20(3): 799-808.
 23. Ma L, Gao C, Mao Z, Zhou J, Shen J, Hu X, et al. Collagen/chitosan porous scaffolds with improved biostability for skin tissue engineering. *Biomaterials*. 2003; 24(26): 4833-4841.
 24. Xu M, West E, Shea LD, Woodruff TK. Identification of a stage-specific permissive in vitro culture environment for follicle growth and oocyte development. *Biol Reprod*. 2006; 75(6): 916-923.
 25. Xu M, Kreeger PK, Shea LD, Woodruff TK. Tissue-engineered follicles produce live, fertile offspring. *Tissue Eng*. 2006; 12(10): 2739-2746.
 26. West-Farrell ER, Xu M, Gomberg MA, Chow YH, Woodruff TK, Shea LD. The mouse follicle microenvironment regulates antrum formation and steroid production: alterations in gene expression profiles. *Biol Reprod*. 2009; 80(3): 432-439.
 27. Michalopoulos G, Sattler GL, Pitot HC. Hormonal regulation and the effects of glucose on tyrosine aminotransferase activity in adult rat hepatocytes cultured on floating collagen membranes. *Cancer Res*. 1978; 38(6): 1550-1555.
 28. Findlay JK, Britt K, Kerr JB, O'Donnell L, Jones ME, Drummond AE, et al. The road to ovulation: the role of oestrogens. *Reprod Fertil Dev*. 2001; 13(7-8): 543-547.
 29. Palermo R. Differential actions of FSH and LH during folliculogenesis. *Reprod Biomed Online*. 2007; 15(3): 326-337.
 30. Fortune JE, Rivera GM, Evans AC, Turzillo AM. Differentiation of dominant versus subordinate follicles in cattle. *Biol Reprod*. 2001; 65(3): 648-654.
 31. Hillier SG. Gonadotropic control of ovarian follicular growth and development. *Mol Cell Endocrinol*. 2001; 179(1-2): 39-46.
 32. Xu Z, Garverick HA, Smith GW, Smith MF, Hamilton SA, Youngquist RS. Expression of follicle-stimulating hormone and luteinizing hormone receptor messenger ribonucleic acids in bovine follicles during the first follicular wave. *Biol Reprod*. 1995; 53(4): 951-957.
 33. Uilenbroek JT, Richards JS. Ovarian follicular development during the rat estrous cycle: gonadotropin receptors and follicular responsiveness. *Biol Reprod*. 1979; 20(5): 1159-1165.
 34. O'shea LC, Mehta J, Lonergan P, Hensey C, Fair T. Developmental competence in oocytes and cumulus cells: candidate genes and networks. *Syst Biol Reprod Med*. 2012; 58(2): 88-101.
 35. Fatehi R, Ebrahimi B, Shahhosseini M, Farrokhi A, Fathi R. Effect of ovarian tissue vitrification method on mice preantral follicular development and gene expression. *Theriogenology*. 2014; 81(2): 302-308.
 36. Sadr SZ, Ebrahimi B, Shahhoseini M, Fatehi R, Favaedi R. Mouse preantral follicle development in two-dimensional and three-dimensional culture systems after ovarian tissue vitrification. *Eur J Obstet Gynecol Reprod Biol*. 2015; 194: 206-211.
 37. Shimasaki S, Moore RK, Erickson GF, Otsuka F. The role of bone morphogenetic proteins in ovarian function. *Reprod Suppl*. 2003; 61: 323-337.
 38. West ER, Shea LD, Woodruff TK, editors. *Engineering the follicle microenvironment*. Seminars in reproductive medicine; 2007; USA. New York: Thieme Medical Publishers; 2007.
 39. Tilly JL. The molecular basis of ovarian cell death during germ cell attrition, follicular atresia, and luteolysis. *Front Biosci*. 1996; 1: d1-d11.
 40. Combelles CM, Cekleniak NA, Racowsky C, Albertini DF. Assessment of nuclear and cytoplasmic maturation in in-vitro matured human oocytes. *Hum Reprod*. 2002; 17(4): 1006-1016.

Advisory Board of Cell Journal^(Yakhteh)
Vol 21, No 1-4, 2019-2020

A	Azizi H	Ebrahimi S
Abdanipour A	Azizollah B	Eghtesad S
Abdi Rad I	B	Ekhteraei Tousi S
Abdollahi M	Babaei F	Esfandiari F
Abdoli A	Badali H	Eskandari N
Abdollahi H	Bagheri F	Esmailnegi N
Abdollahi M	Bahadori M	Ezzatizadeh V
Abedelahi A	Bahmani B	F
Abedini A	Bahramali G	Faghihi F
Abir R	Bahreini F	Falak R
Abouhamzeh B	Bakhshi B	Farjadfar A
Aboutaleb N	Banan M	Fateh A
Aboutorabi R	Bandarian F	Fazeli Sh
Abroun S	Bandehpour M	Ferjani H
Aeri V	Barbakadze T	Forootan SF
Afzal N	Basiri M	G
Aghdam A	Bauer J	Ganji F
Ahmadabadi N	Bayat M	Ghaedi K
Ahmadinejad M	Behjati M	Ghafari SH
Akhavan Taheri M	Behmanesh M	Ghanbarian H
Alavi A	Behzad S	Ghaneialvar H
Alhalabi M	Bijannejad D	Gharbi S
Alizadeh A	C	Gharib E
Alizadeh Sh	Chahardouli B	Ghasemi H
Amani H	Cheki M	Ghasemian F
Amdjadi P	Cheraghi E	Ghazifard A
Amini A	Choudhery M	Ghiaseddin A
Amini P	D	Golipoor M
Amirchaghmaghi E	Dalman A	Goudarzi I
Amiri Yekta A	Dehghani MR	Gourabi H
Andalib A	Demirel Kars M	Guang L
Anifandis G	Dhib A	Gyesik Min
Aoltanian A	Ding L	H
Asgari A	Doosti M	Habibzadeh Motlagh M
Asgharzadeh S	Dormiani K	Haghiralsadat F
Ataee R	D'Souza R	Hajia M
Atashi A	Duisit J	Hajizadeh E
Atlasi M	E	Halvaei I
Azad M	Ebrahimi M	Hamidpour M

Advisory Board of Cell Journal^(Yakhteh)
Vol 21, No 1-4, 2019-2020

Hashemi M
Hashemi Soltanieh A
Hashemzadeh MS
Hernández-Trejo M
Hesaraki M
Homayouni Moghadam F
Hosseini A
Hosseini R
Hosseini S
Hosseini SMA
Hosseinisalekdeh Gh
Hosseinnia P
hosseinzadeh H
Hossini J
Hussein M
I
Ibáñez E
Inanloo K
J
Jafarian A
Jalali A
Jami M
Javeri A
Jebali A
Jia X
Jorsaraei SGh
K
Karabulut S
Karimian M
Karimiani E
Kashani I
Kazemi B
Kazemi M
Kazemi Nejad SR
Keshavarzi S
khademi F
Khamisi Pour Gh
Khanahmmad H
Khochbin S

khodaveisi S
Khoei S
Khoshzaban A
Kiani A
Kido T
Kim J
Kojić S
Koruji M
KP L
Kraus A
Kumar Mageswaran Sh
Kumar S
Kumar Sonkar G
L
Larti F
Lee E
Li Y
Liu H
Lu G
M
Mahdian M
Mahmoudi F
Mahmoudzadeh-Sagheb H
Majidi M
Mardani H
Maroufizadeh S
Masaeli E
Maziar A
Mehdipour P
Mesrian H
Mirfakhraie R
Mirzaee R
Moazzeni SM
Moghadasali R
Moghaddasi MH
Mohammadabadi MR
Mohammadali F
Mohammadi M
Moini A

Mojarad E
Mokhtari M
Montaser L
Moosavi M
Moradi Sh
Mortaz E
Mortezavi Y
Motaleb Gh
Motamedi M
Mousavi Sh
Movaghar B
Mozdarani H
Mudalal M
N
Nabavi SM
Najafi M
Najjari M
Nasoohi S
Navaderi M
Nazari M
Nazari Tavakoli S
Nazm Bojnordi M
Nejad Dehbashi F
Nikanfar S
Nikbakht M
Nikzad H
Nobakht M
Nojoomi F
Noori M
Nourbakhsh M
O
Obeidi N
Omran D
Orazizadeh M
Ostad N
P
Panda S
Parham A
Piryaei A
Ponnuraj Kannan T

Advisory Board of Cell Journal^(Yakhteh)
Vol 21, No 1-4, 2019-2020

Poormoosavi SM
Pour Mohammadi A
Pourhasan-Moghaddam M
Pourteymoor Z

R

Rabiei M
Rafieian-Kopaei M
Rahbarizadeh F

Rajabi S
Ramezani M

Ramos Leal G

Rassouli H

Razavi Sh

Riazipour M

Risso A

Roshangar L

Rostami S

S

Saadatian R
Sabbaghian M

Sadeghi S

Sadroddiny E

Saeedi M

Sagha M

Saghaeian M

Sajadi H

Saki N

Salehnia M

Satarian L

Saylan A

Seifi M

Seifi S

Sellami A

Shafei M

Shahbazi Sh

Shahhoseini M

Shahriari B

Shahryari A

Shajarian M

Shakeri-Zadeh A

Shalaweh S

Shams Mofarah Z

Shamsara M

Sharafi M

Shatizadeh S

Shekaari M

Shekari F

Shekarriz R

Shestakova A

Shirazi A

Shirazi R

Siadat F

Sindhu S

Soleimani J

Soleimanjahi H

Soleymani Z

Soltani B

Soodi M

T

Taghavi K

Taghiabadi E

Taleahmad S

Talebi A

Taravat B

Tavalaee M

Tavana S

Temiz E

V

Vahidi MV

Vaňhara P

Vermeire G

Vincent A

Vosough M

W

Walfridsson J

Wang G

X

Xiao H

Y

Yarahmadi Sh

Yari F

Yari S

Yavari M

Yazdian F

Z

Zahednasab H

Zahedpanah M

Zaimy M

Zamanian M

Zarbakhsh S

Zargar SJ

Zavareh S

Zeinoddini M

Zenclussen AC

Zerbini G

Zhang M

Zhang Q

Zhang SH

Zhang Y

Zhong Y

Ziaee M

Zienolddiny Sh

Index by Authors in Cell Journal^(Yakhteh)
Vol 21, No 1-4, 2019-2020

- A**
- Abbasihormozi Sh (Page: 307)
- Abbaspour MR (Page: 379)
- Abdollahi M (Page: 363)
- Abroun S (Page: 115)
- Acibaeva B (Page: 7)
- Aflatoonian B (Page: 300)
- Afraz K (Page: 307)
- Afzal E (Page: 259)
- Aghaei-Moghadam E (Pages: 70, 337)
- Ahmadalizadeh Khanehsar M (Page: 444)
- Ahmadi Badi S (Page: 57)
- Ajami M (Page: 78)
- Akbaroghli S (Page: 337)
- Akhavan Rezayat K (Page: 268)
- Alavi A (Page: 70)
- Aliasgharzadeh A (Page: 236)
- Alipour H (Page: 253)
- Alizadeh E (Page: 467)
- Allah Bakhshi E (Page: 169)
- Altafi D (Page: 350)
- Amani S (Page: 391)
- Amanzadeh A (Page: 143)
- Amini P (Page: 236)
- Anbarlou A (Page: 78)
- Anvari M (Page: 49)
- Asgari B (Page: 281)
- Asgari HR (Page: 14)
- Asghari MH (Page: 259)
- Ashtari K (Page: 14)
- Atashi A (Page: 78)
- Ayatollahi SAM (Page: 371)
- Azadeh M (Page: 451)
- Azari Sh (Page: 143)
- Aziz H (Pages: 186, 281)
- B**
- Babapour V (Page: 307)
- Badv RS (Page: 307)
- Baek SH (Page: 357)
- Baghaban Eslaminejad MR (Page: 150)
- Bagheri M (Page: 115)
- Baharvand H (Pages: 150, 290)
- Bakhtiyari S (Page: 1)
- Balavandi Z (Page: 419)
- Balmeh N (Page: 451)
- Bang KS (Page: 357)
- Banihashemi S (Page: 337)
- Barzegari Firouzabadi F (Page: 135)
- Başpınar N (Page: 7)
- Bayati V (Page: 379)
- Bazrafkan M (Page: 479)
- Bazrgar M (Page: 35)
- Behjati F (Pages: 70, 337)
- Behrouznezhad F (Page: 99)
- Bodu M (Page: 7)
- Bonakdar Sh (Page: 143)
- Borzouie Z (Page: 300)
- Bucak MN (Page: 7)
- C**
- Chavoshzadeh Z (Page: 337)
- D**
- Darabi S (Page: 1)
- Dayer D (Page: 169)
- Dehghan Gh (Page: 243)
- Delirezh N (Page: 391)
- Didari T (Page: 363)
- Du J (Page: 161)
- Dursun Ş (Page: 7)
- E**
- Ebrahimi B (Page: 479)
- Ebrahimi M (Pages: 124, 259, 467, 479)
- Eftekhari-Yazdi P (Pages: 35, 253)
- Ehsanpour A (Page: 115)
- Ejeian F (Page: 99)
- Elejo Musa A (Page: 236)
- Eliyasi Dashtaki M (Page: 401)
- Emadi-Baygi M (Page: 99)
- Eskandari Hesari M (Page: 70)
- Eskandarian M (Page: 274)
- Eslahi N (Page: 14)
- Esmaeilzadeh A (Page: 268)
- Estiri H (Page: 433)
- Eulsoon Park (Page: 357)
- Eynali S (Page: 419)
- Eyni H (Page: 210)
- Ezzatizadeh V (Page: 124)
- F**
- Fakhr Taha M (Page: 444)
- Fallah A (Page: 433)
- Fan J (Page: 161)
- Fardid R (Page: 204)
- Farhood B (Page: 236)
- Feng H (Page: 161)

Index by Authors in Cell Journal^(Yakhteh)
Vol 21, No 1-4, 2019-2020

Firouzi J (Page: 124)

G

Garssen J (Page: 391)

Geranpayeh L (Page: 467)

Ghadiri A (Page: 169)

Ghaedi K (Pages: 426 ,451)

Ghafari MA (Page: 169)

Ghafouri-Fard S (Page: 331)

Ghasemi Firouzabadi S (Pages: 70, 337)

Ghasemi Hamidabadi H (Page: 186)

Ghasemzadeh M (Page: 150)

Ghassemi A (Page: 268)

Ghiaseddin A (Page: 479)

Ghorbani S (Page: 210)

Gorji M (Page: 350)

Gourabi H (Page: 253)

Güngör Ş (Page: 7)

Guo W (Page: 161)

H

Habibi-Anbouhi M (Page: 143)

Hadipour F (Page: 337)

Hadipour Z (Page: 337)

Haghighat S (Page: 314)

Hajian M (Page: 194)

Hamed M (Page: 401)

Hashemi Tabar M (Page: 169)

Hashemitabar M (Page: 379)

Hassani F (Pages: 35, 253, 479)

Hassani SN (Page: 290)

Hassanzadeh Gh (Page: 479)

Hassanzadeh Taheri MM (Page: 210)

E

Heidarzadeh S (Page: 62)

Hekmatimoghaddam S (Page: 300)

Hemadi M (Page: 401)

Hobbenaghi R (Page: 391)

Hojatian H (Page: 350)

Hoormand M (Page: 419)

Hoseinbeyki M (Page: 444)

Hosseini M (Page: 229)

Hosseini S (Page: 150)

Hosseini Salekdeh Gh (Page: 290)

Hosseini SM (Page: 194)

Hosseini P (Page: 194)

Houshmand M (Pages: 86, 350, 419)

I

İli P (Page: 7)

Irani Sh (Page: 57)

Ismail Hassan F (Page: 363)

J

Jafarpour F (Page: 194)

Jamali P (Page: 337)

Jarahi L (Page: 268)

Javed A (Page: 135)

Javeri A (Page: 444)

Jebali A (Page: 300)

K

Kaka Gh (Page: 220)

Kalantar SM (Page: 135)

Kalarestaghi H (Page: 210)

Kamrava K (Page: 14)

Karami F (Page: 86)

Karimi A (Page: 391)

Karimian L (Page: 253)

Kariminejad A (Page: 337)

Kariminejad R (Page: 337)

Keramati F (Page: 86)

Keramati MR (Page: 78)

Khaki A (Page: 210)

Khaki AA (Page: 210)

Khalaj M (Page: 290)

Khalilifar MA (Page: 150)

Khan F (Page: 363)

Khatami Sh (Page: 57)

Khodadadi A (Page: 401)

Khodaverdi S (Page: 179)

Kholghi Oskooei V (Page: 331)

Khoradmehr A (Pages: 49, 103, 300)

Khosravani P (Page: 124)

Kim MM (Page: 27)

Kim NH (Page: 357)

Kobarfard F (Page: 371)

Koosha F (Page: 419)

Kooshyar MM (Page: 268)

Koruji M (Page: 14)

kouhkan A (Page: 307)

L

Li W (Page: 161)

Liang X (Page: 459)

Lin J (Page: 161)

Liu Q (Page: 161)

M

M Adcock L (Page: 391)

Madjd Z (Page: 14)

Index by Authors in Cell Journal^(Yakhteh)
Vol 21, No 1-4, 2019-2020

- Mahdian R (Page: 143)
Mahdieh N (Page: 337)
Majdi Seghinsara A (Page: 210)
Majid Shokoohi (Page: 210)
Majidi Gharenaz N (Page: 410)
Majidzadeh-Ardebili K (Page: 43)
Maki C (Page: 14)
Maleki Behzad M (Page: 115)
Mansour Ghanaie R (Page: 337)
Mashayekhi P (Page: 179)
Mazaheri F (Page: 49)
Mazaheri Z (Page: 410)
Meyfour A (Page: 229)
Minaee Sh (Page: 70)
Minaii Zang B (Page: 371)
Moazzeni SM (Pages: 92, 274)
Moghimipour E (Pages: 169, 379)
Mohammadi R (Page: 391)
Mohammadiasl J (Page: 401)
Mohammadzadeh A (Page: 337)
Moharrami M (Page: 124)
Mohseni M (Page: 236)
Moini A (Pages: 35, 479)
Mojtahedzadeh M (Page: 363)
Mokhtarian R (Page: 451)
Molla Hoseini H (Page: 300)
Molla Kazemiha V (Page: 143)
Moradi H (Page: 236)
Mortaz E (Page: 391)
Motalleb Gh (Page: 62)
Motamed N (Page: 124)
- Motevaseli E (Page: 236)
Movaffagh J (Page: 379)
Movahedin M (Page: 410)
Mozdarani H (Page: 322)
Mozdarani S (Page: 322)
N
Naderi S (Page: 204)
Naghibzadeh M (Page: 300)
Najafi M (Page: 236)
Najmabadi H (Page: 337)
Nasiri N (Pages: 35, 253)
Nasr Esfahani MH (Pages: 99, 194, 314)
Nejaddehbashi F (Page: 379)
Nemati Sh (Page: 290)
Neshasteh-Riz A (Page: 419)
Niasari Naslji A (Page: 307)
Niaz K (Page: 363)
Nikpour P (Page: 99)
Nikukar H (Page: 300)
Noori-Zadeh A (Page: 1)
Noruzinia M (Page: 179)
Noureddini M (Page: 314)
Nouruzi F (Page: 236)
Nozari A (Pages: 70, 337)
- O**
Ommati H (Page: 268)
Omrani MD (Page: 331)
Orazizadeh M (Pages: 169, 379)
Oryan Sh (Pages: 35, 135, 220)
- P**
Pahlavan S (Page: 229)
Pakizeh Kar S (Page: 350)
Park E (Page: 357)
Park HJ (Page: 27)
Parrish E (Page: 433)
Peymanfar Sh (Page: 426)
Pirhajati-Mahabadi V (Page: 14)
Pourkhodadad S (Page: 220)
Pourrajab F (Page: 300)
- R**
Rahimi M (Page: 467)
Rajaei F (Page: 1)
Rakhshani N (Page: 322)
Rassouli H (Page: 290)
Razi Gh (Page: 243)
Razi M (Page: 243)
Rezaei Kahmini F (Page: 92)
Rezapoor S (Page: 236)
Rezazadeh Valojerdi M (Page: 479)
Riahi Rad Kh (Page: 210)
Roghanian R (Page: 426)
Roshangar L (Page: 210)
- S**
Saadatmand P (Page: 451)
Saber S (Pages: 268, 350)
Sadeghian MH (Page: 78)
Sadeghian-Nodoushan F (Page: 300)
Sadraie SH (Page: 220)
Saffar H (Page: 236)
Saghahazrati S (Page: 371)
Saki G (Page: 401)
Saki N (Page: 115)

Index by Authors in Cell Journal^(Yakhteh)
Vol 21, No 1-4, 2019-2020

Salahshourifar I (Page: 86)
Saleh Gargari S (Page: 331)
Sarli A (Page: 322)
Seyyed Anvari S (Page: 243)
Shabani R (Page: 14)
Shabeeb Dh (Page: 236)
Shafeghati Y (Page: 337)
Shahhoseini M (Page: 124)
Shahidi M (Page: 419)
Shahrooz R (Page: 391)
Shahverdi AH (Pages: 307, 314)
Shakeri-Zadeh A (Page: 14)
Sharifi-Zarchi A (Pages: 35, 467)
Sheikhha MH (Page: 135)
Shervin Badv R (Page: 337)
Shokoohi M (Page: 210)
Shokraii F (Page: 124)
Shokrgozar MA (Page: 143)
Shoorei H (Page: 210)
Siadat SD (Page: 57)
Skutella T (Pages: 186, 281)
Sobhanian H (Page: 229)
Soheily Z (Page: 43)
Soleimani M (Pages: 43, 78, 433)

T

Tabandeh MR (Page: 169)
Tabatabaeian H (Page: 451)
Taheri M (Page: 331)
Tahmasebi M (Page: 210)
Tahmoorespur M (Page: 194)
Takimoto K (Page: 357)

G

Talebi AR (Page: 300)
Tamadon A (Pages: 49, 103)
Tavalaee M (Page: 314)
Tohidi Moghadam T (Page: 14)
Topraggaleh TR (Page: 7)
Torabi Afra M (Page: 350)
Totonchi M (Page: 124)

V

Varmazyar R (Page: 1)
Vosough M (Page: 268)

W

Wang H (Page: 103)

Y

Yakhchali B (Page: 451)
Yari R (Page: 426)

Z

Zadeh-Vakili A (Page: 433)
Zakeri Z (Page: 314)
Zare T (Page: 204)
Zarghami N (Page: 467)
Zarkesh-Esfahani SH (Page: 426)
Zarrabi M (Page: 259)
Zeinali S (Pages: 179, 433)
Zeinaloo A (Page: 70)
Zhang Zh (Page: 459)
Zhou X (Page: 459)
Zolfaghari Z (Pages: 253, 307)
Zorriehzahra MJ (Page: 62)